LOW TEMPERATURE SINTERING OF ZNO-BASED CERAMICS AND INVESTIGATION OF THEIR VARISTOR APPLICATIONS

Gökçe ÖZARSLAN

PhD Dissertation

Department of Ceramic Engineering

Programme in Ceramic Engineering

Supervisor: Prof. Dr. Ender SUVACI

Eskişehir

Eskişehir Technical University

Institute of Graduate Programs

September 2022

This thesis has been supported by the project 20DRP027, which is approved by the SRP Committee.

FINAL APPROVAL FOR THESIS

This thesis titled LOW TEMPERATURE SINTERING OF ZNO-BASED CERAMICS AND INVESTIGATION OF THEIR VARISTOR APPLICATIONS has been prepared and submitted by Gökçe ÖZARSLAN in partial fulfillment of the requirements in "Eskişehir Technical University Directive on Graduate Education and Examination" for the Degree of PhD in Ceramic Engineering Department has been examined and approved on 02/09/2022.

Committee Members		**Title, Name and Surname**	**Signature**
Member	:	Prof. Dr. Emel ÖZEL	
Member	:	Prof. Dr. Nihal ERGİNEL	
Member	:	Assoc. Prof. Bilge YAMAN ISLAK	
Member	:	Asst. Prof. Yasemin ÇELİK	
Member	:	Asst. Prof. Betül YILDIZ	

Prof. Dr. Murat TANIŞLI

Director of the Institute of Graduate Programs

02/09/2022

SUPERVISOR APPROVAL

PhD student Gökçe ÖZARSLAN, whom I supervise, has completed this thesis titled LOW TEMPERATURE SINTERING OF ZNO-BASED CERAMICS AND INVESTIGATION OF THEIR VARISTOR APPLICATIONS. According to my inspections, the work is scientifically and ethically appropriate for the student to the thesis defense exam.

Supervisor

Prof. Dr. Ender SUVACI

ABSTRACT

LOW TEMPERATURE SINTERING OF ZNO-BASED CERAMICS AND INVESTIGATION OF THEIR VARISTOR APPLICATIONS

Gökçe ÖZARSLAN

Department of Ceramic Engineering

Programme in Ceramic Engineering

Eskişehir Technical University, Institute of Graduate Programs, September 2022

Supervisor: Prof. Dr. Ender SUVACI

Cold sintering process (CSP) is a promising ultra low-temperature sintering method that needs an aqueous solution for transition of atoms along with formation of dissolution-precipitation process under high pressures. In this thesis, technical and scientific investigations of the CSP were discussed by using ZnO as model material.

ZnO bulk ceramics with >99.00 % theoretical density (T.D.) were obtained under 540 MPa pressure, at 140˚C temperature after 50 minutes dwell time and 7.00 wt % liquid with pH 5.5 via CSP. Change of liquid film thickness was evaluated during CSP.

For detailed interactions of the sintering variables, responce surface methodology (RSM) using Minitab software was used with Cental Composite Design (CCD) method. pH was obtained as the most effective parameter of the CSP for the given experimental conditions and in the five experimental varibles of temperature, pressure, pH, liquid amount and the time.

In the final part of the thesis, ZnO-Bi_2O_3 and ZnO-Bi_2O_3-Co_2O_3 varistor systems were produced by CSP method. Threshold voltage was expected to be increased for high voltage applications based on fine grains and higher amount of grain boundaries due to CSP. ZnO-Bi_2O_3-Co_2O_3 varistors with > 95.00 % T.D. were produced at 250˚C via CSP. α value obtained as 27 and thereshold voltage was 2200 V/mm, that are compatible with conventionally produced high voltage varistors.

Keywords: Cold sintering process, Response surface methodology, ZnO, Bi2O3, Varistor.

ÖZET

ÇİNKO OKSİT ESASLI SERAMİKLERİN DÜŞÜK SICAKLIKLARDA SİNTERLENMESİ VE VARİSTÖR UYGULAMALARININ İNCELENMESİ

Gökçe ÖZARSLAN

Seramik Mühendisliği Anabilim Dalı

Seramik Mühendisliği Bilim Dalı

Eskişehir Teknik Üniversitesi, Lisansüstü Eğitim Enstitüsü, Eylül 2022

Danışman: Prof. Dr. Ender SUVACI

Soğuk sinterleme prosesi (SSP), yüksek basınçlar altında çözünme-çökelme işleminin oluşumu ile birlikte atomların transferi için sulu bir çözeltiye ihtiyaç duyan, umut verici bir ultra düşük sıcaklık sinterleme yöntemidir. Bu tezde, model materyal olarak ZnO kullanılarak SSP'nin teknik ve bilimsel araştırmaları tartışılmıştır.

>%99.00 teorik yoğunluğa (T.Y.) sahip ZnO yoğun seramikler, 540 MPa basınç altında, 140˚C sıcaklıkta 50 dakika bekleme süresinden sonra ve pH 5.5 ile ağırlıkça %7.00 sıvı kullanılarak SSP ile elde edildi. SSP sırasında sıvı film kalınlığındaki değişiklik değerlendirildi.

Sinterleme değişkenlerinin ayrıntılı etkileşimleri için, Merkezi Kompozit Dizayn yöntemi ile Minitab yazılımı kullanılarak tepki yüzeyi metodolojisi kullanıldı. pH; sıcaklık, basınç, pH, sıvı miktarı ve süre olarak verilen deneysel koşullar içinde SSP'nin en etkili parametresi olarak elde edilmiştir.

Tezin son bölümünde SSP yöntemi ile ZnO-Bi_2O_3 ve ZnO-Bi_2O_3-Co_2O_3 varistör sistemleri üretilmiştir. Yüksek voltaj uygulamaları için uygun varistörlerin SSP yöntemi kullanılarak elde edilebileceği, çünkü üretim yöntemine bağlı olarak ince tanelerin ve tane sınırları miktarının artması ve buna bağlı olarak bozunma voltajının artması bekleniyordu. > %95.00 T.Y.'e sahip ZnO-Bi_2O_3-Co_2O_3 varistörleri SSP ile 250˚C'de üretilmiştir. 27 olarak elde edilen α ve 2200 V/mm eşik voltajı değerleri, geleneksel olarak üretilen yüksek gerilim varistörleri ile uyumludur.

Anahtar Sözcükler: Soğuk sinterleme prosesi, Tepki yüzeyi metodolojisi, ZnO, Bi2O3, Varistör.

ACKNOWLEDGEMENTS

During the execution of this study, I would like to thank my esteemed advisor, my mentor from the first day of undergraduate, who always calmly supporting me, Prof. Dr. Ender SUVACI,

My professors, who were in my PhD thesis monitoring committee and shared their valuable knowledge with me, Prof. Dr. Emel ÖZEL, Assoc. Prof. Dr. Bilge YAMAN ISLAK and Prof. Dr. Nihal ERGİNEL.

To all my professors and colleagues in the Department of Materials Science and Engineering of Eskişehir Technical University, who shared their laboratory facilities and knowledge with all students and created a peaceful working environment,

I would like to thank esteemed Asst. Prof. Yasemin ÇELİK, Assoc. Prof. Ali ÇELİK, Asst. Prof. İ. Özgür ÖZER, Assoc. Prof Erhan AYAS, Asst. Prof. Emrah DÖLEKÇEKİÇ, Prof. Dr. Alpagut KARA, Prof. Dr. Servet TURAN, for their kind helps whenever I need.

To the members of the Suvacı Research Group (SRG), who have never spared their helps and good fellowship during my laboratory studies,

I would like to express my heartfelt thanks for my dear overpatient husband Olçun ÖZARSLAN, who always supported me in every way and never left me alone, to my dear smart and insightful daughter Talya ÖZARSLAN, who is the most valuable asset in my life, and to my parents; Zehra ESİN YILDIRIM and Resul YILDIRIM, making me exist, let me grow and still be there for me.

Gökçe ÖZARSLAN

02/09/2022

STATEMENT OF COMPLIANCE WITH ETHICAL PRINCIPLES AND RULES

I hereby truthfully declare that this thesis is an original work prepared by me; that I have behaved in accordance with the scientific ethical principles and rules throughout the stages of preparation, data collection, analysis and presentation of my work; that I have cited the sources of all the data and information that could be obtained within the scope of this study, and included these sources in the references section; and that this study has been scanned for plagiarism with "scientific plagiarism detection program" used by Eskişehir Technical University, and that "it does not have any plagiarism" whatsoever. I also declare that, if a case contrary to my declaration is detected in my work at any time, I hereby express my consent to all the ethical and legal consequences that are involved.

Gökçe ÖZARSLAN

CONTENTS

Page

LIST OF TABLES

Page

LIST OF FIGURES

Page

GLOSSARY OF SYMBOLS AND ABBREVIATIONS

α	:	Alpha, varistor non-linear coefficient
BSE	:	Backscattered electrons
FAST	:	Field Assisted Sintering Technology
FS	:	Flash sintering
HIP	:	Hot isostatic pressing
HP	:	Hot-pressing
RSM	:	Response Surface Methodology
CCD	:	Central Composite Design
CS	:	Conventional sintering
CSP	:	Cold Sintering Process
E_b	:	Breakdown electric field
EDX	:	Energy dispersive X-ray spectroscopy
EIA	:	USA Energy Information Administration
HCl	:	Hydrochloric acid
J	:	Current density
Min.	:	Minute
SEM	:	Scanning electron microscope
SPS	:	Spark Plasma Sintering
T.D.		Theoretical Density
TG-DTA	:	Thermogravimetric and Differential Thermal Analyses
V-I	:	Voltage-Current
XRD	:	X-ray diffraction
ZA	:	Zinc Acetate

1. INTRODUCTION

Sintering is a thermal energy directed production process, used for the controlled densification of metal or ceramic powders. The sintering of materials is an ancient process that was used to make pottery in prehistoric times. However, systematic scientific studies on this subject mainly started only after the 1940s, [1]. Development of understanding on basics of the sintering is important if reproducible and specific products are desired. Accordingly the research activities on this subject are critical and they enable one to understand role of variables on the sintering process and hence control the process effectively. The driving force for sintering is the reduction in surface free energy of the co-located powder forms. The surface energy can be decreased in two ways, one of which causes densification, but in the other case, the grains in the material grow and this is called grain growth, [1]. In the case of grain growth, the driving force for the densification decreases. This shows that it is very important to know and control which of the mehanisms is dominant during the sintering process, as it is in every engineering treatment, to achieve the desired properties.

Properties of a material can be controlled by tailoring its structure. We see in Figure 1.1 that the chemical composition and production method are effective on the microstructure. Figure 1.2 shows the flow chart of a ceramic material production. Each step involved here influences the resulting microstructure. When we look at the microstructure of a ceramic, we see grains, pores, and sometimes some other phases as shown in Figure 1.3. If the size and shape of the grains and pores as well as their distribution and amount, and presence of other phases are controlled carefully, the properties of the ceramics can be tailored. All the stages, shown in Figure 1.2 play critical on the microstructure development and hence final microstructure. For example, particle size distribution of starting powder determines the microstructure development and the resulting grain size, as well as the density that will occur as a result of sintering. Accordingly, if the process parameters are closely controlled, the desired properties can be obtained. In general, the desired microstructure is the microstructure with a few and homogeneously dispersed pores, a fine-grained structure and the chemical composition of the least component that can provide the desired properties. Some sources describe sintering is a race between grain growth and densification as will be described further below. As a result, if the competition between grain growth and densification is well

understood, this understanding can be used to achieve ceramics with desired microstructures and properties.

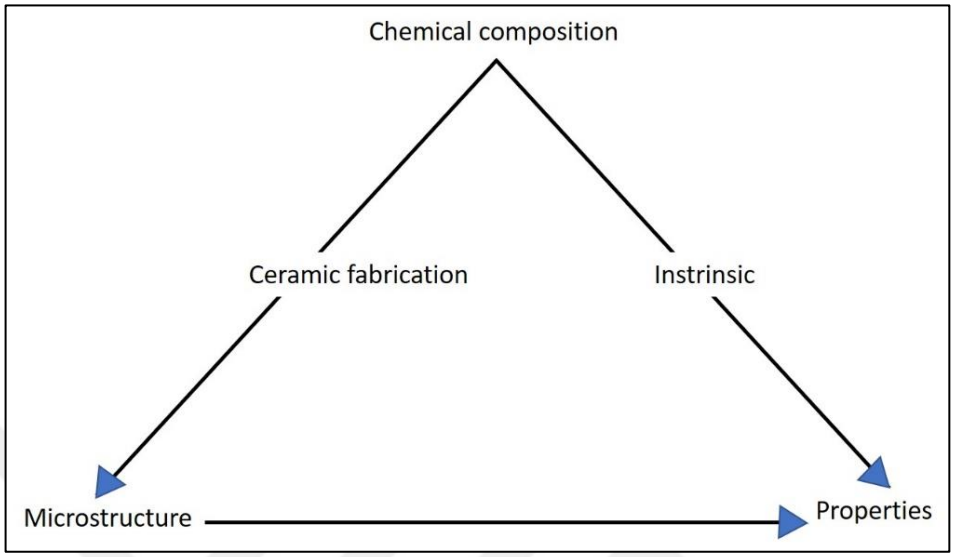

Figure 1.1. *The important relationships in ceramic fabrication, [1].*

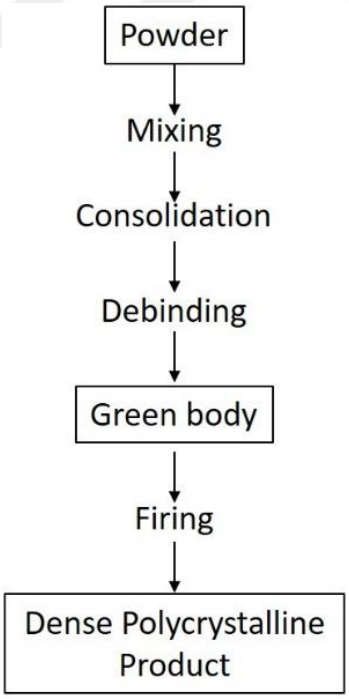

Figure 1.2. *Flow chart for the production of polycrystalline ceramics by firing of consolidated powders, by Rahaman M.N., [1].*

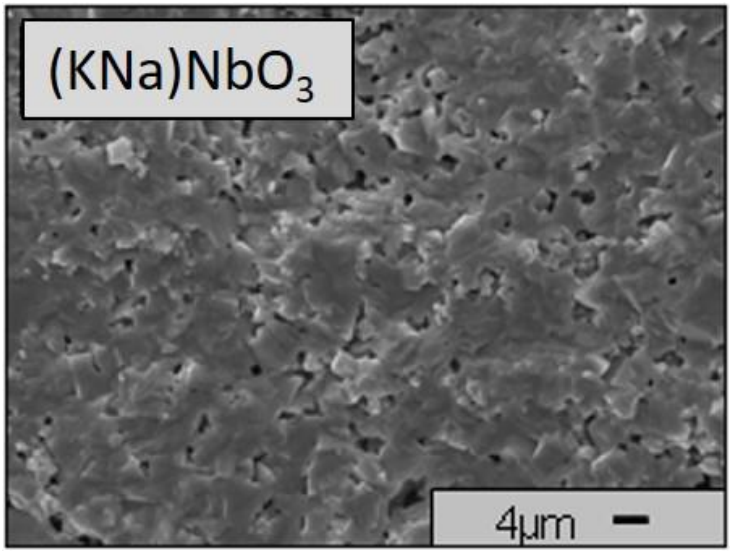

Figure 1.3. *($K_{0.5}Na_{0.5}$)NbO_3, sintered at 1100°C for 5 min.with 91.00 % T.D.,* [2]

The parameters that can be controlled during sintering, are temperature, time, heating and cooling rate. However, since each stage influences the following stage, controlling the entire process is essential. Most of the properties such as dielectric permittivity, dielectric breakdown strength, mechanical hardness and strength, and electrical/thermal conductivity are directly influenced by the density. With the advancement of technology, the desired properties in materials come to the fore even more. For example, if some of the mechanical properties are needed to be improved, after the optimum chemical composition is determined, the targeted microstructure from which we can obtain that property, is determined, and in order to achieve this, the sintering conditions to be applied are chosen. Because the final state of the microstructure will be formed by sintering. The ceramic body with porous structure after the forming step is called as green body. During sintering atomic/ionic mobility (i.e., diffusion) occurs between the grain boundaries and the pores by increasing temperature. The isolated pores are mostly removed from the system at the end of sintering and at the same time grain growth usually occurs in the last stage of the sintering. The final phase created by all these events will also affect the degree of densification. Rahaman states in his book that it is important for the densification of material, not to separate the pores from the grain boundaries in order to prevent grain growth, [1]. In this case, slow grain growth rate and fast densification are necessary to obtain a material with high density and controlled grain growth. Rahaman also indicates that such controlled microstructures can be achieved via use of dopants or fine, inert, second-phase particles, homogeneous packing of fine

particles with a narrow size distribution, sintering with an externally applied pressure, rapid heating rates, and second phases that form a liquid at the firing temperature can be helpful to achieve high densities, [1]. Kang summarizes the variables affecting sintering in Table 1.1. These variables are classified into two groups as material-based and process related variables. Material variables include raw materials' physical and chemical properties and these variables influence the powder compressibility and sinterability. Densification and grain growth are related with raw material characteristics. The process variables in sintering are mostly thermodynamic variables, such as temperature, time, atmosphere, pressure, heating and cooling rate, [3]. These variables are important for all types of sintering and even more comlicated and important in real processing.

Table 1.1. *Sintering variables, [3].*

Material variables	Powder: Shape, size, size distribution, agglomeration, mixedness, etc.
	Chemistry: Composition, impurity, non-stoichiometry, homogeneity, etc.
Process variables	Temperature, time, pressure, atmosphere, heating and cooling rate, etc.

It should be noted that there is more than one type of sintering. The sintering techniques can be grouped as pressureless and pressure-assisted sintering methods in general. The pressureless sintering methods can be classified as solid state, liquid phase and viscous flow sintering. There are similarities as well as differences in the development stages of these sintering types. Before examining a sintering process, it is necessary to know what type of sintering it has in order to evaluate its kinetics correctly.

The curvature of the free surfaces during sintering and the pressure, if present in the system, create the driving forces for sintering. However, to accomplish the process within a reasonable time, we must also consider the kinetics of mass transport. In crystalline ceramics, mass transport occurs predominantly by diffusion of atoms, ions, or other charged species. Solid-state diffusion can occur by several paths that define the mechanisms of diffusion and, hence, the mechanisms of sintering. For sintering to occur, the material must move from high chemical potential energy region to low chemical

potential energy region. The way the atoms move during diffusion determines the mechanism of sintering, [1].

During liquid phase sintering, there is a liquid phase between the solid particles in the system. If the amount of this liquid phase is huge, it is called viscous sintering. Generally, if the liquid phase ratio is between 1 and 30 % by volume, it is called liquid phase sintering, [4]. If the liquid phase content is over 30 vol. %, then sintering type is called as viscous flow sintering. While each sintering method can be developed according to the composition, it can be especially applied to control some parameters. For example, viscous and liquid phase sintering can be preferred over solid-state sintering due to some of its advantages. The most important of these advantages is that the microstructure can be controlled more easily, and the production cost is reduced due to lowering the sintering temperature and time. However, it should be noted that these methods also have some disadvantages. For example, presence of the liquid phase can reduce the mechanical strength. If the desired feature is affected, it should not be preferred. However, there are some cases where viscous and liquid phase sintering processes are particularly preferable. For example, in the production of varistors, which is an electrical material, the liquid phase surrounding the grains is preferred because it provides the desired electrical properties to the material. Liquid phase sintering is still a highly preferred method in the industry despite its disadvantages, due to its ability of reducing sintering temperature significantly. Most of the research in the field of sintering has been done with the aim of decreasing the sintering temperature. Generally, the sintering temperature of a material takes place at a temperature of ½ to 3/4 of its melting temperature. Since the melting points of ceramic raw materials are quite high, their sintering temperatures are above 1000°C. The energy required to produce the material, which remains at this high temperature for some period, is quite high. Today, the importance of energy is increasing day by day. For this reason, many studies have been carried out to reduce the sintering temperatures.

There have been some approaches to reduce the sintering temperature. These techniques can be classified in three main categories: i) optimization of the powders, ii) addition of sintering aids and iii) development of advanced sintering techniques. Refining of the starting powder to decrease the diffusion distance of mobile chemical species and therefore increase the densification rate [5], as well as to remove surface oxides in non-oxide ceramics [6], are well known methods to reduce the sintering temperature. Smaller

particles bond more quickly with the other grain due to greater radius of curvature and hence greater chemical potential energy, so the required sintering time or temperature decreases to echieve a similar density, [7]. For this reason, fine grained powders are preferred when low temperature sintering is desired.

Addition of second phases into the starting composition is also a well established approach to reduce the sintering temperature of ceramic compounds. The sintering additives are more commonly incorporated to form a liquid phase between the particles at high temperature, which generates capillary forces and increases the diffusion rates by partial dissolution of the solid phase and transport through the liquid. This process is known as liquid phase sintering, and is widely used in industry [8], as stated earlier. However, the solidified second phase remains in the microstructure, typically at the grain boundaries, altering the final properties of the material.

Regarding the sintering techniques, a significant progress has been achieved in the last decades. Pressure assisted sintering methods, Hot isostatic pressing (HIP), Hot-pressing (HP), Field Assisted Sintering Technology/Spark Plasma Sintering (FAST/SPS) and the recent flash sintering (FS) enable to reduce the sintering temperature by hundreds of degrees with respect to that of the pressureless sintering [9,10]. These techniques are assisted by pressure and/or by electric current and field. As a result, many materials can be fully densified. A combination of these three main approaches; refining of powder, use of additives and sintering technique is particularly appealing to reduce the sintering temperature and tailor the microstructure. However, it should be noted that the cost of the process to be used to reduce the sintering temperature should be affordable and the equipment should be easily available. When all these aspects are considered, pressure assisted sintering methods have also their own drawbacks. The most important of these may be the high cost of special equipments.

One of the low temperature sintering studies that has been going on for a long time is sintering under hydrothermal conditions. The word hydrothermal first used by the British geologist, Sir Roderick Murchison (1792-1871), to describe the along with the presence of water, therewithal temperature and pressure, leading to the formation of various rocks. Hydrothermal sintering methods are a perspective that imitates the formations in nature. Agglomeration of salt, formation of pearls or diamonds also occur in nature in this way in common with temperature and pressure [11]. Yamasaki et al. were pioneers of the application of hyrothermal processes to sintering of advanced ceramics.

Although they conducted studies on hydrothermal sintering in the 1980s and obtained some results, they could not reach sufficient densities [12]. In the following years, continued studies were carried out and pressure asisted sintering methods were tried to be used together with the liquid phase. This developmental process will be explored in more detail below. However, the bottom line here is that the sintering temperature can be lowered considerably under hydrothermal conditions. The use of water as an auxiliary addition to sintering started with this perspective.

Recently, water assisted sintering was used effectively for densification of several ceramic compounds at very low temperature (<300 °C) by Randall et al. naming the process “Cold Sintering Process” (CSP,) [13-15]. The basic principle is hardly different from the studies published before. It is based on the densification of moistened ceramic powders under very high uniaxial pressures, hence reducing the maximal required temperatures (<300 °C). As for every pressure-assisted sintering technology, it is well known that the external compressive stress is an additional driving force for densification, either accelerating existing densification mechanisms or even triggering new one,s [1]. One of the issues that has been praised is the ease of the CSP process. The moistened ceramic raw pellets can be obtained either by mixing the power with water in a mortar or storing the powder into a humidity chamber, [11]. The drastically reduced temperatures enable to use simple hand press equipment with a heater jacket, which brings a profound advantage. The CSP was also demonstrated for many material at all, [16-19]. In most of the studies, it was possible to exceed 90.00 % theoretical densities. Even when some properties are compared with conventional sintering, close or equivalent results can be obtained. Nevertheless, for some materials like zirconia, CSP is more a compaction process than sintering, and a further thermal treatment at higher temperature is required to fully crystallize the material, [11,20,21]. However, high densities could be obtained in materials such as ZnO, which are easier to sinter and are suitable for the process [25,27-36].

While applying the CSP, moistening can be applied with different liquids and at different pH values. Deciding the most suitable transition solvent for the material depends on the process conditions such as thermodynamics and kinetics. According to the earlier reports, addition of acetic acid into the aqueous solution dramatically changed the final density of ZnO and microstructure, [11]. ZnO with theoretical densities higher than 90.00 % was obtained at T<300 °C, showing equivalent electrical conductivities as for ZnO

sintered at higher temperatures by conventional sintering. It was found that the liquid type and amount used for the powder humidification process is very important due to the mechanism. The CSP is thought to be based on a liquid phase sintering mechanism where particle rearrangement and dissolution-precipitation stages, which creates a supersaturated environment and enables a fast precipitation process on the particle surfaces to reach the final densification. When the studies are examined, it seems that under certain conditions, it is possible to obtain dense oxide ceramics at temperatures even lower than 300°C by partial dissolution of the particles and subsequent precipitation, synthesis reaction or the diffusion of ions from the water molecules into the crystal structure, [14,37,38].Although there are many studies on CSP of ZnO, there are still some points to be investigated in detail to better understanding the mechanism, [11,21,39].

Compared to other methods that lower the sintering temperature, it is very impressive that bulk dense samples can be obtained with the CSP at very low temperatures. Because even with liquid phase sintering, which is one of the mostly used methods, only a temperature drop of 10-20 % can be achieved, [11]. The energy evaluation of the sintering methods used are shown in Figure 1.4.

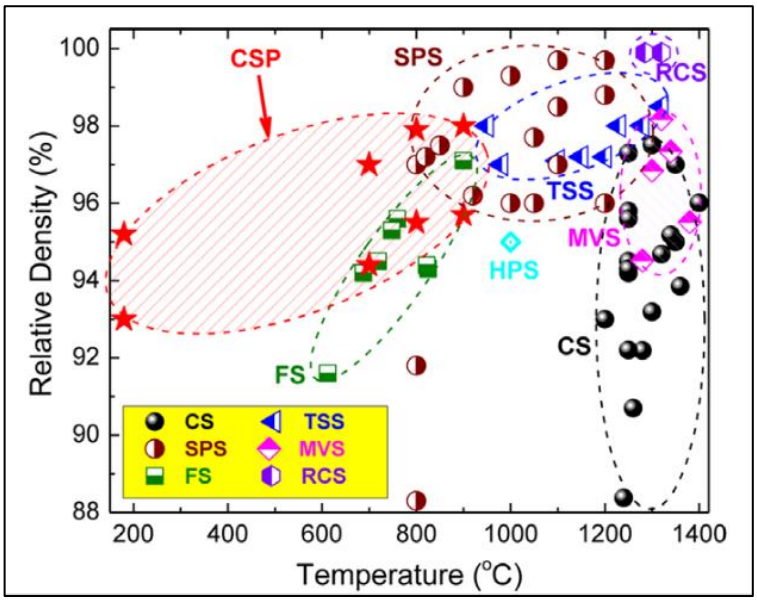

Figure 1.4. *Shows the energy consumption of different types of sintering. Temperature- theoretical density chart CSP:Cold sint. process, MVS:Microwave sint., CS:Traditional sint., FS: Fast sint., TSS: Two-step sint., SPS:Spark Plasma sint., RCS: Ratio-controlled sint., [11].*

1.1. History of the Cold Sintering Process (CSP) Technique

As mentioned earlier, the CSP emerged with the creation of hydrothermal conditions. This process of formation has turned into a structure that many researchers eventually put a stone on, in time. The idea of sintering at room temperature was first tried by Gutmanas et al in 1978, [31]. However, in the experiments, it was mostly studied with materials that could show plastic deformation. Although they were able to sinter some metals under pressure and at low temperatures, the method did not show sufficient success because they could not provide the same behavior in ceramics.

Liao et al. solved the fragility problems of ceramics [32], by decreasing the particle sizes of the powders up to about 18 nm. They obtained samples with 80 % density at room temperature by applying 8 GPa pressure. To get better theoretical densities temperature was increased up to 460°C, and they got densities close to 98 %. Compared to the sintering of alumina with traditional methods (1450°C) [33], the sintering temperature can be reduced three times with this technique. Liao et al. [32] showed thermodynamically that pressure can increase densification by inhibiting grain growth. In this case, the combination of plastic flow and grain internal diffusion by preventing grain growth causes high theoretical densities.

Yamasaki and Yanagisawa in Japan worked on hydrothermal hot-pressing, which is based on an autoclave that is externally heated, the powder with a proper content of water being placed between two pistons, which transmit uniaxial pressure, [12]. The pistons have a space for the release of water included in the starting powder. This space is required to remove the water present in the pore volume of the powder compact that hinders further compaction. As a result, steam pressure in autoclave is kept inside, while the powder is heated and compressed by the pushrods. This method has two characteristics: i) continous compression of the powder under hydrothermal conditions, and ii) removal of water from the interstices of the powder grains into the autoclave free space. The processing parameters in hydrothermal hot pressing are temperature of max. 300°C, heating rates of 10°C/min, pressure of 40 MPa and dwell time of 2 h. Under these conditions, borosilicate glass was fully densified because water diffused into the particles [34], but on the other hand, silica and amorphous titania remained porous, [33,34]. Nevertheless, dense hydroxyapatite ceramics were obtained by hydrothermal hot-pressing, but promoting hydrothermal reactions through the incorporation of precursor compounds, to achieve the expected HA structure. DCPD ($CaHPO_4.2H_2O$) and OCP

($Ca_8H_2(PO_4)6.5H_2O$), whose crystals are plate-like particles, are selected as the precursors, together with $Ca(OH)_2$ or ammonia water, to form HA [36]. Zeolite compounds were also sintered by hydrothermal hot-pressing containing 17 wt % of water with different amounts of NaOH, suggesting dissolution and precipitation as the consolidation mechanism.

In 2007, "cold sintering" of $CaCO_3$ was demonstrated at room temperature, using the combined action of mechanical pressure, CO_2 gas pressure and time. It was proposed that the amount of dissolved limestone available for the reprecipitation is an important factor determining the efficiency of the process and the increase in mechanical strength. High CO_2 pressure combined with high mechanical pressure facilitates the formation of a new calcium carbonate phase that binds the powder particles to an agglomerate.

Another related approach using Field Assisted Sintering Technology/Spark Plasma Sintering has reported by Schwarz et al. in 2012 [40]. The possibility of using high heating rates (100°C/min) in this kind of equipment enabled the densification of humid ZnO powder already above 200°C under 50 MPa. Densification was completed after 10 min at a temperature of 400°C, whereas a dry powder hardly sintered. Similarly, slow heating rates did not enable to achieve theoretical densities higher than ~65 %, [40,42]. When investigated further in great detail this phenomenon, so that highly dense ZnO (99.5 %) with a mean grain size of 200 nm was obtained at 400°C. A controlled, small amount of water (1.6 wt %) was directly added into the green compact. This water had no time to fully evaporate during heating in the graphite die and therefore got trapped at the surface and grain boundaries, with the following consequences: removal of carbonates on the particle surface, dissolution of Zn^{2+} and O^{2-} ions, mass transport through the liquid phase, and diffusion of H^+ and OH^- ions into the crystal structure of ZnO. It was clearly demonstrated that the electric field does not play any role in this process, but the addition of zinc oxide precursors such as zinc acetate considerably fostered densification. In addition, a change in the electrical properties was reported and proton conductivity was observed for the water-containing specimens.

As a result, a new form of cold sintering has been developed for ceramics, called CSP, [13-15,19,43]. According to this method, diffusion between particles is enhanced by a carrier solvent. Thus, while the temperature remains usually at 120-200°C, the pressure remains low at 350 MPa instead of 8 GPa. In order to distinguish between recent cold sintering studies and other previous low temperature sintering studies, the new

technique is called as the cold sintering process. The Pennsylvania State University researchers stated that 90-98 % densities can be reached with the cold sintering process in various ceramics including $BaTiO_3$, ZrO_2, Li_2MoO_4, CsBr, $NaNO_2$, KH_2PO_4, V_2O_5, and $Na_2Mo_2O_7$ [44].

1.2. The Advantages of the CSP and Energy Consumption Comparisons

In the modern world, everything requires energy and energy has become a very important need. However, as technologies progress, it becomes difficult to provide the necessary energy for the production. In addition to the research of new energy sources, many studies are carried out to use the used energies much more efficiently and economically during its consumption.

Many advanced sintering methods have been tried and some combination of them have been used to decrease energy consumption. Three parameters were taken into consideration in the comparison of energy consumptions. These parameters were increasing ramp rate of sintering, using electric field and inserting additives to the composition. Sohrabi et al. indicates decreasing techniques of energy consumption in Figure 1.5 [38]. Kimura et al. studied on energy consumption with electric field and also by additive concentration [45]. It was mentioned the use of additives can reduce energy consumption by 1.4 times and is known as the simplest method to be used. Using electric field and rapid heating is a more effective method and can reduce energy consumption by 2.6 to 20 times [38]. In Figure 1.5, fast firing technique, increasing the power used increases the heating rate, because the sintering time will decrease more than the energy requirement, so the rapid firing curve slope is negative. Conversely, the FAST and liquid phase sintering curve slopes are positive. This is due to the fact that the electric field and sintering additives reduce the sintering temperature, and therefore energy consumption decrease.

In the last decade, microwave sintering, one of the sintering methods that has been studied on various material systems by several researchers. Dorner-Reisel et al. compared conventionally sintered $BaTiO_3$ with the microwave sintered one. According to their results, energy consumption in microwave sintering can be as low as 5.4 MJ, that means 5.1 times lower than in the conventional sintering. SPS (Spark Plasma Sintering has the advantages of rapid heating, use of pressure and electric field, [46-49], together in one case. Different mechanisms are dominant during SPS sintering, [9]. It was considered,

energy consumption can be low due to the presence of more than one mechanism [50]. Using some of the techniques together can give the advantage of less energy consumption with the complex mechanisms.

Anselmi-Tamburini et al. [51], demonstrated, when the density was kept constant at 95 %TD during the sintering of ZrO_2 powders with SPS, the calculated energy consumption was 6 MJ at a pressure as low as 25 MPa. Compared to the conventional sintering of ZrO_2 (23 MJ), it was 4 times lower. These results show that utilization of electric field and rapid heating reducing the energy consumption. If the pressure used is increased to 800 MPa, the energy consumption can be further decreased down to 4 MJ levels.

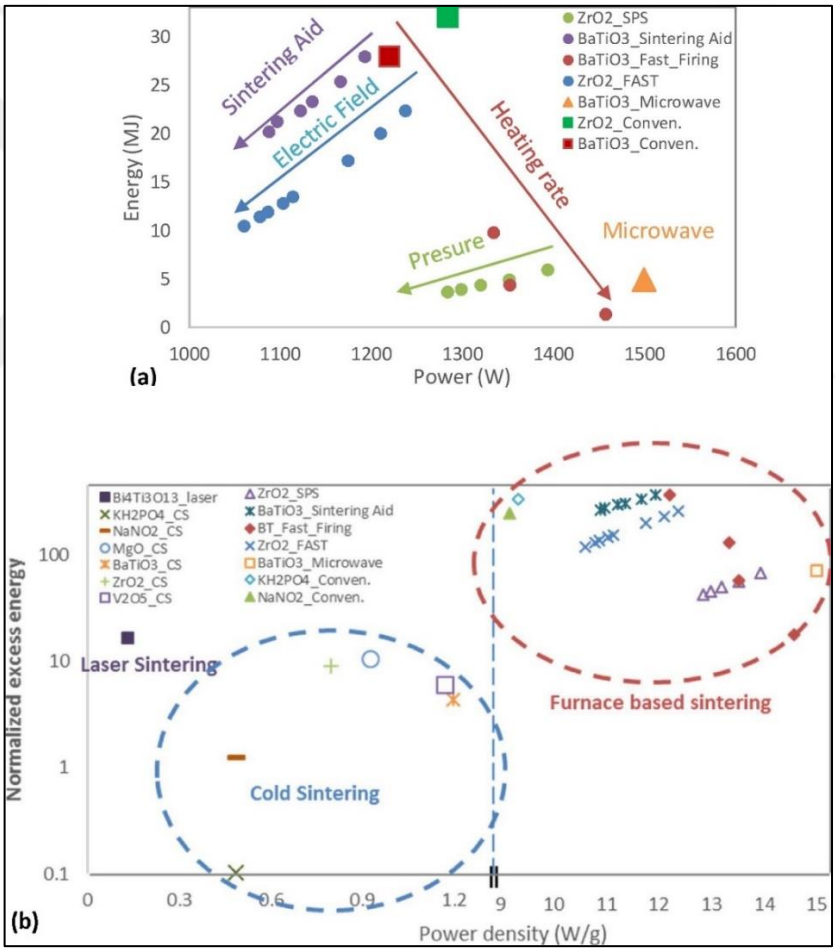

Figure 1.5. *a) energy consumption according to different techniques b) extra energy use according to different techniques, [50].*

The sintering time comes into prominence when making energy calculations on sintering with the CSP. Because the sintering time can vary from 1 min at 120°C to 30 min at 180 °C. In this case, finding the suitable solvent for the CSP and ensuring

dissolution and precipitation is the key parameter for the CSP, [50]. According to EIA (USA Energy Information Administration) data, in the USA, 34 % of all energy consumption (i.e., 25.85 × 1018 J), belongs to the energy industry sector in 2013, and this is expected to increase to 31.65 × 1018 J in 2025, [50]. Almost half of this energy is used in high temperature processes that occur usually above 1000°C. Reducing the energy used in such high temperature processes can save a lot of energy. For example, reducing sintering temperature from 1300°C to 180 °C by cold sintering process provides ~93 times of energy savings. The energy required to press a pellet with a diameter of 25 mm and a thickness of 5 mm was determined as 245 J, [50]. The applied pressure changes with the density, but for simplicity, the highest pressure value was taken as 350 MPa, and the energy expenditure is calculated. The thermal energy was measured as 2.91 kJ and the total energy required for KH_2PO_4 CSP was 3.16 kJ for 1 min. hold at 120°C. It was very difficult to compare this energy exactly with the energy used in other technologies because the unsintered product properties such as powder amount, powder physical properties must be similar for comparison, [50].

1.3. Basic Sintering Theories and Their Application to the CSP

In order to understand the CSP, it will be useful to benefit from other sintering theories available. Although some of the mechanisms change, there are still common points of sintering such as basics of densification and grain growth.

Two particle model is often used to describe the solid state sintering. The behavior of two particles in contact with each other over time is examined in the Figure 1.6. What is essential during sintering is the formation of a neck between two grains and the increase of this neck formation with material transfer from convex surfaces to flat and concave surface regions and then they are coming together and forming flat grain boundaries between the two grains. In Figure 1.6, X represents the neck radius and R represents the grain radius. The neck radius increases over time. The approach described here is to evaluate the sintering mechanism according to the law of measurement. In addition, according to the analytical model, which is one of the sintering theories, there are three stages of sintering. These are the initial stage, the intermediate stage, and the final stage. In the initial stage, neck formation occurs through diffusion, vapor convection, plastic flow, or viscous flow behavior. For a system in which sintering mechanisms are active, densification is observed up to about 65 % of the theoretical density. In the intermediate

stage, the pores still has continuity, as this stage ends, the pores are isolated at the beginning of the last stage and the density reaches 90 % theoretical density at the end of the middle stage, [52]. The point that draws attention here is that the densities in the initial parts of the thesis, did not exceed the 90 % theoretical density, except for a single sample. In this case, it may be possible to say that sintering stopped at the end of the 2nd stage in most of the studies carried out in the first trials.

At the last stage of sintering, densities over 90 % are reached. In the last step, the following equation is used when examining the change of densification rate according to grain size. The densification rate changes with the temperature constant K and the grain size G, and m is determined according to the type of diffusion mechanism. Here m = 3 for lattice diffusion and m = 4 for grain boundary diffusion, [52] .

$$1/\rho\ (d\rho/dt) = K/G^m \tag{1.1}$$

In the studies carried out, the gradual densification rate has not been determined yet. However, once the best conditions have been determined, the m contained here can be evaluated by performing gradual experiments. Such a study will be useful when describing diffusion mechanisms.

The scaling laws for the other mass transport mechanisms can be described as following equation by Herring. m is te exponent, changing due to sintering mechanism, Δt is the time change during sintering, λ is a numerical factor, R is the Radius of the grains due to time, as seen at Figure 1.6.

$$\frac{\Delta t_2}{\Delta t_1} = \lambda^m = \left(\frac{R_2}{R_1}\right)^m \tag{1.2}$$

The table below shows the transport mechanisms formed according to the m value according to Herring's law of scaling. These mechanisms show how the transport of atoms occurs in the system and the condensation as a result of which transports, see in Table 1.2. Its importance in our study is that it is necessary for the way of diffusion at grain growth or densification mechanisms in the future.

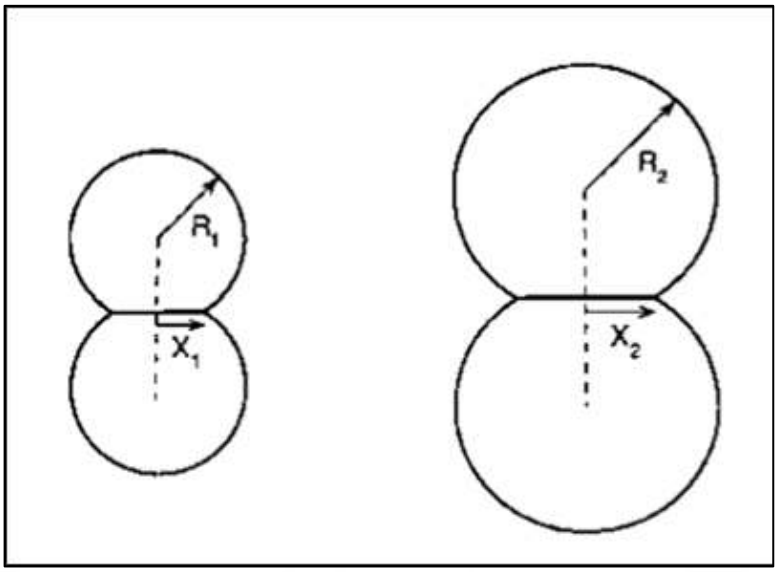

Figure 1.6. *View of two touching grains of different diameters during sintering, [52].*

Table 1.2. *Table of m values according to diffusion mechanism according to Herring's scaling law*

Sintering mechanism	m scale
Surface diffusion	4
Latice diffusion	3
Vapor transport	2
Grain boundary diffusion	4
Plastic flow	1
Viscos flow	1

At the CSP, the mechanism is explained mainly as a dissolution and precipitation process, similar to liquid phase sintering. Dissolution is the process that determines where the atom will be moved from (i.e., convex surfaces) during the diffusion in sintering. That is, the initiation, shape and speed of dissolution are important. Afterwards, the region where the precipitation (i.e., concave surfaces) will occur is important as observed during the liquid phase sintering.

1.4. Liquid Phase Sintering: A Path Towards Understanding the CSP

In the liquid phase sintering, the liquid completely wets the solid surfaces, the surfaces between the gas and solid phase are eliminated and the pores turn into round

spaces in the liquid. With the reduction of the surface areas between the liquid and the vapor, shrinkage, that is, densification, takes place. Figure 1.7 indicates two particle model for solid state sintering and liquid phase sintering. Diffusion paths going through the liquid phase, so the densification rate changes due to way of atomic transport.

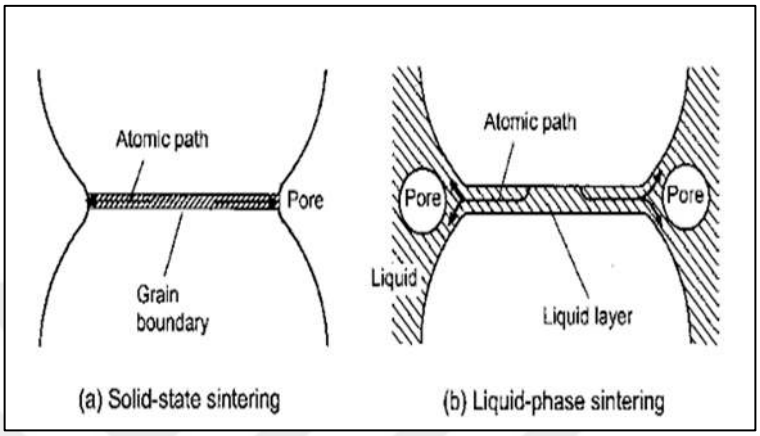

Figure 1.7. *Solid state sintering and liquid phase sintering two grain model representations, [52].*

The simplest and most effective way to reduce the sintering temperature and energy requirement is liquid phase sintering. The process is based on adding a low temperature melting phase to the system. The secondary phase melts during sintering and flows between the particles. It facilitates the liquid phase diffusion process and reorganization of the grains. This sintering method has been studied in detail by many people, [8,42]. As mentioned before, Kimura et al. investigated the relationship between the concentration of Li_2CO_3 addition to $BaTiO_3$ and the sintering temperature, [45]. The sintering temperature of $BaTiO_3$ powders can be reduced from 1300°C to 1000°C with the addition of 0-0.03% mol % Li. It can even be reduced to 800°C with the addition of 0.15 mol % LiF, [53]. There are many additives that lower the sintering temperature, some of them BaB_2O_4, YB_6, Li_2O-SiO_2, ZnO-B_2O_3, PbO-B_2O_3, and ZBS (ZnO–B_2O_3–SiO_2). However, none of them can reduce the sintering temperature below 900°C, [54].

When sintering was done by covering the Ni particles with Li_2CO_3, the microstructure analyzes showed that the Ni grains were surrounded by residual Li_2CO_3 at the grain boundaries, [45].

One of the most popular examples of liquid phase sintering is the use of liquid phase in ZnO varistors, [55-59]. Bi_2O_3 powder melts at 817°C and is used as a sintering additive for ZnO. In a typical conventional varistor structure, the Bi_2O_3 phase is visible at the grain

boundaries, they are seen brightly in Figure 1.8. This shows that the Bi_2O_3 powder melted and flowed between the grains in the early stages of sintering. The advantage of using Bi_2O_3 is that it both reduces the sintering temperature and creates unique electrical properties, [48]. In the CSP process, the liquid phase formation feature of Bi_2O_3 will not be utilized by going to high temperature. However, changes in electrical properties due to the homogeneous distribution of this addition in the matrix and sintering at low temperature should be examined.

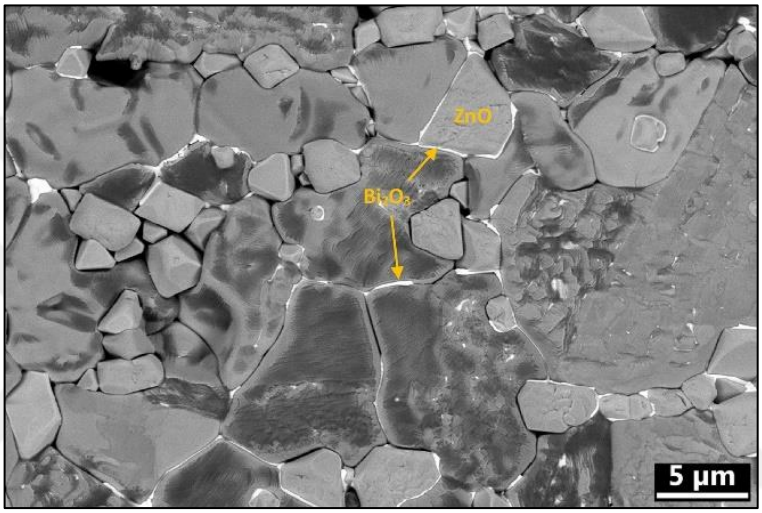

Figure 1.8. *ZnO varistor structure, [48].*

There are three essential conditions for the liquid phase sintering:

- There must be sufficient liquid phase
- The liquid phase must wet the solid
- Solid must have solubility in liquid

There are three stages at liquid phase sintering. Figure 1.9 shows these stages, summarized by Rahaman [1]. Mostly, the material all in solid form at the beginning and during the temperature rise, some sufficient material with low melting point creates liquid phase and rearrangement of the particles occure by the assistance of the liquid phase. At the second stage, some of the solid particles dissolve into the liquid phase and the ions in the solute begins to saturate and there is precipitation on the less energy sites and there is densisfication occurs. Density increase is proportional with surface energies and inversly proportiona with the rise of viscosity and particle size, see in Equation 1.2. It is well known that smaller the particle that there is an increase of solubility. Accordingly, solubility of the solid particle in the solute is a key factor. In liquid phase sintering, driving

force of the rearrangement part is capilar forces. Grain size distribution, different grain shapes, internal density fluctuations, anisotropic material properties are some of the important key factors that effect liquid phase sintering at rearrangement part.

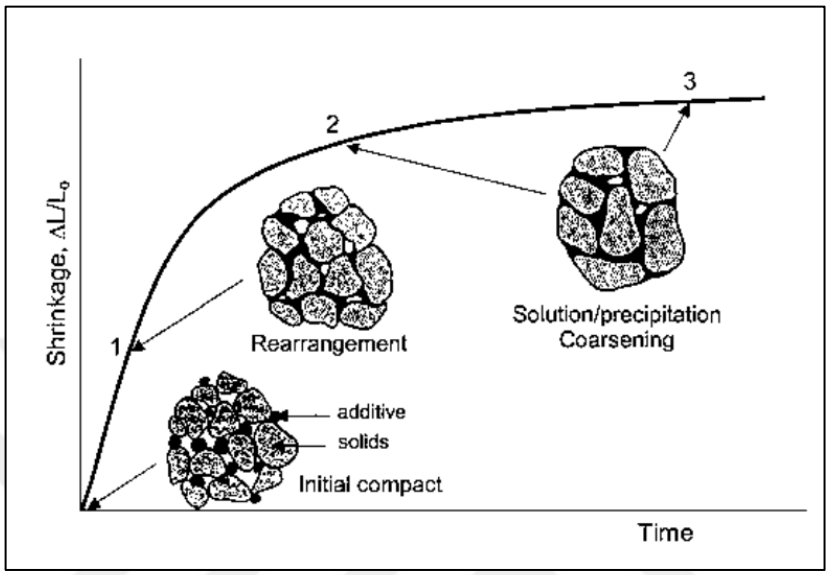

Figure 1.9. *Stages of liquid phase sintering by Rahaman M., [1].*

$$\frac{d(\Delta\rho/\rho_0)}{dt} = A_{(g)}\frac{\gamma_{lv}}{\eta r_s} \tag{1.3}$$

When there is a Newtonian liquid between the particles, the deformation rate is proportional to the shearing stress occured on the particles. Accordingly, the resulting densification rate is given by Equation 1.3, where ρ is the theoretical density, ρ_0 is the initial compact density, Δρ is the density difference, t is the time, A(g) is the geometrical constant, that is a function of V_1, ρ and the contact geometry, η is the viscosity of the liquid, and r_s is the radius of the solid particle. A (g) increases with increasing volume fraction of solid and liquid, and decreases with increasing theoretical density, [3]. Kingery and Narasimhan demonstrated that actual particle compacts, full densification can be achieved by rearrangement alone at approximately 30-35 vol% liquid, [3].

For the second and third part of the sintering, there is dissolution and precipitation in the system. There can be two mechanisms that can effect the rate of sintering. There are two mechanisms, [4].

1. Diffusion rate determinant over the liquid phase
2. Interface reaction

These two mechanisms can be seen at the formulations 1.3 and 1.4 Driving force for the sintering is capilar forces, [4]. In general, there are two rate limiting processes for solution-precipitation. When material transport is limited by diffusion through the liquid phase, the densification rate is:

$$\frac{d(\Delta\rho/\rho_0)}{dt} = B(g)\frac{\delta D_b C_l \gamma_{lv} \Omega}{kT} r_s^{-4} \tag{1.4}$$

where B(g) is the geometrical constant which depends on V_s, V_1, ρ and the apparent dihedral angle, δ is the thickness of the liquid boundary (typically 1-3 nm), D_b is the grain boundary diffusion constant of the solute, and c_1 is the solubility of the solute. , k is the Boltzmann constant, and T is the absolute temperature. If material transport is controlled by the interface reaction, the densification rate is:

$$\frac{d(\Delta\rho/\rho_0)}{dt} = C_{(g)}\frac{K_{C_1}\gamma_{lv}\Omega}{kT} r_s^{-2} \tag{1.5}$$

Elimination of the pores occurs in the last part of the liquid phase sintering. It starts when the pores become closed and isolated (i.e., 90-95 % TD.) The closed pores can contain; sintering atmosphere, evaporating liquid, decomposed solid and these all will affect the elimination of the pores.

$$DS = \frac{2\gamma_{lv}}{r_p} - \sigma_p \tag{1.6}$$

Driving force for elimination of the pores can be expressed as the formulation above, at Equation 1.6. σ_p is pore inside pressure. Pore size should be small for elimination and there is a negative effect of the vapor pressure inside the pore. When there is pressure in the system the last stage changes due to formulation 1.6. Pressure enhances driving force for liquid phase sintering at all stages. During the final stage of pressure assisted LPS, the driving stress while under an applied stress is given by Equation 1.7, and σ_a is applied stress.

$$DS = \frac{2\gamma_{lV}}{r_p} + \sigma_a - \sigma_p \tag{1.7}$$

Another situation that can be seen frequently in liquid phase sintering is grain growth. Different dissolution rates of the particles because of theis shaper or sizes may result in grain growth by Ostwald ripening. Amount of liquid phase is an important variable for grain growth. Driving force for grain growth is surface energy difference. Small particles have high surface energy and sintering starts with their high sinterability.

If there is no small grains at the mixture powder of the green body, then the pressure difference at the contact points of the touching large particles will be driving force for dissolution, [4].

Moreover, in pressure assisted sintering methods, they can be classified as closed and open systems as shown in Figure 1.10. While hydrothermal sintering is a closed system with isostatic pressing, the cold SPS and the cold sintering process are open systems that water in the system can escape intime and they are both under uniaxial pressing. During continuous pressing, water in the system extrudes and escapes from the system that density increases also at the last stages as mentioned in Equation 1.6.

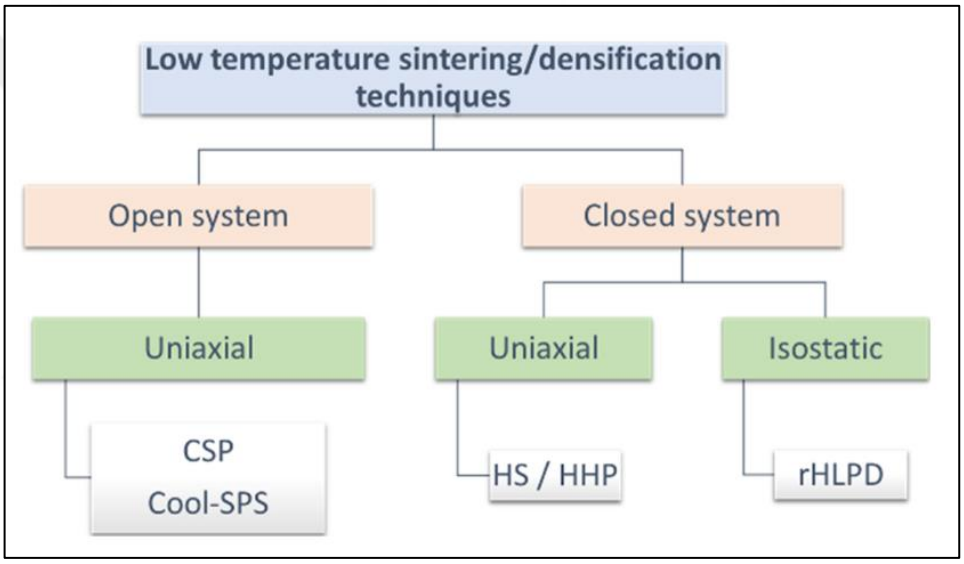

Figure 1.10. *Types of some low temperature sintering processes, [60].*

1.5. Fundamentals of The Cold Sintering Process (CSP)

The Cold Sintering Process (CSP) can be thought as the derivative of liquid phase sintering of the CSP, material transfer during sintering can be achieved with the advantage of the liquid phase. However, in the liquid phase sintering, there is a molten (liquid) phase at high temperatures that improves the diffusion process, while in the CSP this situation is replaced by solvent and high pressure, [38].

In a typical CSP, the powder is exposed to moisture, thus creating a layer of water around the grains, [38]. The particles are then pressed at a pressure of around 350 MPa and kept at a temperature of 120-200°C for 1-30 min. The presence of the liquid phase around the grains acts as a lubricant during pressing, causing them to slide around each other more easily and settle for a better compression level, [38]. The average density of

the samples reaches around 60 %TD after this rearrangement stage. In the second step that the density increases from 60 % to 90 %TD via dissolution precipitation process, [1]. The pressure applied to the powder concentrates at the contact points of the particles. In a powder with 70 %TD, a pressure of 350 MPa becomes 500 MPa with the rise in the contact points. This pressure is equivalent to the yield point in some ceramics. The pressure at the non-contact points on the surface is zero, this pressure difference creates a chemical potential gradient for the atoms or lumps at the contact points to dissolve into the water and precipitate to the non-contact points. At the same time, the sample is heated above 120°C, allowing the water to evaporate and the solution to become saturated. This aids precipitation and crystallization on particle surfaces. Guo et al. [13] showed that during the sintering of $Na_2Mo_2O_7$ compound with the CSP, the interfacial crystal growth is layer by layer, as in the Terrace-Ledge-Kink model, and the atoms are placed one by one in the corner and stepped positions where the energies are appropriate, [61]. Eventually all the water evaporates, and the sample density reaches to 95 %TD. However, in some cases, as in $BaTiO_3$, the precipitated materials form an amorphous structure due to the low temperature and limit the solid state diffusibility. Annealing was applied to form a fully crystalline structure. Annealing also allowed the material density to increase from 95 % to 98 %TD (Figure 1.11) [15,62]. Furthermore, a hybrid technique using the CSP and FAST (the field assisted) sintering was also tested for the ZnO system, [29,41].

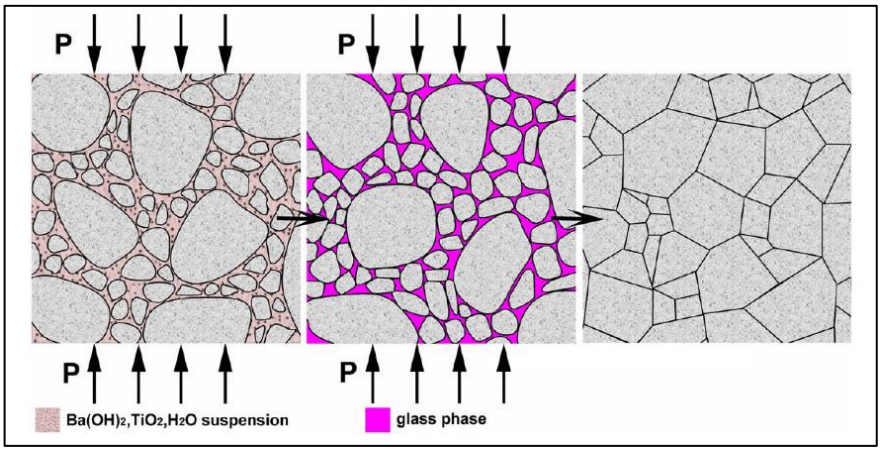

Figure 1.11. *The evolution of the internal structure of $BaTiO_3$ ceramics during the CSP and annealing, [15].*

There are some processing variables that are affecting the CSP. These are type of the ceramic particle, particle size, amount of water addition, pH, solution addition,

pressure applied, sintering temperature, holding time and heating rates, [18]. Mostly used liquid for the CSP is water due to easy abundaced, reasonable price, also suitable for CSP due to vaporization temperature and ability of solving most of the materials. The cold sintering process temperature and pressure should be congruous with the phase diagram as shown in Figure 1.12.

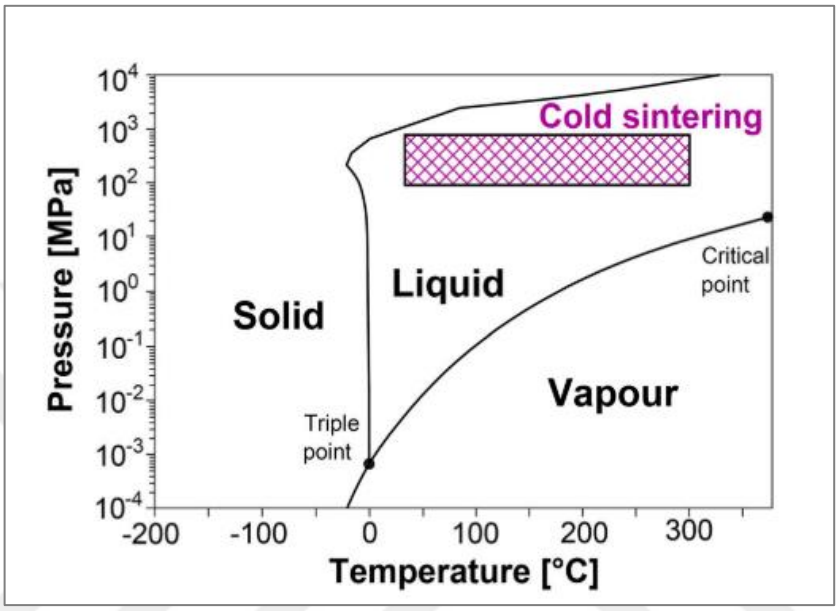

Figure 1.12. *Phase diagram of water and CSP conditions due to temperature-pressure variables, [63].*

There are three stages of sintering at the CSP, as like liquid phase sintering. These are, dissolution, material transport, and precipitation. For the dissolution stages of the sintering, the dissolution takes place following the chemical potential difference between the stressed solid μ(s,1) and the liquid phase in contact with it μ(l,1). The driving force for dissolution μ(D) and is defined by:

$$\Delta\mu_D = \mu_{s,1} - \mu_{l,1} \tag{1.8}$$

at a strain e_v, accumulated by postelastic creep, the grain-to-grain contacts becomes a circle with an area A_c (Fig. 1.13 b). The stress intensification factor (B) is then defined by the Eq. When the area A_c is smaller, dissolution increase due to increase of dissolution:

$$B = -\frac{6\,d^2(1-e_v)^{2/3}}{A_C} \tag{1.9}$$

mass transport stage was expressed as the following formulation by the A. Ndayishimiyea et al. difference between the liquid phase with a high concentration of solute μ(l,1) and

the liquid phase with a lower concentration of solute μ(l,2). The driving force for mass transport μ(T) and is defined by Eqn 1.10, [64].

$$\Delta\mu_T = \mu_{l,1} - \mu_{l,2} \tag{1.10}$$

The precipitation takes place following the chemical potential difference between the liquid phase with a certain concentration of solute μ(l,2) and the less stressed solid, generally located at pore walls μ(s,2). The driving force for precipitation μ(P) and is defined by Eqn 1.11, [64].

$$\Delta\mu_p = \mu_{l,2} - \mu_{s,2} \tag{1.11}$$

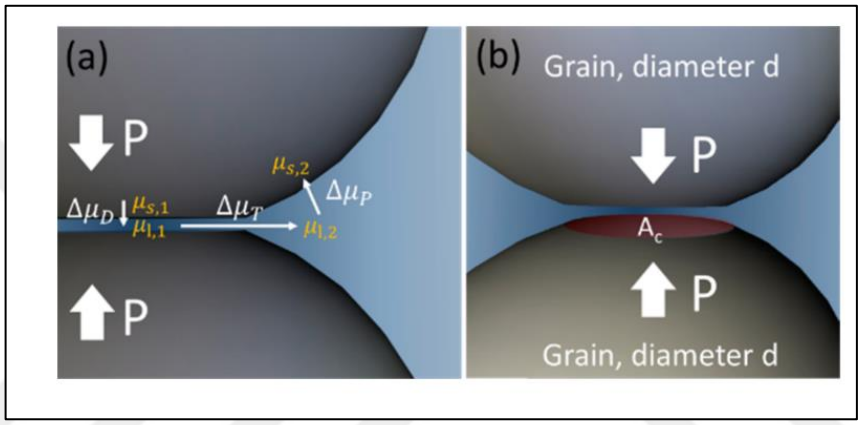

Figure 1.13. *Two particle impression for CSP . ΔμD, ΔμT and ΔμP are driving forces for dissolution, mass transport and precipitation, respectively. (b) Schematic of the model with two grains with a diameter d and a grain-to- grain contact with an area Ac., [60]*

While trying to learn more about the mechanisms that occur in the CSP process, many studies are proceeding to learn about how the process is going on in details, [25,66]. A. Ndayishimiye et al. [60] discussed the system mechanism in three stages, in the first stage, the particles are mixed with liquid. It is coated and begins to dissolve from solid contact points with pressure. Grain reorganization occurs by capillary pressure. At the end of the first stage, a liquid film image separating the packed grains is mentioned. In the second part of the cold sintering process, high stress points are formed at the contact points and the dissolution at these points increases with the chemical potential difference. In the second stage, it is stated that the dissolved material diffuses from the grain boundaries and settles in pores or low potential energy points. In the last stage, the liquid moves away from the system. Here, the diffusion rate is the rate-determining condition that determines grain growth or densification. In addition, Maria et al. determined that the grain size decreased in their study, [25]. The reason for the decrease in grain size was

explained by Maria as the morphology was changed during the CSP. In order to examine this situation in more detail, it is necessary to examine the morphology and grain size changes in samples sintered for different times.

Randall also states that in the first stage, the fluid in between ensures the rearrangement of the grains with the help of capillary force, [62]. However, a detailed analysis of this situation has not been presented. In the studies carried out, detailed examination with the size, shape and distribution of the pores is not presented. In the first stage, the degree of capillary pressure can be clearly revealed by examining the pore sizes. For this

$$P=-2\gamma_{lv}\cos Q/a \qquad (1.12)$$

equation can be used, [42,52]. The above equation is given as the calculation of the capillary force created by the pore channel filled by the liquid in Rahaman's book. Here, P: capillary force is given as γ_{lv}: surface energy between liquid and vapor, Q: angle of contact.

Continuous channels formed by open pores in the first stages of sintering are mentioned, but there are not enough studies on the closed pores formed in the later stages and in this case the steam in the system and the vapor pressure. The determination of open and closed pores for different sintering stages by Archimedes and gas adsorption (BET) method will be very useful in explaining the mechanisms. Another point mentioned in the studies is the hydroxyl ions formed on the surface, a hydroxyl layer is formed on the surface of the material during sintering and the dissolved ion during diffusion exceeds this layer. However, as Randall points out, temperatures as low as 120°C are not capable of removing hydroxyl ions from the system. The amount of ions can be determined via Thermogravimetric and Differential Thermal Analyses System (TG-DTA analyses). TG-DTA analyses, which can also be applied to samples sintered with the cold sintering process, to determine whether hydroxyl ions remain in the structure and to determine the removal of water from the structure at different sintering stages and conditions. Maria determined the weight changes of the samples that dried at 80°C after sintering. He also reported that there was less than 0.3 % weight loss in the sintered sample by TGA analysis. By performing this experiment at different stages of sintering, the time-dependent variation of hydroxyl ions can be determined. In addition, in this way, the liquid film thickness in the time-dependent system can be calculated depending on the

grain size. The presence of water, hydroxyl ions and water vapor in the system are important parameters for sintering.

Mechanism studies in the cold sintering process continue to increase validation and understanding. In previous studies, the mechanism was tried to be defined. When the mechanism studies are examined in general, they can be summarized as follows: The cold sintering process consists of three stages. During development of the sintering, the settlement and rearrangement of the grains occur rapidly at first, but then the sintering speed slows down with the increase in density. As shown in Figure 1.13, Rahaman graphically illustrated this situation in his book while describing liquid phase sintering, [1]. The CSP has a similar mechanism sequence, as depicted in Figure 1.14, [67]. There is an additional pressure effect in the CSP system. The presence of the external pressure is very effective during the convergence of the grains and the elimination of the pores. In addition, with the temperature, steam pressure is formed in the die and a system is created in which hydrothermal conditions are effective.

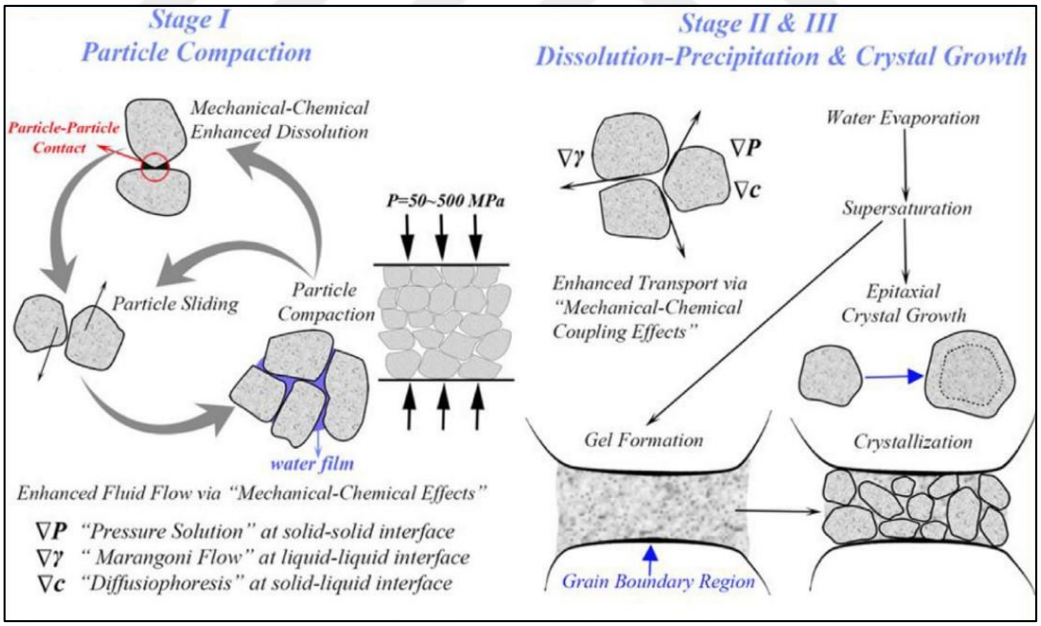

Figure 1.14. *CSP sintering steps, [67].*

During the liquid phase sintering, the grains touch each other during precipitation and the dissolution will be more at the flat points. The difference between the chemical potentials allows for material transfer, and as the inclination increases at the contact points, the chemical potential difference decreases. The material transfer is controlled by

the slower of the two mechanisms. These; diffusion over the liquid and the other is the inter-surface reaction that provides precipitation on the grain surface. This situation is similarly described in the CSP process [25,32,66].

Theoretical density of a material, grain size change due to time and pore size and shape give us some important sintering mechanism informations. There are some studies that deals on liquid film during the CSP. Liquid amount in the system is an important parameter since diffusion is related with the film thickness.

Liquid phase plays a critical role at all stages of the CSP. It can be considered as a low-temperature liquid phase sintering, utilizing water vapor or aqueous solutions as a transient solvent. The water is initially introduced to wet the particle−particle interfaces so as to dissolve the sharp edges of the particles, under external uniaxial pressure. The liquid phase fills the particle−particle interstitials, and this yields an initial compaction through particle rearrangement; subsequently, raising the temperature up to 100°C creates a supersaturated environment for the liquid phase, with evaporation of the water, which enables a fast epitaxial precipitation process on the surfaces of particles to reach the final densification, [15]. Firstly, it aids particle reaarengement under pressure, [20]. pH adjusted liquid helps the particles to dissolve and with the help of temperature and pressure, increased dissolved particles results in supersaturation. The liquid amount is important to determine the supersaturation time. When the liquid evaporates and extrudes due to pressure and temperature, there is less liquid in the system. It should be also noted that as the liquid amount decreases the distance of diffusion becomes less. In the last part of the sintering, pores become isolated, closed and their amount defines the final density.

1.6. Statement of the Problem

The CSP process is a newly understood process. Unknown know-how about this process needs to be established for each laboratory. Because changes in laboratory conditions affect the process. Although variables have been identified and studied in the CSP method, their effects on current conditions are unknown. Moreover, the interaction of process variables in one or more ways with each other has not been systematically examined. In the continuation of this, it is striking that there are some missing points in the literature. It is not clear enough in the literature whether there is residual fluid in the system. In addition, the film thickness formed by this remaining liquid is not known exactly. There are studies in systems containing more than one component, and studies

for a specific device have started, albeit a little. Studies for the production of varistor, one of these technical devices, are limited. When the electrical properties of a varistor system containing more than two components and produced with CSP were examined, successful results were obtained. The reproducibility of these results by mixing in the mill should be examined how they will affect a dissolution dependent process. What can be done if insoluble particles are preventing CSP when they are included in the system. There is not much study yet. The introduction of additives into the system with powder coating method that has not been studied before.

1.7. Research Objectives of the Thesis

With this thesis, a new process, CSP, will be introduced to our laboratory and our country. The know-how obtained will pave the way for different studies that can be done in the future. This process is a process that can be preferred in the future for energy saving as it allows sintering at low temperature. Its industrial use will provide high profits for the future. For this reason, the details of bulk material production using ZnO powder, which is taken as the basis in this thesis, were examined. By increasing these details, the interactions with each other were made with the central composite design, which is a statistical method. As a result of these trials, the interactions of more than one variable could be determined. This data will shed light on future studies. In addition, although the presence of liquid phase in low temperature sintering causes a decrease in the thermodynamic driving force and a decrease in the sintering temperature, it is important whether liquid remains in the system during the closure of the pores. this situation will be examined and can also be calculated as the film thickness. The film thickness between grains will be measured at different sintering moments. Thus, the behavior of the liquid in the system during sintering will be determined.

The studies, which started with ZnO and created a scientific infrastructure, will continue with the production of varistors. First of all, the sintering of ZnO with Bi_2O_3 by CSP method will be examined and its electrical properties will be examined. Afterwards, Co_2O_3 and MnO/Mn_2O_3 and occasionally Sb_2O_3 will be added to the system. In case some of these additives affect the CSP system negatively, coating trials will be carried out with the selected additive. The aim here is to obtain varistor material with fine grains in the microstructure and its non-linearity is high; 30-50 and threshold voltage is over 1000 V/mm.

1.8. Structure of the Thesis

After evaluating the CSP process literature in detail in Chapter 1, in Chapter 2, the parameters to be included in the process will be determined by using ZnO powder, these parameters will be examined and the remaining liquid in the system will be analyzed and evaluated with TG-DTA. The change in grain size will be examined with the images obtained by scanning electron microscopy of the instantaneous test results and the activation energy required for grain growth will be calculated. Along with some hardness values, the mechanical properties of the high-density ZnO bulk material will be examined and its conductivity will be measured.

In the 3rd Chapter, pure ZnO will be studied again and the variables of the CSP process, for which a working range has been determined by examining previously, will be discussed in more detail. Experiment set will be created with central composite design. The individual and binary effects of temperature, pressure, pH, liquid ratio and time on the density will be determined. At the end of this section, the density equation will be obtained depending on the variables examined.

In Chapter 4, it will be tried to densify the ZnO-Bi_2O_3 system with the CSP method. In these experiments, mixed oxide method and coating method will be used and the density and electrical properties of the bulk samples obtained will be compared. MnO/Mn_2O_3, Co_2O_3 and Sb_2O_3 will be added to the binary ZnO-Bi_2O_3 varistor system by mixed oxide method and sintering of powders will be done via CSP. It is deliberated that insoluble particles may affect the sintering behavior in multiple systems. Only Co_2O_3 will be added to the binary ZnO-Bi_2O_3 system using the coating method if mixed oxide method does not give required test results. The internal structure and properties of the materials that will be formed via CSP will be investigated. It will be discussed whether the varistors used at high voltages have the necessary structure to obtain them.

1.9. Model System for the Thesis

ZnO is the model system for the thesis since there are many researches on this material due to its easy sintering behavior. It is an advantage that there is data to compare almost with the entire results. ZnO is an easy handling powder with many application areas. Varistors are one of these applications, with CSP, it is possible to achieve a desired feature in production. Since the high temperature is not reached, the grain size is generally

fine and this can generally be an advantage. In varistors, fine grain size are preferred for high voltage applications, depending on the area of use. In this case, the sintering method with CSP is suitable for the production of this product. Although varistors use additives for a variety of reasons, most of them are necessary to regulate the internal structure and will not be needed in most CSP production. However, it would be beneficial to use the additives that increase the non-linearity feature in the system. The ratios of these additions are between 0.5 - 1.0 %.

2. PROCESSING PARAMETERS EFFECTS ON MICROSTRUCTURE DEVELOPMENT OF ZINC OXIDE CERAMICS DURING THE CSP

2.1. Introduction

Zinc oxide is a multi-featured material due to its high chemical stability, high electrochemical coupling constant, ability to absorb radiation in a wide range, high photostability and unique physical and chemical properties. Zinc oxide, in materials science, is a semiconductor material in the II-VI group, whose degree of covalent character is at the border of ionic and covalent semiconductor. It has a wide energy band of 3.37 eV, has a high bond energy of 60 meV, and is thermally and mechanically stable at room temperature. Due to its unique properties, it can be used in sensors, converters, energy generators and photocatalysts in hydrogen production. Since it is an environmentally friendly material, it is used in biological applications in the ceramics industry. It is a material that can have a wide range of applications in the field of nanotechnology, [68].

Since the 1960s, the production of ZnO thin films has an important area for sensor, converter and catalyst applications. In one-dimensional material production, ZnO has a great importance due to its structure, [69]. There are also areas of use in two-dimensional and three-dimensional applications. In two-dimensional applications, nanoplates, nanofoils, nanopellets can have structures like flowers, snowflakes, dandelions and chestnuts in three-dimensional applications. Zinc oxide offers a great variety of microstructure, [68].

The point defects inherent in ZnO material are oxygen vacancies and Zn cation interstitial atoms, leaving behind dominant carriers, thus forming an n-type semiconductor. ZnO has application areas such as varistors against electrostatic discharge, protection of sensitive electronic devices, gas sensors, surface acoustic wave devices, piezoelectric and thermoelectric materials. Being a binary system, ZnO is used as a model ceramic system in many studies. Some of the recent studies, employed zinc oxide as a model system, are for testing of microwave sintering, FAST/SPS and FLASH sintering techniques, [19].

In 2012, Schwarz et al. [40] presented their work with FAST/SPS. Due to the high heating rates, ZnO was sintered in a humid state at a pressure of 50 MPa above 200°C. Densification was completed in 10 minutes at 400°C, as mentioned before. However, the

dry powder could not be fully sintered at this temperature. Likewise, when the sintering heating rate was slow, only 65% density could be reached. When Dargatz et al. examined this phenomenon in more detail, they were able to reach full density ZnO with a grain size of 200 nm with a density of 99.5% at 400°C, [29]. For this, a small amount of water, up to 1.6 % by weight, was added to the raw material. This water used could not evaporate completely during heating and was trapped on the surface and in the grain boundaries, thus ensuring the removal of carbonates on the particle surface, dissolution of Zn^{2+} and O^{2-} ions, as well as matter transfer with the liquid phase and diffusion of H^{+} and OH^{-} ions in the crystal. In this process, although the system was with SPS, the electric field did not play any role. However, a very small amount of zinc acetate was added to the system, which was the impetus for sintering. After this trial, Randall et al. [20,43], in many trials, they have used water to sinter ZnO at low temperatures. In these studies, the addition of acetic acid to the system significantly changed the resulting density and microstructure. With CSP, ZnO, which has densities higher than 90 % and has electrical properties equivalent to ZnO obtained at higher temperatures by conventional methods, could be obtained at temperatures such as 300°C, [22].

For a successful application of the CSP, solubility of the material in the solvent (i.e., usually water) is very important since all stages of the sintering since it directly affects dissolution. When the solvent is water, solubility of ZnO material in water is limited. In the studies carried out, the addition of acetic acid was used to ensure dissolution. As stated in the literature, the pH value of ZnO material is close to 7. It is difficult to provide dispersion in water without addition. If the pH value is far less from 7, it allows ZnO to dissolve in water, [70].

It has been noted that during sintering with CSP, the matrix grains are small because low temperatures are used. While this has been reported for many materials, grain growth was observed in some conditions in experiments with ZnO. In cases where ZnO is sintered by the addition of acetic acid, the grains are larger than when using only water, Figure 2.1. The grain size in ZnO-H_2O-AC samples were > 500 nm. It is seen that there are particles smaller than 100 nm with only water. This difference in grain size occurred with the use of only 0.5 % by weight zinc acetate, [22]. ZnO grains and grain boundaries formed by CSP can be detected in Figure 2.2, as well, [19]. Small grains (~ 200nm) and very thin grain boundaries observed.

Although the CSP has been tested for ZnO ceramics by other researchers previously, since the process has many varibles and each lab has its own capabilities and conditions; therefore, it is critical to understand the effect of each processing parameter on microstructure development during the CSP. Consequently, the research objective of this chapter was to investigate powder and process related parameters effects on microstructure development during the CSP.

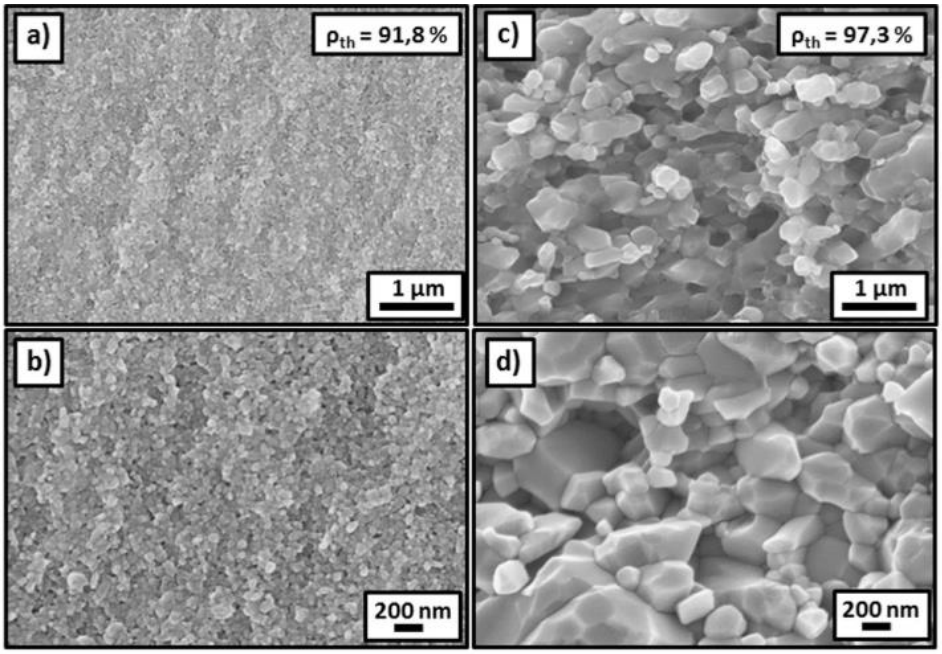

Figure 2.1. *SEM micrograph of fracture surfaces a) and b) ZnO+H_2O, c) and d) ZnO+H_2O+AC*

Funahashi et al., As stated, the activation energy required for grain growth during the sintering of ZnO with the cold sintering process is as low as 43 kJ/mol, [22]. This required energy for grain growth also examined at our studies.

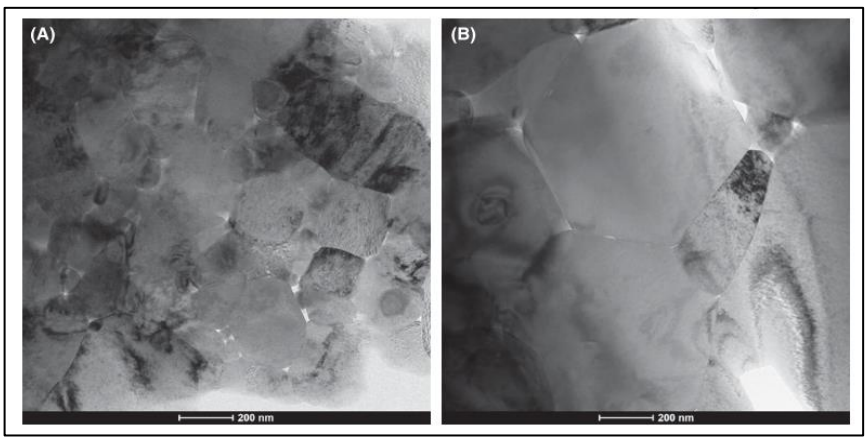

Figure 2.2. *Bright field TEM image of ZnO with 1M acetic acid at 387 MPa and 77 MPa pressure a) 126° C, b)305° C, [19].*

2.2. Experimental Procedure

The starting ZnO powder was purchased from Sigma Aldrich. Alumina mortar and pestle were used for humidifying the powder. Hydrolic hand press and Carver lamination press with heating plates (up to 342°C) were used for pre-pressing and the CSP, respectively. Citric acid, hydrochloric acid (HCl), zinc acetate and nitric acid were used for pH adjustments. Sintering studies were performed at 100-330°C and under 150-350 MPa pressure with the appropriate liquid ratio (the appropriate liquid ratio was determined during the studies). After the CSP, size, and shape of the samples were controlled and their densities were determined by Archimedes and/or geometric measurement methods. The phase development was monitored via x-ray diffraction (XRD) analysis. In addition, the microstructure development was analyzed by scanning electron microscope (SEM). Details of the used methods and experimental details are presented below.

The process flow chart, which was created after some trials, is shown in Figure 2.3. Moistening of the powder was done after weighing the powder and the treatment was done in alumina morter with the pestle. There was no pre-pressing process at the first trials to investigate the CSP system. Prepressing was not a proper stage at the process. It was adjoined after some of the trials done to prevent cracks. Systems with pre-pressing were indicated at the discussion.

The lamination press can be pre-heated or heating can be done at the time of sintering, the latter was implemented. Heating ramp rate is standard for the lamination heating press and it is 6.7°C/min. Dwell time at sintering temperature, performed was 10 minutes to 1 hour. After required time at sintering temperature, pressing ends and mould can be handled. Cooling of the mould was done at room temperature and at the end bulk material was taken from the mould.

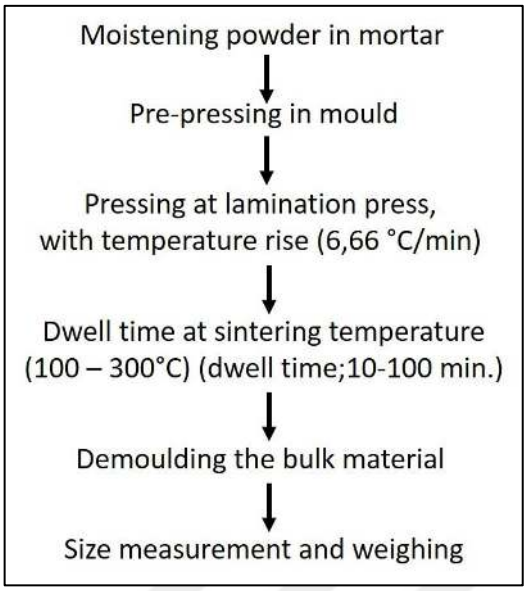

Figure 2.3. *Process chart of cold sintering process*

As given in Figure 2.4, studies were carried out to evaluate the theoretical densities of bulk samples or to obtain the highest density by performing internal structure analysis with SEM to ensure that the samples were crack-free. Initially, the powders to be used were characterized, since the powder size is critical for the sintering. ZnO powders with different sizes ZnO-1 (larger) and ZnO-2 (finer) were tested for the CSP in this study. As mentioned above, ZnO powder of Sigma Aldrich was used for the experiments. The particle size distribution was measured with Malvern Nano Zeta Sizer device, the suspensions were prepared with water as the liquid. An ultra sound wave was used for 20 seconds rather than a dispersant in the system, at the measurements.

Two different sized particles were cold sintered at the same conditions. For humidifying, 12.0 % water with pH 5.0 was used. Acid type was citric acid for both samples. After then, pressing 80 MPa for 10 minutes at 90°C and then at 320°C for 45 minutes at 170 MPa was utilized for sintering.

Humidification process was developed and studied to ensure good dissolution of particles. There are three main parts of humidifying; acid type to be used, pH of the solution and quantity of the solvent to be used for humidifying the powder. Initial trials were done at many different pH values using 3 different acids. However, the most important experiment to see the effect of pH on the system was made between pH 4.0 - 6.0 by using HCl acid.

The CSP conditions were adjusted as 1.5 grams of powder and 12.0 wt % of liquid, under 170 MPa, 45 minutes of dwell time and the sintering temperature was 330°C.

For the rest of the trials, zinc acetate was choosen for pH adjustment of the liquid, pH 5.5 was used and different values of liquid phase was utilized for humidifying. 7.0 % wt liquid was used for the interrupted tests to adjust residual moisture during sintering period.

The pressure is expressed as

$$P=F/A \tag{2.1}$$

P is pressure, F is force and A is area of the mold. In terms of practicality in the experiments, the load values processed in kg were converted into pressure values with this formula. The mold diameter used was 13 mm. When the pressure was calculated for 13 mm diameter mold, a 2030 kg load should be applied with to obtain 150 MPa pressure. For the press used, the load values could be set 100 by 100. For this reason, a load of 2100 kg is used for 150 MPa. In other studies in the literature, it is seen that it reaches up to 300 MPa values. For 300 MPa, the load to be applied to the 13 mm mold should be approximately 4000 kg. Although our press can reach up to 13000 kg, it has been determined that the maximum load that can be used on a 13 mm dia. mold is 8200 kg. For this reason, the maximum load used during working with 13 mm dia. mold is 7400 kg. The pressure value in the experiment with a load of 7000 kg is approximately 500 MPa. During pressure, temperature and dwell time effects on the sintering studies, it was observed that employing pre-pressing step was more efficient.

It was obtained by trying some other conditions due to internal structure disorders and fragmentation in the early stages of laboratory trials. Open and closed mould sytems, 13 mm and 16 mm mould radiuses, different lubricants were examined.

Experimental variables selection was done as given in Figure 2.4. After reaching over 92 % T.D., internal structure analyzes were made with batch experiments, the remaining moisture and initial humidity in the system were determined and theoretical studies were carried out. TG-DTA was used to obtain residual moisture in the samples instantly. Samples were cracked just after sintering was completed or interrupted and density measurements from dimesions, moisture analysis with TG-DTA and SEM analyses for microstructural observations were carried out.

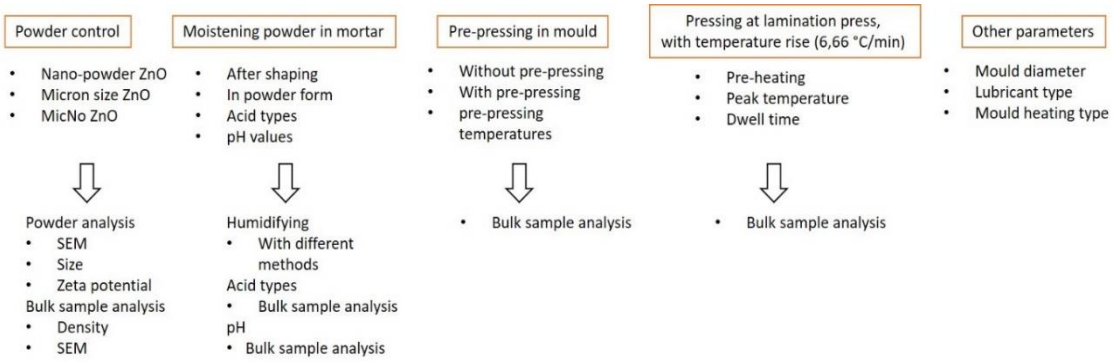

Figure 2.4. *Experimental parameters tested during the CSP studies*

2.2.1. Designed interrupted experiments to analyze the CSP in detail

One of the issues that was not addresssed clearly in the previous studies [25] is whether all of the water evaporates in the system, although TG-DTA analyzes are included in thoses studies. Maria et al. [24] states that after process temperatures above 100°C, there is no residual water in the system, and in the measurements, they made with TG-DTA, they found a maximum of 0.2 % water by weight. In addition to this information, they performed Raman analysis and emphasized that although they saw some very small peaks next to the ZnO peaks, they were not very important. In our laboratory, we made some experiments with the remaining water in the system. First, the powder moistened with 6.5 % water before sintering was analyzed with TG-DTA. Analysis performed up to a maximum of 500°C.

To verify this situation, we designed interrupted experiments. In this study, density measurements of the sintered samples were determined geometrically by taking the dimensional measurements of the pellets. ZnO (Sigma Aldrich, 99-100.5 purity, average particle size ~300 nm), zinc acetate and citric acid were used as raw materials. The moistening of the ZnO powder was done by beating it with a pestle for 2 minutes. Uniaxial press with heating plates up to 342°C for heating and pressing samples Carver Inc. Lamination Press was used. The molds were not sealed during the sintering process. Moisture of the starting powder and after sintering were carried out with both the EM-120-HR Moisture Analyzer (at 105°C) and the TA Instruments SDT 600 TG Analyzer at 600°C. During the sintering, the samples were taken from the press and instant analyzes were made. Microstructure examinations were taken with SEM, and particle sizes of instantaneous measurement samples were made with ImageJ 1.50 software.

Film thickness calculation was made due to equation:

$$\tau = \frac{v_{liq}}{SA_p} \quad (2.2)$$

At equation 2.2; τ is film thickness, V_{liq} is the volume of the residual water in the system and SA_p is the surface area of the powder at pores. SSA of the ZnO powder analysed with BET and was determined 5.6852m^2/g. 1.5g of powder was used for each densification process. Such interrupted experiments enabled us to analyze the CSP process from thermodynamics and kinetics perspective, presented below in the Results and Discussion section.

2.2.2. Hardness tests

The Vickers Hardness test was used to evaluate ZnO hardness after CSP. Test was done for two materials that were sintered at 135°C and 300°C at all. These were the process temperatures which maximum densities were obtained. Hardness vary due to deformation of the material against applied load. A square-based pyramid indenter whose opposite sides meet at the apex at an angle of 136° is employed in Vickers hardness test. Imprint size is measured with the aid of optical microscope.

(ISO 6507) is used to characterize hardness of various solid materials (metals, ceramics, etc.). A diamond pyramid is pressed against the solid with a certain normal load and the hardness is calculated based on the imprint left on the surface. Hardness may vary as a function of load, therefore, it is advised to specify applied when HV hardness is reported. A square-based pyramid indenter whose opposite sides meet at the apex at an angle of 136° is employed in Vickers hardness test. Imprint size is measured with the aid of optical microscope.

Hardness test obtaining Hv formulations

$$H = 0.1891x \frac{9.8}{1000} x \frac{F}{d^2} \quad (2.3)$$

d is the average of the diagonals. F is applied load in kgf/cm^2 and hardness is in GPa as the result.

For the hardness test, the specimens were polished and the Vickers hardness test was applied.

2.3. Results and Discussion

2.3.1. Powder caharacteristics and their role on CSP

The particle size distribution of the powders used in this study is shown in Figure 2.5. According to Figure 2.5, it is seen that the particle size of ZnO powder, which is indicated by the green curve has smaller particle size distribution than the red curve impression. The average particle size obtained is 1167 nm for the red curved ZnO powder, entitled as ZnO-1. For elles, ZnO-2, the mean grain size was measured as 334 nm. However, in powders with fine particle size, particle size measurement analyzes must be done with precision. The actual size measurement may not be obtained due to aglomerations. For this reason, images of the powders were also obtained with a scanning electron microscope (SEM). When the SEM images are examined in Figure 2.6, grain size of the ZnO-1 powder is between 100-300 nm, and the grain size of the other ZnO-2 powder used as an alternative and tested is 50-200 nm, respectively.

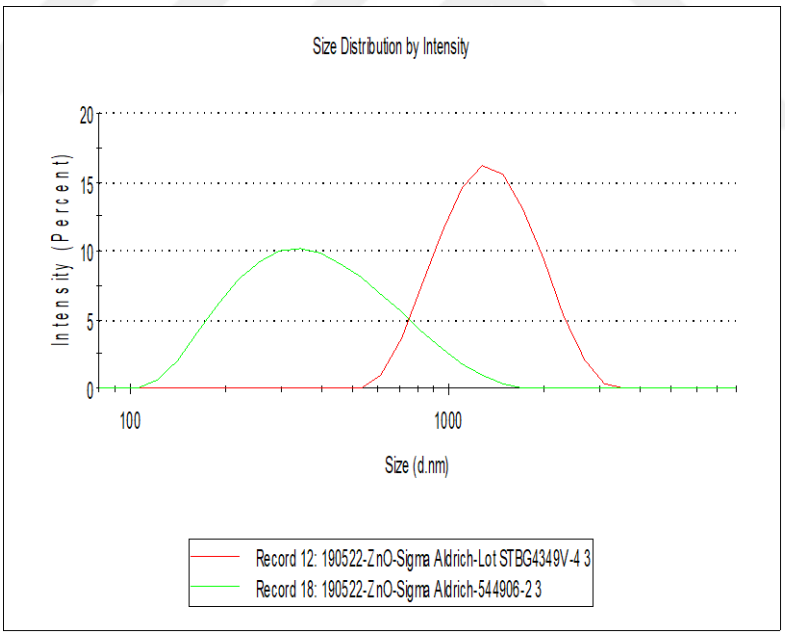

Figure 2.5. *Particle size distribution of powders ZnO-1 and ZnO-2*

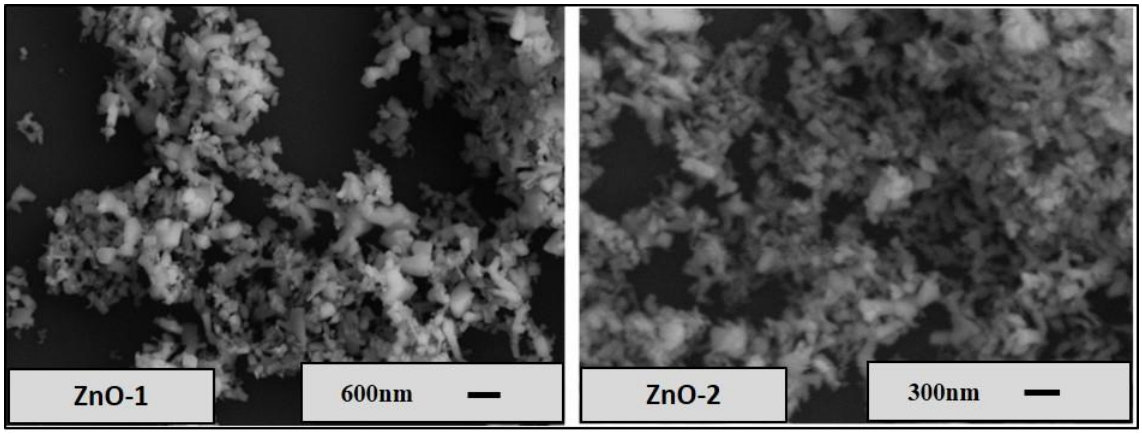

Figure 2.6. *Raw material SEM analysis*

After pressing under 170 MPa at 320˚C for 45 minutes, bulk material exhibited 66.38% TD and 76.72% TD for ZnO-1 and ZnO-2 powders, respectively. The 13.5 % theoretical density difference shows clearly the impact of the particle size on desification process during the CSP. The particles size can be changed to enhance the density under current conditions. The most obvious reason for the increase in density with particle size reduction is related with the dissolution which is one of the main principles of the cold sintering process. The dissolution mechanism is strongly related with the particle size. At Table 2.1, the dissolution rates of ZnO powders with different particle sizes are shown, [71].

Table 2.1. *Dissolution of ZnO Nanoparticles at pH 7.5 depending on grain size,* [71] .

Particle radius (nm)	Zn^{2+} concantration (mg/L)
4	57
15	22
241	10

The parameters affecting the dissolution rate are given in the equation below.

$$dm/dt = DA/h\ (cs\text{-}c) \tag{2.4}$$

Where dm/dt is the dissolution rate, D is the dissolution coefficient, A is the surface area, h is the thickness of the diffusion layers, cs is the precipitation concentration, and c is the bulk concentration.

From a thermodynamic point of view, it can be seen that the modified Kelvin equation depends on the Ostwald Freundlich equation, see in Eqn. 2.5.

$$S/S_0 = \exp(2\gamma V/RTr) \quad (2.5)$$

In this equation, S represents the solubility of particles of r diameter. V is the molar volume, γ is the surface free energy, R is the gas constant, T is the temperature. In addition, nanoparticles have more atoms at the corners than coarse grains with a layered structure in terraces. Due to this difference, surface ions can be separated from the lattice more easily and increase the solubility, [71].

Along with the particle size, the dissolution capacity of the powder is also important for the studies. ZnO powder is known to dissolve in water. However, the dissolving capacity of the powder varies according to different pH values. In the next section, experiments based on pH are included.

2.3.2. Roles of acid type and amount on the humidification and the CSP

Three different pH adjusters were used in the experiments, zinc acetate hexahydrate (ZA), citric acid and hydrogen chloride. Citric acid and HCl were used in comparison at the same sintering conditions, while ZA was used at higher level pressures and evaluated within itself.

Table 2.2 shows all the trials that were made with different type of acids. The CSP conditions were also set in the table. There is not much difference in the results with the use of citric acid and HCl under the same conditions. When citric acid was used, maximum theoretical density of the sample 89.28 %T.D. was obtained when 4.0 wt % liquid with pH 5.0 was used, on the other hand, 78.72 % T.D. was obtained with HCl, with 12,0 % wt liquid with pH 5.5. Theoretical densities increase when the acid is zinc acetate and even very close to 100.00 % T.D. could be obtained. When zinc acetate-water solution with pH 5.5 was used by 7.33 wt %, and sintering was done at 539 MPa pressure, 140°C for 50 minutes dwell time. More than 99.00 % TD was obtained.

When citric acid or HCl were used under the same conditions, 12.0 wt % liquid with pH 5.0 and 170 MPa, 320°C and 45 minutes dwell time, 66.38 and 68.60 % T.D. were obtained, respectively. Densities are very close to each other for these acids but not close to the values obtained in the zinc acetate containing systems. On the other hand, pressure may be more effective for this situation.

The densities of the samples sintered under the same conditions but using three different solutions for moistining the powder were examined. Theoretical densities

obtained when using 4.01 % by volume of liquids with pH 5.0 and sintered at 300˚C for 45 minutes under 155 MPa pressure were evaluated. In the experiments where the solution used was ZA, citric acid and HCl, the densities were obtained as 89.1, 88.8 and 69.10 % T.D., respectively. Although the use of citric acid allows close results to be obtained with ZA, it was still observed that the highest values were obtained with ZA. Theoretical densities of the all trials were given at Table 2.2.

Table 2.2, 26 of the samples could reached more than 95.00 % T.D.. All of these high density results are with zinc acetate solution with pH 5.5, with various liquid amounts at temperatures of 135-140°C under pressures more than 530 MPa and dwell time of 50 minutes. The next best result was 92.00 % T.D. and it was observed with the sample sintered under 155 MPa pressure at 300°C temperature for 40 minutes dwell time. This is also with zinc acetate salt. By using citric acid, the highest density, achieved was 89.28 % T.D.. The CSP conditions were 177 MPa, 330°C and 25 min. dwell time, with pH 5.0 and 4.01 wt % solution. By using HCl, the highest density, achieved was 78.72 % T.D. conditions were 517 MPa, 320°C and 45 min. dwell time, with pH 5.5 and 12.00 wt % solution.

In Figure 2.7, blue squares show citric acid, while the red ones show HCl acid solutions. Citric acid with higher pressure gives higher theoretical densities. However, here more impressive one is when the liquid amount is higher, high pressure is not the key value to able to get high densities. If there should be an optimum liquid amount for sintering, this should probably be around 4.0 wt %. Some studies were also reported on 4.00 wt % liquid as optimum value for humidification, [25].

pH trials were made with using HCl as the acid type. The highest density was obtained at pH 4.5, looking at points 4.0 to 6.0. However, it is seen that all the densities were still under 90.00 % TD. In this case, it was decided to do experiments with different acids. The aim here was to find the most accurate CSP path in the light of some information in the literature.

The amount of liquid used is another parameter that affects the effectiveness of dissolution in the system as much as the acid and pH used. The ratio of the liquid to be used is important because of wetting capacity, homogeneous dispersal ability and ultimately determining the degree of saturation.

Table 2.2. *Theoretical densities due to acid type at different CSP conditions*

Acid Type	Liquid (wt %)	pH	1st Stage Pressure (MPa)	1st St. Dwell time (min.)	Peak Temp. (°C)	2nd St. Pressure (MPa)	2nd St. Dwell time (min.)	Peak Temp. (°C)	T.D. (%)
Citric acid	3,00	5.0	74	3	30	251	35	205	66.68
Citric acid	4.01	5.0	89	15	50	155	45	300	81.86
Citric acid	4.01	5.0	89	15	50	163	45	330	66.76
Citric acid	4.01	5.0	89	15	90	170	45	330	64.77
Citric acid	4.01	5.0	74	3	100	177	25	330	89.28
Citric acid	4.01	5.0	74	5	90	155	45	300	58.32
Citric acid	6.67	5.0	74	10	70	170	45	300	65.36
Citric acid	8.00	5.0	74	10	70	170	45	320	67.16
Citric acid	10.67	5.0	74	10	90	170	45	320	67.57
Citric acid	12.00	5.0	74	10	90	170	45	320	66.38
Citric acid	13.33	5.0	74	10	90	170	45	320	68.44
HCl	12.00	6.0	74	10	90	170	45	320	69.80
HCl	12.00	5.5	74	10	90	170	45	320	67.92
HCl	12.00	5.0	74	10	90	170	45	320	68.60
HCl	12.00	4.5	74	10	90	170	45	320	73.50
HCl	12.00	4.0	74	10	90	170	45	320	67.66
HCl	12.00	5.5	74	10	90	170	45	320	52.07
HCl	12.00	5.5	74	10	90	517	45	320	78.72
HCl	24.00	5.5	74	10	90	170	45	320	61.23
HCl	12.00	5.5	74	10	90	369	45	320	77.17
Zinc acetate	3.75	5.5	89	15	20	155	45	300	87.63
Zinc acetate	2.83	5.5	89	15	45	155	45	300	88.48
Zinc acetate	5.66	5.5	89	15	20	155	45	300	89.15
Zinc acetate	5.66	5.5	89	15	40	155	45	300	85.68
Zinc acetate	1.89	5.5	89	15	20	155	45	300	87.20
Zinc acetate	2.01	5.5	89	15	50	155	45	300	87.56
Zinc acetate	2.47	5.5	89	15	20	155	45	300	87.42
Zinc acetate	2.47	5.5	89	15	20	155	45	300	87.98
Zinc acetate	2.62	5.5	89	15	20	155	45	300	87.05
Zinc acetate	2.77	5.5	89	15	20	155	45	300	87.48
Zinc acetate	2.93	5.5	89	15	55	155	45	300	88.16
Zinc acetate	3.09	5.5	89	15	55	155	45	300	83.39
Zinc acetate	3.09	5.5	89	15	55	155	45	300	82.99

Table 2.2. (continue) *Theoretical densities due to acid type at different CSP conditions.*

Zinc acetate	3.39	5.5	89	15	40	155	45	300	92.97
Zinc acetate	3.70	5.5	89	15	20	155	45	300	87.58
Zinc acetate	4.01	5.5	89	15	55	155	45	300	89.14
Zinc acetate	4.32	5.5	89	15	20	155	45	300	88.37
Zinc acetate	4.63	5.5	89	15	40	155	45	300	87.89
Zinc acetate	2.31	5.5	89	15	30	155	45	300	86.15
Zinc acetate	3.09	5.5	89	15	40	155	45	300	88.14
Zinc acetate	2.47	5.5	89	15	30	155	45	300	87.66
Zinc acetate	2.01	5.5	89	15	20	155	45	300	88.92
Zinc acetate	1.85	5.5	89	15	45	155	45	300	85.06
Zinc acetate	2.16	5.5	89	15	20	155	45	300	89.69
Zinc acetate	7.00	5.5	89	4	100	539	50	140	97.94
Zinc acetate	8.00	5.5	89	4	100	539	50	135	97.86
Zinc acetate	8.00	5.5	89	4	100	532	50	135	96.27
Zinc acetate	8.00	5.5	89	4	100	547	50	135	96.73
Zinc acetate	8.00	5.5	89	4	100	539	50	135	95.88
Zinc acetate	8.00	5.5	89	4	100	539	50	135	98.19
Zinc acetate	8.00	5.5	89	4	100	539	50	140	98.28
Zinc acetate	8.00	5.5	89	4	100	539	50	130	97.40
Zinc acetate	8.00	5.5	89	4	100	547	50	135	98.04
Zinc acetate	8.00	5.5	89	4	100	532	50	135	97.39
Zinc acetate	7.33	5.5	89	4	100	539	50	135	99.28
Zinc acetate	7.33	5.5	89	4	100	539	50	130	98.41
Zinc acetate	7.33	5.5	89	4	100	539	50	140	99.93
Zinc acetate	7.33	5.5	89	4	100	547	50	135	97.89
Zinc acetate	7.33	5.5	89	4	100	532	50	135	97.26
Zinc acetate	8.67	5.5	89	4	100	532	50	135	98.49
Zinc acetate	8.67	5.5	89	4	100	547	50	135	98.67
Zinc acetate	8.67	5.5	89	4	100	539	50	135	97.44
Zinc acetate	8.67	5.5	89	4	100	539	50	130	98.71
Zinc acetate	8.67	5.5	89	4	100	539	50	140	99.08
Zinc acetate	6.67	5.5	89	4	100	539	50	130	98.93
Zinc acetate	6.67	5.5	89	4	100	539	50	140	98.24
Zinc acetate	6.67	5.5	89	4	100	532	50	135	98.12
Zinc acetate	6.67	5.5	89	4	100	547	50	135	97.13
Zinc acetate	6.67	5.5	89	4	100	539	50	135	97.21
Zinc acetate	7.00	5.5	89	4	100	539	50	140	97.54

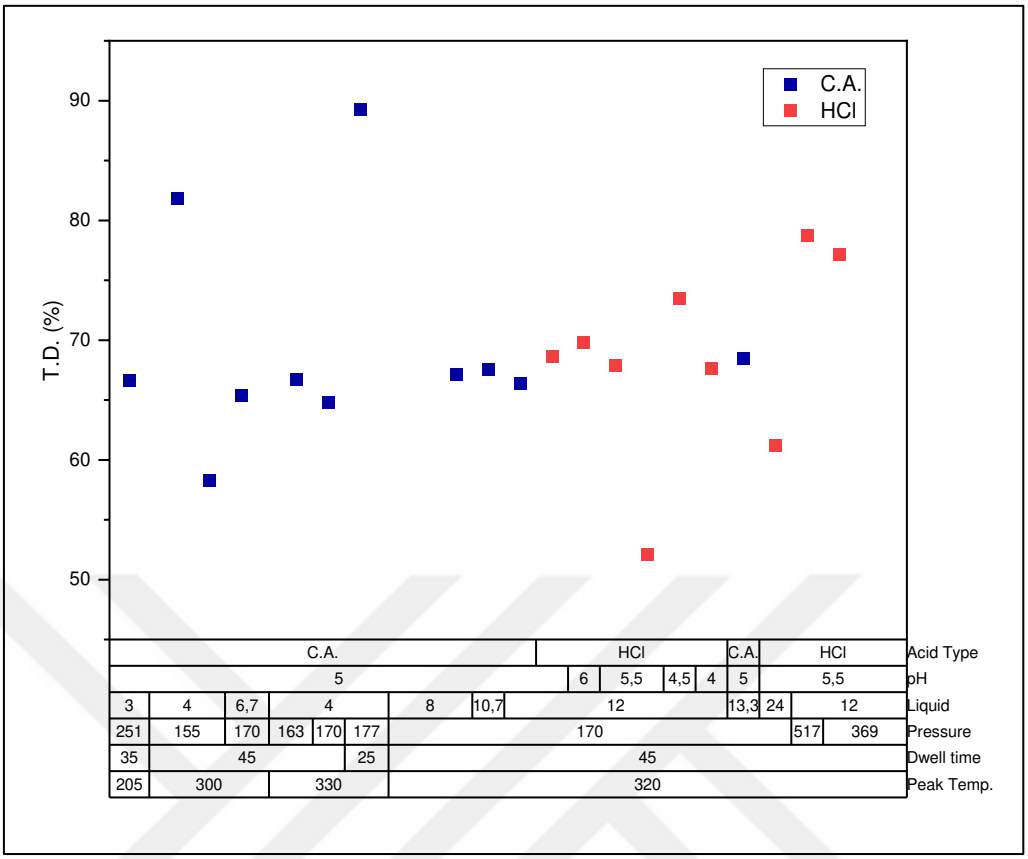

Figure 2.7. *Citric acid and HCl acid type and theoretical density graph due to different variables*

When all the trials with ZA in Figure 2.8 are examined, it is directly striking that the studies are divided into two parts. The main factor here is the temperature and pressure variation. It seems that high pressure and an optimum temperature are suitable for CSP studies, although the temperature-pressure evaluations required to achieve high density will be discussed in the next sections.

Figure 2.9, shows the effect of liquid amount on final theoretical densities of the CSPed samples. At the bottom, pressure is shown, for the T.D. results, 540 MPa give higher densities also for the same temperatures. Maximum density is with red dots, means 7.3 wt % liquid amount, 140°C and for all the trials, 50 minutes dwell time and pH 5.5 are likewise.

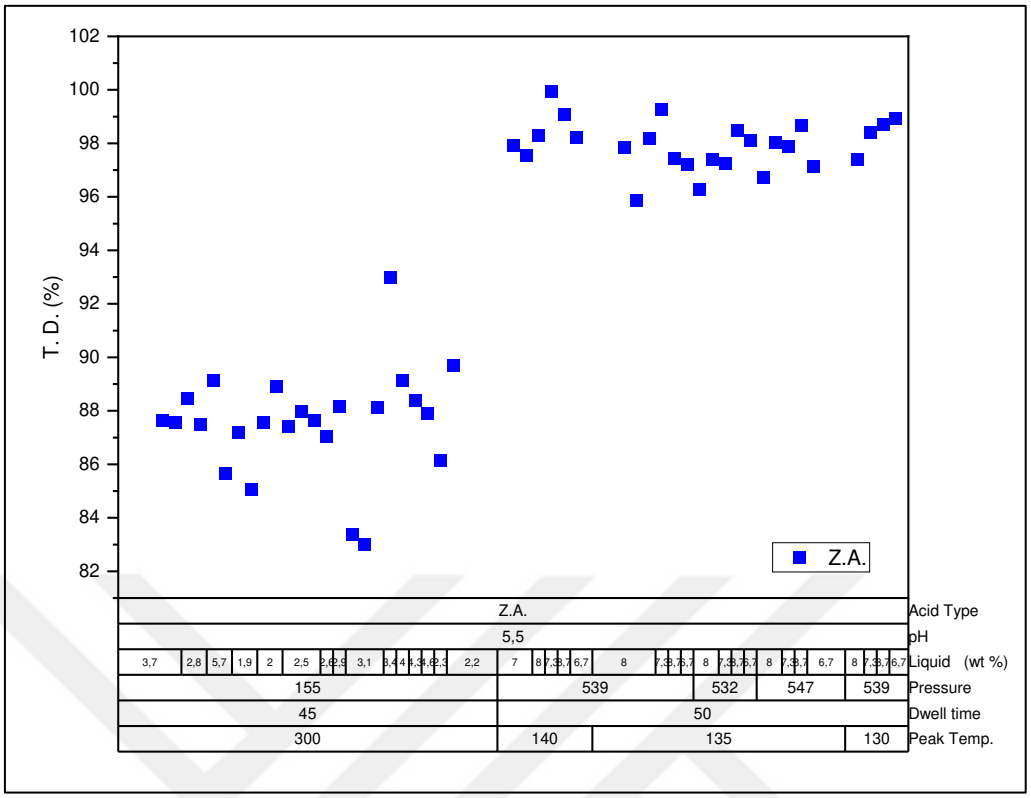

Figure 2.8. *Zinc acetate and theoretical density graph due to different variables*

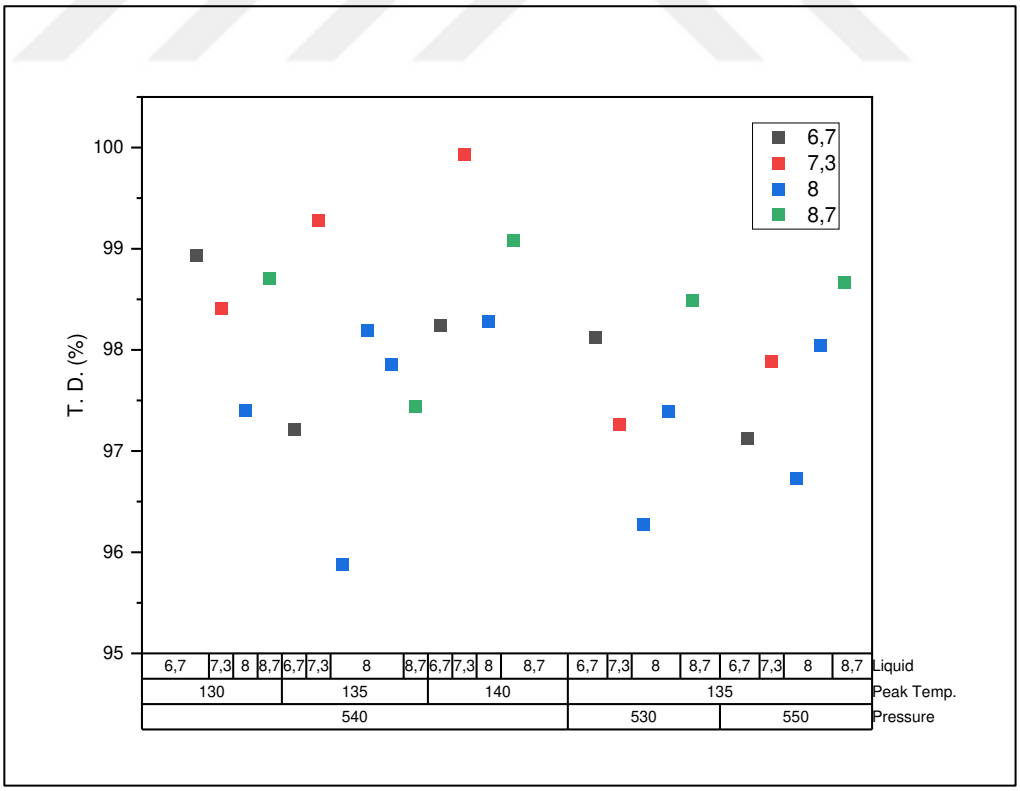

Figure 2.9. *Amount of liquid, T.D. % change graph*

Figure 2.10 shows higher temperature and lower pressure results with zinc acetate at pH 5.5 and with different liquid amounts. On the other hand, Figure 2.10 shows the results with high pressure and low temperature results. Theoretical densities are under 90.00 % with low pressure while it upgrades more than 90.00 % densities when the pressure is 540 MPa. Sintering liquid ratios are different, it wasn't able to obtain bulk material with liquid amounts under 6.0 wt %, see at Figure 2.11. This may be due to extrusion of liquid is higher with high pressure and water disappears from the system too early when it is less than 6.0 %.

These results showed that the amount of water was also related to other variables. When the effect of pressure was examined in the literature, it was seen that it was effective first in the settlement of the particles, then in the rearrangement and precipitation processes. The first studies done by changing the variables are shown in the graphs below, Figures 2.10 and 2.11. Subsequently, the results are detailed with more systematic experiments, see at Section 2.3.3.

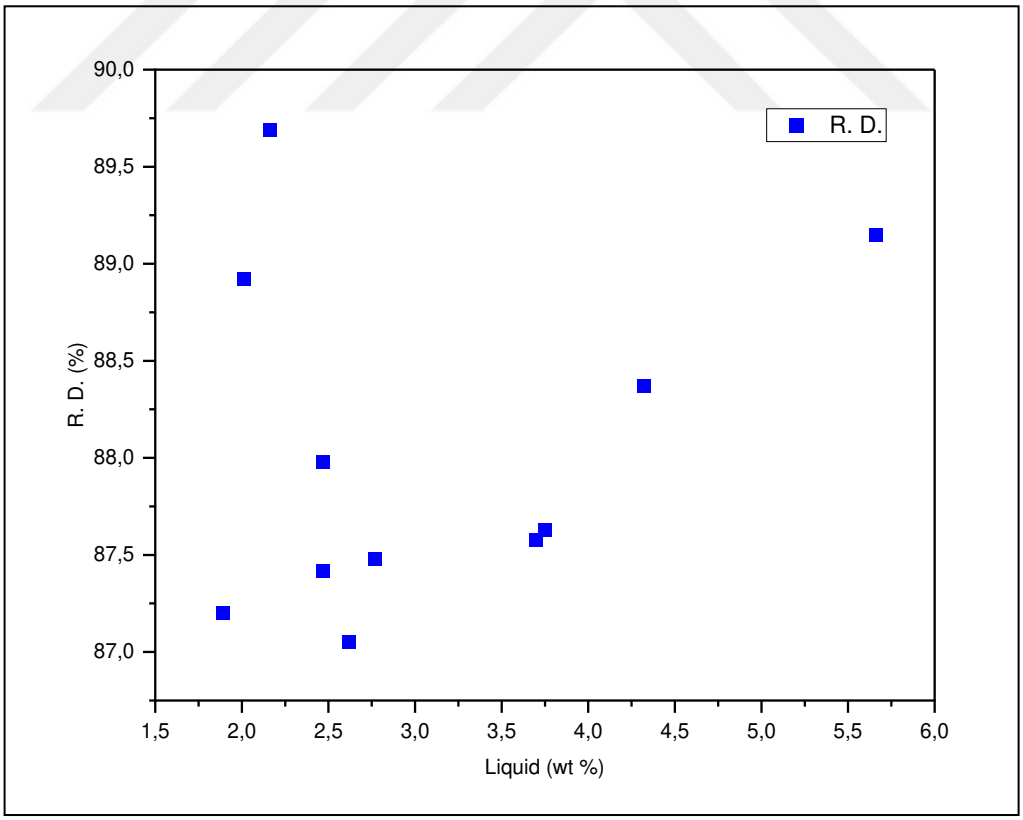

Figure 2.10. *Effect of liquid amount on the density, Zinc acetate liquid with pH 5.5, pre-pressing with 89 MPa for 15 minutes at 20°C and afterwards 155 MPa, 45 minutes at 300°C.*

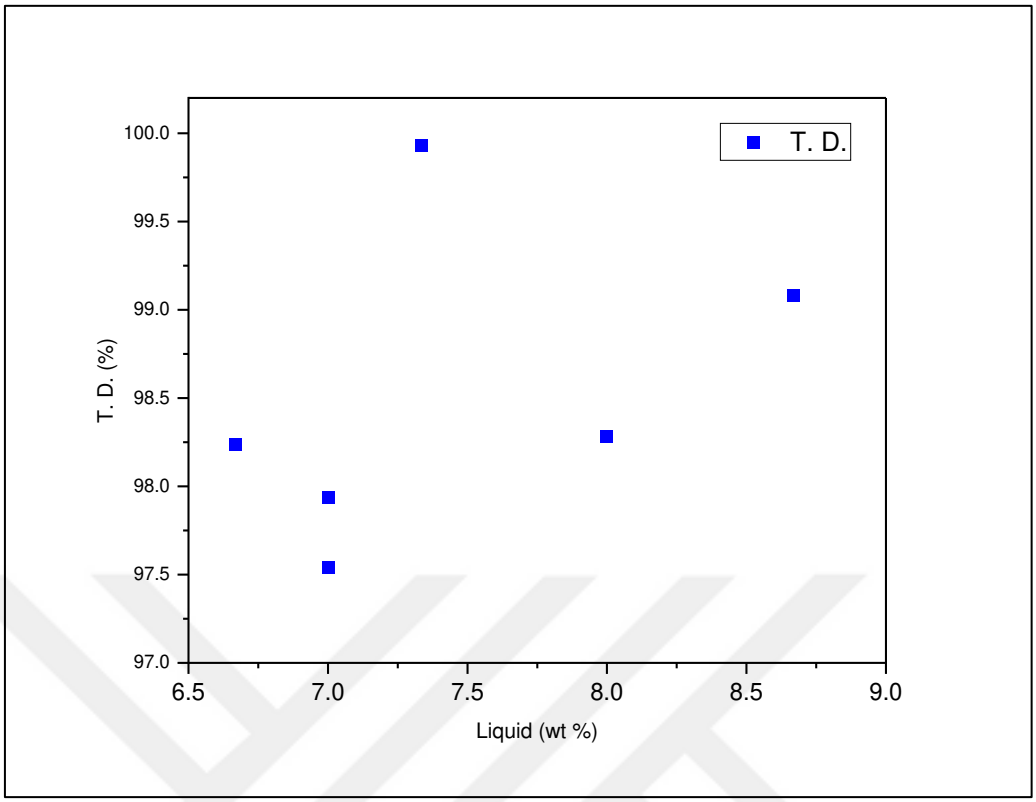

Figure 2.11. *Effect of the liquid amount on theoretical density. Zinc acetate liquid with pH 5.5, pre-pressing with 89 MPa for 4 minutes at 100°C and afterwards 540 MPa, 50 minutes at 140°C.*

2.3.3. Roles of pressure and temperature on the CSP

Theoretical densities of samples that were sintered by the conditions of 7.33 wt % liquid, zinc acetate, with pH 5.5, pre-pressing with 89 MPa for 4 minutes at 100°C and afterwards 50 minutes at 135°C with three different pressures were investigated. For the given conditions, the best result, greater than 99 % TD, was obtained under 540 MPa pressure. Looking at the pressure vs theoretical density graph at Figure 2.12, it was observed that the theoretical densities increased up to 540 MPa pressure and then started to decrease, under the same sintering conditions.

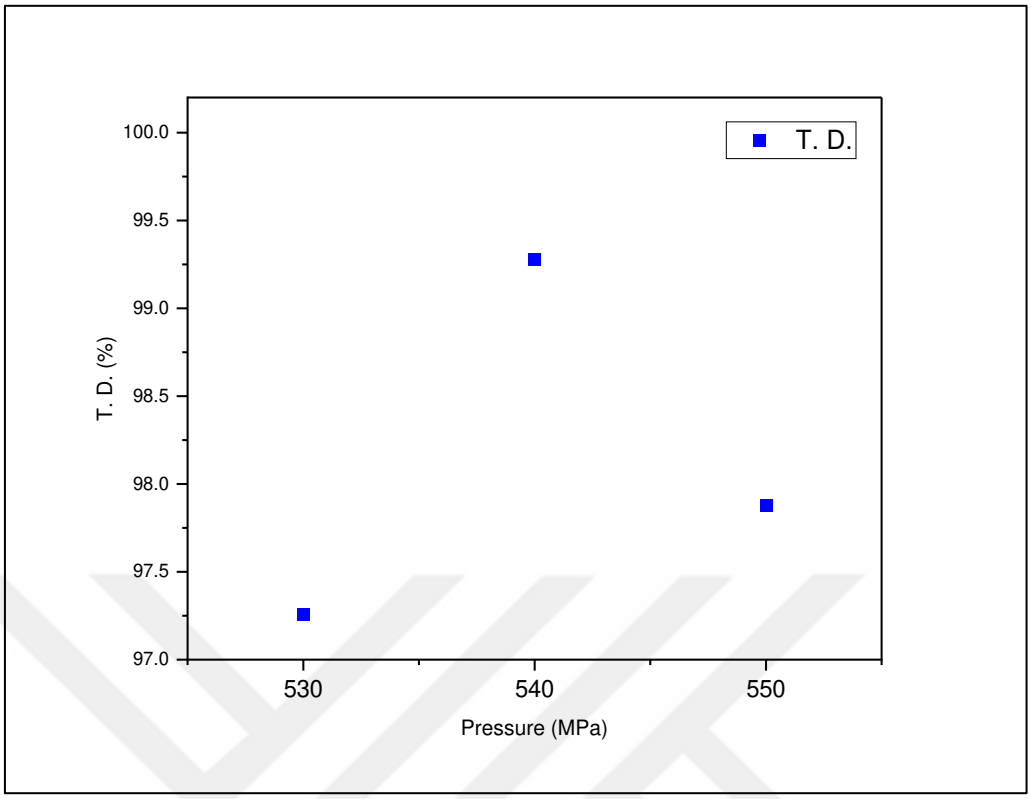

Figure 2.12. *Role of the sintering pressure on density of the samples.*

Temperature and pressure are both very effective parameters in the system together and their influence depends on time. Because the basis of hydrothermal sintering is based on temperature and pressure association, when the temperature is decreased, the pressure should be increased or vice versa in the literature studies. Systematic studies on temperature were continued.

Figure 2.13 shows theoretical density changes as a function of temperature at 7.33 wt % liquid, zinc acetate, with pH 5.5, pre-pressing with 89 MPa for 4 minutes at 100°C and afterwards 50 minutes at 540 MPa with three different temperatures were investigated. Among the tested conditions, the best result which was greater than 99.00 % T.D., was obtained at 140°C.

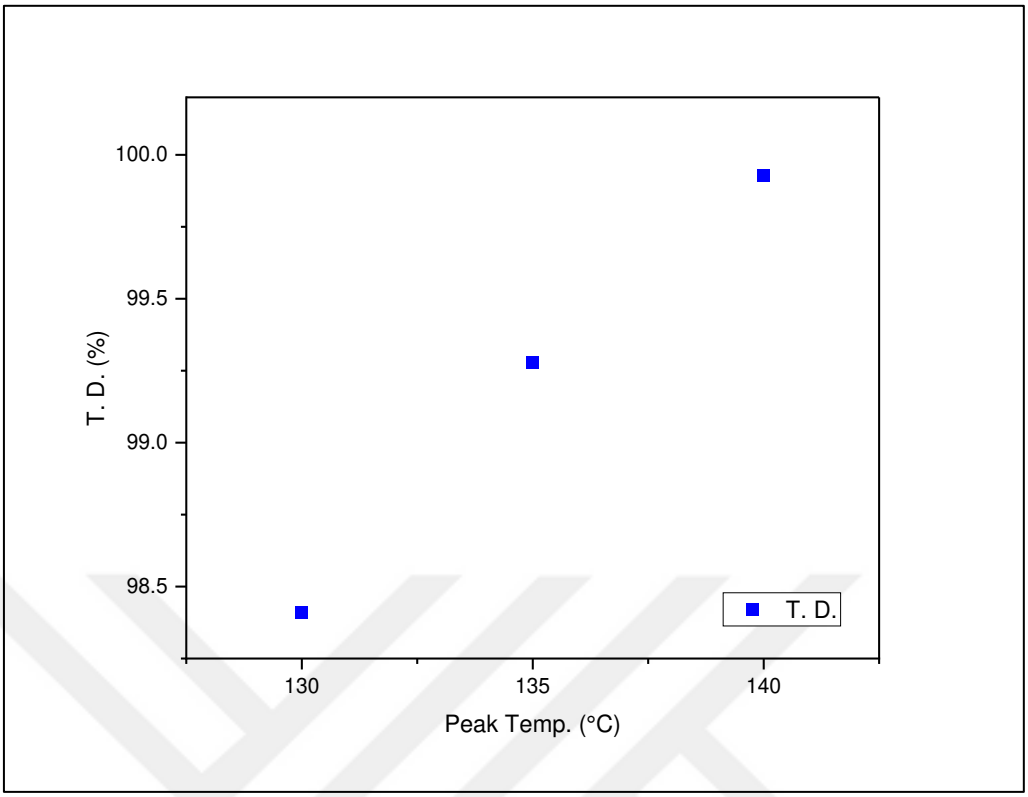

Figure 2.13. *Theoretical Density of the samples as a function of the sintering temperature*

These studies showed that if the parameters are closely controlled during the CSP, ZnO ceramics with greater than 99.00 % TD can be achieved. However, in some studies, it was observed that higher temperatures are more suitable to reach traditionally sintered ceramic properties. S. Funahashi et al. presented the average conductivity of the CSP of ZnO sintered at various temperatures, 126°C, 305°C, and conventional sample sintered at 1400°C. 0.00002 S/cm, 9 S/cm and 5 S/cm conductivities were measured, respectively [19]. According to this study it seems that CSP at 305°C give even better result than conventional sintering.

We could not obtain high densities at temperatures such as 300°C in our previous acid tests, in Table 2.2. However, when these conductivity values in the literature were examined, we realized that the temperature could be effective in improving the properties, although high densities were achieved during the CSP at relatively lower temperatures. For this reason, we decided to expand the high temperature trials. Trials at 300°C and 300MPa pressures, which had not been done before, were carried out and electrical conductivity was measured for two different temperatures, see at Table 2.3. Conductivity values are even not close to conventially sintered ZnO values. This may be due to small pores at grain boundaries, bond type, dislocation types or hydrated grain boundaries. S.

Funahashi et al. attributed low electrical conductivity to defects at grain boundaries that limit transport across the grain boundary. Post heat treatment was discussed for further enhancement of the electrical properties, [72]. Y. Jing et al. [72] approved different atmospheres for post heat treatments and measured conductivities of ZnO samples. There was an electric conductivity of $5x10^{-4}$ S/cm for cold sintered ZnO samples but there is an improvement with the post heat treatment at 500°C at argon atmosphere. It's not similar for the air atmosphere heat treatment, as seen at Figure 2.14. The electrical conductivity increases continuously by increasing post-heat-treating temperature and reaches a maximum of 16.4 S/cm at 500 °C, which is almost 3×104 times higher than that of as-cold-sintered ones. However, Y. Jing et al. deals with cracking of samples with the post heating treatment, [72]. This cracking on process induces additional troubles herewith.

Table 2.3. *CSP sintering temperature and property relationship*

Pressure (MPa)	**Temp. (°C)**	**Dwell time (min.)**	**Cycle Complete time**	**T.D. (%)**	**Conduct. (S/cm)**	**Hv Hardness (GPa)**
540	135	50	50	98.25	$1.94x10^{-5}$	-
540	135	50	50	96.38	-	2.98
560	150	50	50	98.74	$3.95x10^{-5}$	-
300	300	1	50	98.30	-	1.70
350	300	1	50	97.86	$1.27x10^{-6}$	-
250	300	1	50	99.25	$7.17x10^{-6}$	-

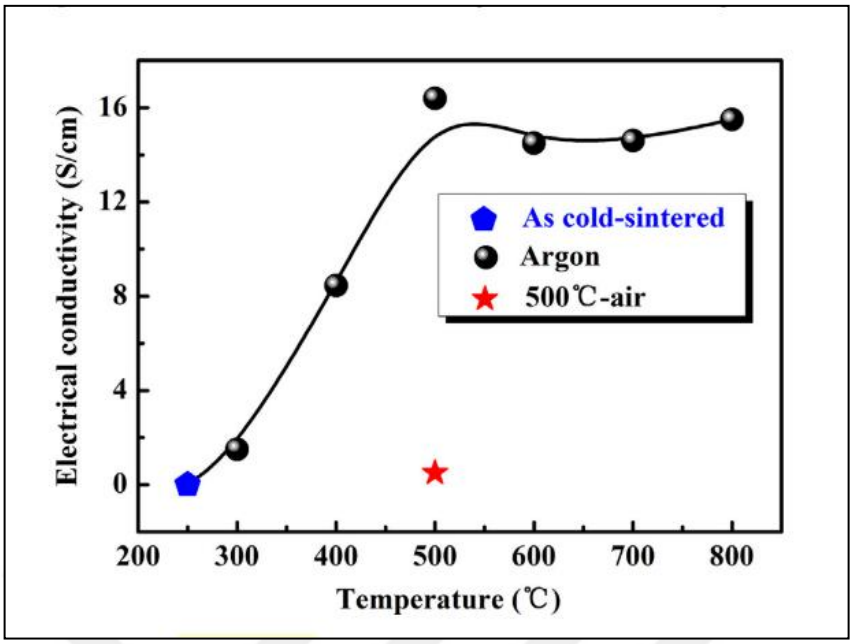

Figure 2.14. *Electrical conductivity of cold sintered ZnO before and after post heat treatment, [72].*

Even sintering at higher temperatures were studied, seen at Figure 2.15. At 250 MPa pressure, 300°C and 1 minute dwell time at 300°C and 50 minutes complete cycle was the highest theoretical density result was obtained. Hardness test and conductivity tests were enforced to the samples, comparative with 140°C sintering. When the dwell time is more than 1 minute at high temperature as like 300°C, it was obtained the sample cracked in the mould. 10 minutes dwell time at 300°C, caused the fragmented sample.

In Table 2.3, study due to sintering temperature is shown, effects ZnO bulk sample properties due to sintering temperature even at cold sintering process were detected. In this study however it affects the property, its not so much as like the literature. The conductivity of the samples sintered at different temperatures and conditions were investigated. Accordingly, although the conductivity varies depending on the temperature and other sintering conditions, it is seen that they are not in a position to be compared with the material sintered by conventional sintering.

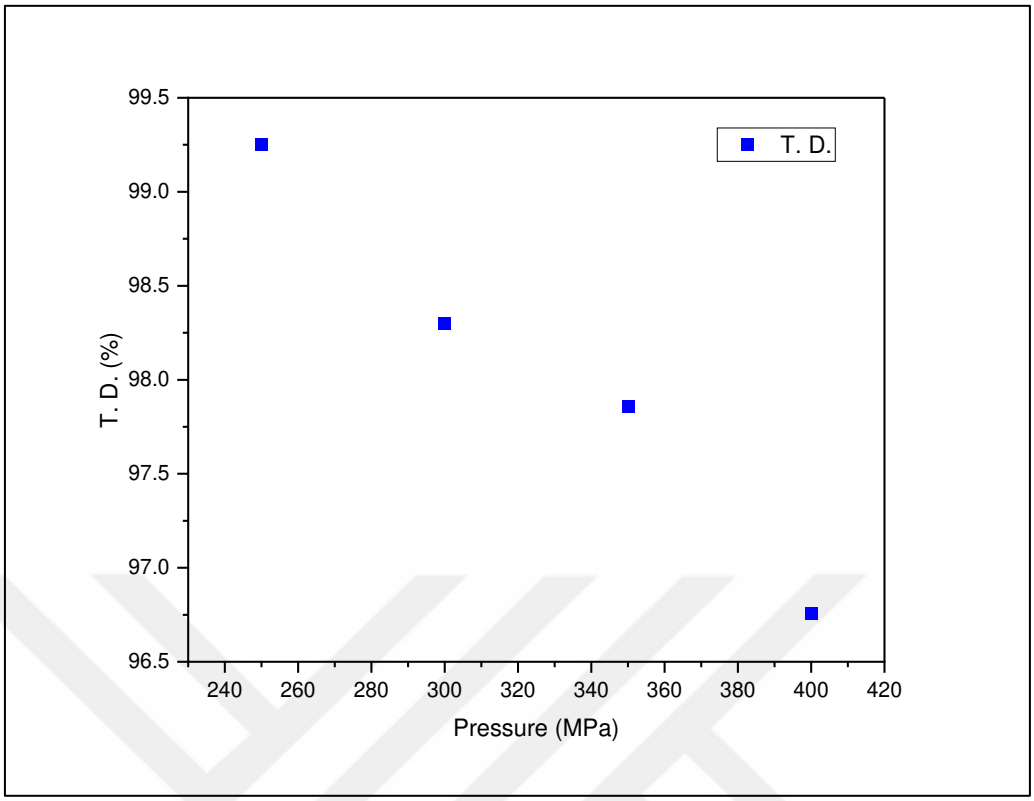

Figure 2.15. *300°C, 1 minute dwell time, for different pressures*

Considering the hardness test results, the hardness of the sample sintered at 135°C was higher than that of the sintered sample at 300°C. This is surprising. Although both samples have a well sintered appearance, and the conductivity tests in the literature, the conductivity of the sample sintered at high temperature is similar to the traditional sintered ZnO, but this was not the case in our study. The hardness values of the samples sintered at 135°C were at a level that could compete with the samples sintered with the traditionally sintered. 2.98 GPa hardness was calculated for the CSP handled sample and it is between 0.5 to 3.0 for conventionally sintered ZnO ceramics, [73,74]. Stereo microscope images of the indentations for both samples can be seen at Figure 2.16.

K. Nur et al. demonstrated hardness of ZnO samples are even better hardness values than the conventially sintered samples, see in Figure 2.17, [75]. Hardness was 4.88 GPa for conventially sintered samples and 5.56 for cold sinetered with air atmosphere samples.

As a result of the hardness test performed on alumina sintered with CSP before, the values were even ten times lower than the conventionally sintered ceramic. This is explained by the low bond strength, but for the densisties of 85.00 – 90.00 % T.D. in the literature, [17]. In this case, it can be said that the bond strength of the material, whose hardness is similar to that of conventional sintered samples, is also good.

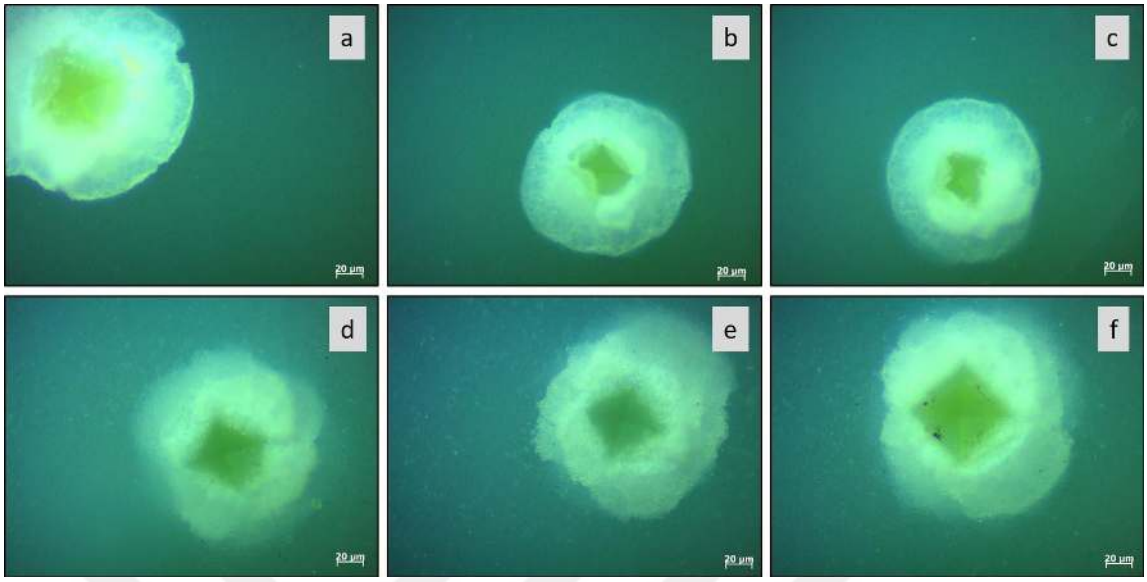

Figure 2.16. *HV hardness test indentation images, a, b, c) CSP temperature at 140˚C and, d,e,f) CSP temperature at 300˚C*

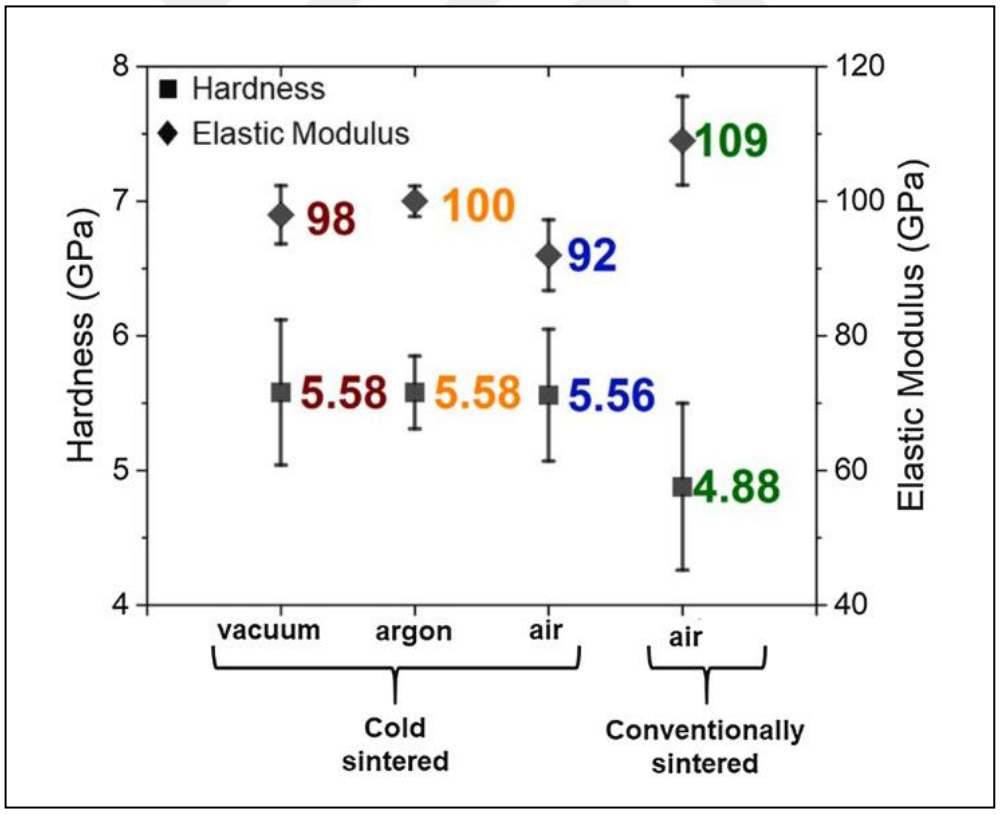

Figure 2.17. *Average values of hardness and elastic modulus for cold and conventionally sintered ZnO samples, [75].*

When the temperature is the variable, the highest theoretical density was obtained at 140˚C as shown in Figure 2.18 In the samples with varying water content 5.0 - 8.0

wt%, a density of 98.91%TD was reached. When different pressure and temperature studies were examined depending on different liquid ratios, the graphs below were obtained, see at Figures 2.19 and 2.20. When the theoretical density values of the materials with constant liquid contents, sintered with different pressures are examined, Figure 2.19 was obtained. Sintering conditions were 50 min at 140°C. Experiments were repeated for each different liquid ratio for three times and 4 different curves were obtained. The liquid pH is 5.5. When the pressure, which is generally used in these curves, was increased, the theoretical density decreased. It was observed that the highest density value was obtained when 7.33 wt % liq with a pH of 5.5 and zinc acetic salt was used, at a pressure of 532 MPa. As the liquid ratio increases, that is, 8.00 % and above, the effect of the pressure changes and the pressure increase has a positive effect.

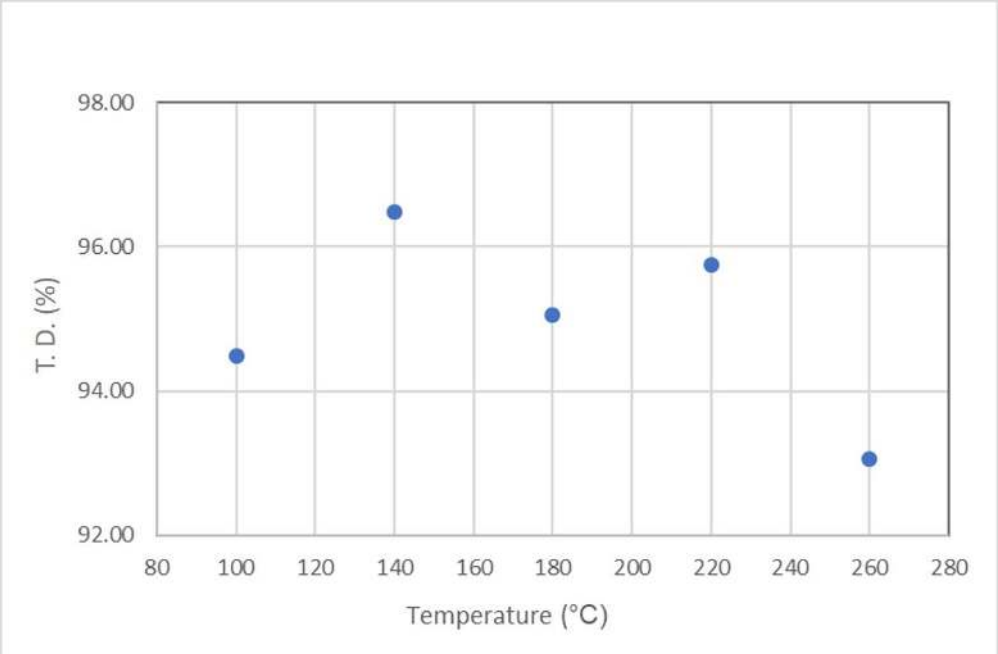

Figure 2.18. *% theoretical density change according to the temperature of pure ZnO*

In Figure 2.20, the effect of temperature on the theoretical density of pure ZnO was investigated. The effect of temperature was also examined using different liquid ratios. Here the pressure is constant and is 539 MPa in all trials. Accordingly, as a result of the studies carried out at 130, 135, and 140°C, it is seen that the theoretical densities slightly decrease when the temperature is 135°C, but then re-increase. The highest density value was obtained at 140°C when 7.33% liquid was used.

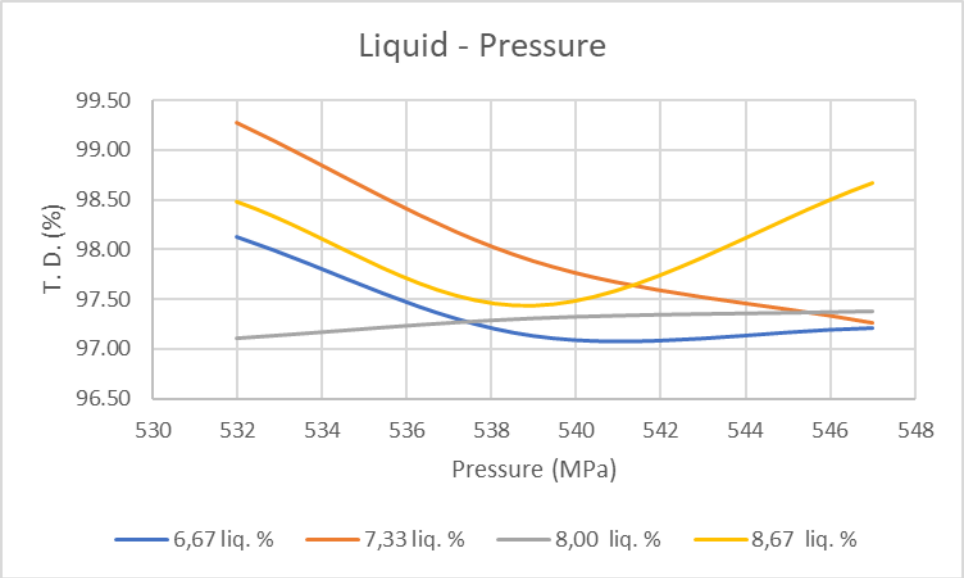

Figure 2.19. *Pure ZnO, pressure of samples sintered with CSP at 140°C with different water ratios, T.D. % curves*

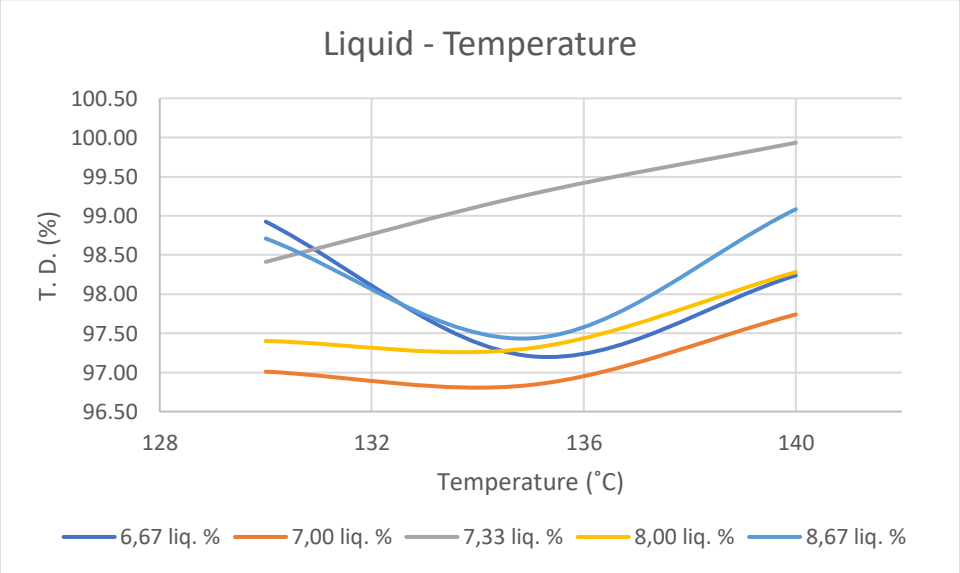

Figure 2.20. *Pure ZnO, temperature of samples sintered with CSP at 539MPa with different water ratios, T.D. % curves*

As the sintering conditions are; temperature of 140°C, dwell time of 50 minutes, pressure of 539 MPA and ZA solution with, pH of 5.5 was used as optimum sintering condition for ongoing experiments. The liquid ratio varied according to the material and the experiment. Accordingly, the scanning electron microscope (SEM) images shown in Figure 2.21 are images of samples sintered under the same conditions and with different liquid ratios. When the internal structure of the material with a liquid ratio of 7.33 % is examined, it is seen that the grains are between 150-300 nm. These grains are larger than

material containing 8.00 % liquid. This may be due to the greater dissolution with 8.00 % liquid. Another possibility is that they may be at different stages of sintering. When there is less liquid, the liquid with dissolved particles will reach saturation faster and precipitation will begin. In this case, it may be possible to say that sintering starts faster. Considering the densities, the density of the material containing 7.33% liquid is higher than the material with the other two liquid ratios. The densities stated herein are taken by measuring size and weight, see at Table 2.4. In previous studies, density measurements were started with Archimedes. However, since some samples fell to pieces in water during this measurement, density calculations were continued by dimensional measurement.

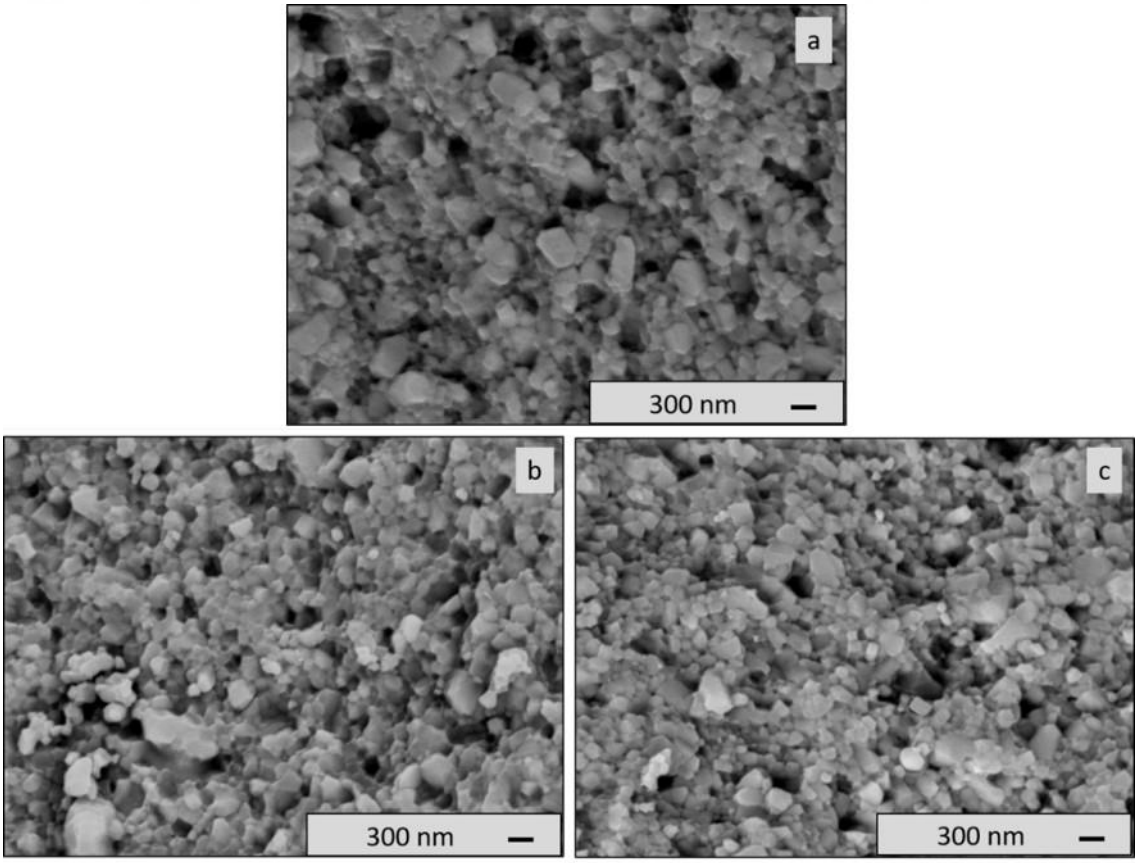

Figure 2.21. *BSE-SEM images of pure ZnO samples sintered with CSP at 140°C, 539MPa pressure with different water ratios, a)7.33 wt %, b)8.00 wt %, c)8.67 wt %*

Table 2.4. *BSE-SEM images of pure ZnO samples sintered with CSP at 140°C, 539MPa pressure with different water ratios*

SEM	Liq. (%)	T.D. (%)
a	7.33	99.28
b	8.00	98.19
c	8.67	97.44

When the liquid ratio was reduced to 5.6 wt %, T.D. value decreased to 96.38 %. The microstructure is as in Figure 2.22, there are regions determined to have different grain sizes and degrees of sintering. This may be an indication that the amount of liquid used is low and it is insufficient to wet the whole particles homogeneously.

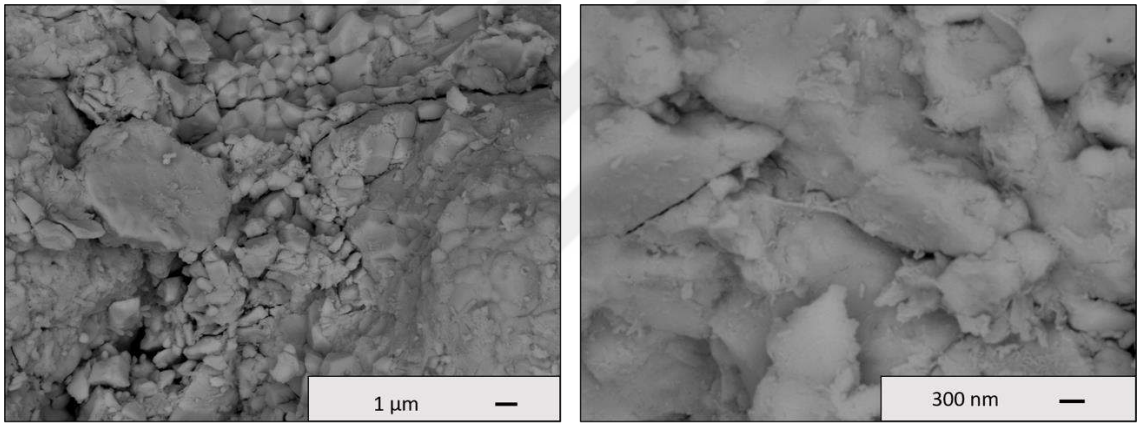

Figure 2.22. *Pure ZnO BSE-SEM images of the sample sintered with CSP at 140°C, 539MPa pressure, 5.6 wt % liquid*

There was not much structural change in the materials sintered at different pressures, Figure 2.23. However, the grain size distribution was lower in the sample sintered at 532 MPa pressure. While there are grains larger than 300 nm in the sample sintered with 539 MPa pressure, the grains are generally below 300 nm in the sample sintered with 532 MPa pressure. The density of the sample sintered with 532 MPa pressure is higher than the others, see at Table 2.5. A similar result was obtained in the graph where the effect of pressure was examined before, and it was determined that the densities at 532 MPa were higher than the materials sintered with high pressure.

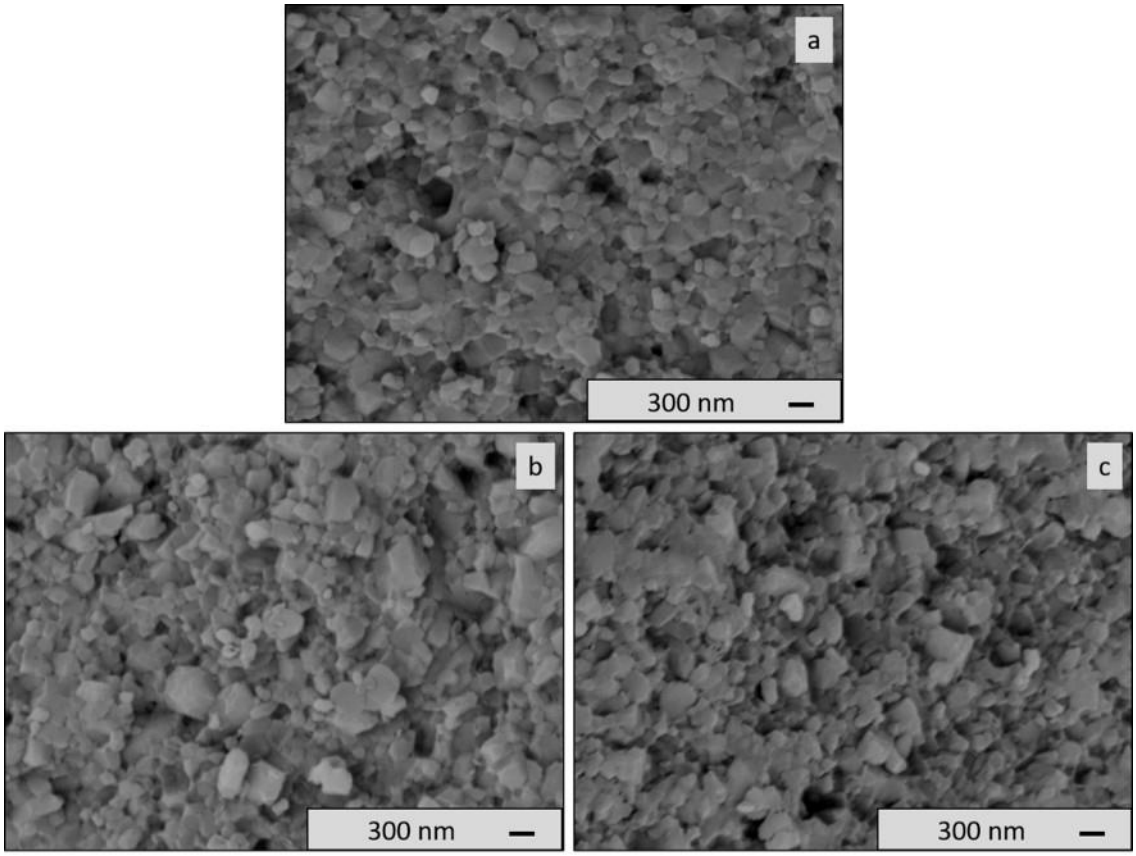

Figure 2.23. *Pure ZnO BSE-SEM images of samples sintered with CSP at different pressures, at 140°C and 6.67 wt. % liq, a)532MPa, b)539MPa, c)547MPa*

Table 2.5. *Pure ZnO BSE-SEM images of samples sintered with CSP at different pressures, at 140°C and 6.67 wt. % liq*

SEM	Pressure (MPa)	T.D. (%)
a	532	98.12
b	539	97.21
c	547	97.13

The microstructure, obtained at 130°C, shows that it is quite homogeneous in materials sintered at different temperatures, Figure 2.24. The grain size is stable and in the range of 200-300 nm. Grains below 100 nm are also seen in the material sintered at 135°C. In addition, there are grains with size of 300 nm. The lower density in this sample also suggests that the internal structure affects the density, see at Table 2.6. In the material sintered at 140°C, the theoretical density again reached 97.00 %. However, it is seen that this material, which is sintered at 140°C, also contains some fine grains, at all.

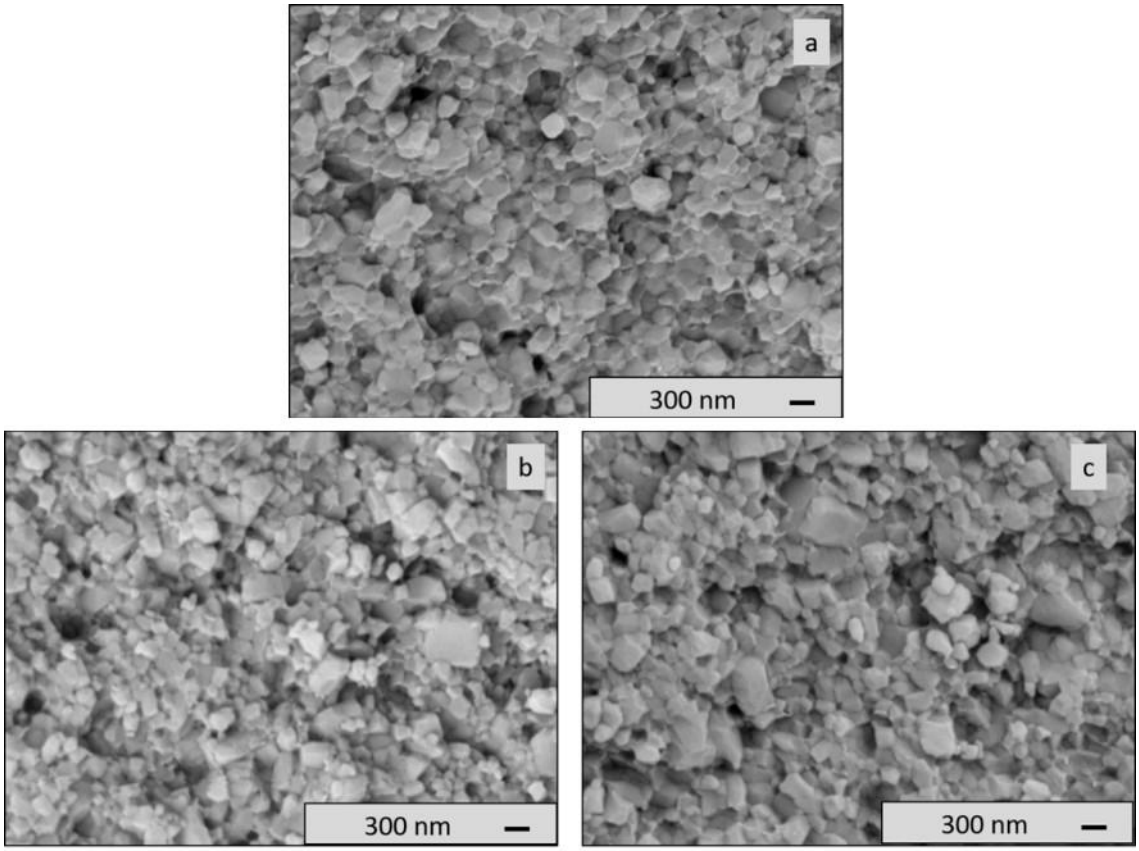

Figure 2.24. *BSE-SEM images of pure ZnO samples sintered with CSP at different temperatures, 539MPa pressure*

Table 2.6. *BSE-SEM images of pure ZnO samples sintered with CSP at different temperatures, 539MPa pressure*

SEM	Temp. (˚C)	T.D. (%)
a	130	97.01
b	135	96.84
c	140	97.74

2.3.4. Water loss during the heating and its role on the CSP

One of the parameters that can affect the CSP process is the water loss during the heating and sintering. Furthermore, the heating rate can play a significant role on water loss. However, it is not simple to control the rate of temperature rise in the system available in our laboratory. The use of a heat jacket is one of the options that can be used to heat the system in a controlled manner. Greater than %99.00 theoretical densities could be obtained without extra heating in the system. The key parameter is to be able to evaluate hydrothermal conditions at the system. In addition, some experiments were

carried out by closing the air outlet chamber in the mold. The aim was to prevent the water loss in the system due to water evaporation with the increase in temperature. However, there were still steam escape points in the system. Studies can be done to isolate the system a little more. With the same conditions open and closed systems were investigated by using the following conditions: 300°C, 155 MPa and 45 minutes dwell time, pH 5.0 citric acid 4.0 wt % liquid. For the open system density was 81.86%TD while for the closed system, it was 58.32 % TD. Table 2.7 show all the experiments, performed with the closed system. The highest theoretical density, achieved, was 78.72 % T.D. even under 517 MPa pressure.

Table 2.7. *Closed system CSP theoretical density results*

Acid Type	Liquid (wt %)	pH	1st Stage Pressure (Mpa)	1st Stage Dwell time (min.)	Peak Temp. (°C)	2nd Stage Pressure (Mpa)	2nd Stage Dwell time (min.)	Peak Temp. (°C)	T. D. (%)
C. A.	4.01	5.0	74	5	90	155	45	300	58.32
C. A.	6.67	5.0	74	10	70	170	45	300	65.36
C. A.	8.00	5.0	74	10	70	170	45	320	67.16
C. A.	10.67	5.0	74	10	90	170	45	320	67.57
C. A.	12.00	5.0	74	10	90	170	45	320	66.38
C. A.	13.33	5.0	74	10	90	170	45	320	68.44
HCl	12.00	6.0	74	10	90	170	45	320	69.80
HCl	12.00	5.5	74	10	90	170	45	320	67.92
HCl	12.00	5.0	74	10	90	170	45	320	68.60
HCl	12.00	4.5	74	10	90	170	45	320	73.50
HCl	12.00	4.0	74	10	90	170	45	320	67.66
HCl	12.00	5.5	74	10	90	170	45	320	52.07
HCl	12.00	5.5	74	10	90	517	45	320	78.72
HCl	24.00	5.5	74	10	90	170	45	320	61.23
HCl	12.00	5.5	74	10	90	369	45	320	77.17

2.3.5. Effect of pressing parameters on the CSP

Experiments were performed to investigate effect of die diameter, that is related to the surface area, on the CSP. The pressure values that could be reached with a large-diameter mold were somewhat more limited. The measurements from such large die

pressed could not be taken because the samples from the experiments with a 31 mm diameter mold were broken due to low densities induced by unsufficient pressures, applied during the sintering. On the other hand, the samples from the experiments with 13 mm diameter were not broken.

Process errors were also observed in most of the trials at the beginning of the experimental activities. Most of the process errors, observed in the samples with a density above 90.00 %TD were similar to the pressing errors mentioned in James Reed's book. These errors are in the form of hat-shaped cap formation, ring-shaped cap formation, lamination. In his book, James Reed explains the causes and prevention methods of errors, [76].Generally, it is stated that most of the errors occur with the "springback" difference. The reasons for this difference are explained as follows:

1. Pressure gradients due to friction on the mold wall.

2. Uneven distribution in elastic compression in the compact due to variable granule structure, uneven filling, air compression

3. Restriction of movement by friction caused by insufficient lubrication on the mold wall and/or surface roughness

4. Springback differences between the exiting part and the part remaining inside the mold during demoulding

Lamination breaks are repetitive circumferential breaks on the friction surface perpendicular to the pressing direction. In Figure 2.25, there is a photograph of the broken sample, sintered powder containing 6.00 wt % liquid with pH of 5.5 after sintering at 300°C and 370 MPa. The sample had a 87.90 %TD. At the broken surface, repeated lamination cracks were seen. Although this situation occured in almost all samples, it was seen that some samples also have more than one error. It was stated that the simplest way to prevent lamination fractures is to reduce the press pressure. In the studies carried out in this direction, a trial was done by reducing the pressure from 155 MPa to 125 MPa and enhancement in the internal structure was observed. It was seen that the lamination decreased but not completely disappeared. However, with the decrease in pressure, the densities began to decrease from 94.00 % to 92.00 %TD at all.

One other study to reduce lamination was the usage of lubricant. It was used to decrease die friction between the die wall and the sample. A silicone-based lubricant was used, although it did not match the temperatures we work on. In some cases, sticking was experienced while removing the sample from the mold. In this period, additional

experiments were carried out with steric acid. In the trials, there are applications such as lubricating the mold with steric acid and also coating the powder with steric acid. Coating powder with steric acid was not sufficient and even prevented the densities to exceed 90.00 %. The most important reason for this situation is that steric acid is hydrophobic. It was observed that when the coated powder came into contact with water in the mortar, the water did not wet the powder and rolled as droplets. For this reason, it was thought that steric acid could not act as a binder in the powder, but could be tried as a lubricant. In this case, different methods have been explored to prevent lamination. Some more experiments were done with bornitrides lubricant. Mould release agent or protectoragent can be more exact for the bornitrides, since it was not a slippy surface on the mould. But the results were interestingly more effective rather than all other lubricants. This is thought to be due to its ability to close gaps rather than its lubricating effect. Thus, Zahabi et al explains use of polyvinyl pyrrolidone (PVP) adhesive as a sealant against water escape was reported to reduce the pressure needed to obtain full density from 250 MPa for unsealed zinc oxide samples to 140 MPa, [77].

During sintering, the water in the material evaporates and most of it leaves the system over time. If the evaporation is too fast, lamination cracks may occur perpendicular to the side walls of the mold, which are the points where the water moves away from the system. Rahaman explains this situation with Scherer theory in his book [2]. Accordingly, macroscopic forces occur in the liquid while drying the gels. These forces, called ∇p, increase with rapid evaporation and cause a high difference between the regressions. Drying should be done more slowly to reduce these stresses. Trials were made at temperatures below 300°C, where the first trials were made. The temperature, which was 300°C in the first trials, was reduced to 220°C. In Figure 2.25 a and b, there are photographs of the samples at different temperatures. It can be seen that the lamination is almost absent and the density increases. In the samples 191001-2 and 191209-1, the density was 87.9%, while the liquid ratio was increased from 6.0% to 6.5%, the press pressure was increased from 370 MPa to 540 MPa and the final temperature was reduced from 300°C to 220°C, and the internal structure was tested. Microstructure could be improved and the density increased at such conditions. It was observed that the sample could not be broken by hand and the surface smoothness increased. When the temperature is reduced, that slowed down the evaporation rate, it is predicted that the sample will not receive enough energy for sintering while at the same pressure. As a matter of fact, [25]

obtained a transition pressure value of 140 MPa in their study, and showed that 90.00 % density could not be exceeded at pressures below this value. When our previous studies are evaluated, approximately 150 MPa pressure was used and 90.00 % theoretical density could not be exceeded. Again, Paula et al. conducted most of their work at 120°C and 530 MPa, [25]. They stated that the density increase could not be achieved after a certain pressure. However, this issue will be clarified in the future, as we have not done our optimum pressure value studies as well.

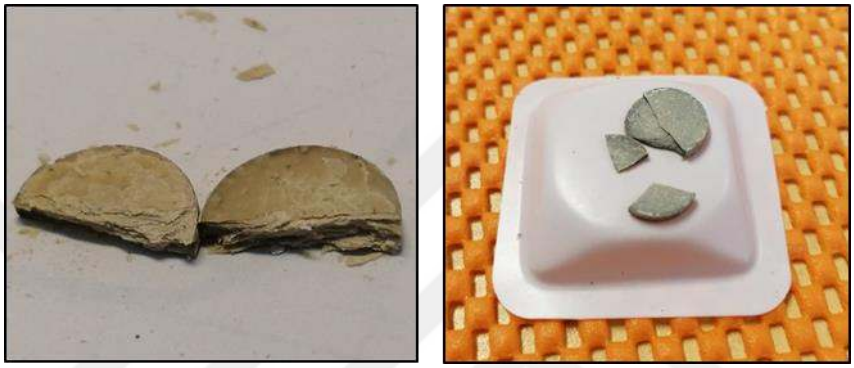

Figure 2.25. *a) 191001-2 (87.9% theoretical density) b) 191209-1 internal structure photographs showing the decrease of lamination*

Early on thesis, with pure ZnO, the highest theoretical density reached was 92.97 %. However, this situation occurred in a single sample and in general, about 90.00 % theoretical density could not be exceeded, at the same time, proper measurements could not be taken from many samples due to errors. For these reasons, it was decided to carry out studies to determine the causes of errors in the internal structures of the samples and to resolve the process errors.

At the end of the studies, bornitride mould release agent was used and it was seen that the defects in the mold are somewhat improved in this way. In addition, the increased strength of the specimens by changing CSP conditions, such as temeperature ensured that ring-shaped ruptures or cap fractures were almost never seen. Even the densities were much more higher, as seen at Table 2.8.

Elimination of process errors is of great importance for the development of the process. Thereafter, more methodological studies can be performed.

Table 2.8. *Theoretical density variation of pure ZnO with designed CSP procedures*

1st Stage Pressure (Mpa)	1st Stage Dwell time (min.)	Peak Temp. (°C)	2nd Stage Pressure (Mpa)	2nd Stage Dwell time (min.)	Peak Temp. (°C)	Liquid (wt %)	pH	T.D. (%)
89	4	100	540	50	100	6.47	5.5	94.49
89	4	100	540	50	140	6.47	5.5	96.49
89	4	100	540	50	180	6.47	5.5	95.05
89	4	100	540	50	220	6.47	5.5	95.75
89	4	100	540	50	260	6.47	6.5	93.06

2.3.6. The analysis of the CSP of ZnO from thermodynamics and kinetics point of view

Figure 2.26 shows moisture content in the starting powder just before sintering. It was determined that the weight loss in the system was 2.46 %. This amount is less than the water amount given to the system in the mortar, 6.5 wt %. At the following, the sample, which was sintered at 530 MPa pressure and 220°C for 50 minutes, was crushed, powdered in a mortar and TG-DTA was checked again. In this case, the weight loss was 1.04 %. It is seen that the weight loss after sintering occurs only after 300°C at the TG-DTA, see at Figure 2.27. This may be related with the hydrates at the system or the zinc acetate that was used for the pH arrangement. In order to examine this situation in more detail, TG-DTA will be applied to the sample intermittently during sintering, and the amount of water in the system will be found instantly. The presence and accuracy of this information will be very important when creating sintering models. Kang et al. showed at different sintering temperatures, humidity of the system changes and when sintering finishes at 140°C, the residual humidity of the system is close to zero, at Figure 2.28 [25]. These test results are also observed at TG-DTA, while the upper temperature limit for the investigation wasn't indicated.

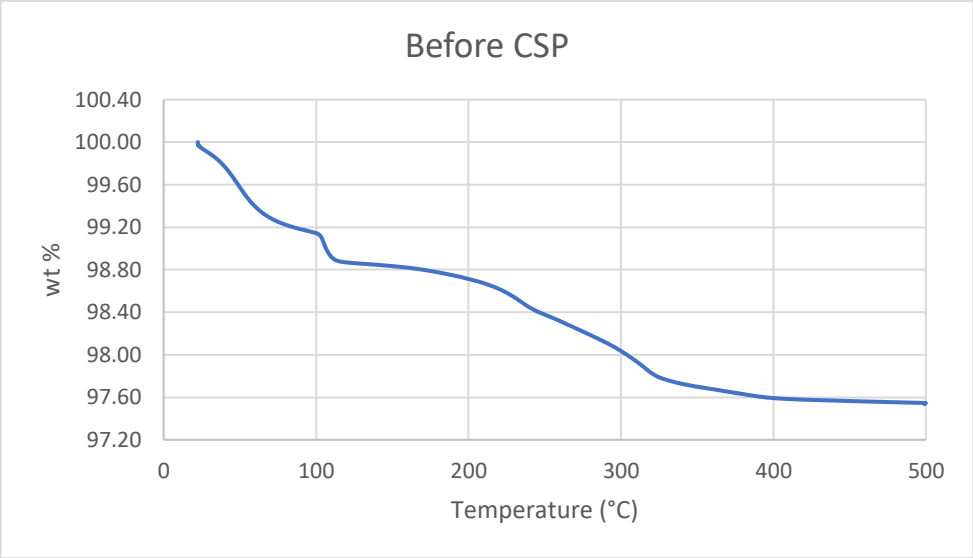

Figure 2.26. *TG-DTA graph of the powder moistened before sintering*

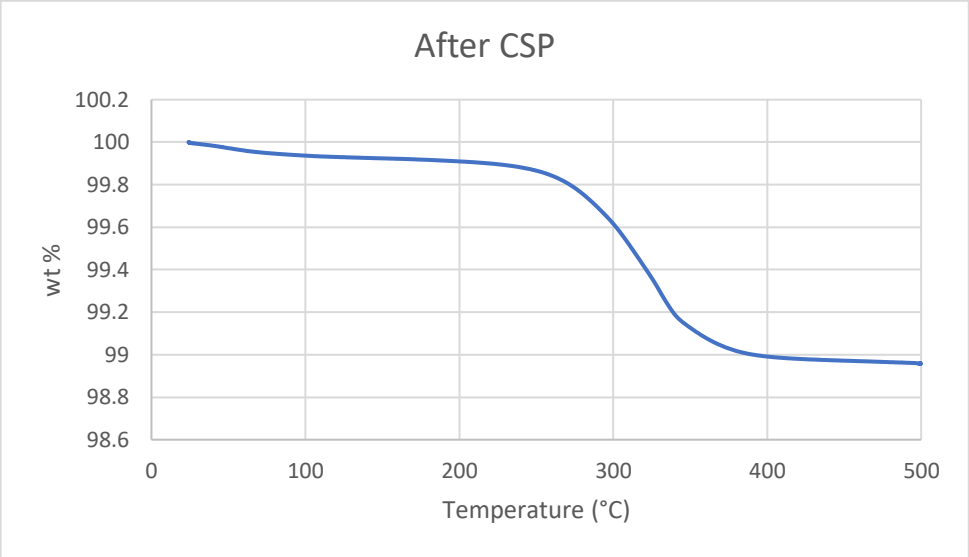

Figure 2.27. *TG-DTA graph of the pellet milled after sintering*

Humidity studies with TG-DTA was advanced, and the pressure created by the capillary forces on the system will be tried to be calculated based on the liquid film thicknesses and pore distributions during sintering. For this purpose, moisture determination and TG-DTA analyzes was performed to determine the amount of water in the system at different stages of sintering, and SEM analyzes will be performed to determine the grain sizes. BET analysis and Archimedes analysis will be used to find the amount of open and closed pores in the system.

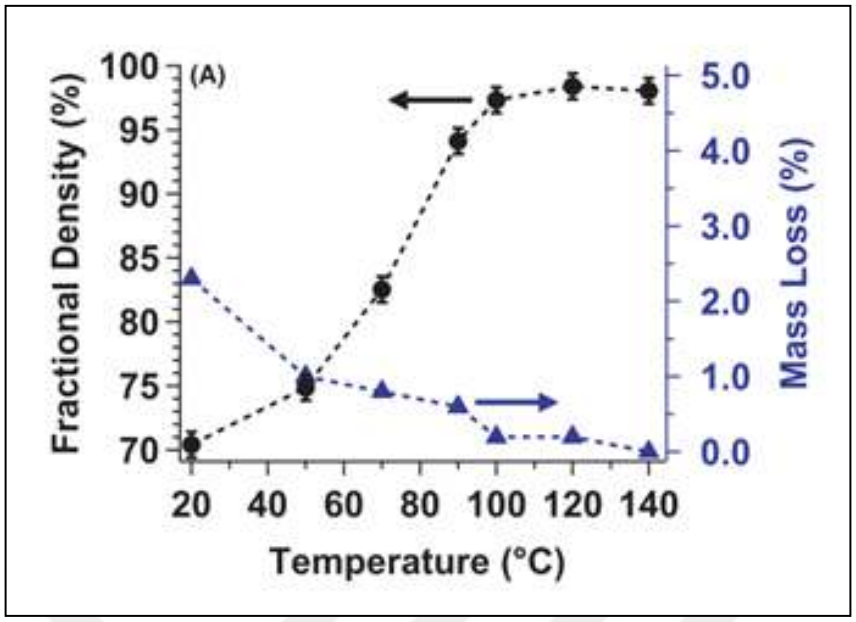

Figure 2.28. *Kang et al. Weight losses after sintering, [25].*

In the TG-DTA analyses, moisture determinations of the samples taken from the press were made instantly. The sintering times are shown in the first column of the Table 2.9. The sintering times were rearranged. Because the point where the press reaches the sintering temperature of 140°C is taken as the zero point. Since sintering did not start during pre-period (appropriate hydrothermal environment is not provided), it was only taken as pre-pressing and all times were rearranged accordingly. The time shown as 1 minute is shown for the sample standing at 140°C for 1 minute. The weight loss at 100°C in the second column indicates the amount of liquid evaporated up to 100°C in TG-DTA. The reason why 100°C and 600°C are taken separately is to see if the water is in physical or bonded form. The theoretical density value was determined according to the weight and dimensional measurements made immediately just after the sample was taken from the press. Grain size analysis and pore size analyzes were obtained by measuring the diameters of grains and pores in the SEM images with the ImageJ program. Three different SEM images and at least 50 of measurements were done for each image for the calculations. Dimensional fluctuations due to the two-dimensionality of the images were not taken into account.

Table 2.9. *Moisture values and film thickness from interrupted analysis*

TG-DTA wt losses (%)				T.D.	Grain R	Pore R	Film thickness
Time (min)	100°C	600°C	TOTAL	(%)	(nm)	(nm)	(nm)
powder	2.95	1.11	4.06	-	259	-	-
0	-	-	-	71.65	186	99	-
1	0.69	1.05	1.75	84.80	192	100	20.61
5	0.32	0.97	1.29	93.17	184	78	33.65
15	0.19	0.59	0.78	96.12	189	94	35.64
25	0.21	0.55	0.76	97.11	206	89	46.62
35	0.18	0.57	0.74	97.66	196	70	56.04
45	0.19	0.56	0.76	97.59	225	70	55.91

After the powder sample was moistened with 6.5 wt % water in a mortar, analysis was carried out immediately. The obtained humidity was determined as approximately 4.0 %, Table 2.9. In this case, it can be said that some of the added water evaporates or is not distributed homogeneously. The average particle size of the powder was measured as 259 nm from the SEM images. It is seen that the amount of water in the system gradually decreases until the 15th minute, and then it is constant, seen at Figure 2.29. Figure 2.29 was created due to Table 2.9, which are TG-DTA weight loss results at different temperetaure time snaps at CSP. Water remains in the system up to 0.8 % when the sintering is close to the end. It is seen that approximately 0.6 % of this water is probably chemically bound and evaporates only when 600°C is reached. Looking at Figure 2.30 and Figure 2.32, it is seen that the bound water remaining in the material is removed at 350-400°C. 100-150°C is the removal temperature hydrated water, [78,79]. Zinc acetate, removes at 350-400°C from the system, as seen from Figure 2.33. Maria states that after process temperatures above 100°C, there is no residual water in the system, and in the measurements they made with TG-DTA, they found a maximum of 0.2 % water by weight. Figure 2.28 shows the graph obtained as a result of the residual water amount experiments. In addition to this information, they performed Raman analysis and emphasized that although they saw some very small peaks next to the ZnO peaks, [25].

C. A. Randall et al. [80], demonstrates ZnO cold sintering employs acetic acid solution as a transient phase in an open system, allowing it to mostly evaporate during the heating ramp, the rapid linear shrinkage between times of 3 and 6 minutes may be

recognized as the combined effects of powder densification and liquid evaporation. However, thermal gravimetric analysis (TGA) of the wet green body showed that the weight loss was only 3 % of the total weight up to 120°C, despite the initial 15 wt % of the added transient phase. Hence, the TGA result indicates that following points:

(1) excessive transient liquid can be extruded from the wet green body during the 5 minute pressure stabilization prior to cold sintering and (2) liquid evaporation can be considered as only a minor effect for the linear shrinkage, as the remining liquid will be likely located in the pore spaces between particles, [80].

It is seen from the endothermic peak that the reaction takes place at approximately 400°C and the remaining moisture in the system is removed. This peak is quite evident in the powder sample where the humidity is high. As stated in the literature, water components are removed from the system before 200°C, [81]. If it is above 300°C, zinc acetate decomposes and an endothermic peak is formed. Afterwards, it is recrystallized at around 400°C. In the TGA graph in Figure 2.35 [82], the decomposition of zinc acetate occurred at 329°C. In this case, the humidity in our system moves away from the system up to 200°C.

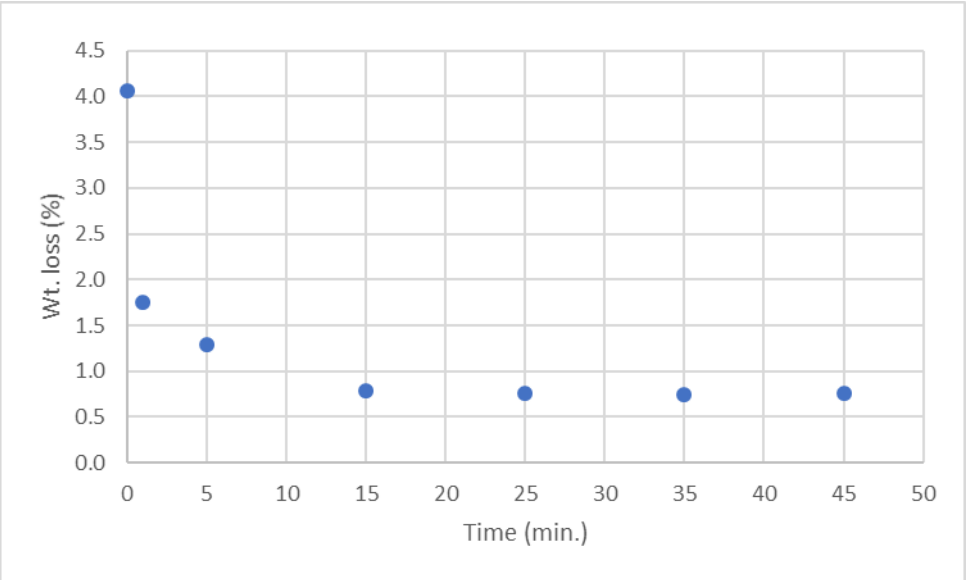

Figure 2.29. *Time-dependent weight loss graph in TG-DTA analysis*

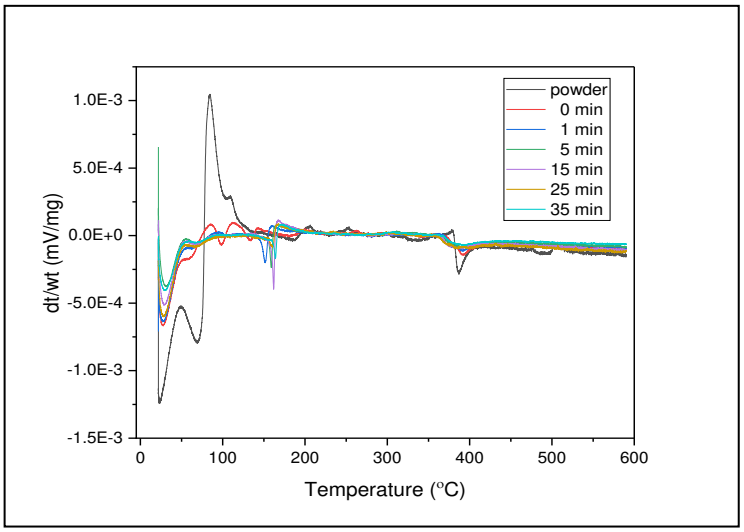

Figure 2.30. *Temperature dependent heat exchange derivative curves in TG-DTA analysis*

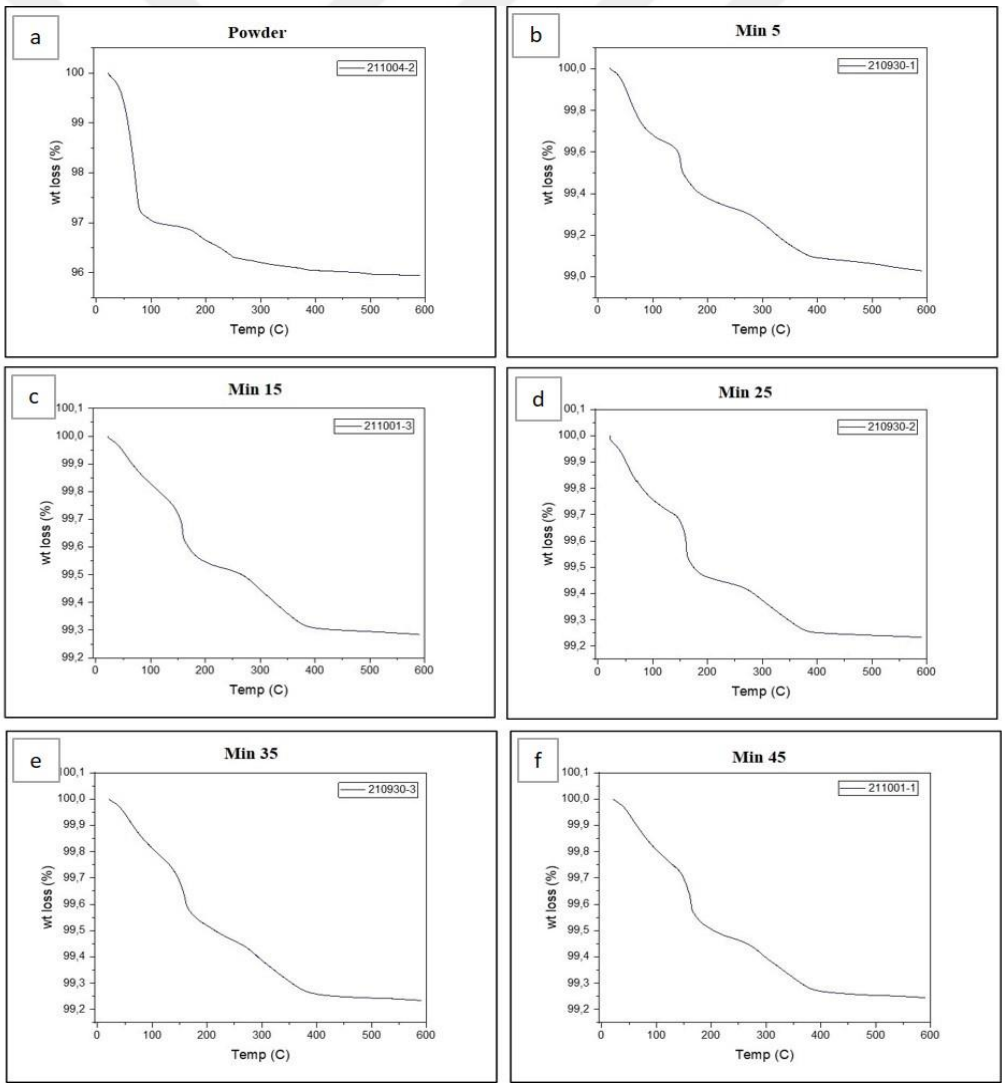

Figure 2.31. *Weight loss graphs of interrupted tests, for a)powder, b)min 5, c)min 15, d)min 25, e)min35, f)min 45.*

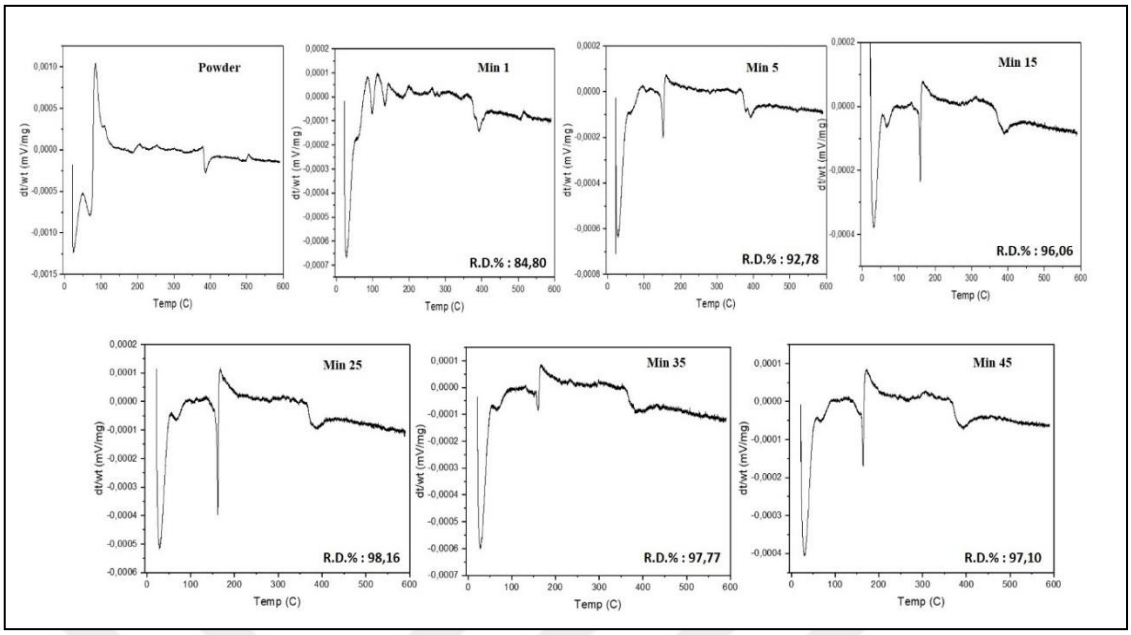

Figure 2.32. *DSC graphs of interrupted tests*

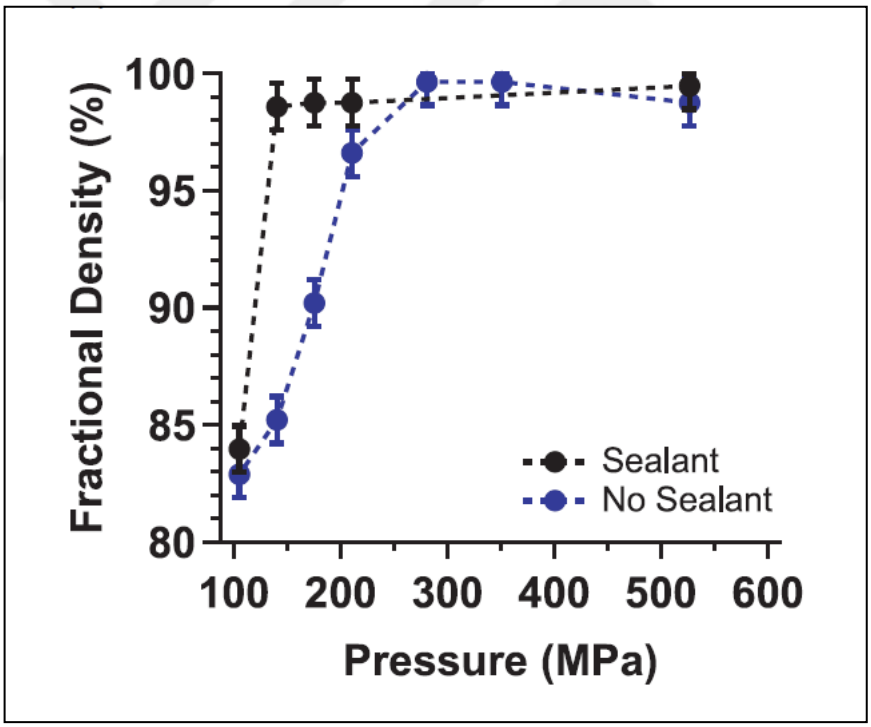

Figure 2.33. *Maria et al. Weight losses after sintering, [24]*

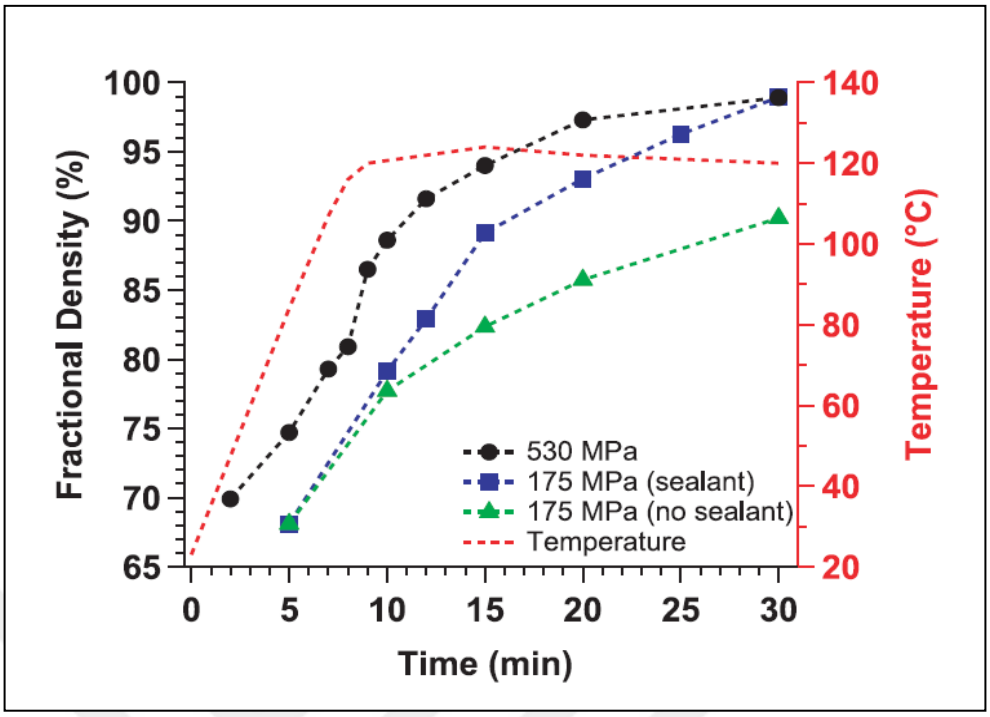

Figure 2.34. *Maria et al. sintering time theoretical density change, [24]*

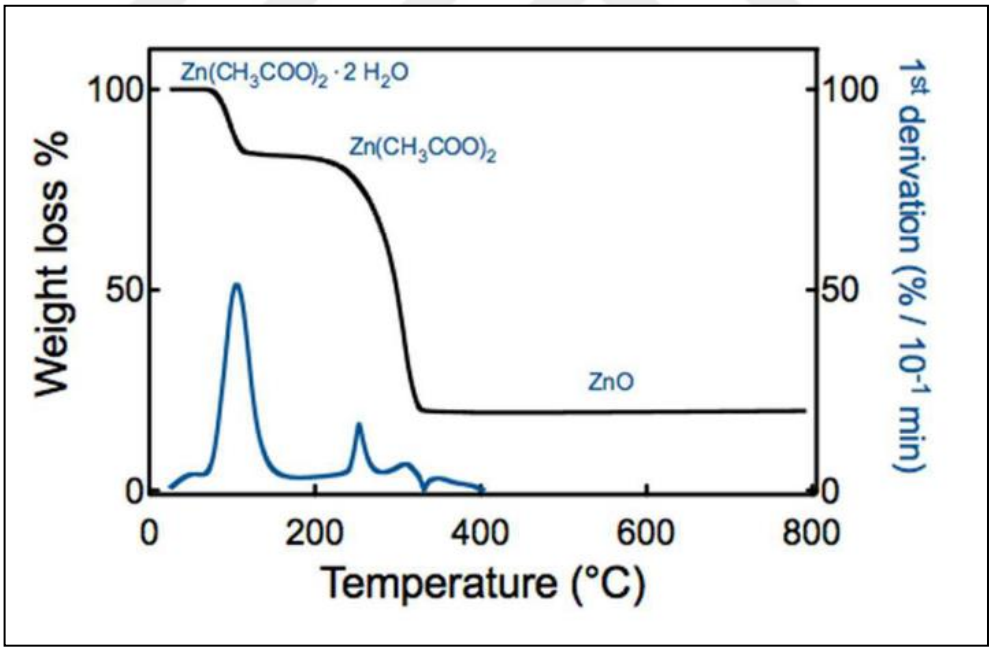

Figure 2.35. *Zincacetate TGA graph, [82].*

In the wiev of such information obtained in Table 2.9, the number of grains per unit area and the amount of moisture at that moment were calculated together with the liquid film thickness in the sample. The liquid film thickness seems to increase in time. However, the water in the system at this time consists of as hydrates. The important thing

here is the change of the film thickness in the second stage of sintering, that is, in the first 10 minutes. In Figure 2.32, the variation of the system density depending on the time show that the final intensity is approached after the first 18 minutes, [25]. Rahaman was making a mention on capillary force and says it is large and compressive for all amounts of liquid and decreases strongly with increasing values of h. h is distance between two spheres at sintering, [52] .

Scanning electron microscope (SEM) images show the internal structures of samples sintered for different times. In the image in Figure 2.36 a, it is seen that the grain size has finer grains compared to the other samples. In Figure 2.36 e and f, the grain sizes are getting larger. This situation was examined in more detail by dimensional analysis on the grains in the SEM images in ImageJ program. In Figure 2.37 a, the grain size distribution averages of the samples sintered at different times, as well as the lowest and highest values are shown. These are the results of three different SEM images. During the analysis, 70-250 measurements were taken from each SEM image. This process was applied for three SEM images for each separate period, and then the average of each particle size analysis was taken and the average, highest and lowest values of the values obtained as a result of all three SEM analyzes are shown. In the grain size analysis, it is seen that the grain growth is not much. Indeed, this is a feature of CSP. However, it is possible to say that grain growth increases after a certain period of time. Grain growth increased after 15 minutes and grain growth rate increased after 35 minutes. The pore size distributions are seen in the scatterplot in Figure 2.37 b. The pore size distributions were also measured similarly to the particle size distributions. It can be said that there is a general decrease in pore size distribution depending on the time. However, the pores may be located inward like channels, or the measured part may be only a visible part of the pore. It may not be accurate to give information about the pore size distribution in unpolished samples.

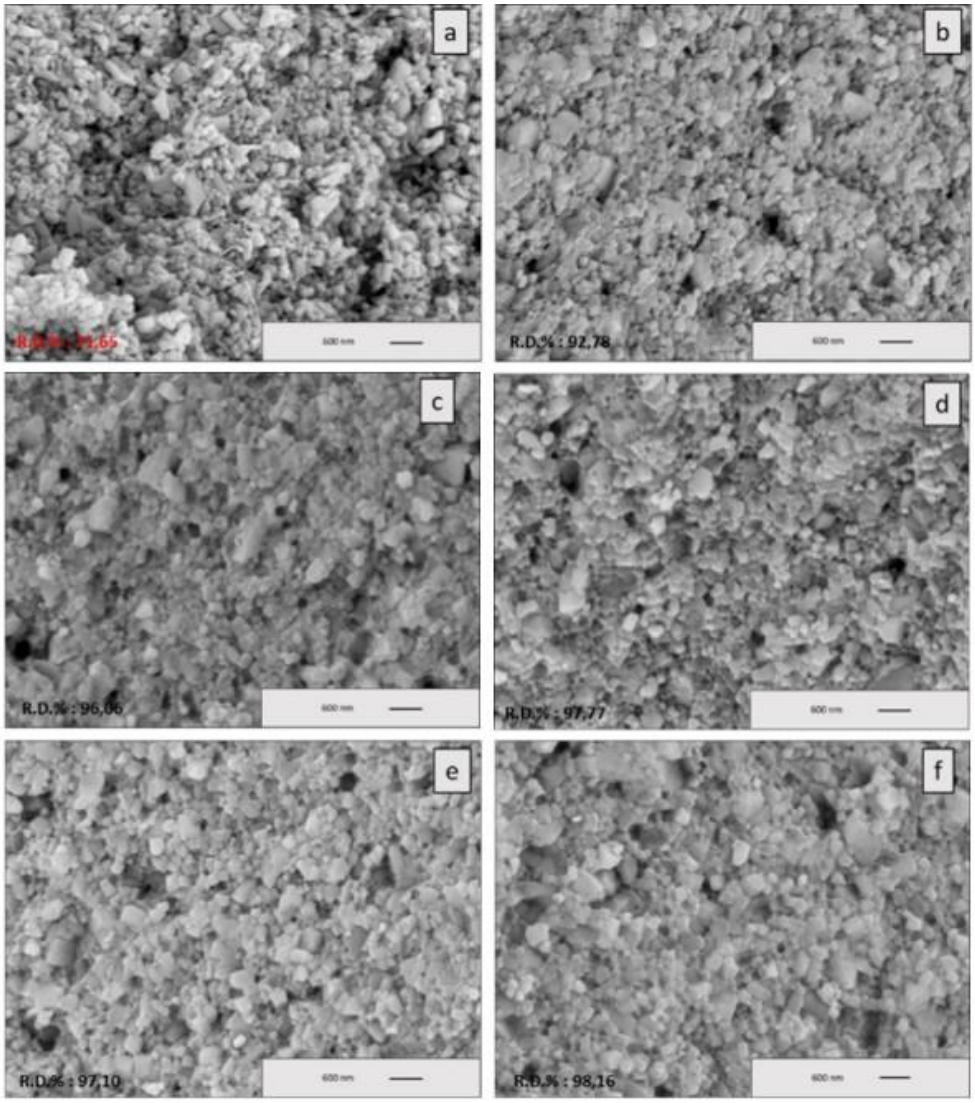

Figure 2.36. *Fracture surface BSE SEM images of samples sintered at different times. a)1min, b)5min, c)15min, d)25min, e)35min, f)45min*

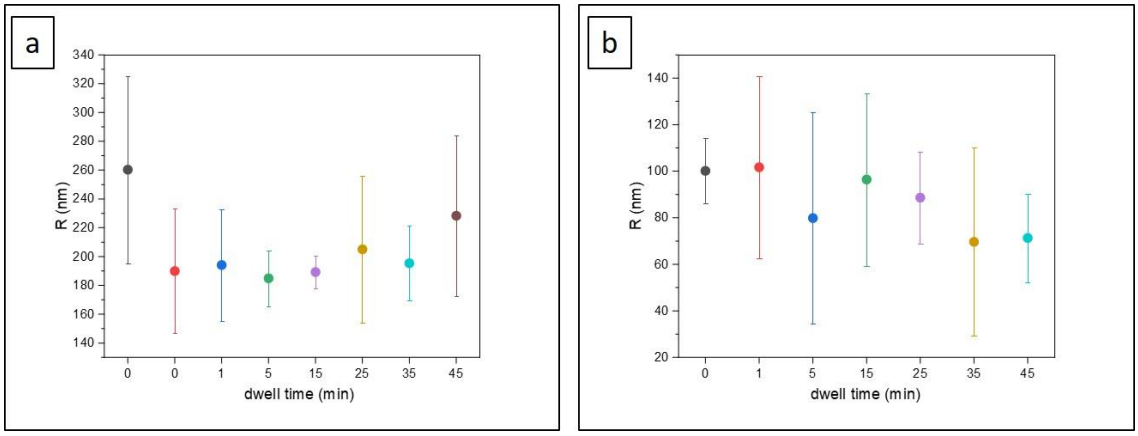

Figure 2.37. *Dependence of a) grain size and b) pore size on the dwell time.*

Based on the grain size data and its dependence to temperature and time, thermodynamics and kinetics analyses can be made about which mechanism is active depending on grain growth and growth rate. Rahaman formulated it as follows in his book about sintering [52]. Here, the value of n gives the diffusion rate. When n=2, there is interface reaction and when n=3 there is lattice diffusion. In the calculations made accordingly, the value of n was determined as 2. In some sources, it is stated that the n value is 3 in the analyzes made with CSP [19]. Temperature and temperature output rates may have changed the mechanism by adjusting this value.

$$G^n - G_0^n = kt \tag{2.6}$$

Equation showing the variation of grain growth depending on sintering time. G: grain size, G_0 initial grain size, k: sintering constant due to Arhenius equation

n=2

$$192^2 - 186^2 = 25k$$
$$k = 90.72$$

$$196^2 - 186^2 = 35k$$
$$k = 109$$

n=3

$$192^3 - 186^3 = 25k$$
$$k = 25721$$

$$196^3 - 186^3 = 35k$$
$$k = 31276$$

In the calculation made, it is seen that the k values are closer when n=2. In this case, it would be correct to take the value of n as 2. The k value here is the constant value in the Arhenius equation. Equation showing the connection between grain growth and activation energy.

$$G^n - G_0^n = AM\gamma t \exp\left(-\frac{\theta_b}{RT}\right) \tag{2.7}$$

When the Arhenius equation is examined, the slope of the log G – log t curve is expected to be around ½. It is seen that this value is low in the first parts of sintering. This is the reason why the grain growth is low in the first stage of sintering. In the last stage, the system energy caused grain growth. On the other hand, -Q/R gives the energy of the system. This value was determined as 40.7 kJ in our study. J. Guo et al. They determined this value as 43 kJ, [19]. The activation energy required for grain growth in conventional sintering is given as 200 kJ/mol. It is seen that the activation energy required for grain growth in the CSP system is quite low.

The study to find the film thickness as a result of batch tests was also carried out for the samples sintered at 300°C with CSP. However, although it was applied intermittently at 300°C, no results could be obtained. Because the pressure formed inside caused an explosion when the press pressure was removed. Only the sample cooled at the end of sintering could be examined. At the end of the sintering of the sample, after cooling at room temperature for 8 minutes, density and humidity measurements were made.

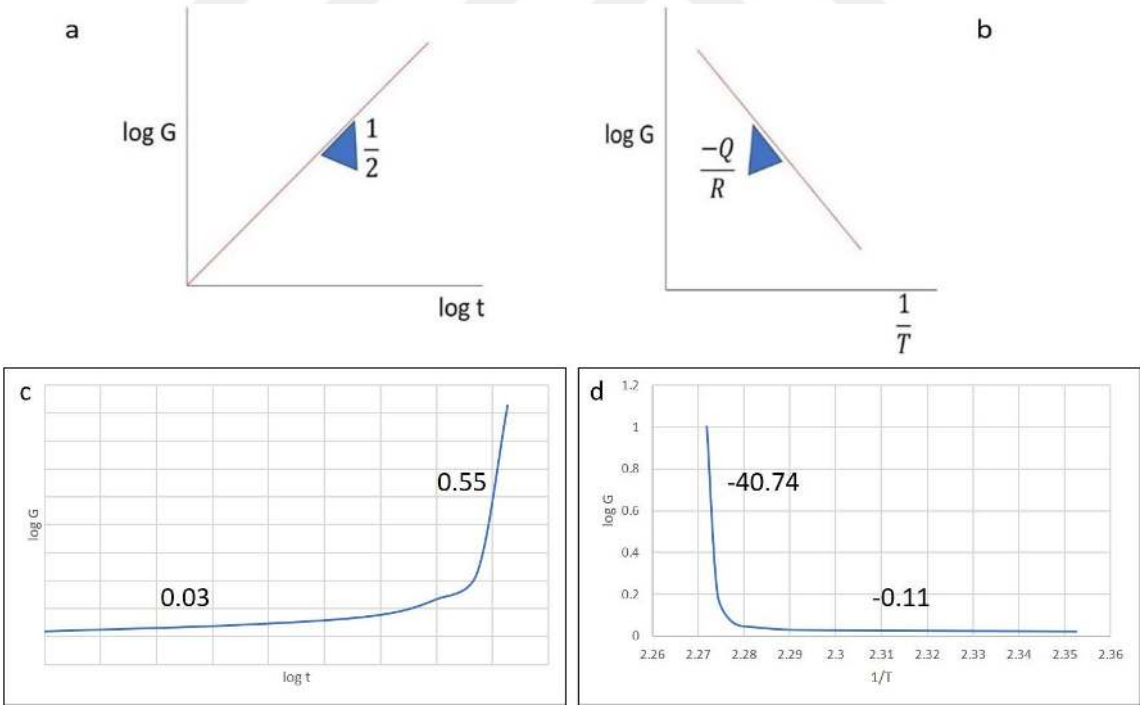

Figure 2.38. *Grain growth and grain growth activation energy graphs a) Grain growth graph expected slope, b) Activation energy required for grain growth, c) Slopes due to particle size distributions in samples produced with CSP, c) CSP produced and particle size distribution measured Calculation of activation energy in samples*

Accordingly, the sample theoretical density was 99.78 %TD. The sample was sintered at 300°C for 1 minute and under 250 MPa pressure, the entire sintering time was 50 minutes. The humidity measured with TG-DTA is 0.4968 %. Therefore, the film thickness was calculated as 0.004 nm at the end of the sintering process. This value is quite low when compared to the calculations made for samples sintered at 140°C. That is, in this case, the diffusion path decreases over time by sintering at higher temperatures. Also, bursting of samples during batch experiments indicates higher internal pressure with higher temperatures.

2.4. Conclusions

In order to understand the each processing parameters including particle size, sintering temperature, time, pressure, amount of liquid used, acid type, die diameter and die gas output range, role on the CSP process, the experiments were conducted in a systematic approach. It has been found that all of the parameters play a role during the CSP and influences the final densities of the products.

Two process conditions where the highest densities are achieved:

1- Water - Zinc acetate liquid with pH 5.5, pre-pressing with 89 MPa for 4 minutes at 100°C and afterwards 540 MPa, 50 minutes at 140°C.

2- Water - Zinc acetate liquid with pH 5.5, pre-pressing with 89 MPa for 4 minutes at 100°C and 250 MPa, 1 minute at 300°C.

For both process conditions, theoretical densities were more than 99.00 %. For the sample that was sintered at 140°C exhibited higher Vickers hardness of 2.98 than the sample sintered at 300°C.

Interrupted experiments were performed to analyze the CSP process from thermodynamics and kinetics perspective. Zinc acetate liquid with pH 5.5, pre-pressing with 89 MPa for 4 minutes at 100°C and afterwards 540 MPa, 50 minutes at 140°C samples. Film thickness calculations were done and even the sintering density is rising in time, film thickness is getting thicker, due to lack of evaporation at 140°C. This is changing at 300°C, since evaporation and acetate vaporization is available. The growth constant n was determined as ~2 that indicates the grain growth process is controlled by interface reaction during the CSP conditions, used in this study. Furthermore, the activation energy for the grain growth was determined as 40.7 kJ, that is consistent with the literature.

3. UNDERSTANDING THE RELATIONSHIP BETWEEN PROCESSING PARAMETERS OF THE CSP VIA DESIGN OF EXPERIMENT APPROACH

3.1. Introductıon

The CSP process, a type of sintering, has recently caught everyone's attention when it started to come to the forefront by Clieve A. Randall in 2016. It is important that sintering can be carried out at low temperatures, at about < 300˚C. How has this been achieved with CSP, while trying to reduce ceramic sintering temperatures from about 1000˚C for many years? The answer to this can be clarified by the process mechanism, which will be explained soonly. Another point is what we will encounter if we want to apply this process. Because, although the variables affecting the system and their effects have been studied for a while, the details and the examination of more than one effect are still in a weak structure.

Densification mechanism is a leading an in order of events as dissolution/rearrangement and recrystallization of the material in the presence of atransient phase as also mentioned by Sengul et al. and also many other researchers as well, [65].

The densification process with the CSP occurs under limited exposure to water vapor and/or aqueous solutions to provide a transient liquid phase that becomes evaporated under a uniaxial pressure with a controlled heating above 100°C, in a die that is not completely closed, [20]. It is different from the hydrothermal sintering by the way there is no sealing, means it’s not a closed system. The CSP utilizes aqueous solutions as transient solvents to aid densification by a mediated dissolution-precipitation process. There are several sequential stages at the CSP process. These stages are particle rearrangement actualizes under certain temperatures and pressures, with the help of liquid phase between particles, and then dissolution of the powder by the solvent. This solvent can be choosen up to powder properties. However, basically and mostly water can be used. pH of the solution can be adjusted due to dissolution kinetics. Particles dissolve and reprecipitate from a supersaturated solution under pressure and the established temperature. Variables that impact dissolution and precipitation process affect the sintering period at all, [18]. As discussed in the 2nd chapter of this thesis in detail, the variables that impact the CSP can be summarized as particle size, amount of water

addition, pH, solute addition, pressure applied, sintering temperature, holding time, and heating rates.

Funahashi et al. followed a very simple way while describing the mechanism of the CSP process and the necessary equipment [20]. The fact that the devices used are quite simple, this makes the method more interesting. Normal die and a press together with two hot plates controlled by a temperature controller, or a normal press and a die wrapped with an electrical controlled heater jacket is enough to get densification. As the temperatures to be reached do not exceed 300°C, there is usually no need for an extra oven. The material used is somewhat moistened before putting it into the mold. During sintering, this moisture inside is allowed to evaporate from the mold edges. First, the liquid phase aids the particle rearrangement under the applied pressure; the heating, pressure, and acidity accelerates chemical dissolution of the chemistry from the powders into the aqueous liquid phase. With continued heating, this liquid evaporates, driving a high concentration of the solute, and eventually supersaturates the liquid and drives the precipitation and subsequent a pseudo hydrothermal epitaxial crystal growth process that completes the final stages of sintering [20].

The solubility limit can also be affected by external physical conditions, such as temperature and pressure, and internal chemical parameters such as pH and the nature of the solvent also be effective [83]. The higher the solubility limit the higher the quantity of dissolved species taking part in the sintering [84]. By the experience, these parameters all can change due to the material itself and the process conditions as well. Grain size, grain morphology, particle size distribution, die sealing, rate of pressure application, and liquid phase viscosity are some other factors that can be discussed. When all parameters are handled separately and their effects on the system are examined, the map of what we should do can be formed gradually.

Main difference of the CSP from other pressure assisted sintering techniques is the usage of an aqeous phase. A little amount of liquid is used at the beginning, for moustirising the powder. Liquid phase coats the inorganic powder surface. Under external pressure, powders rearrange just as like forming bodies. Solute at the system and pH of the solution, controls the solubility of the inorganic material at the second stage of the process. Solubility is affected by solute, solvent, pH, pressure, temperature and time roughly as mentioned before. Corners of the powders dissolve under external pressure and after supersaturation value is reached, precipitation starts to occur. High stresses at

the contact points of the grains results in more dissolution rates at these points. Supersaturated material starts to settle down at less energy sites and the neck formation begins. Diffusion and pore modification are other sites for the saturated atoms as expressed by Sengul et al. [65]. Densification and grain growth can be actualized due to diffusion of atoms at this stage. Dissolution, adsorbtion and diffusion rates are important at this stage and these results are affected by the parameters which were mensioned before. As the solvent moves away from the system from the openings of the mold system, densification is higher and at the last stage highly dense ceramics can be obtained with CSP.

Mold and system design will of course be influential in the development of sintering. We are already familiar in our studies with the equipment adjustments for obtaining high density acquired samples without cracks. Besides, one of the parameters to be examined first has always been the powder particle size. Because it is known that grain size has a direct effect on sintering. Particle size analzes were done at Chapter 2.3.1 and not surprisingly, it was specified that samller particle size improves CSP theoretical densities.

The task of the fluid in the system is to provide diffusion. In order to obtain a homogeneous structure, the amount of water or the other solvent used must be large enough to surround the grains in the material. At the same time, adding more than a certain amount of liquid to the powder will cause sludge, and there may be problems during pressing. The rate of water amount to be used will vary depending on the material and grain size. The rates of water used in many studies vary between 1.0 % and 20.0 %. Kang et al. had found 4.0 wt % water is optimum emount to get highest density at their process conditions, [25]. On the other hand, the increase and decrease of the determined liquid ratio is also related to the rate of increase in temperature. We made some liquid ratio examinations and 7.33 wt % liquid was the optimum amount for sintering at 140˚C, at CSP studies.

T. Yu et al. describing the temperature – water amount relationship as if there is decrease at temperature ramp, the water amount should be increased. They could get 93.4 % theoritical density with ZnO, by increasing water amount, [85]. The reason why the water ratio is associated with the temperature increase is that evaporation increases at low temperature increases and there is not enough liquid in the system for the last stage of sintering. If it will affect the amount of liquid and ensure the development of diffusion, it

is the type of liquid used. First of all, it should be determined which liquid to use. Water is the most approprite liquid for our system with ZnO. On the other hand, of course, the pH of this liquid will also be important for the process.

Since it is the solubility of the material that is important, acid or base solutions can be used. J.P Maria tells about cationic group doped solution is also can be used as like ZnO material with the zinc acetate solution, [86]. In the CSP process of ZnO, an acidic solution is used instead of just water to prevent hydrolysis, [17].

It was found that adding acetic acid to an aqueous solution dramatically changed both the densities and the grain microstructures of the ZnO ceramics, [20].

For cold sintering of MgO, some different acids were examined and Table 3.1 shows the densification results. 10 % acetic acid gives best densification for the MgO with the given experiment conditions, [87].

Table 3.1. *CSP results of sintered MgO at 110°C and 530 MPa, [87].*

Solutions	Liquid phase content (%)	Density (g/cm^3)	Normalized density to pure MgO (%)
10% acetic acid	13	2.81	79%
10% citric acid	6	2.74	77%
pure water	16	2.76	77%
50% methanol-water	15	2.66	74%
5% nitric acid	5	2.36	66%

Kang et al. studied different pH values of the same acetate containing solutions and had nearly the same densities around 98.00 – 99.00 % theoritical. They claimed that CSP process results are independent from the pH, if Zn^{2+} and acetate ions are present in solution [25].

Moreover, we know that pH of the solvent strongly affects the dissolution kinetics and lower values of pH increase the kinetics of dissolution of ZnO in aqueous solution as Grasso et al. indicates [17]. Although it is stated that it is not necessary, pH is also an important parameter in terms of solubility. Studies have shown that pH is an effective parameter. We used pH 5.5 as the optimum pH for ZnO in Chapter 2, but it would be better to investigate this parameter together with other variables more systematically. Since CSP is a pressure and temperature based process, these two parameters are at least as important as the other parameters.

If there is no selaing at the system Kang says pressure should be higher than a sealed system, to be able to reach the hydrothermal conditions [25]. He determined 140 MPa minimum pressure is needed to can reach hydrothermal conditions, otherwise densities are under ~ 85 % [25]. Kang has experienced that if the pressure is 280 MPa, full densisfication could be done due to die sealing conditions [87]. The remarkable point is that loading is important around the critical pressure value that will provide the thermodynamic conditions. At this point, densification is more sensitive to pressure. We mensioned minimum 250 MPa pressure should be used to get densified ZnO ceramics at Chapter 2. Optimum conditions were observed with the pressure of 539MPa. At our previous studies, for sintering at 135˚C, prssures of 530 – 540 – 560 MPa were investigated, see at Figure 2.12. Highest density could be obtained at 540 MPa for sintering at 140˚C, on the other hand, fort the sintering temperature of 300˚C, it was observed theoritical density was decreasing by increament of pressure (200MPa to 400MPa), see at Figure 2.15. Kang examined many variables, including insulation, in his thesis. Some of the samples were poorly densified because of the evaporation of the liquid phase from the die wall and punch gap. He then defined that hydrothermal condition and densification would then rely on die sealing conditions. Many researchers agree that hydrothermal conditions are the most important mechanism for cold sintering of the material. However, in his detailed study of Kang, he mentioned at pressures above 300 MPa, full densification can be achieved even without intentional sealing [87]. When we made experiments on insulation, high densities couldn't be obtained when insulation was applied. However, other determination was importance of gas output from the die outlet to ensure essential hydrothermal conditions for the sintering time.

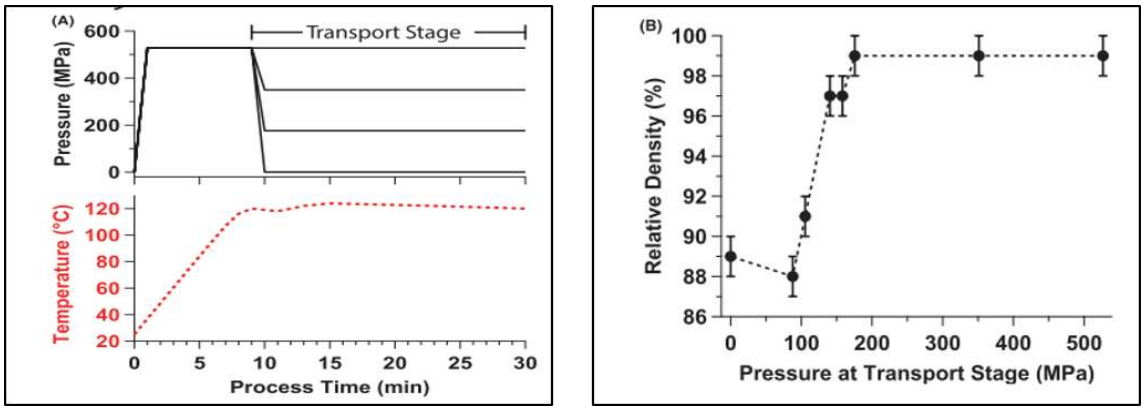

Figure 3.1. *a, Pressure and temperature profiles for densification a series of CSP ZnO pellets and b, final density as a function of pressure at the transport stage*

It is believed to have a transition stage pressure to observe densities up to 99.00 % and this pressure is related with the temperature. Kang et al. described this relationship due to experiments done with ZnO material. He found 140 MPa pressure is enough for the densification of ZnO material with their own equipment. And this relationship is also related with the pressure temperature diagram [25].

However, hydrothermal conditions are not the only effect of pressure in the CSP process. At the same time, it acts as a factor that provides condensation by mechanically bringing the particles closer to each other. Kang et al. explain this situation as follows; temperature and pressure will provide solubility, but alone will not be sufficient for densifiying. Densification can be achieved at different values such as 350 MPa pressure or 530 MPa pressure, depending on the equipment used in cold sintering process studies carried out under different conditions [25,39].

In the cold sintering process, temperatures between 100 and 300°C are mentioned. Since cold sintering process is a dissolution precipitation process, solubility again is one of the main factors. It is known that temperature increase enhances solubility of particles. In equation 2.5, it has been seen that solubility is increasing by the temperature. The effect of temperature on condensation is not just solubility, in fact the initial driving force required for condensation comes from temperature and pressure energies. Therefore, a critical temperature is required for sintering to occur. This temperature must be modified to achieve higher densities.

Biesuz et al. expressed that the temperature should be between 100°C and 300°C, if the transient liquid is water as usual. The temperature selection is due to the phase diagram of the water as like pressure selection [63]. Gonzalez-Julian et al. gave some more specific information on temperature selection. He mentioned about onset temperature of densification as the starting of the shrinkage as a function of temperature. This temperature can be more less if the pressure is getting higher. However, pressure is not the only effective parameter. The liquid phase used is also very effective at the beginning of sintering. Even when water containing acetate is used instead of water, it has been observed that sintering begins even at room temperature under sufficient pressure [22].

For the ZnO samples cold sintered temperatures are changing from 120°C to about 300°C in many studies. In some cases related properties of the material due to sintering temperature [19,24]. Sengul et al. made some simulations and saw that 300°C temperature

was a need for the migration of the Zn^{2+} ions to change the site, but it was also indicated that it can be lower temperatures for the experimental trials [65].

We consolidated pre-trials for our experiments and choosed the center point of the temperature when we saw the maksimum density. This temperature was 135°C in our experiments. Upper and lower limits had to be choosen with a correlation with the conditions that all results had to give an useful density result. The holding time at the temperature determined during sintering gains importance in terms of completing the reactions.

In conventional sintering, the sintering and temperature ramp time can be quite long. However, in the CSP process, the sintering process takes place in 1 hour or even less. Considering that the temperatures are also low, this is a situation that can save a lot of energy consumed. At Figures 3.1 and 3.2, it can be seen that at some conditions, theoretical densities higher than 90.00 % could be reached in less that 30 minutes. The sintering time will also be effective in the microstructure development.

$$G^N - G_0^N = tk_0\, exp(Q\ /\ RT) \tag{3.1}$$

Equation 3.3. show coarsening of particles, [52]. G_0 is initial grain size, t is the sintering time, and N is the kinetic grain growth exponent, k_0 is a constant, Q is the apparent activation energy for grain growth, R is the gas constant, and T is the absolute temperature. Since grain coarsening is a function of time and temperature, dwell time at the sintering temperature is effective for coarsening. Grain size is an important factor for the materials to get the desired properties. If the desired material property is closely related to the grain size, the temperature and time must be carefully controlled. For materials with fine grain size, low temperature and short time will prevent grain size coarsening. Rahaman is giving example to this phenomena in his book as, the electrical breakdown strength of ZnO varistors used in electrical surge suppressors increases as 1/G, while the dielectric constant of $BaTiO_3$ capacitors is found to increase with decreasing grain size, [52].

At most publications, they are agree that CSP process is taking place in a very short period of time. That means in first 10 to 20 minutes material reaches more than 90.00 % density already. For sintering at room temperature, we see from some studies that most densification occurs within the first 10 min, then approaches completion in about 20 min., [86]. X. Kang et al also found the similar results that material was densified nearly fully

in 30 minutes as seen in Figure 3.2. In some cases, time is extended up to 1 hour or more at some studies, [20]. At the instant analzes in our studies, it was observed theoretical densisties are not changing significantly after about 20th minute of sintering at 140˚C, see at Table 2.9. However, this time may vary depending on temperature and other factors. In this section, it will be useful to examine the density change by making studies at different times in relation with the other variables.

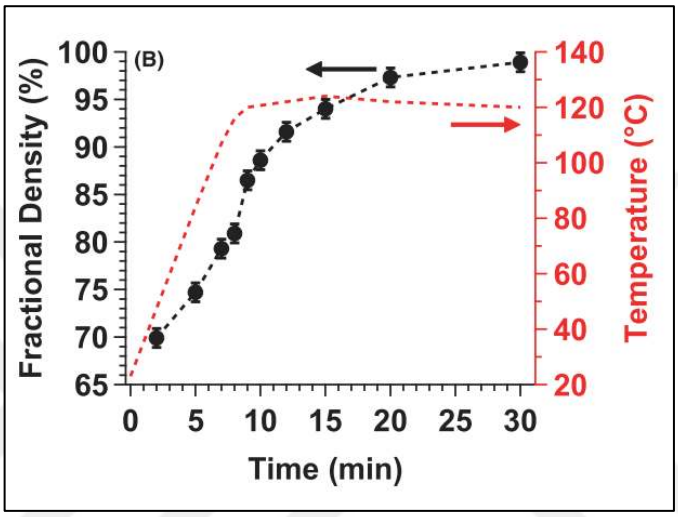

Figure 3.2. *Sintering of ZnO due to time (0.86 mol/L $Zn(OAc)_2$, 4 wt. % liquid phase, 120°C temperature, 530 MPa uniaxial pressure) [25].*

Since very high temperatures are reached during conventional sintering, the ramp rate used becomes important as mentioned before. With a slow ramp rate, the heat exposure time of the material is prolonged and diffusion begins, or vice versa, the grain size can be changed when ramp rate is too fast. Ramp rates of 5 to 80°C/min were used by many researches for CSP [18,24,88,89]. In some cases it was observed heating rate can change some properties of the final product.

J. Guo and friends described CSP with a slow heating rate improved the permittivity of the some of the $(LiBi)_{0.5}MoO_4$ samples, [18]. On the other hand, according to the information described, in some cases, since the slow heating rate will cause more evaporation, there will be not enough liquid required for diffusion in the system and this may adversely affect the sintering process, [85].

When the variables are examined one by one, it is seen that there are different opinions and/or study results as well. In this case, it is obvious that the studies will be continued any way. Examining the variables from a systematic point of view may provide

a different interpretation, and in fact, the existence of all studies within themselves can be discussed. To be well versed in most effective variables on CSP, structure-property relationships can be predominated. For this reason, many variables were examined separately in the studies carried out. Although these have been identified in the previous chapters, it is clear that there are more complex interactions within the system. For this reason, the system has been examined by examining the interactions between the variables with a different methodology. Respose surface methodology was used for this study. When determined parameters are examined, we see that there are actually ideas and studies related to all of them. However, there are very few studies in which their effects and all parameters are studied systematically together.

Response surface methodolgy (RSM) is a statistical method which can describe the relationship between the different factors at different levels, and the responses demonstrating this relationship with a polynominal.

Assuming all factors are measurable, the response surface can be explained using the following equation, Equation 3.2 response surface equation:

$$y = f(x_1, x_2, x_3, \ldots) \tag{3.2}$$

where y is response and x_1 to x_n are process variables or inputs affecting the y response. Basically, RSM consist of three stages: 1)designing and performing the experiments, 2)RSM modeling using regression and 3) optimisation, [90].

It has been described above that pressure and temperature are together important for hydrothermal conditions. At the same time, other parameters have different effects together. However, studies have not sufficiently examined their interactions with each other. When all parameters are evaluated, the parameters that affect or have little effect on the system should be evaluated. This review can be done if the parameters can be analyzed together. Although variables have been examined and interpreted in the literature, there is no examination of the multiple effects of these variables.

At this thesis, an experimental set up was prepared to examine the interactions together. This experimental set was determined with the Minitab program and response surface methodology was used for analyzes. ZnO is the model system for the investigations. Temperature, time, pressure, humidity and pH were choosen as variables to be examined. Other variables were kept constant due to already determined effects, such as importance of particle size on sintering. Center points of the variables were

choosen due to Chapter 2, since density observation was a must for the statistical analyzes. Limiting points were choosen in a wide range and the terminal experiments of the given experimental set were tasted. For example, 7.00 wt % liquid is the centre point, while the limiting points are 6.33 wt % for minimum and 7.66 wt % maximum at the experimental design. Minimum liquid amount can give a density result at many points of the given experimental set from the program, but it will be hard to work at a point with maximum pressure and temperature points, all together with minimum liquid amount. Because extrusion with pressure and vaporisation would work together to inhibit sintering. So Table 3.2 was evaluated with the prediction of Chapter 2 and some tests of the limiting points for the given experimental design.

It is critical to understand the effect of each processing parameters under different conditions and also binary effects of the varibles, as well. There is no observation at the literature on binary effects and effectiveness of the variables. Statistical measurements were not done yet with a program that is used only for these purposes. Consequently, the research objective of this chapter was to investigate process parameters affect on CSP, together with a statistically designed and modeling program. Effects of the variables can be determined as an equation, so that density estimation can be done for a given condition.

This situation was examined in the first part of the thesis and high pressure and optimum temperature were determined. We could reach the optimum conditions as when 7.33 % liq. at pH 5.5, with zinc acetate was used for moistining, pre-pressing with 89 MPa for 4 minutes at 100°C and afterwards 540 MPa, 50 minutes at 140°C. These conditions surely not the only one choice to get high theoritical densities. Studies have shown that the sample sintered at 300˚C can also have high densities. This is exactly what is related to hydrothermal conditions. The sample was sintered at 300°C for 1 minute and under 250 MPa pressure, and the entire sintering time was 50 minutes, more than 99.00 % T.D. could be also achieved. But sintering time couldn't be prolonged, because of the cracking of the samples.

3.2. Materials and Methods

3.2.1. Cold sintering process

Commercially available ZnO powder (Sigma Aldrich, 99-100% purity, average particles size ~300 nm), zinc acetate and citric acid were used as raw materials.

Lamination press, Carver Inc., with heating plates up to 342°C was used for heating and pressing the samples. Molds were not sealed during the sintering operation. Moisturising of the ZnO powder was made with an alumina mortar and pestle, with 2 minutes crushing. The powder was pre-pressed by hand press by 200 kgf/cm^2, for 2 min. Pre-pressed mold was taken to pre-heated lamination press for the cold sintering process. Initial temperature of the heated press was 100˚C. Heating ramp rate was constant for all trials and was 6.6 ˚C/min. Final temperatue, time of sintering, pressure, liquid amount and pH of the used liquid were adjusted cccording to the test set given by the Minitab Programm.

3.2.2. Fabrication of ZnO samples

In order to investigate the effect of five parameters, intervals of the parameters to be invesitgated were determined with the pre-experiments. ZnO powder was moistured within the morter by pH adjusted solution. pH 5.5 was selected due to past studies of cold sintering of ZnO. The initial studies were persented at the previous section. Moistured powder was put into the mold and pre-pressing with 200 kgf/cm^2 was applied to the samples. The mold with pre-pressed pellet was transmitted to the pre-heated lamination press. At previos works it was shown that pre-pressing is preventing some cracks at the final product. Two-step pressing/sintering was utilized to the samples: 1)4 minutes dwell time at 89 MPa, 100°C, then 2) 50 minutes dwell time at 540MPa, 135°C was the best processing conditions that was discovered during pre-experiments. Density of the samples were measured both geometrically and by the Archimedes method as well. To ensure the accuracy and repeatibility, modelled test was repeated three times and two of them were reported as the test results as repetation of the model.

3.2.3. Design of experiment

Experiments were designed by responce surface methodology (RSM) using Minitab software. RSM provided to be suitable for determination of the interaction between the independent variables, modeling the system mathematically, and saving time and cost by reducing the number of trials For this purpose, Cental Composite Design (CCD) was selected which is well suited for fitting of quadratic surfaces and it is also suitable for optimisation of the process. This method is based on two level full factorial and partial experiment design. Experimental variables were considered over five levels.

Alpha value is -1.414 to +1.414. The selcted variables with their levels are listed in Table 3.2.

Table 3.2. *Selected variables with their levels*

FACTOR	NAME	LOW	HIGH
A	Temperature (°C)	125	145
B	Pressure (MPa)	525	555
C	Time (min.)	40	60
D	pH	5.1	5.9
E	Moisture (wt %)	6.33	7.66

In the experimental design, there are 16 cube points, 5 center points in cube, 10 axial points at the two-level factorial, and it is half fraction central composite design. α is 1.414 choosen as indicated before and it indicates borderline of the points from the choosen 5 factors' therminal points. The measured responses were theoretical density measurements of the cold sintered ZnO samples. The goal of this study is to figure out the optimum condition of the variables which results in maximum values of the aforamentioned responses. For this purpose, Design of Experiments (DOE) was conducted on the suggested models. Table 3.3 shows the designed experiments order and conditiones that were established by the software, with the responses already.

3.3. Results and Discussion

31 experiments were done according to Table 3.3. The experiments were done due to given placement and last two columns are the responses of the tests, named T.D. – 1^{st} % and T.D. – 2^{nd} % . All the results were obtained over 90.00 % of the theoretical densities which demonstrate the computable response functional design. Density results at the table all were done with Archimedes method. When we compute these values at the DOE and analyze it with the software, we obtained a regression equation as mentined below.

Normal plot of the standardized effects show us general results of the effective variables. Red square dots indicate the variables that are effective. Sometimes variables are more effective in the sytem in binary or square form as well.

At the normal plot of the standardizied effects it can be seen clearly that square of temperature, square of time and pH are effectable on the model. Pressure x time, temperature x time, temperature x pressure and time x moisture have significant effects

on the model. These effectiveness can be seen clearly also at the Annova table as well. According to final annova table, lineer effect of the pH is the most effective factor on the percentage of the theoretical density. F 0.05 ; 1.00 ; 49 = 4.08 < F_{pH} = 182.14 shows that pH is effective on the model. Square effect of the temperature, time and pH can be also seen from the Annova table as well. Interaction effects of the temperature x pressure, temperature x time, pressure x time and time x moisture remain important according to table. The effect of pH on the system will be discussed in detail later.

Table 3.3. *Designed experimenral run and the responses*

Std Order	Run Order	Pt Type	Blocks	Temp (°C)	Pressure (Mpa)	time (min.)	pH	Moisture (wt. %)	T. D. - 1st (%)	T. D. - 2nd (%)
1	1	1	1	125	525	40	5.1	7.66	91.41	91.67
2	2	1	1	145	525	40	5.1	6.33	94.58	93.51
3	3	1	1	125	555	40	5.1	6.33	94.82	94.90
4	4	1	1	145	555	40	5.1	7.66	94.47	94.84
5	5	1	1	125	525	60	5.1	6.33	93.68	93.95
6	6	1	1	145	525	60	5.1	7.66	95.65	95.28
7	7	1	1	125	555	60	5.1	7.66	94.09	94.36
8	8	1	1	145	555	60	5.1	6.33	92.78	92.60
9	9	1	1	125	525	40	5.9	6.33	95.53	95.56
10	10	1	1	145	525	40	5.9	7.66	97.32	97.29
11	11	1	1	125	555	40	5.9	7.66	96.71	96.43
12	12	1	1	145	555	40	5.9	6.33	97.94	98.47
13	13	1	1	125	525	60	5.9	7.66	97.32	97.53
14	14	1	1	145	525	60	5.9	6.33	97.25	96.43
15	15	1	1	125	555	60	5.9	6.33	96.46	96.07
16	16	1	1	145	555	60	5.9	7.66	95.04	95.67
17	17	-1	1	121	540	50	5.5	7.00	98.52	97.33
18	18	-1	1	149	540	50	5.5	7.00	96.20	96.38
19	19	-1	1	135	519	50	5.5	7.00	95.80	95.33
20	20	-1	1	135	561	50	5.5	7.00	96.75	97.07
21	21	-1	1	135	540	36	5.5	7.00	96.33	96.05
22	22	-1	1	135	540	64	5.5	7.00	95.03	94.44
23	23	-1	1	135	540	50	4.9	7.00	92.82	92.55
24	24	-1	1	135	540	50	6.1	7.00	96.23	97.20
25	25	-1	1	135	540	50	5.5	6.05	95.23	94.76
26	26	-1	1	135	540	50	5.5	7.94	96.43	96.02
27	27	0	1	135	540	50	5.5	7.00	95.08	95.42
28	28	0	1	135	540	50	5.5	7.00	94.64	95.98
29	29	0	1	135	540	50	5.5	7.00	95.44	94.99
30	30	0	1	135	540	50	5.5	7.00	96.67	96.55
31	31	0	1	135	540	50	5.5	7.00	96.06	96.30

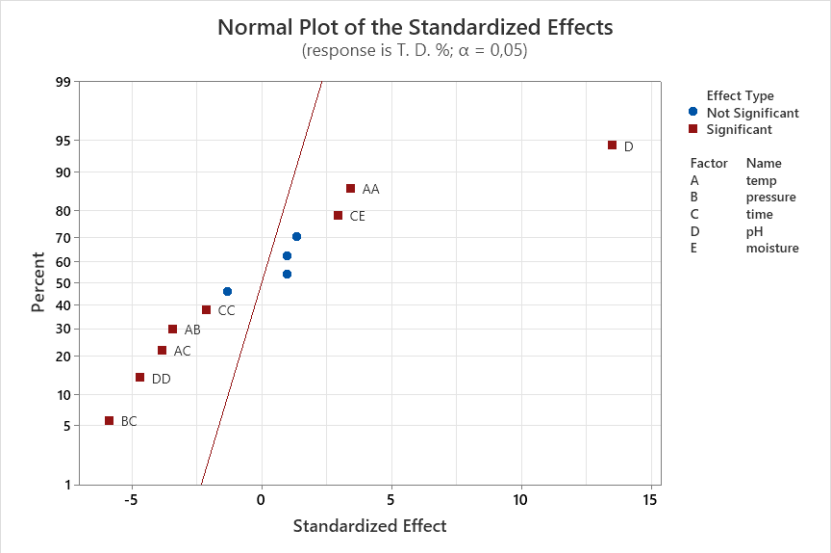

Figure 3.3. *Normal Plot of the standardized effects*

Table 3.4. *Annova table of the variables, analysis of variance*

Source	**DF**	**Adj SS**	**Adj MS**	**F-Value**	**P-Value**
Model	12	124.956	10.4130	24.34	0.000
Linear	5	80.212	16.0425	37.50	0.000
temp	1	0.401	0.4013	0.94	0.338
pressure	1	0.755	0.7546	1.76	0.190
time	1	0.730	0.7303	1.71	0.197
pH	1	77.921	77.9206	182.14	0.000
moisture	1	0.406	0.4057	0.95	0.335
Square	3	14.993	4.9975	11.68	0.000
temp*temp	1	5.047	5.0465	11.80	0.001
time*time	1	1.918	1.9181	4.48	0.039
pH*pH	1	9.414	9.4140	22.01	0.000
2-Way Interaction	4	29.751	7.4378	17.39	0.000
temp*pressure	1	5.032	5.0324	11.76	0.001
temp*time	1	6.257	6.2570	14.63	0.000
pressure*time	1	14.756	14.7560	34.49	0.000
time*moisture	1	3.706	3.7060	8.66	0.005
Error	49	20.962	0.4278		
Lack-of-Fit	41	16.757	0.4087	0.78	0.723
Pure Error	8	4.206	0.5257		
Total	61	145.919			

Analysis of variance has three assumptions. The errors are normally distributed, the errors have constant variance, and the errors are independent of each other. We see the effective linear, square and 2-way interactions. P values are close to zero means more effective value it is. Moisture had taken as linear effect even the P value is higher, but it is effective at the 2-way interactions already. It's the same with time, pressure and temperature. But we see that interactions of the variables are much more important as it should be. We do not see pH x temperature effect at the table although we know they together effect the solubility together. Sengul's assumption is, at low temperatures, some of the acetate can not decompose and prevents diffusion from grain boundaries. While 300°C is enough for decomposition, 120°C is not enough. But also she is agree that it may change due to experimental conditions, [66]. Although it does not appear to be a dual effect, separately pH and pressure are essential factors for the CSP process as predicted in this study (please Chp. 2) and also by other researchers previously, [20]. While time x moisture are affective parameters, for 2-way interactions, pressure x moisture seems not affective. Pressure is needed for extrusion of water from the sytem, so that grains come closer to observe densification. But degree of importance to the system kinetics come through here.

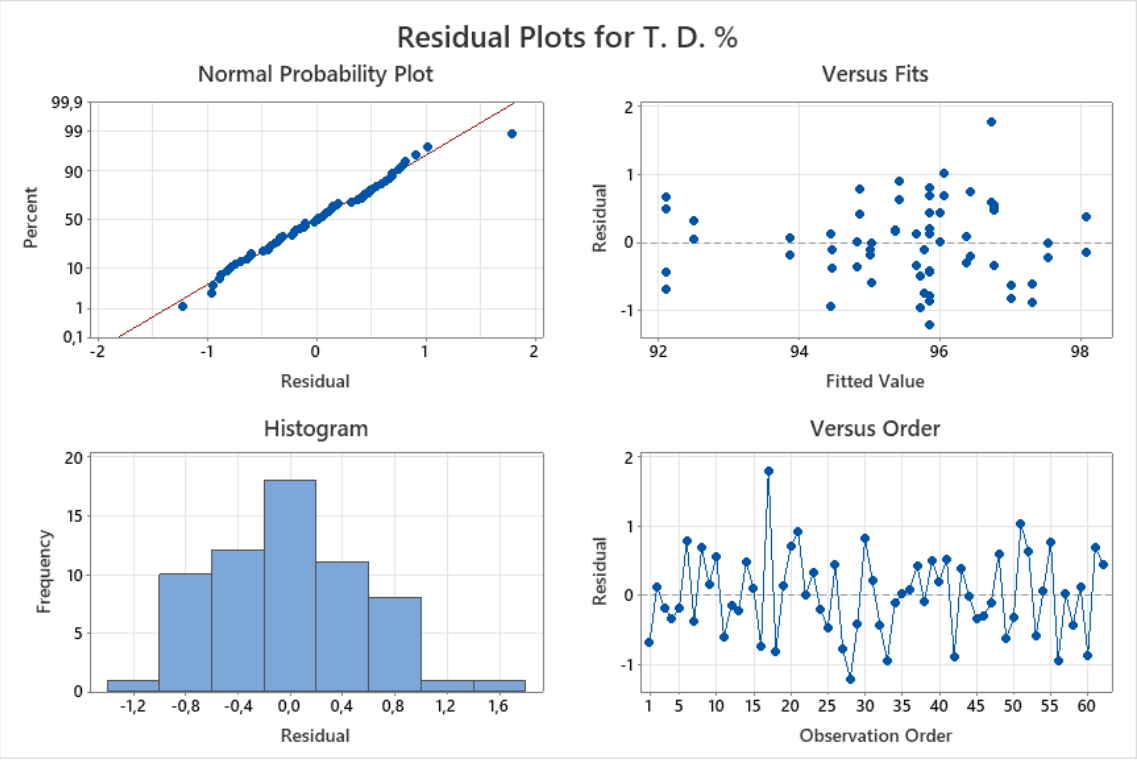

Figure 3.4. *Residual plots of the model*

Normal probability plot and histogram of residuals shows the normal plots of the residuals and can be seen from the Figure 3.3. It can be determined residuals are spreaded normally. According to versus fits graph, it can be seen that residuals have constant variance. According to versus order graph, it is observed that errors are independent of each other. It has all been detected from Table 3.5 that model may contain accurate results, so it would be appropriate to examine the r^2 value, that is explaining the total variability. R^2 adjusted value of the model is 82.12% and it is an approprite value for an agrreable model explanation. 82.12 % of the total variability is explained with the given experimental design results. R^2 is called the coefficient of determination and is the square of the correlation coefficient. Model is explained the amount of the variability in the data with 82.12 % by the model.

Table 3.5. *Model summary values*

S	R-sq	R-sq(adj)	R-sq(pred)
0.654065	85.63%	82.12%	77.43%

Predicted value of the theoretical density can be calculated by using following regulation equation, Equation 3.3. Uncoded unit of the variables shows every given unit is suitable with the equation that were used as in the model. Regression Equation in Uncoded Units seen at Equation 3.3 :

T.D. % = -303.4 + 0.285 temp + 0.592 pressure + 2.984 time + 51.3 pH - 2.407 moisture + 0.00509 temp*temp - 0.00314 time*time- 4.345 pH*pH - 0.002644 temp*pressure - 0.00442 temp*time - 0.004527 pressure*time + 0.0512 time*moisture (3.3)

The reviewed results of the model observation above show appropriate for the further analysis evaluation. It was started by analyzing the binary interactions. Pressure x time, temperature x time, temperature x pressure and time x moisture were shown to be effective on the model.

Time x moisture binary effect was the first determined interaction of the model. There appear to be two usable results. The peaks of the curves are where the density is highest. When the moisture is 7.66 %, 55 minutes sintering gives maksimum theoritical density and while the moisture is 6.33 % wt., best time for sintering is 42 minutes, as seen from the curves below. Since it is better to set the sintering time shorter, 42 minutes

sintering with 6.33 % wt moisture can be used to get the highest theoretical density for the given experimental design. On the other way, 43 minutes for the 6.33 % wt moisture, 47 minutes for the 6.99 % wt and 54 minutes for the 7.66 % wt moisture shows highest theoretical density ratios. If it is not possible to controll moisture amount well enough, it can be possible to work for 47 minutes sintering times to get best theoretical density regardless of humidity.

While the water vaporization does continue during the CSP, time is important to have enough or optimum value of moisture inside the system. This is also related with the temperature and ramp rate as discussed before. In our experiments 6.6°C/min. ramp rate was used for all the experiments. However, when temperature is constant, and its 145°C at the experiment numbers 4, 8, 12 and 16, for different pH values, for less sintering time, densities are higher even the moisture amounts are not the same. Floyd et al. made some experiments for this phenomenom and after some TGA analysis he observed after 30 minutes, there is so little amount of water in the system and even process time was as long as more 5.5 hours, densities could reach up to 97.00 % with that residual little amount of water, [89].

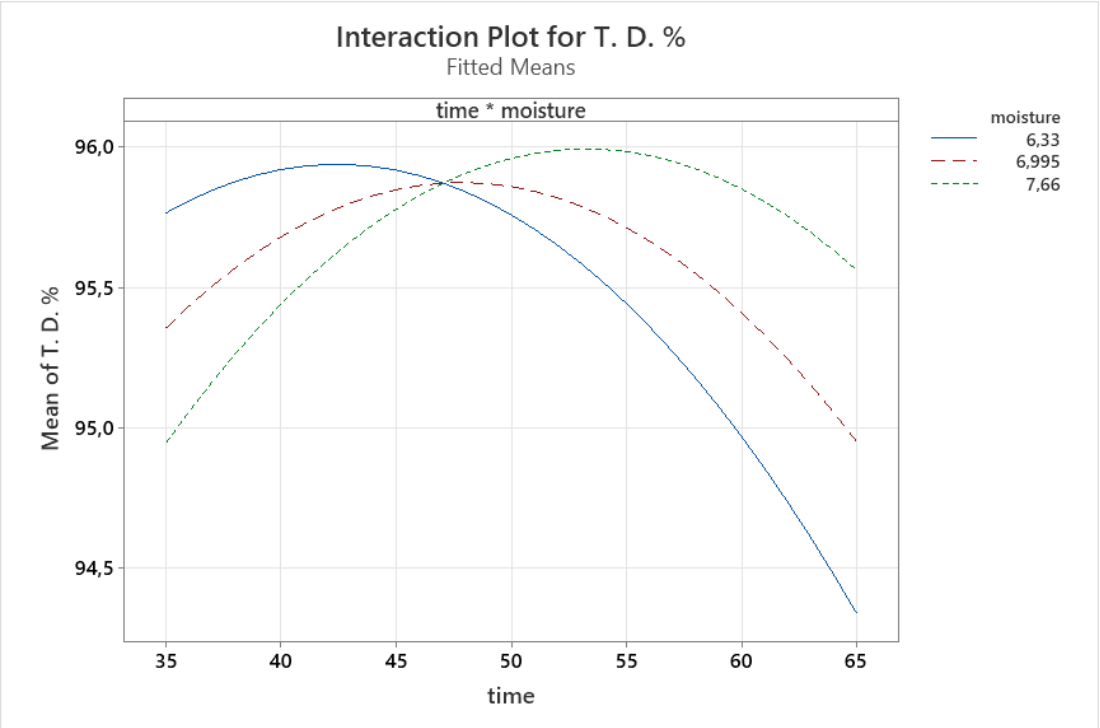

Figure 3.5. *Binary interaction plot of time x moisture.*

Figure 3.6 show that 555 MPa pressure and the 120°C sintering temperature give maksimum density at the experiments. Second option that is close theoritical density to get a close theoritical density is 525 MPa density with the temperature of 150°C as well. If it is important to work at lower temperature instead of lower pressure value, first option should be preferred.

When temperature and pressure are together, necessary conditions for sintering occur. In a hydrothermal vessel, sintering will not occur without isostatic pressure. Therefore, isostatic pressure at the appropriate temperature creates the driving force for sintering. Kang et al. requires this pressure gives an additional driving force by extruding the liquid and adduct particle centers together, [25].

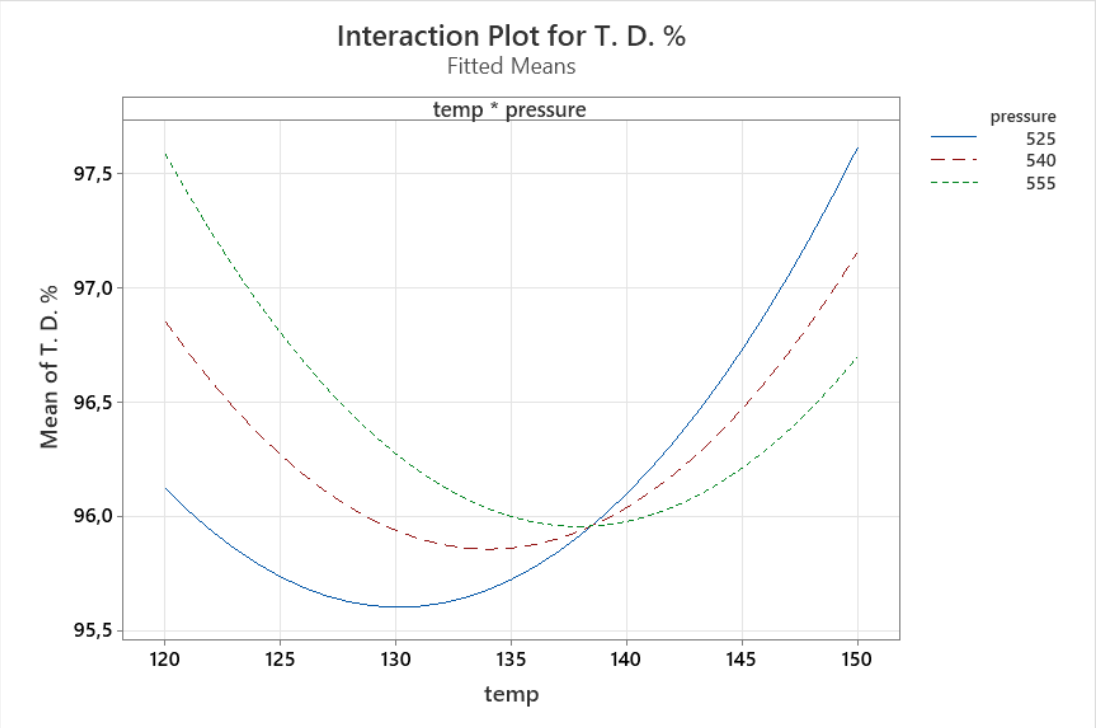

Figure 3.6. *Binary interaction plot of temperature x pressure.*

Temperature x time plot shows that it is available to reach theoretical densities up to 97.00 %, with 40 minutes waiting at 150°C temperatue or 50 minutes waiting at 150°C, Figure 3.7. Funahashi et al. reported that temperature and time were associated with grain growth and this situation was similar to liquid phase sintering, [20]. At Table 3.6, eight of the results were discussed. Two different pH studies, 5.1 and 5.9 are discussed in themselves. For pH 5.1 when we look at the results number 1 and 6 have the same moisture. For number 1, 125°C and 40 minutes and for number 6, 145°C and 60 minutes.

Theoretical densities are 91.00 % and 95.00 % respectively. But when moisture is less, the results become nearly the same at experiment numbers 2 and 5. When we do the same perspective for the pH 5.9 samples, its nearly the same with higher densities as seen. But when the pH is 5.9, moisture percentage is affecting the system conversely, means densities are higher with higher moisture percentage. This may be related with the pressure, temperature and moisture are all affecting the system together. If the pH is linearly affecting the system and as pH 5.9 is the best pH to work with, it's a normal result to have little higher results, and for the ideal pH, time and temperature are not so effective together.

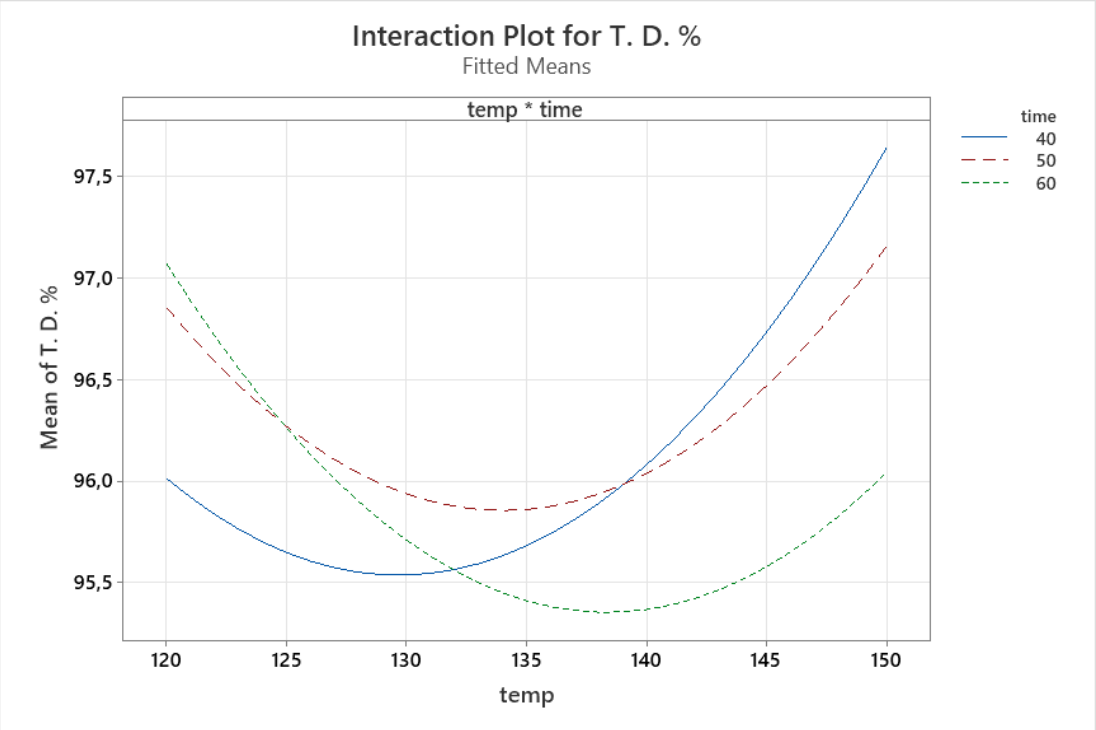

Figure 3.7. *Binary interaction plot of temperature x time.*

It is seen from Figure 3.8 that to reach maksimum theoretical density 560 MPa pressure and 40 minutes waiting time is determined due to test conditions and given variables. In fact, it has been stated in previous studies that pressure loses its importance after a certain value. There is no doubt about the accuracy of these results. Kang et al. described it as pressure-independent in their study, [87]. However, when the bilateral interactions were examined, it was seen that the pressure and time together could affect the density. As the pressure increases, the time required to reach high density decreases. The reason for this may be that the water in the system evaporates over time and then a

high pressurization process is continued when there is no water in the system, and the high pressure may even cause damage to the material. At the same time, the time to achieve hydrothermal conditions may be shortened as the pressure increases. In line with this notion, Kang et al. demonstrated that this critical pressure originates from hydrothermal condition and is dependent on degree of die-sealing. Even die sealing is a very important value to describe critical values, its not discussed at this study and sealing kept constant.

Table 3.6. *Temperature x time effect partial results*

Std Order	Run Order	Pt Type	Blocks	Temp (°C)	Pressure (Mpa)	time (min.)	pH	Moisture (wt. %)	T.D. - 1st (%)	T.D. - 2nd (%)
1	1	1	1	125	525	40	5.1	7.66	91.41	91.67
2	2	1	1	145	525	40	5.1	6.33	94.58	93.51
5	5	1	1	125	525	60	5.1	6.33	93.68	93.95
6	6	1	1	145	525	60	5.1	7.66	95.65	95.28
9	9	1	1	125	525	40	5.9	6.33	95.53	95.56
10	10	1	1	145	525	40	5.9	7.66	97.32	97.29
13	13	1	1	125	525	60	5.9	7.66	97.32	97.53
14	14	1	1	145	525	60	5.9	6.33	97.25	96.43

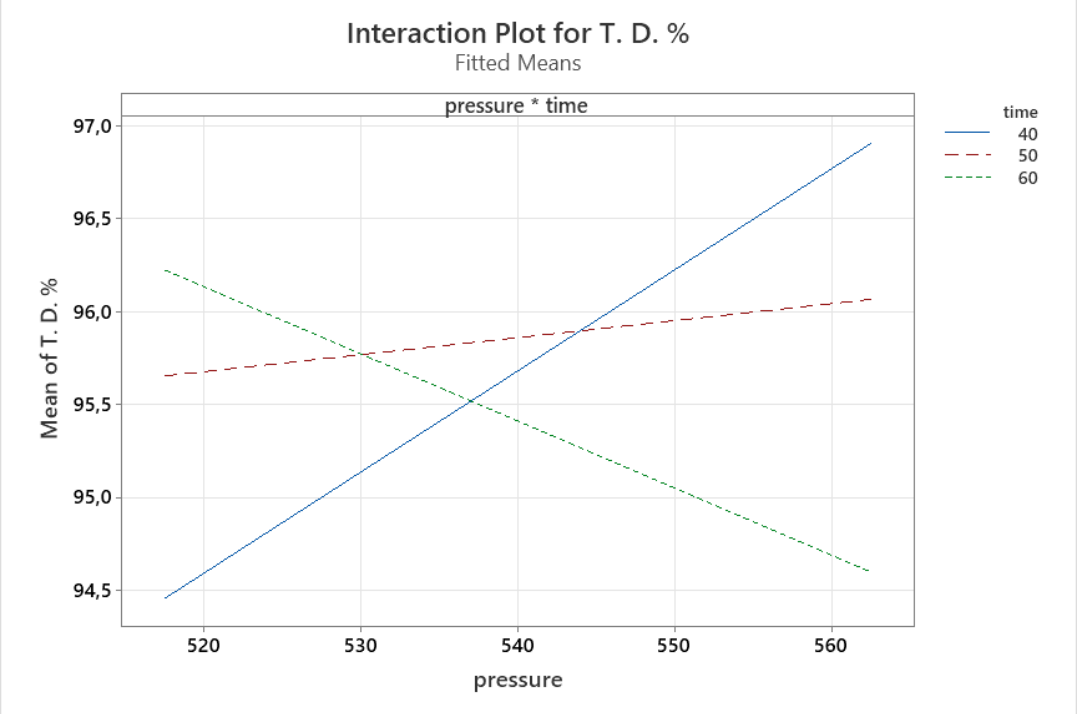

Figure 3.8. *Binary interaction plot of pressure x time.*

Since pH is the most effective varible for the system, to see which pH value is the most effective during sintering, main effect plots are examined. pH 5.9 gives the maximum theoretical density as a main effect, seen from Figure 3.9. pH is not dependent to other variables. When Kang et al. studied on pH effect, they saw that there is a pH independency at the system. In fact, presence of Zn^{2+} and acetate ions in solution is effective here rather than pH [25]. So why its not the same in our study, we can discuss about it. When we look at number 23, 24 and 27 of the experiments from Table 3.3, at the same conditions and with different pH solutions, densities are decreasing with increasing pH. With only the pH 4.9 and 5.1, we added citric acid to the system to can decrease the pH. But also, still there is more zinc acetate at the system. If we search also for is it the same for other pH values, we looked at the experiment numbers 4 and 12. For the pH 5.1 and 5.9 for the same conditions again, densities for the pH 5.9 are higher. Just before than these systematic experiments, we made some acid type experiments and at none of them we could get good results as zinc acetate. This means Zn^{2+} and acetate ions has really significant role on densification. One of the driving force for precipitation can be the starting ions are already in the system. But may be pH can be still has importance on the system, especially dissolution of the particles. If at the all sintering system, dissolution time, vaporization time, pressure-temperature consistency are important, dissolution is also an important factor. But it seems its not have to be fast that normally can be thought. Dissolution can be slower if there is enough ion already at the system, since dissolution precipitation had started and slow precipitation may also mean giving time for choosing a good energy state and getting higher density.

Sengul et al. stated that low pH values are not affected by the surface hydrolysis of Zn^{2+} ions, and that the hydroxyl layer on the surface increases the diffusion of ions by creating a high void concentration [65]. Also it was shown by the experimental results that lower the pH value means lower grain size and density values. Increased acidity and dissolution decreases diffusion rates and had negative effect to CSP [65].

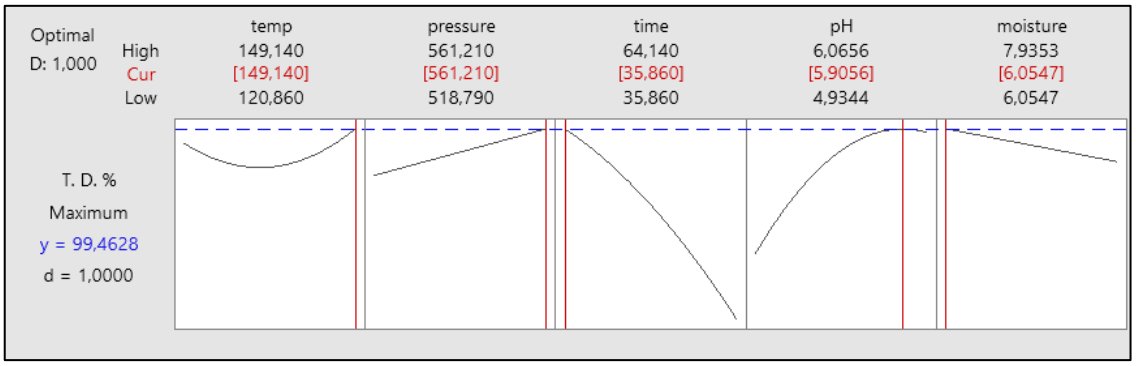

Figure 3.9. *Main effect plots of variables*

For the given parameters, datas of the model, Table 3.7 gives best conditions to get maximum density. When these results are compared with the binary and main effect results, to get best result experimentally, at pH 5.9, with 560 MPa pressure, 40 minutes waiting time at 150°C and with the moisture 6.33 wt. %, should give high density values. Time and moisture are optimized due to binary effect values with the given data. Assumed values optimized with the results that were achieved.

High temperature and high pressure are the choices for the model. It is well known that pressure and time effect the solubility together and also both two are effective for the formation of hydrothermal conditions. But for the pressure, we also saw that after some value, it shouldn't be a need to use higher pressures. But this pressure line, I believe is related to the system all together, means e.g sealing. J. While Guo et al. was describing CSP for the ceramics, he mentioned higher temperature and pressure values give rise to the densification [13].

Table 3.7. *Responses due to model, Multiple Response Prediction*

Variable	**Setting**
temp	149.14
pressure	561.21
time	35.86
pH	5.90563
moisture	6.05469

Response	**Fit**	**SE Fit**	**95% CI**	**95% PI**
T. D. %	99.463	0.611	(98.235; 100.691)	(97.664; 101.262)

When we replace the variables in the regression equation, we see that theoretical density can be achieved above 99.00 % of the theoretical, see in Equation 3.4.

Experimental work was conducted to observe the accuracy of this situation. Equation 3.4 is the calculation of expected density values with given values:

$$\begin{aligned} \text{T.D. \%} = &-303.4 + 0.285\,(149.14) + 0.592\,(561.21) + 2.984\,(35.86) \\ &+ 51.3\,(5.90563) - 2.407\,(6.05469) + 0.00509\,(149.14)\,*(149.14) \\ &- 0.00314\,(35.86)\,*(35.86) - 4.345\,(5.90563)\,*(5.90563) - 0.002644\,(149.14) \\ &*(561.21) - 0.00442\,(149.14)\,*(35.86) - 0.004527\,(561.21)*(35.86) \\ &+ 0.0512\,(35.86)\,*(6.05469) = 99.444\ \text{\% T.D.} \end{aligned} \tag{3.4}$$

We made seven experiments and used given variables. Densities were examined with Archimedes method. Measured theoretical densities were : 97.48 – 97.49 – 97.68 – 97.47 – 98.69 – 99.04. Mean theoretical density is 97. 98 %. It is competable 98.52 % with the desired result. To understand effectiveness of process variables some conductivity testes were performed, see in Table 3.8. These tests were performed with some of the choosen trails due to time and temperature variables. Conductivities were much more less than the reported at some studies e.g., [20]. It was 2 x 10^{-5} S/cm for the sintering at 126°C and 9 S/cm for the sintering at 305°C at the reports. Differentiation may be because of the defect concentration as he reported. When the results we obtained were compared within themselves, the electrical conductivity of the samples sintered at high temperature was relatively higher. In order to see whether the remaining hydrates in the system are effective in low conductivity, some samples were annealed at 300°C for 3 hours and conductivity measurement were reviewed. However, it was observed that the electrical conductivity did not increase and even decreased in most samples. Electrical conductivities are dependent on the CSP temperature, and the conductivities of ZnO sintered at around 300°C are essentially equivalent to that sintered at conventional high temperatures, [20].

When the SEM images were examined in Figure 3.10, no excess grain growth was observed depending on the temperature or time of the samples. The slightly better conductivity results of the sample sintered at 150°C may be due to the more homogeneous distribution of grain sizes. All densities are 97.00 – 98.00 % theoretical density range at all.

Table 3.8. *Conductivity of samples due to different process variables*

Temp. (°C)	Pressure (MPa)	Time (min)	T. D. (%)	Conductivity (S/cm)	After an. Cond. (S/cm)
121	540	50	97.19	2.6×10^{-5}	3.2×10^{-6}
135	540	36	99.45	2.7×10^{-5}	1.7×10^{-6}
135	540	50	98.30	1.8×10^{-5}	4.2×10^{-6}
135	540	64	97.18	2.3×10^{-6}	2.3×10^{-6}
149	540	50	96.45	1.8×10^{-4}	3.2×10^{-6}
150	555	40	99.04	3.4×10^{-4}	1.4×10^{-5}
135	540	36	97.96	2.5×10^{-5}	
135	540	50	98.25	1.9×10^{-5}	
135	540	64	98.12	1.1×10^{-6}	
150	550	40	96.95	8.7×10^{-4}	
150	555	40	98.74	4.0×10^{-5}	

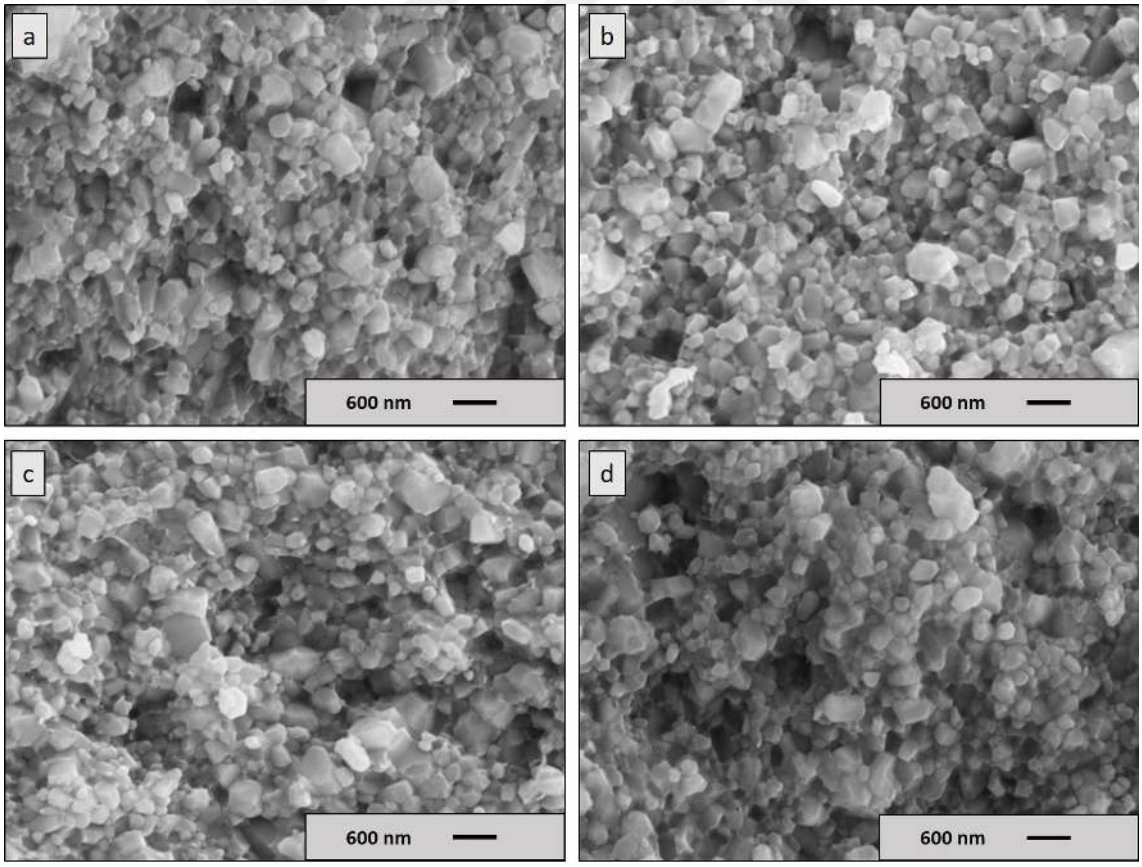

Figure 3.10. *SEM of cracked surfaces of samples; a) 540MPa, 135°C, 36min, pH 5.5, b) 540MPa, 135°C, 50min, pH 5.5, c) 540MPa, 135°C, 64min, pH 5.5, d) 555MPa, 150°C, 40min, pH 5.9.*

3.4. Conclusions

The CSP is a dynamic process small quantities of liquid can escape from the mold, finite liquid evaporates during high pressure, and the polycrystalline bodies or composites undergo densification [86]. Hydrothermal conditions change the sintering kinetics and the final properties can be different at all. Temperature, pressure, moisture ratio all are important and should be different for these two similar systems. It is important to understand process variables and the possible effects to work with new materials.

For the tested variables, most effective parameter is pH and can effect the system linearly, on the other hand while other parameters are also effective, mostly seen as binary effect. Optimal conditions due to the according research, at pH 5.9, with 560 MPa pressure, 40 minutes waiting time at 150°C and with the moisture 6.33 % wt should give best sintering conditions. Theoretical densities were obtained above 97.00 % in the validty experiments. Although the results could not reach 99.00 %TD, it can be seen that the internal structure is more homogeneous as a result of sintering at given conditions. Electrical conductivities are not high for all the samples. Higher temperatures may be an essential for higher conductivity results.

4. ZNO-BASED VARISTOR PRODUCTION VIA THE CSP

4.1. Introduction

Varistors show non-linear voltage-current behavior. The material, which is an insulator at low voltages, suddenly becomes conductive at a certain value, which is called breakdown or threshold voltage. This variability is useful in protecting electrical circuits. With the advancement of technology, number of devices, used with electricity, has increased quite a lot in the last decades. For the last 60 years, varistor are protecting electronic, electrical and power distribution and transmission circuits from the destructive voltage levels induced by lightning impulses or switching surges [91].

In general, there are two types of varistors, SiC varistors and metal oxide varistors (MOV). As a matter of fact, while SiC was recognized as the best varistor material in the 1960s, research on ZnO introduced to yield results in the 1970s, and ZnO began to be defined as the most important varistor material in the 1980s, [92,93]. The history of varistors dates back to the 1950s, in the early 1970s metal oxide varistors were introduced and started to be produced by small products that can react as quickly as nanoseconds have begun to be produced by General Electric Co. [94]. Due to the structure of the material, at low voltage values, metal oxide varistors behave like an open circuit. That is, the varistor is an insulator and no current flows through it. However, when the voltage increases and a certain value is reached, the varistor material becomes conductive and passes the current over itself [94]. In this case, the circuit to which the varistor is connected will be protected against a sudden voltage increase.

One of the most important value of varistors are α (non-linear coefficient) values, which are the numerical indicator of an electrical behaviour. This value is expected to be high for the varistor property to be good. Because, this value indicates the stability of the electrical conductivity transition zone. Typical α values of ZnO varistors are from 30 to 100; therefore, the current varies by orders of magnitude with only small changes in voltage. Generally, α values of SiC varistors do not exceed 10 [95]. After the realization of this situation, the production of ZnO varistor had definitely accelerated.

The I–V characteristics of ZnO varistors are classified into three regions, as seen in Figure 4.1, [95,96]. In region I (low electrical field region, or pre-breakdown region), below the breakdown voltage/threshold voltage (typically a voltage at 1 μAcm^{-2}), the nonohmic property is not so evident and can be approved as ohmic. At this region, the

leakage current is highly temperature dependent. In region II (medium electrical field region, nonlinear region, or breakdown region), between the breakdown voltage and a voltage at a current of about 100Acm^{-2}, the nonohmic property is very prominent and almost independent of temperature. In region III (high electrical field region or upturn region), above 100Acm^{-2}, the nonohmic property gradually degrades, and the varistor is again ohmic. These three regions in engineering applications are also called as the low current region, medium current region, and high current region, respectively [96].

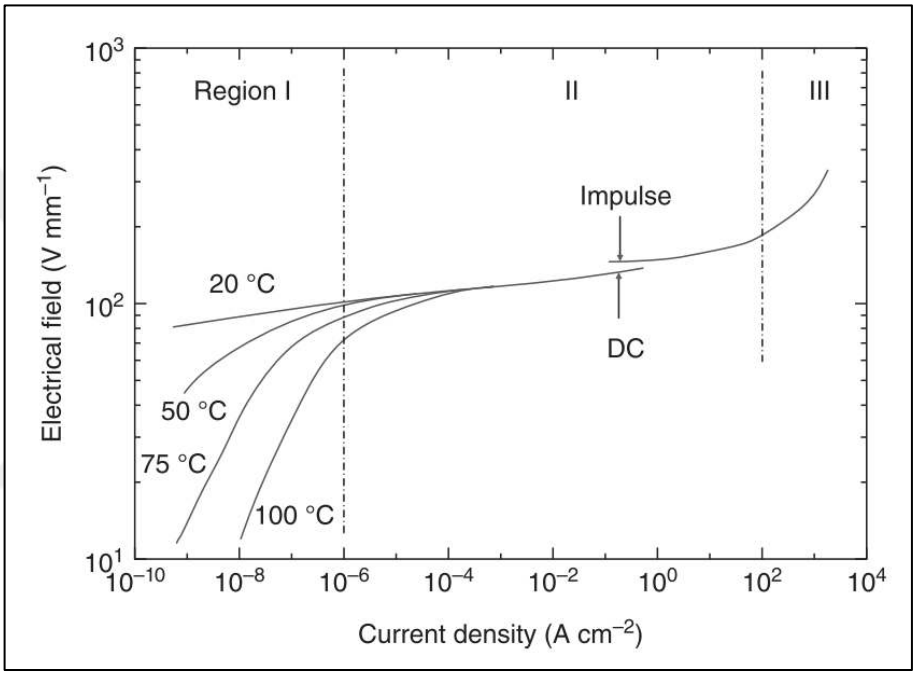

Figure 4.1. *I–V characteristics of a typical ZnO varistor [96].*

In conventional varistors, the threshold voltage is specified as 200 – 400 V/mm [96]. In some varistors, this value can reach up to 10000 V/cm, but 10000 V/cm is a varistor that can be used for very special applications, and values below may also be suitable for high voltage applications [97]. It can be increased up to 10000 V/mm voltage values in high voltage varistors [97]. The alpha (α) values which is an indicator of non-linear electrical property, are about 40-60 for ZnO varistors [98].

A major application of ZnO varistors is for the protection of electric power distribution and transmission systems. ZnO surge arrester have quick response speed, large handling capability and good protectors for power systems. Mitsubishi Corporation produce three types of varistors, named type A, B and C. A type is more conventionally used varistors. Type B and C are superior ones, anda re used for UHV arresters in Japan.

B-type arrester is used in 1000kV systems whose rated voltage is 826kV. In Figure 4.2, large power station arrester containing hundreds of ZnO varistor disks, each one is more than 100cm^3, can be seen [99]. These high voltahe varistors are used at most power stations, seen at Figure 4.3 [91]. The ZnO varistor station arrester discs are surrounded by a silicone rubber collar and pressed against the side of a porcelain insulating housing to enhance thermal transfer.

Figure 4.2. *1000 kV ultrahigh voltage AC surge arresters with porcelain houses [95].*

Figure 4.3. *ZnO varistor components used in the construction of high voltage station arrester shown in Figure 4.2 [91].*

Today, the size of the metal oxide varistor industry is USD 8,693.25 million for 2021 according to The Global Metal Oxide Varistor Market. Expected annual growth rate

of this market is 4.17 % [100]. While the market is growing rapidly and energy is gaining importance in all over the world, perhaps one of the most important issues to be studied on processes and materials may be to reduce production energy. All ceramics, including varistor ceramics, use more energy during production. Most of this energy is used during sintering, as mentioned before. In this case, sintering ZnO varistors conventionally sintered at 1000-1200°C replace with 300°C via the CSP method will be a huge step for the sector in question [38]. Studies should be carried out for technical issues that need to be overcome. It can be said that these studies have started [24]. While the working principle of varistors and the structure-property relationship are examined, the usability of the CSP method in the production of varistors can be more easily evaluated.

As mentioned above, ZnO-based varistors are leading the varistor sector since decades [101]. The working principle of varistors, as mentioned before, is based on the fact that the insulating material at some voltages becomes conductive after a certain voltage. Considering ZnO varistors, although ZnO is a very important material on its own, it does not provide this feature alone. The varistor property of ZnO, that is, the non-linear Voltage-Current (V-I) property, is provided by other additions present in the material and in small amounts together with ZnO. The most important of these additives is Bi_2O_3. Varistors can provide these properties thanks to an electrical barrier called Schottky barrier formed between ZnO and Bi_2O_3 grains, [102,103]. In this case, the grain boundaries formed between ZnO and Bi_2O_3 are very important, because each grain boundary acts as a barrier. The higher the grain boundary quantity, the higher the voltage value that the varistor can provide protection [103]. Means higher the amount of barriers, higher the breakdown voltage for the varistor.

The breakdown or threshold voltage, i.e., the voltage at which a varistor becomes conductive, is expected to be high for certain applications. If the grain size is not small, it is necessary to make larger varistor devices to meet this breakdown voltage, although this is sometimes not possible, since nowadays electronic devices are getting smaller and smaller. For these reasons, fine-grained varistor production is a necessary instance. Many studies have been carried out to increase the number of grain boundaries, in other words, to produce materials with smaller grains. However, the sintering process of varistors in traditional ways actually has the opposite effect on the production of fine-grained materials. Bi_2O_3, which is located together with ZnO, forms a liquid phase after temperatures of about 750°C and wraps around the ZnO grains, allowing the varistor to

reach the microstructure it should be. However, at the same time, grain growth occurs during liquid phase sintering, [104].

Depending on the area in which the varistor will be used, but generally and for high voltage varistor applications, it is clear that grain growth is not a desirable situation. Sintering a varistor containing Bi_2O_3 with the traditional method causes grain growth in the opposite way. This grain size control can be critical in some circumstances than it might seem. For example, according to a study conducted in China, if a ZnO varistor with a voltage gradient of 300 V/mm is used in a 1000 kV ultra high transmission system, the length of GIS surge arrester is 5880 mm. If this value is 350 V/mm, the device size decreases to 5340 mm, for both situations, complicated capacitors must be used for better potential distribution. If the value is 400 V/mm, the dimension will be 3000 mm and an additional homogenizer may not be needed [105]. If it is necessary to increase the number of grains per unit area by decreasing the grain size in order to increase the threshold voltage, various ways have been discovered to achieve this.

There are two accepted methods to improve the voltage gradient. The first method is to use some rare-earth metal oxides at the varistor in hand composition. If it is added to the system with rare earth, the varistor grain size is both reduced and a more homogeneous grain size distribution can be achieved for ZnO systems, [106,107]. Tailoring the microstructure by changing it with the sintering process parameters is the second method, [108]. Some sintering methods for fast sintering such as SPS or flash sintering also were used for sintering varistors, [52,110-112]. However, for most cases, it was not preferred because the equipment was expensive and difficult to use for mass production by the industry.

Many studies were performed to reduce the sintering temperature [113]. The sintering temperatures of varistors can be reduced from 900-1000°C to 700-800°C with the new equipment and additives that have been tried. Meng et al. tailored the gradient, residual voltage and energy absorption capacity by using multiple dopants and optimising preparation technology comprehensively. Voltage gradient of 444 V/mm evaluated as a huge innovation [108]. However, the high temperature and the long time required for the heating of green samples in conventional sintering (CS) lead to a significant energy loss, an overgrowth of grains, [115,116] and a loss of volatile elements, [107,118,119]. As disccused in the previous chapters, the cold sintering process, on the other hand, can provide sintering at lower temperatures than all the methods used. It has been stated that

sintering temperatures can be reduced from 150° to 300°C, [13,23,34]. Subsequently, in one of the last studies by X. Zhao, Clive A. Randall et al., they have succeeded in obtaining a varistor material with high breakdown voltage by sintering at low temperature by using CoO, Mn_2O_3 and Bi_2O_3 together with ZnO, with the CSP method [24].

Tan et al. summarized the physical and microstructural formations that the additives used should create in the system to increase the breakdown voltage. Accordingly, when Figure 4.4 is examined, since the varistor breakdown voltage is provided by the barriers occurring at the grain boundaries, it is necessary to increase the barrier height. This situation can be achieved with some supplements. If equation summarizing barrier height

$$(\phi_B = n_0 d^2 / 4k) \tag{4.1}$$

of a grain boundary, when charge concentration (n_0) in the grain boundary and grain boundary width (d) becomes larger, and grain permittivity (k) becomes lower, and barrier height becomes higher. As a result, electron tunneling becomes more difficult and results in a higher breakdown voltage since a higher bias voltage will be needed to alter the energy band structure and to lower the potential barrier. Modifying grain boundary phase and reducing ionic conduction associated with Zn interstitials and O vacancies will be necessary to increase the breakdown voltage of the barriers, and current density as well [97].

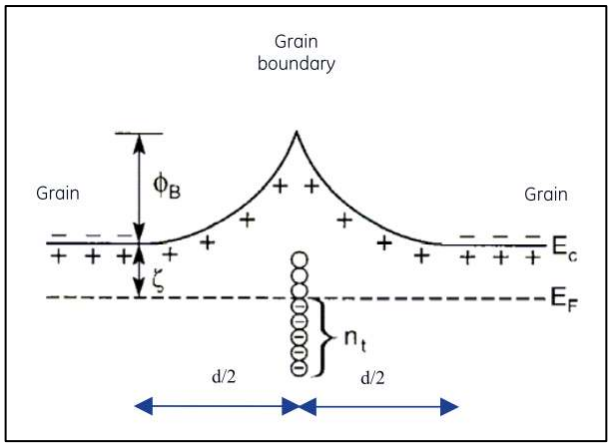

Figure 4.4. *Barrier charge distribution of a MOV [97].*

Studies have been carried out to design the interior structure and the proportions of additions have been determined. Previously determined optimum value of 1.0 mol % Bi_2O_3 as addition to ZnO material [121,122], sintered by the CSP method under different

conditions were investigated at this study. Density, final grain size and electrical properties are key points to get desired varistor property. While measuring the electrical properties of varistor materials, I-V curves are evaluated, [123]. Because the I-V curve allows us to see the nonlinear behavior between current and voltage. Another important parameter to be considered is the α value. The α value in the

$$I=c(V)^{\alpha} \tag{4.2}$$

formulation in varistors α is the coefficient of nonlinear behavior. V is the voltage across the body, I is the current flowing through the body, C is non-linear resistance constant. This value of α is expected to be higher than 1.00 at varistors, [124]. For some varistors, this value can go up to 50.00. Clieve Randall et al., on CSP with ZnO containing Bi_2O_3 and some other additions, was published as an article, [24]. Randall et al., in their study using ZnO-Bi_2O_3-Mn_2O_3-CoO, reached an α value of 33.5 and a high breakdown voltage of 3550 V/mm, by using CSP method, [24]. Our prediction in our study is that the breakdown voltage would be high via the CSP due to small grain size and Co_2O_3 addition to the Bi_2O_3-ZnO varistor system, as well, with Co_2O_3 as additive. Randall et al. used mixed powder method for powder preparation, availability of the densifiying by this method will be discussed.

Pure ZnO, pure Bi_2O_3, ZnO-Bi_2O_3 and Co_2O_3-Bi_2O_3-ZnO systems were investigated in order to identify the material during the measurement of electrical properties. Since the covered ZnO grains by Bi_2O_3 is critical for varistors [124], the first powder preparation of Bi_2O_3-ZnO with different methods has also been tried for achieving homogenization. As discussed in detail he critical point in the cold sintering process (CSP) is dissolution, [63]. During CSP, sintering occurs by the mechanism of dissolution and reprecipitation. In the meantime, it will be preferred that Bi_2O_3 dissolves quickly and is located at the grain boundaries. However, since ZnO dissolves easier, it is located at the grain boundaries and causes the regression of varistor properties. In this case, wrapping the ZnO grains' circumference with Bi_2O_3 with the coating method and then sintering with the CSP method can improve the varistor properties. Another application in the literature that can be used to improve varistor properties in the continuation of the study is annealing. Annealing is the mass material obtained after sintering, being brought to a certain temperature and waiting, [126,127]. Annealing can in some cases provide unique mechanical or electrical properties in materials.

The threshold voltage value of 842.6 V/mm was obtained by sintering the ZnO powder coated with Bi_2O_3 powder with CSP. However, besides this value, the α value being as high as possible will increase the behavior of the varistor. It is stated in the literature that the α value of the product sintered with CSP is 33.5 [24].

Grain boundary design is very important for a varistor. In order for the ceramic to gain varistor properties, the grain boundary must have a certain structure as shown in Figure 4.5. This behavior can occur in traditional varistor production due to the encapsulation of the ZnO grains by the Bi_2O_3 together with the liquid phase sintering.

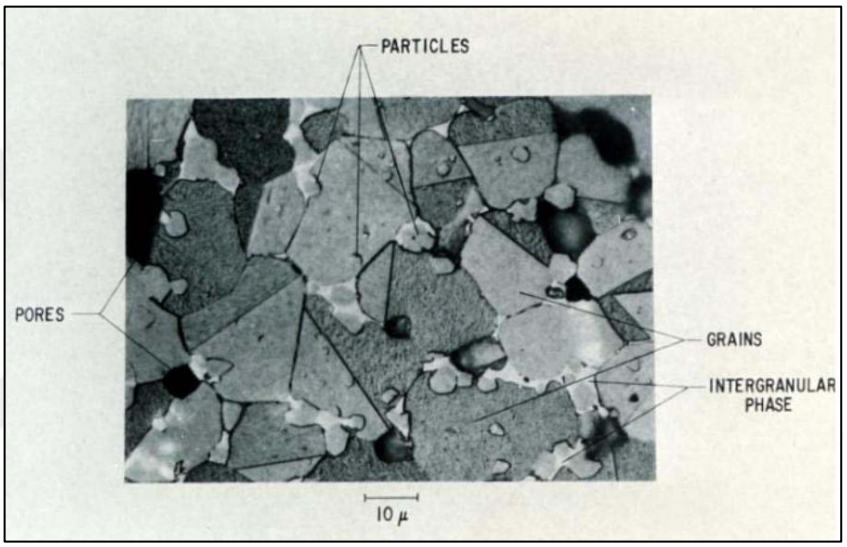

Figure 4.5. *Optical microscope image of a polished and etched surface of a ZnO varistor [128].*

Eda et al. drew attention to the effect of heat treatment on stability. The stability can be explained by the phase transition of the O-rich intergranular layer in the Bi_2O_3-rich phase, because the β phase is much more oxygen-conducting than the γ phase. For example, the reduction of oxygen at heterojunctions is shown schematically in Figure 4.6 a. Oxygen ions migrate to the positive and bulkier parts of the Bi, O-rich intergranular layer due to the electric field. As a result, Schottky barriers will deform as shown in Figure 4.6 b. This model is consistent with the fact that the forward-looking Schottky barrier deforms more easily than the reverse-biased barrier because oxygen reduction occurs more readily near the forward-looking barrier than near the reverse-biased barrier, Figure 4.6 a. In case of AC decay, oxygen reduction occurs at both interfaces [129].

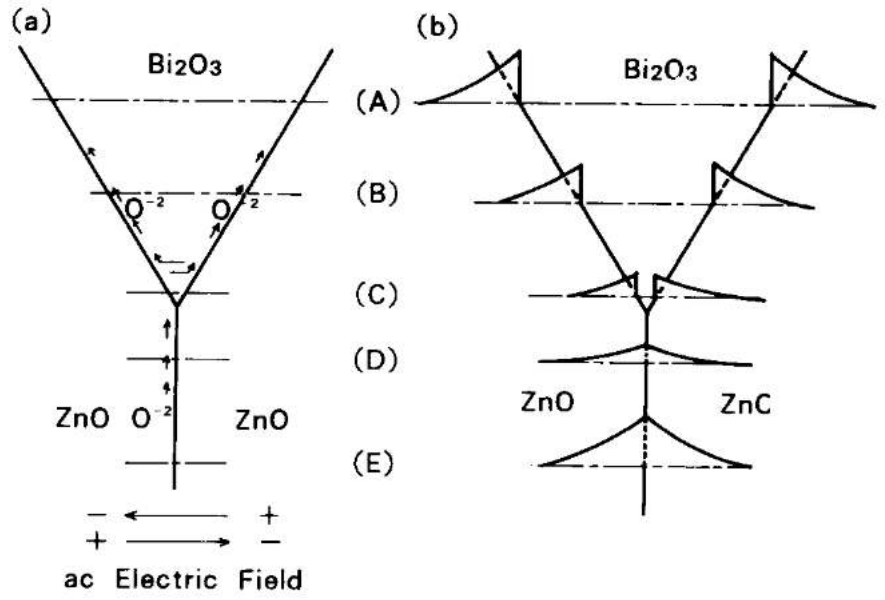

Figure 4.6. *Schematic expressions for oxygen reduction and deformation of Schottky barriers at the grain boundary caused by AC stresses. a) The 0 ion is swept towards the Edt side in the Bi, O, rich intergranular layer by the electric field. The oxygen reduction at point C causes this at point D due to the gradient of oxygen content. (b) Schottky barriers corresponding to each position (A-E) deform symmetrically [129].*

When the internal structure of the materials produced with CSP is examined, it is seen that the Bi_2O_3 grains are dispersed throughout the structure, but this dispersion does not show a structure that will surround the grain boundaries. For the solution of this situation, the dissolution and sintering parameters are examined.

The main microstructure purpose in varistor design is to surround the ZnO grain with Bi_2O_3, Figure 4.7. At conventional sintering, liquid phase formed at high temperature is provided to surround the grain by molten Bi_2O_3 [102]. However, it does not seem possible to achieve this during sintering with CSP. Since the liquid phase does not form at low temperatures, a situation occurs depending on the ions dissolved in the environment at the grain boundaries. Bi_2O_3 material has been studied in order to get to know the Bi_2O_3 material further and to understand its behavior during CSP. CSP trials were carried out and its electrical properties were examined for the pure Bi_2O_3 as well.

Another situation that can influence the varistor behavior is the phases formed in the varistor material. Six different polymorphs of Bi_2O_3 were mentioned in the literature [103]. In previous years, only four of these polymorphs were known. In addition to the combination of different phases at grain boundaries, different polymorphs of Bi_2O_3 can also be mentioned [121]. Grain boundary phases in varistors are usually complex

structures consisting of ZnO, Bi_2O_3, Sb_2O_3, MnO and Co_3O_4 and sometimes different or more compounds [106]. In addition to Bi_2O_3, a small amount of dissolved ZnO mixed into the liquid phase during sintering is mentioned at the grain boundaries. If we examine for the CSP, different polymorphs may also affect dissolution and precipitation behaviors during the CSP and/or the resultant electrical properties may change.

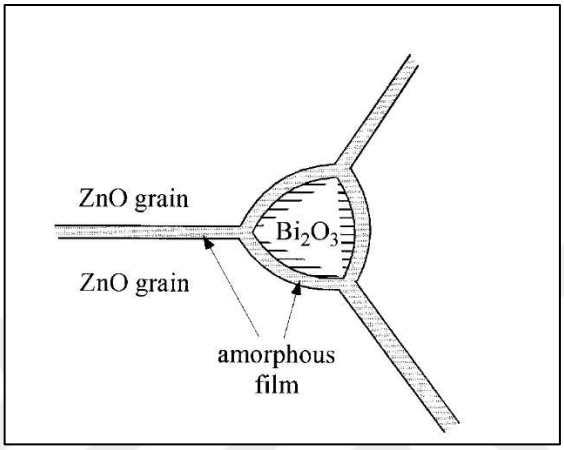

Figure 4.7. *Triple intersection points of grains and varistor morphology [130].*

Bi_2O_3 has polymorphs with different structures formed at different temperatures as shown in Figure 4.8. Among these, the Bi_2O_3 phase at room temperature is the α phase. Although it is stated that there is some β-Bi_2O_3 phase, this phase is not much. α-Bi_2O_3 transforms into ϱ-Bi_2O_3 phase at 730°C. The conductivity of this phase is higher. In general, it is stated that all phases can be found in the varistor structure. In addition, the fact that the annealing, which is generally applied in varistors, is done to ensure this phase change, is also explained as one of the reasons for annealing [107]. The α- β- ɣ- ϱ- phases in Bi_2O_3 are mostly ionic. Oxide ions can have carriers. The ionic conductivity in the α-phase is about 3 times that of other intermediate phases. It is an electronic conductor between 400°C – 700°C [121].

The Bi_2O_3 polymorph in varistors depends on the initial powder and sintering conditions. Any of the α- β- ɣ- ϱ-Bi_2O_3 phases can be found. The ɣ-Bi_2O_3 phase is believed to provide the best varistor properties. ɣ-Bi_2O_3 is metastable but can be stabilized with some additions. These additions can be: ZnO, PbO, B_2O_3, Al_2O_3, SiO_2, MnO_2 etc. [121].

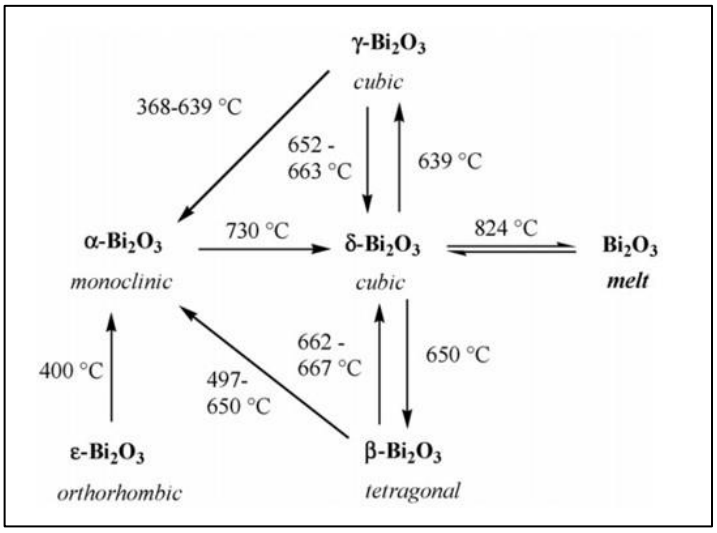

Figure 4.8. *Bi_2O_3 polymorphs and change temperatures [103].*

Particle size consideration is one of the key factors. Under the same conditions in the first phase of sintering, the densification rate increases as the initial grain size gets smaller [3]. For this reason, it is a good method to reduce the grain size in order to reduce the sintering temperature or time. According to Herring's Scaling Law, the sintering times of a material with two grains of initial diameter a_1 and a_2 vary according to the following relation. If $a_2 = \lambda a_1$, the change of sintering times is t_1 and t_2;

$$t_2 = (\lambda)^{\alpha} t_1 \tag{4.3}$$

Here α is an exponent. In this case, when looking at two grains with a grain size of 3 times the value, the sintering time will also change in proportion to the exponential function of 3. In the first stage of sintering, the effect of grain size on sintering is quite clear. However, when it comes to the final stages of sintering, the grain size effect becomes a bit more complex.

At the final stage of sintering, grain growth or densification mechanisms may be active. Since there will still be pores in the system, the movement of the pores at the grain boundaries will be achieved by grain boundary diffusion or lattice diffusion. If grain growth occurs in the system, one or more of the surface diffusion, lattice diffusion or gas phase transport mechanisms will be active. While examining the densification process depending on the grain size, if the grain size used for densification is expressed as m and the grain size used for grain growth is n, the situations that will occur are expressed by Kang as follows: m>n, m=n or m<n. In cases m<n and m=n, the condensation rate is inversely proportional to the exponential function of the grain size. This is one of the

indicators of the importance of grain size during sintering. However, since a similar situation exists for grain growth, a situation competing with densification may occur with increasing growth rate of small grains, [3]. For example, when m<n the following equations, 4.4 and 4.5 can be active for grain growth and densification. Figure 4.9 shows the graph of the relationship between grain growth and densification. Accordingly, fine particle size is more important for densification anyway. This graph applies to when densification is controlled by lattice diffusion and grain growth by surface diffusion [3].

$$\frac{1}{\rho}\frac{d\rho}{dt}\alpha\frac{D_l\gamma_s v_m(1-\rho)^{1/3}}{RTG^3\rho} \tag{4.4}$$

$$\frac{1}{G}\frac{dG}{dt}\alpha\frac{D_s\delta_s\gamma_b v_m}{RTG^4(1-\rho)^{4/3}} \tag{4.5}$$

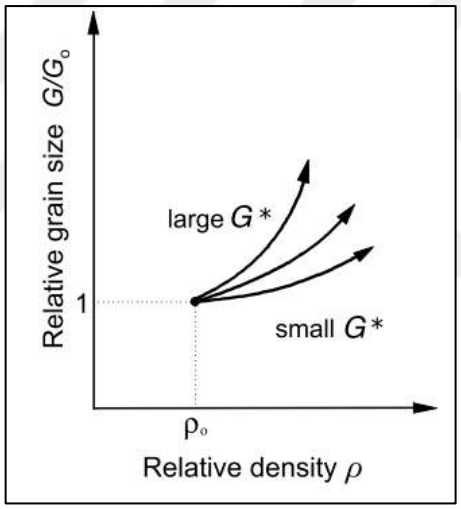

Figure 4.9. *Microstructure development when densification is controlled by lattice diffusion and grain growth by surface diffusion [3].*

Particle size and particle size distribution are very important in liquid phase sintering. Densification rate is inversely proportional to grain size, Figure 4.9. A low grain size will have a positive effect on densification, but on the other hand, it will also cause rapid grain growth. That is, while sintering continues, the advantage of small grain size is lost [110].

In Figure 4.10, the variation of the density formed in the liquid phase sintering of Fe-22Cu compound according to the initial grain size is given. As the grain size decreases, it is seen that the density approaches the theoretical densities. The reasons for this are given as the shortening of the diffusion distance between the grains, the increase in

capillary forces as the grain size decreases, and the acceleration of liquid phase sintering [110]. It should also be noted that grain size is very important for the dissolution and precipitation behavior involved in liquid phase sintering.

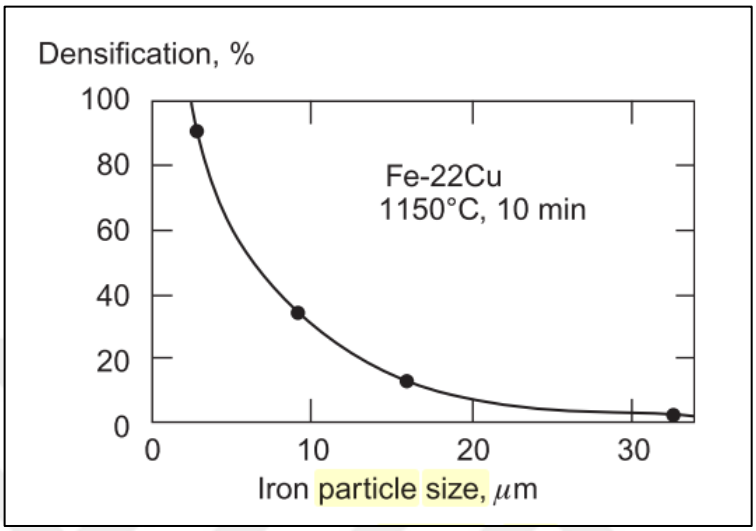

Figure 4.10. *Sintering densification versus iron particle size for the liquid phase sintering of Fe-22Cu at 1150°C [110].*

Capillary pressure plays an important role in the realization of sintering in liquid phase sintering. Capillary pressure will affect grain size, volumes of liquid phase and solid phase. In this case, the particle size is also effective with the surface area during the liquid phase sintering, [111].

$$\ln\left(\frac{s}{s_0}\right) = \frac{2\gamma_{sl}\Omega}{kTa} \tag{4.6}$$

In equation 4.6, s represents the solubility of a particle of diameter a in the liquid. Where γ_{sl} is the energy of the solid and liquid interface, Ω is the atomic volume. T is the absolute temperature and k is the Boltzmann constant. According to this equation, particles with smaller grain size will have a higher dissolution rate. However, another point to be considered here is that if the grain size is not balanced, smaller particles in the system will dissolve and cause grain growth, [52].

When the solubility is examined alone, it is known that the grain size is effective. Experimentally, it was determined that the solubility increased depending on the decrease in grain size. The Noyes Whitney equation is used for the dissolution process of solid drugs.

$$dm/dt = DA(C_s - C)/h \quad (4.7)$$

According to equation 4.7, the solute (t) time is its weight (m), and the diffusion coefficient (D) and the liquid thickness h are used. C_s is the equilibrium solubility, and t(C) is the amount dissolved during t. Although this equation is precise and clear, it has been determined by the experiments that the amount of C_s changes according to the grain size, [112]. The resolution increases as the grain size decreases. In the Kelvin equation in the Gibbs-Kelvin relationship, it was determined that the grain size may affect the solubility due to the increase in pressure due to the curvature of the surface, [112].

Dissolution during the sintering of ZnO with the liquid phase is involved in the current production of varistors. ZnO varistors sintered by traditional methods, the liquid phase is formed together with Bi_2O_3. The phase diagram of ZnO-Bi_2O_3 is given in Figure 4.11. Accordingly, when it contains 86 % Bi_2O_3, the eutectic is formed at approximately at 740°C. After this formation, dissolution can be mentioned.

Examining the concepts of solubility and precipitation a little more will enable us to have information about the way we can follow to develop varistors with the CSP. Because it is understood that one of the most fundamental aspects of the CSP process is dissolution and precipitation. In addition, according to the varistor microstructure design, what should be done to ensure that the Bi_2O_3 predominate phase is at the grain boundaries should be decided.

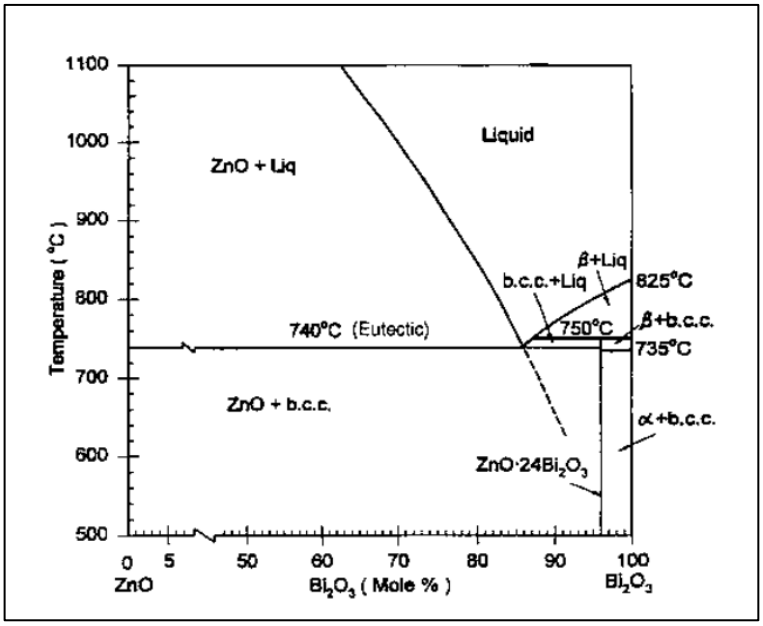

Figure 4.11. *ZnO- Bi_2O_3 phase diagram, [52].*

Solubility, dissolution and dissolution rate are different but related terms. Solubility indicates the dissolving capacity of a solute in a pure solvent. Beyond the precipitation concentration (i.e., solubility limit), a solute cannot be dissolved any more.

Parameters affecting the overall solubility and hence dissolution:

- The nature and strength of the interactions between the solvent and the solute
- Solvent and solute polarity
- Thermodynamics of dissolution
- Heat
- Ionization of the solvent and solute and the pH of the solvent, [131].

The reactions began immediately after immersion of ZnO in deionized water by the hydrolysis of the ZnO particle surface that took place as a result of the adsorption of water molecules with the simultaneous formation of $Zn(OH)_{2s}$ layer. It is also noticed that zinc hydroxide is soluble in water, and becomes more soluble when pH is lowered or increased. The predominant reactions are the dissolution of $ZnO_{(s)}$ to $Zn^{2+}{}_{(aq)}$ and $O^{2-}{}_{(aq)}$ and surface hydroxylation to $Zn(OH)^{+}{}_{(s)}$ which takes place based on the following Eqs 4.9 – 4.10.

$$ZnO_{(s)} \leftrightarrow Zn^{2+}{}_{(aq)} + O^{2-}{}_{(aq)} \quad \text{metal oxide dissolution} \tag{4.8}$$

$$ZnO_{(s)} + H^{+}{}_{(aq)}\ Zn(OH)^{+}{}_{(s)} \quad \text{metal oxide hydroxylation} \tag{4.9}$$

Some important reactions are noted that occur when the pH is lowered from 7.7 to 6.4 and the pH after 5.5 and 4.5.

$$Zn(OH)^{+}{}_{(aq)}\ Zn^{2+}{}_{(aq)} + OH^{-}{}_{(aq)} \tag{4.10}$$

$$Zn(OH)_{2s}\ Zn(OH) +_{(aq)} + OH^{-}{}_{(aq)} \tag{4.11}$$

$$Zn(OH)_{2(s)}\ Zn(OH)2_{(aq)} \tag{4.12}$$

$$Zn(OH)_{2(s)}\ \ Zn^{2+}{}_{(aq)} + 2OH^{-} \tag{4.13}$$

$$O^{2-}{}_{(aq)} + 2H^{+}\ \ H_2O_{(aq)} \tag{4.14}$$

One of the objectives of the study is to increase the Bi_2O_3 dissolution rate. It is known that the solubility changes depending on the grain size as shown in Figure 4.12, [115]. For this reason, experiments were made with powders with different particle sizes. Factors affecting the dissolution rate:

- Chemical and surface properties of the particles
- Particle size and distribution
- The environment around the particle

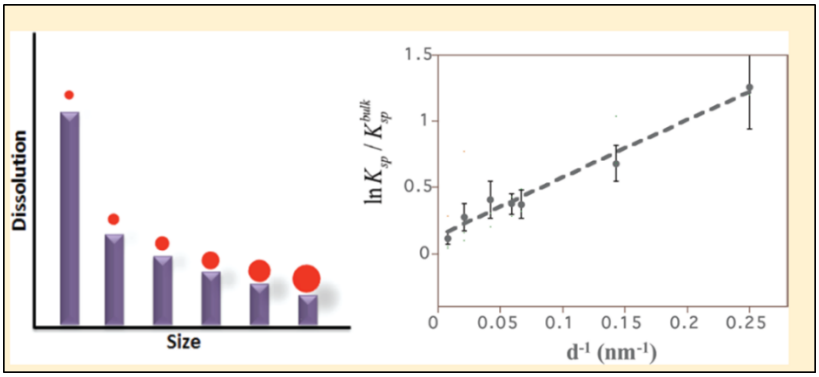

Figure 4.12. *Dissolution chart and graph based on particle size [115].*

Dissolution is important for both coating and the CSP. Considering the factors affecting the dissolution rate, the three most important ones are as follows. In solutions with high acidity, H^+ ions from HCl react with the ZnO surface, allowing ZnO to dissolve and Zn^{2+}(aq) and H_2O are formed. If the addition of HCl continues, the proton concentration in the solution will increase and if the H^+ ions exceed the amount of Zn^{2+} ions, the pH change will not occur [116]. This explains the absence of pH change below a certain pH in our zeta measurements, and the fact that the pH does not change no matter how much acid is added. In ZnO measurements, when the pH was 6.5, the pH could not be lowered and ZnO suddenly dissolved.

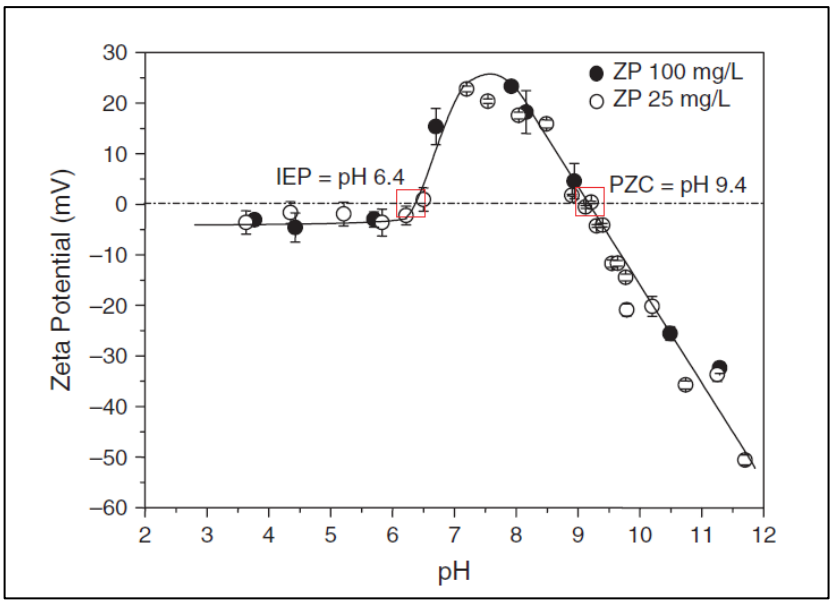

Figure 4.13. *Zeta potential profile for ZnO at concentrations of 25mg/L ve 100mg/L [116].*

Sintering with CSP is also similar to a pressurized liquid phase sintering. In this case, the grain size will gain importance especially in terms of dissolution. Particle size distribution is at least as important as particle size. On the other hand, it is advantageous to use fine-grained powder during sintering with CSP, since the particle size will be important during the formation of capillary forces. Bi_2O_3 powder particle size can be used as smaller than the ZnO particles for more dissolution.

In cases where the dissolution is not sufficient for Bi_2O_3, the initial contact between ZnO and the liquid phase can be reduced by using the coating method. The coating method has also been tried before for varistor applications. The purpose of coating in these applications is to distribute the additives more homogeneously in the system, to form the liquid phase homogeneously and to wrap the grains more quickly.

Coating one powder with another powder is a method used in high-tech ceramics. It can be used to impart many properties to the material. In our studies, the purpose of coating ZnO powder with Bi_2O_3 is to ensure that Bi_2O_3 is dissolved beforehand, in order for the skeletal structure to be formed by the grain boundaries to be formed as like at Figure 4.14. In this way, it is aimed to improve the varistor properties with the increase of the existence of the Bi_2O_3 phase at the grain boundaries. Coating has also been tried and tested method in conventional sintering [118].

In our studies, two different ways were followed for the coating of ZnO grains with Bi_2O_3. The first of these is the dissolution of the bi-nitrate powder in nitric acid and then its re-precipitation as oxide by increasing the pH [119]. In fact, this method is used as a synthesis method, not powder coating. However, we aimed to use ZnO grains as cores by adding ZnO powder to the medium during precipitation.

Another process to increase the α value and improve the varistor properties is to improve the microstructure design by adding different additives to the powder mixture. Many additives are used in varistors sintered by conventional methods. These additives are added to the system at rates determined by long studies in order to provide different properties. Additions used to improve the α value are given as Co, Mn, Sb and Cr [128].

Figure 4.14. *Scanning electron microgpaph of sintered polycrystalline Zn0-0.5 mol% Bi_2O_3 after the ZnO grains were dissolved in NH_4C1 solution (x1780) [122].*

The important thing in this study is to see the sintering process of systems containing more than one powder system with the CSP, as well as to obtain a varistor microstructure and hence varistor properties. There are not enough results about varistors produced via CSP, yet. Microstructure design and feature development with CSP is a new era. In varistor microstructures, Bi_2O_3 should surround the ZnO grains, to be able to form Schottky barriers. In addition, high density and fine grain size via limited/no grain growth are the target material structure. Methods to further dissolve Bi_2O_3 can be used to reduce the particle size, control the phase solubility of Bi_2O_3, and if these conditions are not sufficient, covering the ZnO powder with Bi_2O_3 should be evaluated. The method to be tried first is to experiment with different Bi_2O_3 powders and ZnO powders to obtain a high density and then a suitable I-V measurement. It is expected that threshold voltage value will increase with fine grain size. If necessary, different additions will be used to increase the alpha value. Although it is aimed to add these additives to the system with the mixed powder method first, the coating method can also be applied again, since the insoluble additives will not be located in the desired grain boundary regions in the CSP system. The target alpha value is to be over 30 and threshold voltage is to reach 1000 V/mm for high power applications of varistor system. Microstructure should be investigated carefully to see the CSP effect on the structure-property relationship.

To achieve the desired microstrucre, some requirements should be investigated first of all. If dissolution and precipitation is an indispensable process step for CSP, then it has not been understood how some additives, which dissolve much slower than ZnO, can dissolve and precipitate in the system and take place in the grain boundaries. In order to

cut off the contact of the acid-containing solvent medium with ZnO, which causes the rapid dissolution of ZnO, the way of coating the additives on ZnO has been tried. Coating was tried firsly at ZnO-Bi_2O_3 system, then oncoming ZnO-Bi_2O_3-Co_2O_3 system. During the studies, importance of phases and solubility parameters were also carried out, since microstructure of the varistor is the key point for desired properties.

Research objectives of Chapter 4 is to develop varistors by using Co_2O_3 and Bi_2O_3 in addition to ZnO with non-linear I-V characteristics via the CSP. By using only two additives, named Bi_2O_3 and Co_2O_3, in the production of ZnO varistor, by lowering the sintering temperature (~250°C), and samples with fine grain size can be obtained, threshold voltage can exceeded 1000 V/mm, for high voltage applications.

4.2. Experimental Procedure

4.2.1. The Cold sintering process

The CSP procedure used for single ZnO sytem was also used for binary (ZnO-Bi_2O_3) and ternary (ZnO-Bi_2O_3-Co_2O_3) systems. However, the mixing of Bi_2O_3 powder with ZnO must be done before the CSP process. In this case, it should be determined how the mixing method will be. Mixing in the mill will be more appropriate in terms of homogeneity and convenience. In this case, studies were made for the most appropriate mixing time and the type of dispersant to be used in the mill. Results of these studies are described in Section 4.3.1.5. Mixed powders were sintered by the CSP. When the electrical properties were not as desired, coating ZnO by Bi_2O_3 was utilized.

In the case where Bi_2O_3 is included in the system by coating, ZnO powder is coated with Bi_2O_3 before the CSP treatment. In this case, the mixing process was not applied in the mill.

The CSP conditions were finalized by trials for each system. Electrical characterization samples were produced using the conditions with the highest intensity value.

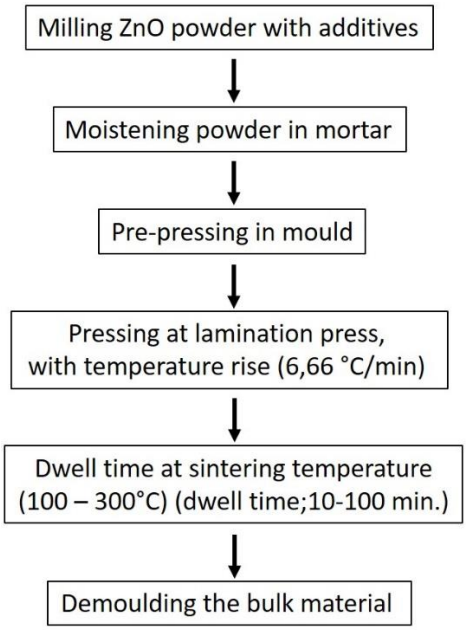

Figure 4.15. *The CSP flow chart*

In this part of the thesis, firstly, Bi_2O_3 and ZnO-Bi_2O_3 systems were studied and then Co_2O_3 added to these systems. These Bi_2O_3, ZnO-Bi_2O_3 and ZnO-$Bi_{12}O_3$-Co_2O_3 systems will be discussed in detail below.

For ZnO and Bi_2O_3, first trials were carried out to choose the appropriate powder for mixture. Two different types of ZnO and two different types of Bi_2O_3 were investigated. Crystallographic phase identifications were made during the selection of Bi_2O_3 powder via x-ray diffraction method. In addition, phase development and electrical conductivity measurements were done for the CSPed Bi_2O_3 samples.

Due to the importance of obtaining a homogeneous structure for the ZnO-Bi_2O_3 system, first of all, the sedimentation test for the dispersant selection and then the mixing time in the mill were tried. Appropriate dispersant and mill mixing time were selected based on these studies. The electrical properties were investigated by making CSP trials with the powder mixed under appropriate conditions.

Besides mixing in the mill, powder preparation by coating ZnO with Bi_2O_3 were carried out to see if the electrical properties would improve or not. Two different coating methods were carried out. Powders were obtained by both methods. After the characterizations were made, bulk samples were produced using CSP with both. The electrical properties of these samples were investigated. The CSP conditions were tested for pure Bi_2O_3, Bi_2O_3-ZnO milled powder and Bi_2O_3 coated ZnO systems, and the characterization methods, used in this study are presented in Figure 4.16.

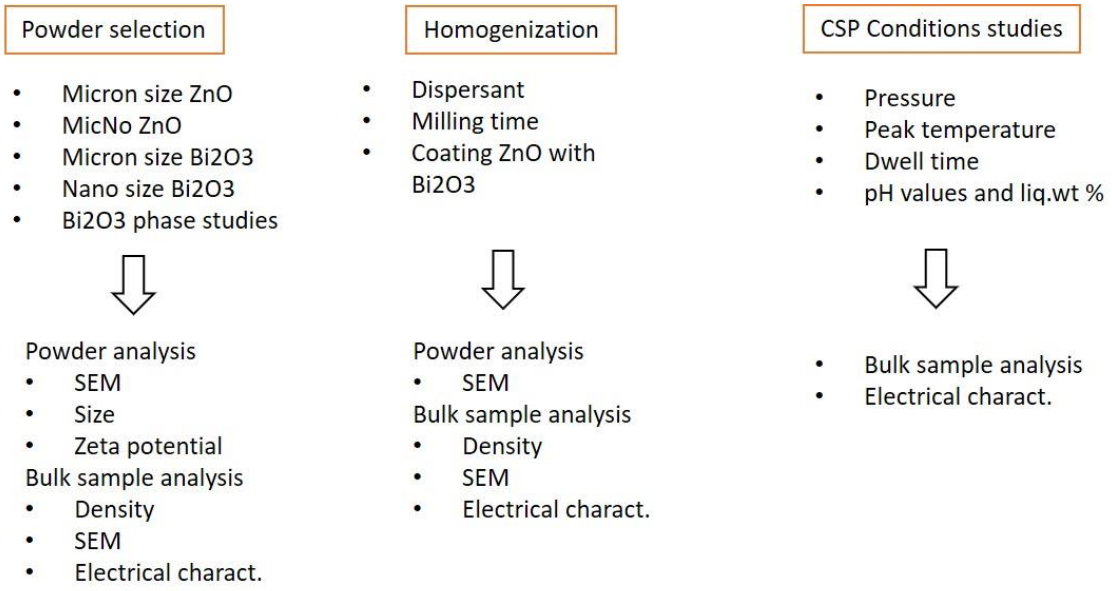

Figure 4.16. *Experimental procedure chart*

4.2.2. The CSP of ZnO-Bi_2O_3 production

Two kinds of Bi_2O_3 powder were used at the experiments. Particle size analyzes of these two powders were carried out. Powders were named as micron-Bi_2O_3 and nano-Bi_2O_3 after the size measurement results. Particle size was measured with Malvern Nano Zeta Sizer. The phases of two different powders were determined by XRD. XRD measurements were done as powder form and just after sintering to see if there is phase change after sintering. The resulting Bi_2O_3 phases determination was done to the samples sintered via CSP at different temperatures. Sintering procedure was used dur to Chapter 2, some parameters changed due to powder characterstics. Sintering procedure will be given with the results. I-V analyzes were performed after sintering of pure Bi_2O_3.

Impact of Bi_2O_3 and ZnO powder size in order to obtain varistor microstructure

Particle size experiments were done in two paths. Aim of the experiments were to see the densification difference due to different particle size combinations. On the other way, the real aim is to observe the microstructure change that will arise from the difference in resolution. Figure 4.17 shows experimental varibles. ZnO, as the main phase of the varistor, two different types of powders were tasted. ZnO was used 99.00 mole % and Bi_2O_3 was used 1.00 mole % for all the trials. Mole percents were constant due to traditional ZnO-Bi_2O_3 varistor systems.

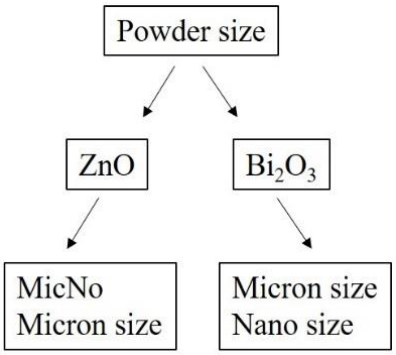

Figure 4.17. *Experimental pathway for particle size researches*

ZnO particle size: In order to design the grain boundary, it is necessary that the Bi_2O_3 powder dissolves and the ZnO powder dissolves less so that the grain boundary can have a Bi_2O_3-rich phase. However, the higher solubility of ZnO powder complicates this situation. For this reason, it has been tried to produce a solution by experimenting with powders of different grain sizes. Increasing the ZnO grain size and decreasing the Bi_2O_3 grain size is the point of the experimental design.

In the raw material trials, a trial was made with MicNo as ZnO powder. Micnos are plate-shaped ZnO structures formed by combining nano ZnO grains. It is produced by Prof. Dr. Ender Suvacı and his team and has the opportunity to be used in many areas [132]. In this study, it was used at the experimental aspect to observe the dissolution rates. 1 mol % Bi_2O_3 was mixed in a plastic jar with zirconia balls for about 30 minutes. Afterwards, Bi_2O_3 added MicNo powder was sintered by CSP method. Results were compared with the micron size ZnO trials.

Bi_2O_3 particle size: to prevent unimely dissolution of ZnO, by the Bi_2O_3 side, it was purposed to increase the solubility by decreasing the grain size with an opposite point of view. Trials were made with two different Bi_2O_3 powders. Micron-sized ZnO powder, which was used as a standard in the trials, was mixed with micron-sized and nano-sized Bi_2O_3 at the rate of 1% mol in the mill. CSP trials were carried out with the obtained mixture powders. Densities and SEM images were examined. Electrical characterization was carried out to understand whether Bi_2O_3 is dominantly at grain boundaries and gives varistor properties as expected.

Dispersing: Milling time and dispersant

Mixing processes of powders is also another matter that needs to be worked on. The selection of the appropriate dispersant is related to the nature of the powder in the mill and the liquid medium to be used. Although we have some experience in this field as a laboratory, experiments were carried out with three different dispersants in order to clearly determine the theoretical background. Among these, Darvan C and Tego dispers are some dispersants used previos ZnO studies. Polyacrylic acid (PAA) dispersant, on the other hand, is the information obtained from the literature and has been used in trials and was available in our laboratory [133]. From the trials to choose the appropriate dispersant, micron size ZnO and micron size Bi_2O_3 were used.

Selecting the Dispersant:

1. Darvan C
2. Tego Dispers
3. Poly acrylic acid

OBJECTIVE: Selection of suitable distributor for the mill

Powder : ZnO + Bi_2O_3

Medium : Ethanol

TESTS:

- Powder SEM (BSE and EDX)
- Bulk SEM
- Bulk Density
- Dust sedimentation test

Another study to ensure homogeneity was to examine the effect of milling duration on homogeneity after selecting the appropriate dispersant. 3 different milling jars were prepared. The prepared jars with exactly with the same content were taken from the rotation at different times, sintering was done with all three powders after drying, and the sintered samples were examined to obtain appropriate mixing time. ZnO was milled for 1 hour only with dispersant and after Bi_2O_3 added to the jar.

Trial milling durations:

1. 1 hour + 4 hours
2. 1 hour + 8 hours
3. 1 hour + 16 hours

OBJECTIVE: Determination of homogeneity of Bi_2O_3 distribution

TESTS:

• Powder SEM (BSE and EDX)

• Bulk SEM

• Bulk Density

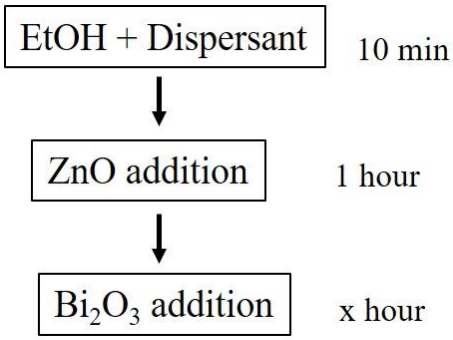

Figure 4.18. *Mill preparation flow chart*

4.2.2.1. CSP of ZnO-Bi_2O_3 mixed powder

1.0 mol % with the rest ZnO powder mixture was dried after milling process. The CSP process was applied to the milled powder.

The optimum CSP conditions were resulted in more than 90.00 % T.D. for all trials. These conditions for CSP are; 7.0 wt % pH adjusted water by weight. The pH was 5.5 with zinc acetate (ZA) dissolved in water. The powder moistened with this liquid by mortar and pestle. Pre-pressing was used as 200kgf/cm^2 for 1 minute. Carver lamination press with heating plates was used for sintering. Dwell time was 50 minutes at 540 MPa pressure and the 140°C as the temperature for sintering.

4.2.2.2. Coating ZnO by Bi_2O_3

The second method used when adding Bi_2O_3 to the system was coating. Two different methods were used for coating ZnO by Bi_2O_3. These methods can be summarized as pH controlled coating and coating with slurry mixing method. The powder obtained from the pH controlled coating was named S1 and the powder obtained from the mixing method was named S2. Powder characterization methods were applied to the obtained powders. After that, sintering was applied with the CSP method.

Coated powder phase analyzes were carried out by XRD, Bruker D2 Phaser. Coating specifications were performed by FTIR, Shimadzu IRTracer-100 and by Raman,

Renishaw inVia Raman Microscope, zeta differences' determination were done by Malvern Zetasizer Nano series. Images of the particles and samples were acquired by SEM, Supra 50VP.

The pH controlled coating method (S1)

The pH controlled coating method was created by adapting the methods used for powder synthesis to the coating method. The powder production method used is the powder production method was unique of heteronucleation. The core used here is ZnO powder.

Figure 4.19 shows the flow chart of the process. Bismuth nitrate powder dissolves in 65% nitric acid. After the dissolution process, approximately two times by volume of water was added onto the liquid and thenslurry was taken onto the stirrer. Afterwards, the system pH was increased by adding ammonia solution. Meanwhile, the mixing process was continued. Precipitation begins when the pH is 13.00. ZnO powder was added to the system at the point where precipitation was just beginning, before pH was 13.00. system pH continues to be controlled and mixing continued for 2 hours. During the procedure, when it started to precipitate as Bi_2O_3 powder at pH 13.00, ZnO powder acts as the core and coated by Bi_2O_3. Yellowish powder was taken from the stirer and washed 3 times by water and 2 times with ethanol. Achieved powder was dried at etuv for 24 hours.

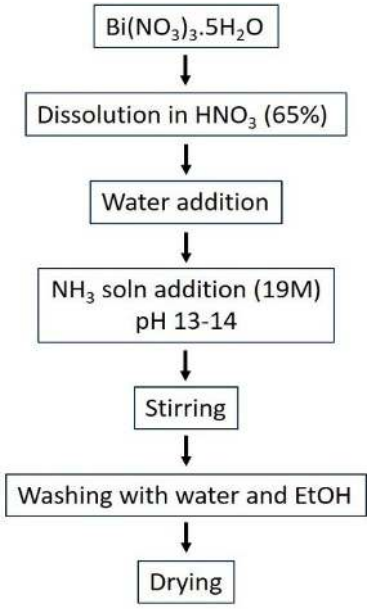

Figure 4.19. *pH controlled powder coating method flow chart*

The slurry based coating Method (S2)

The coating of ZnO with Bi_2O_3 was tried using a different method. This study was done to see effectiveness of the different coating methods. In this coating method, pH control was not provided [126]. More simply, the powders were dispersed in alcohol and then dried and calcined, as at seen Figure 4.20. The flow chart of the method is given below.

Bismuth nitrate was dispersed in ethanol and mixed in alcohol for 2 hours before ZnO addition. While the stirring was proceeding, ZnO was added to the system and stirring was remained for 1 hour. Slurry was heated to 80˚C, for evaporation of the alcohol and powder mixture was dried while stirring was going on.

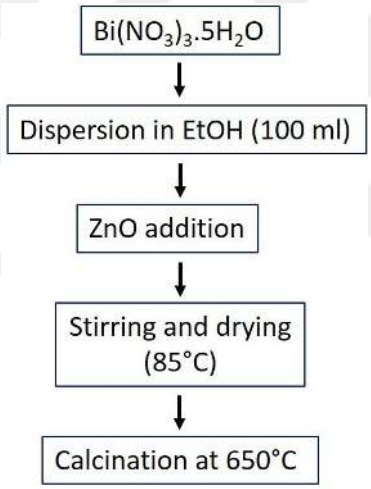

Figure 4.20. *Flow chart of powder coating method by dispersing in solution*

4.2.2.3. Annealing of ZnO-Bi_2O_3 varistors

Mixing powder by milling process and two different type of coated particles were cold sintered and their electrical caharacterizations were made. Later on, for improving electrical behaviour of the samples, annealing was tried out.

Annealing is a method applied for varistor materials to improve their electrical properties, [126,127]. Another advantage of the materials produced with CSP is that the internal structure is homogenized and the particles are surrounded by the liquid phase. Of course, some other internal structure changes may also occur. For this reason, the

electrical properties that will occur as a result of annealing are important for scientific view.

The sintering conditions of the annealed samples were: Waiting for 50 minutes at 140°C, at 539 MPa pressure, moistened with 7.81 wt % water with a pH value of 5.5. The samples produced with S1 powder were kept at 400°C, 600°C and 800°C temperatures for 1 hour and then XRD analyzes were done. Electrical characterizations were performed after annealing, as well.

In our studies, we tried to determine whether the electrical properties changed by applying annealing at 400°C, 600°C and 800°C for only ZnO-Bi_2O_3 system, to see the benefits of annealing, if there are.

4.2.3. ZnO-Bi_2O_3-Co_2O_3 varistor production via the CSP

4.*2.3.1. Mixed powder method*

Bi_2O_3, Co_2O_3 and MnO/Mn_2O_3 and occasionally Sb_2O_3 were added to the ZnO containing plastic jar respectively and mixed in the mill. The mixing process was 16-20 hours, as determined more finely. Process chart is the same as Figure 4.18**,** Mill preparation flow chart. After Bi_2O_3, other additives as in the list below were put in the jar 10 minutes apart.

Four compositions were named ZBCM and ZBCMS with the production numbers. First two compositions were with MnO powder. 3rd and 4th compositions are with Mn_2O_3 powder. Mn_2O_3 was produced by calcination of Mn_2CO_3 powder. Powder characterization was made with XRD analysis.

Although the 3rd and 4th compositions are the same, Bi_2O_3 powders are different as given at section 4.2.2. While micron size Bi_2O_3 was used in ZBCM-211120-1 mill composition, nano sized Bi_2O_3 powder was used in ZBCM-211120-2 mill composition. The aim was to be able to see the interactions in multi-component systems.

Varistor powder compositions by mole percentages:

1)ZBCM-2109 : 98.0 % ZnO-1.0 % Bi_2O_3-0.5 % Co_3O_4-0.5 % MnO

2)ZBCMS-2109 : 97.5 % ZnO-1.0 % Bi_2O_3-0.5 % Co_3O_4-0.5 % MnO-0.5 % Sb_2O_3

3)ZBCM-211120-1 : 98.0 % ZnO - 1.0 % Bi_2O_3 - 0.5 % Co_3O_4 - 0.5 % Mn_2O_3

4)ZBCM-211120-2 : 98.0 % ZnO - 1.0 % Bi_2O_3 - 0.5 % Co_3O_4 - 0.5 % Mn_2O_3

4.2.3.2. Coating ZnO by cobalt oxide

Previously, two different methods were used during the coating of ZnO with Bi_2O_3. In the system containing Co_2O_3, the coating method called S1 among these methods, with a pH controlled method was applied. Additionally to the S1 method, Cobalt-nitrate compound used for coating. Figure 4.21 shows flow chart of coating method. Procedure was similar with the Bi_2O_3 coating method. Co-nitrate is soluable in pure water, so no more extra acidic liquid was needed. Solution of cobalt nitrate was heated to 85˚C at the stirrer. After reaching the temperature, ammonia was started to be added just until pH was 8.0. ZnO was added to the slurry despatch while pH was adjusted to pH 9.0. pH was tried to be kept constant while the stirring was proceeding for more 2 hours. After cooling the slurry, powder was washed with water for 3 times and 2 times with alcohol. Washed powder was dried 24 hours at drying oven, at 100˚C.

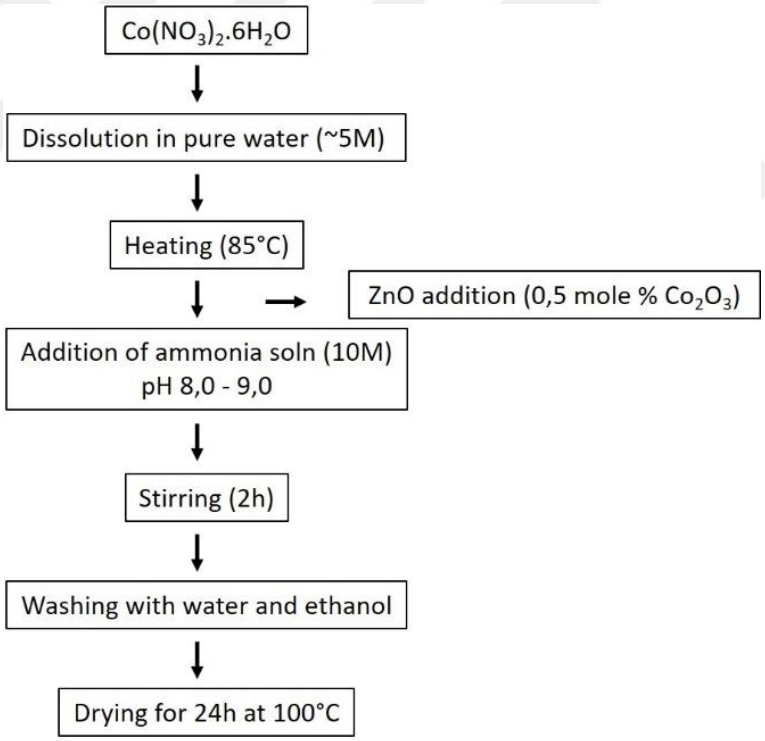

Figure 4.21. *Flow chart of oxide coating of ZnO powder with Co-nitrate starting powder*

Afterwards, Bi_2O_3 was added to the ZnO powder coated with cobalt and sintered with CSP. CSP trials were performed powders without calcination, initially. Afterwards, the powders calcined at 500°C or 600°C for 2 hours were sintered with CSP and analyzed.

Figure 4.22 illustrates effect of coating on final microstructure. In Figure 4.22 a, soluable pure ZnO particles at the beginnig of the process are shown. After coating with Cobalt oxide phase on ZnO, particles are insoluable and ready for CSP, see at Figure 4.22 b. In Figure 4.22 c, Bi_2O_3 powder is mixed with coated particles for CSP. At this point, coated particles are insoluable and Bi_2O_3 is soluable. This mixture of powders meet with pH adjusted liquid and CSP can be performed. After sintering, expected microstructure is like at Figure 4.22 d. This microstructure design is required to reach varistor properties. In order for the grain boundary phase to be bismuth-rich and for the grains to be composed of ZnO, the ZnO grains must be coated with the insoluble phase, cobalt oxide.

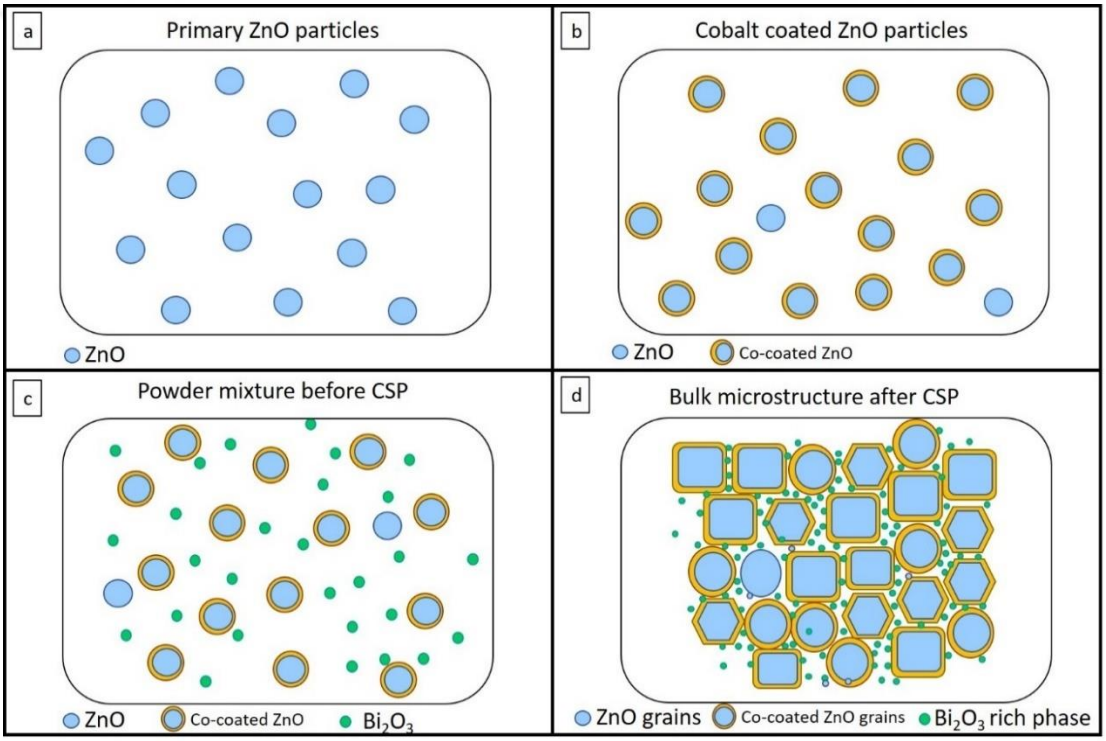

Figure 4.22. *The formation scheme of the varistor microstructure to be formed with the Co_2O_3 coated ZnO particles*

4.2.3.3. ZnO-Bi_2O_3-Co_2O_3 varistor production with CSP

Powder mixtures, the production of which is described in Sections 4.2.3.1 and 4.2.3.2, were sintered by the CSP method.

Powder mixtures were prepared using the compositions. ZBCM-2109, ZBCMS-2109, ZBCM-211120-1, ZBCM-211120-2 powder mixtures were used for CSP trials. In order to obtain high density, experiments were carried out by changing the pH, moisture

content, temperature, pressure and times. The coating method was tried to improve the density results and to provide a homogeneous structure. In the coating method, experiments were done with only ZnO-Bi_2O_3-Co_2O_3 powder system.

For the sintering of Co_2O_3 coated ZnO powder, uncalcined powder was first used and densities of 90.00 % were achieved in the first trials. However, it was determined that there was a need for calcination in the direction of the analyzes made on the powder, and the trials were continued with the calcined powder.

-CSP with uncalcined Co-coated-ZnO

-CSP with ZnO co-coated-calcined with Bi_2O_3

- CSP with ZnO co-coated-calcined without Bi_2O_3

Trials have been done as above-mentioned. The calcination conditions for calcined powders were 2 hours at 500°C at box furnace.

4.2.4. Electrical characterization

I-V characterizations were made with Keithley 2410 power supply system. α value was calculated due to equation 4.15.

$$\alpha = \frac{\log(J_2/J_1)}{\log(E_2/E_1)} \tag{4.15}$$

E_2 and E_1 are the electric fields at standard current densities of J_2 and J_1, respectively. Breakdown electric field (E_b) was calculated at a current density of 1 mA/cm^2. Instance I-V graph of a varistor is given at Figure 4.23.

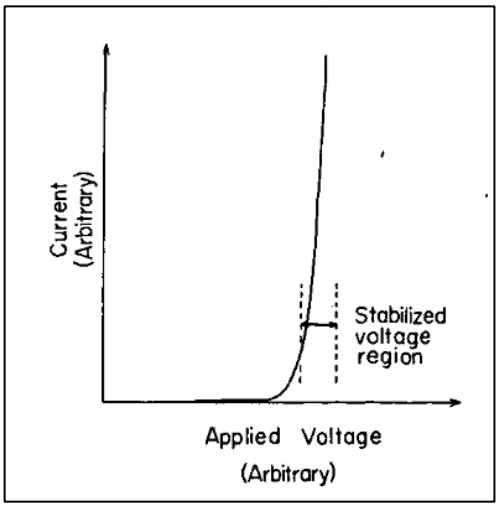

Figure 4.23. *Voltage-current graph of a typical varistor with arbitrary units [127].*

4.3. Results and Discussion

4.3.1. Cold sintering studies of ZnO-Bi_2O_3 system

4.3.1.1. The CSP of pure Bi_2O_3

Phase changes during the CSP of Bi_2O_3

Two different Bi_2O_3 powders were used in the studies. One of them was nano-Bi_2O_3 and the other one was micron-Bi_2O_3 powder. SEM images of both powders are served up. Micron-sized Bi_2O_3 powder has coarse agglomerates (Figure 4.24). Coarse agglomerates reaching 10 μm size and consist of finer grains of 0.5 – 1.0 μm. At nano-sized Bi_2O_3 powder, the particles are more equiaxed and completely spherical. The grain size is between 200 – 300 nm. As has been dealt with before, particle size is a parameter that can be effective in dissolution behavior. On the other hand, when the XRD results of both powders were examined, it was determined that there were differences in their crystal phases, as well, as shown in Figure 4.25. Nano- Bi_2O_3 consists of β-phase while the micron Bi_2O_3 powder consisted of the α-phase. In the CSP studies, experiments were done with both powders and it was tried to determine how effective it was on electrical properties.

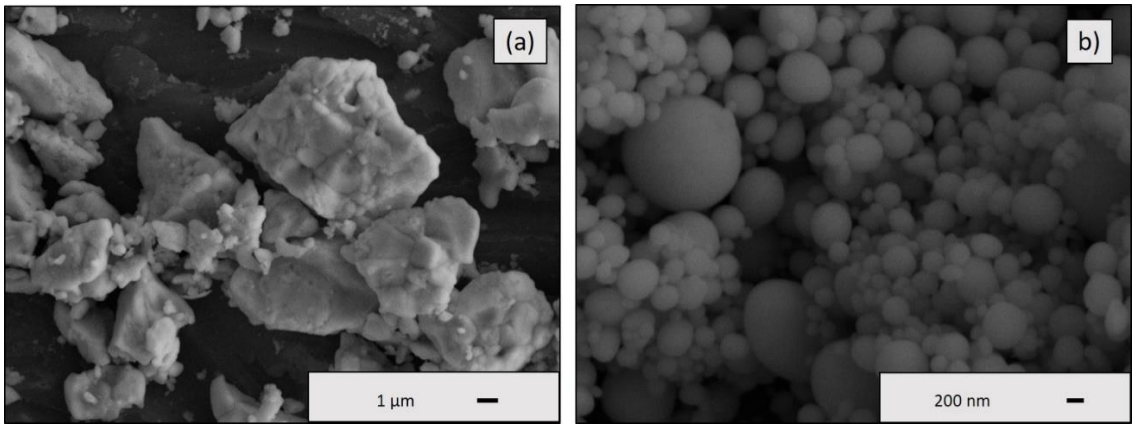

Figure 4.24. *BSE-SEM images of a) Micron-Bi_2O_3, b)Nano-Bi_2O_3 raw materials*

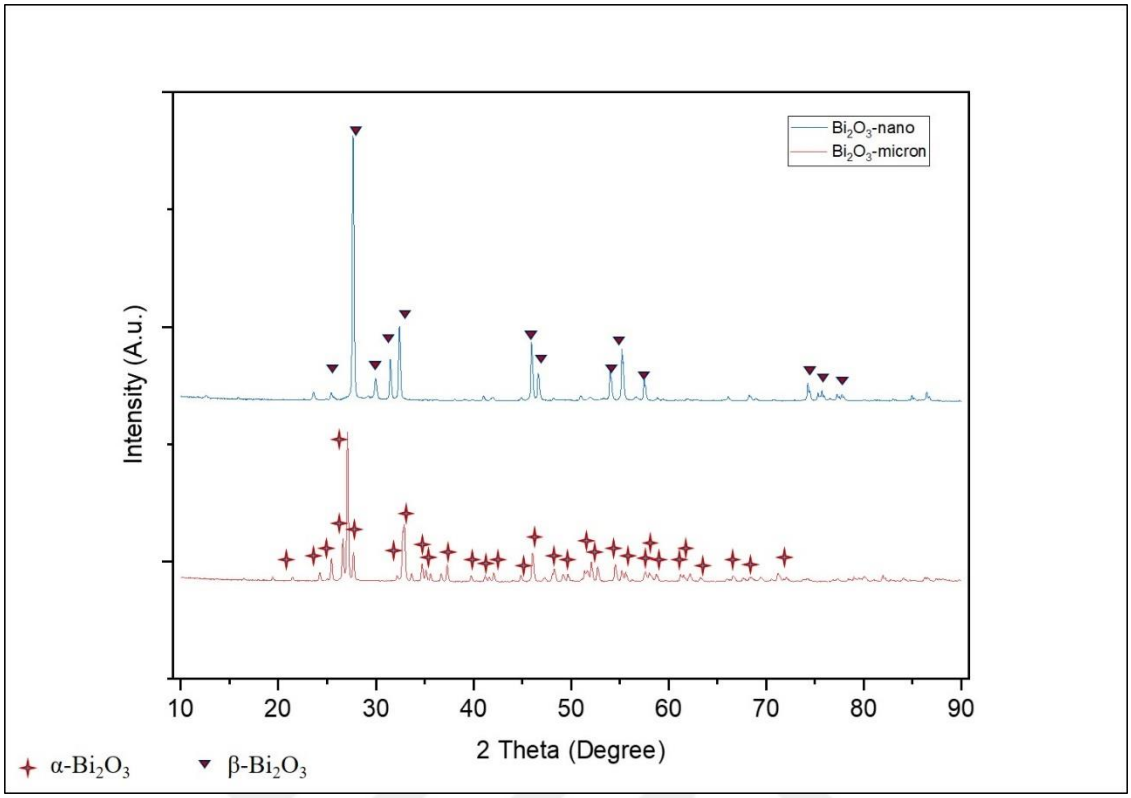

Figure 4.25. *XRD patterns of Micron-Bi_2O_3, Nano-Bi_2O_3 particles*

Pure Bi_2O_3 samples were sintered under the same conditions and at 140°C using Micron- Bi_2O_3 and Nano- Bi_2O_3 powders. The samples sintered at 140°C for 50 min. were subjected to XRD analysis after sintering. In Figure 4.26, it is seen that there is no phase change for Micron-Bi_2O_3 after sintering and there is still α-Bi_2O_3 phase in the structure. In Figure 4.26, the α-Bi_2O_3 phases can be seen, [134-136].

When the XRD analysis of the sample containing nano-Bi_2O_3 is examined, it was determined that there were some changes in the phases as shown in Figure 4.27. While the nano-Bi_2O_3 contained only β-Bi_2O_3 phase at first, it exhibited both α- and β- phases after the sintering. Changing the cooling regime to control the phases during the CSP was not possible with the available equipment. However, if necessary, the cooling regime can be changed with annealing and the phases can be brought to the desired point.

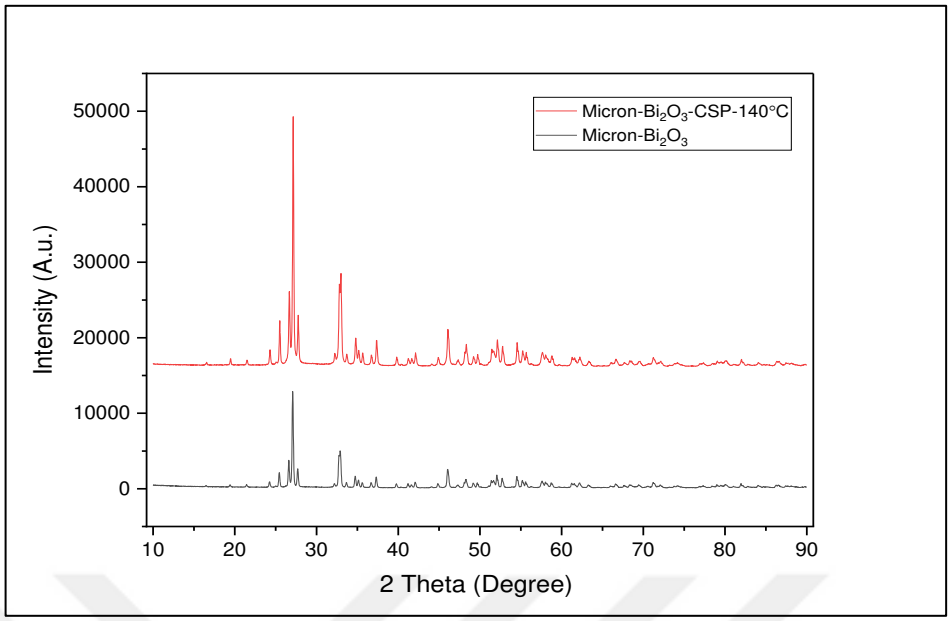

Figure 4.26. *XRD plots of Mikron-Bi_2O_3 raw material powder and Micron-Bi_2O_3 bulk sample after CSP at 140°C*

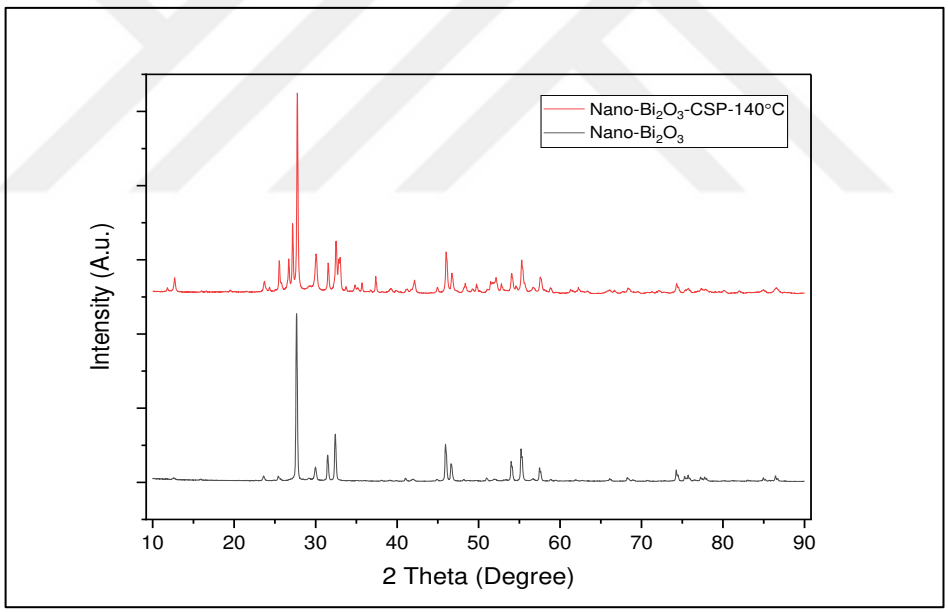

Figure 4.27. *XRD plots of Nano-Bi_2O_3 raw material powder and Nano-Bi_2O_3 bulk sample after CSP at 140°C*

The Microstructure Development During the CSP of Pure Bi_2O_3 System

Pure Bi_2O_3 CSP results show us the sinterability of the powder in pure form. Theoretical densities and sintering conditions are shown in the Table 4.1. Accordingly, 90.00 %TD. values have been reached. Trials were not made with different acids, but it was determined that the ZA (zinc acetate) salt solution at pH 5.5 was sufficient. It was observed that the densities did not change much when nano and micron size Bi_2O_3 were

used. However, the required liquid ratio for the system changes depending on the particle size due to change in total surface area. The optimum liquid ratio required for the nano-size powder was approximately 1.0 wt % higher than for the micron-size powder.

The microstructures of the samples were characterized by scanning electron microscope. The microstructural features of the samples in the broken surface BSE-SEM images are shown in Figure 4.28 and densities of the samples are given in Table 4.2. All samples have theoretical densities over 90.00 %TD. Figure 4.28 a shows the sample produced with nano-Bi_2O_3 powder and the production conditions are the same as the sample, shown in Figure 4.28 b. The only difference between them was the starting powder. It is seen that the grain size of the material produced with nano-sized powder in Figure 4.28 a is much finer even after the sintering. It can be seen that some grains maintain their initial a spherical form. The structure is different in the sample that produced with micron particle size powder. The heterogeneous particle size distribution in the starting powder was ultimately reflected to the final microstructure. It is seen that the grains have angular structures in micron grain size samples.

Table 4.1. *Sintering conditions and T.D. % of the samples made with pure Bi_2O_3 CSP.*

Sample	Pressure (MPa)	Time (min.)	Temp. (°C)	Liq. (wt %)	pH	T. D. (%)
Micron-Bi_2O_3	539	50	140	4.00	5.5	94.31
Micron-Bi_2O_3	539	50	140	4.00	5.5	95.34
Micron-Bi_2O_3	539	50	140	4.25	5.5	96.48
Micron-Bi_2O_3	539	50	140	3.75	5.5	95.62
Micron-Bi_2O_3	539	50	140	4.50	5.5	94.79
Micron-Bi_2O_3	539	50	150	4.25	5.5	96.06
Micron-Bi_2O_3	539	50	130	4.25	5.5	95.24
Micron-Bi_2O_3	547	50	140	4.25	5.5	96.29
Micron-Bi_2O_3	532	50	140	4.25	5.5	94.95
Micron-Bi_2O_3	539	50	140	4.50	5.5	90.62
Micron-Bi_2O_3	539	50	140	4.00	5.5	96.59
Nano-Bi_2O_3	539	50	140	5.33	5.5	96.11
Nano-Bi_2O_3	539	50	140	4.50	5.5	92.05

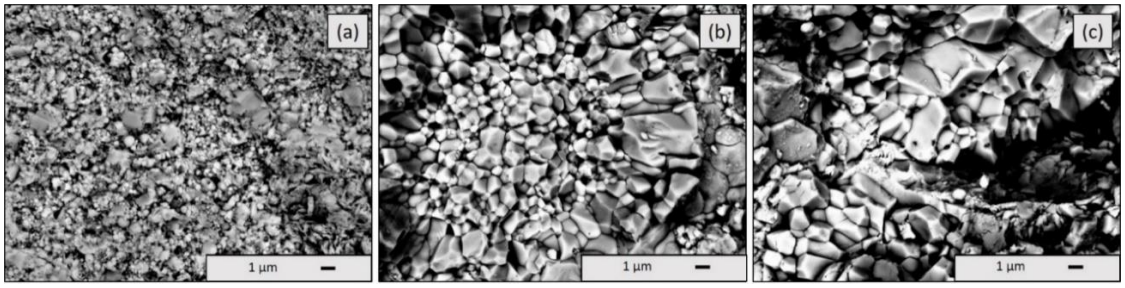

Figure 4.28. *BSE-SEM micrographs of pure Bi_2O_3 after the CSP at140°C for 50 mins. a) nano-Bi_2O_3 powder b) micron-Bi_2O_3, c) micron-Bi_2O_3*

Table 4.2. *SEM samples specifications*

SEM sample	Bi_2O_3 powder size	Liq. (wt %)	T.D. (%)
a	Nano	4.50	92.05
b	Micron	4.50	90.62
c	Micron	4.50	96.59

Electrical characterization of pure Bi_2O_3

The electrical properties of pure Bi_2O_3 bulk samples were examined. Compared with pure ZnO, the behavior of Bi_2O_3 appears to be quite different (Figure 4.29). Although it seems to show an increasing conductivity value, material couldn't be reached 1mA value, the material was actually an insulator. Despite reaching high voltage values such as 8000 V/cm, the material did not transmit electric current. For this reason, the threshold voltage and α value of the material cannot be calculated. It is already known that this material does not have varistor properties. These results were not surprising because in the ZnO-based varistor system while ZnO grains are conductive, the grain boundaries which are usually bismuth oxide rich regions are non-conductive. These two-mode nature of the microstructure results in non-linear I-V characteristic as mentioned above. In fact, high non-conductive nature of the Bi_2O_3 after the CSP can be a good indication that when they are mixed with ZnO and then sintered via the CSP, these mixture can exhibit non-linear I-V behavior that means varistor characteristics. I-V test samples that are mentioned at Figure 4.29 are the samples as in Table 4.2, respectively.

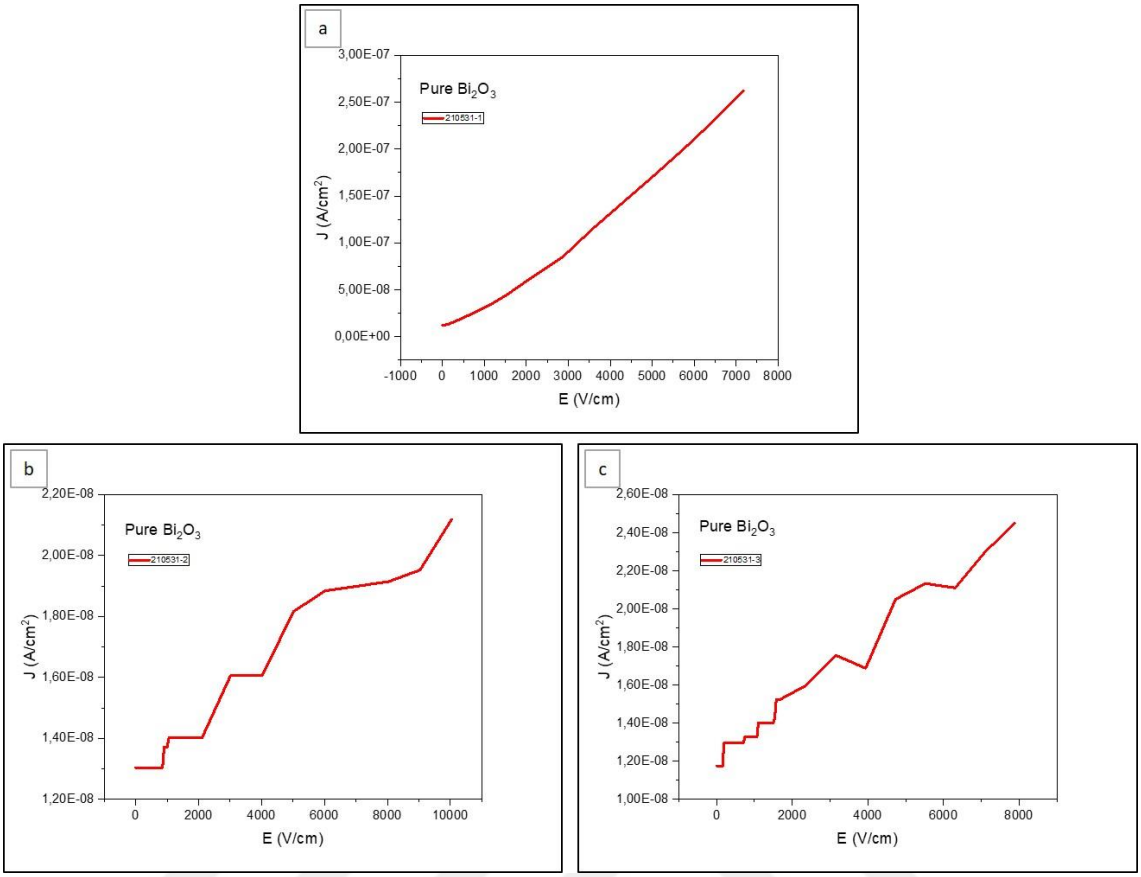

Figure 4.29. *Pure Bi_2O_3, I-V curves pure Bi_2O_3 after the CSP at140°C for 50 mins. a) nano-Bi_2O_3 powder b) micron-Bi_2O_3, c) micron-Bi_2O_3*

4.3.1.2. The CSP of ZnO–Bi_2O_3 ceramics

Particle size effect on the CSP

Figure 4.30 a) and b) shows the Bi_2O_3 raw materials used in the trials. Figure 4. 30 a) is the Bi_2O_3 powder used as a standard, it is seen that there are micron-sized grains and agglomerates. The powder particle size range is approximately 1-50 µm. On the other hand, Bi_2O_3 in the SEM photograph in b) is very fine-grained and homogeneous. It has nano grains. The powder particle size range is approximately 50-100 nm. It was already determined for Bi_2O_3 that the microstructures were different when sintered alone. However, to see the behavior in the binary system, experiments were done with Bi_2O_3 with both grain sizes. Figure 4. 30 shows the ZnO powder used as a standard in c and the Micno image in d. Although the MicNo powder is actually composed of nano grains, the fact that it is in the form of plates has caused it to be among these trials. Powder morphology has an effect on dissolution. If the dissolution behavior of MicNo is slow compared to ZnO used as standard, during CSP, Bi_2O_3 can save time to surround the

plates. Sintering trials were carried out under the same conditions using powders with these different grain sizes.

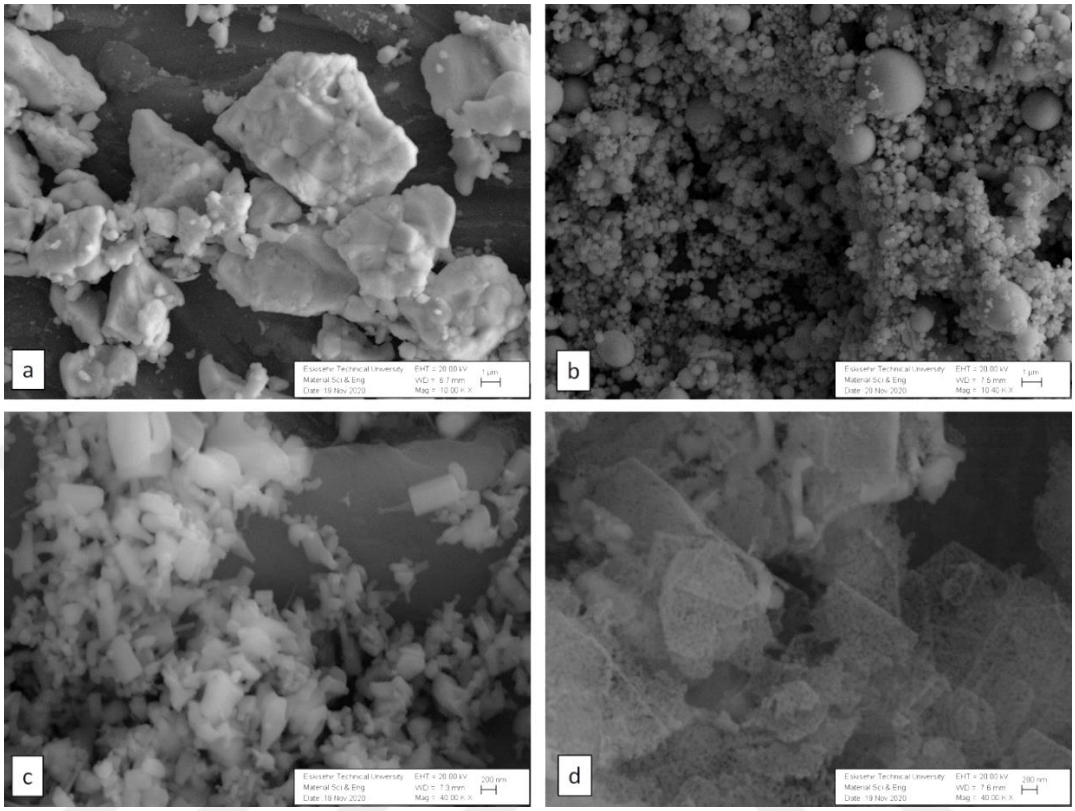

Figure 4.30. *SEM images of the raw materials used a) micron sized Bi_2O_3, b) nano sized Bi_2O_3, c) ZnO, d) MicNo ZnO*

The image of the sample containing micron-sized Bi_2O_3 in CSP trials using different raw materials is given in Figure 4.31 a). The theoretical density value is 93.76 %. The sample containing Nano-Bi_2O_3 is shown in Figure Figure 4.31 b). The theoretical density of the sample was 94.66 %. Both samples were densified as well. The pores of the sample containing Nano Bi_2O_3 are more prominent. Sintering conditions were given at section 4.2.2.1, CSP of ZnO-Bi_2O_3 mixed powder.

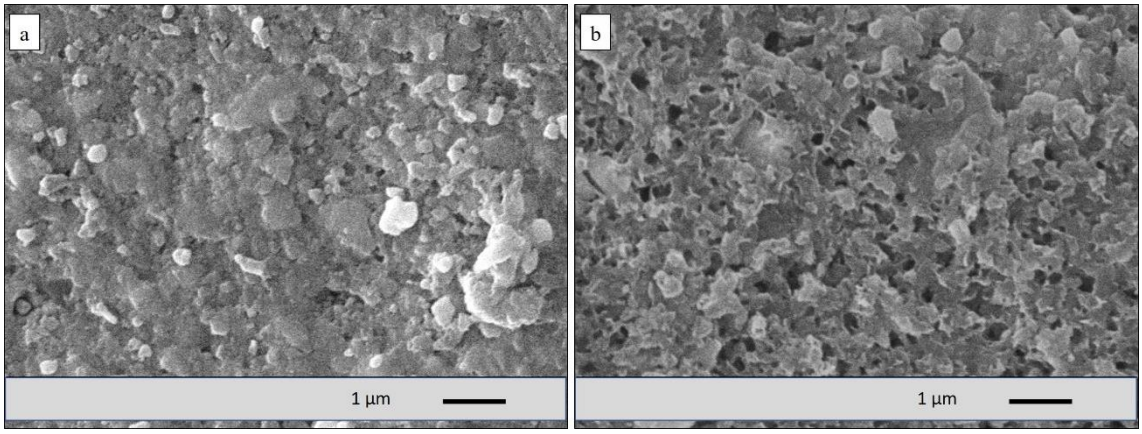

Figure 4.31. *a) ZnO containing 1% mol micron-sized Bi_2O_3 b) SEM images of bulk ceramics produced with ZnO, CSP containing 1 % mol nano-sized Bi_2O_3*

Another raw material trial was the use of MicNo powder as a source of ZnO. As mentioned before, Bi_2O_3 powder was added to the system in the mill, but the mixing process was done by hand to prevent the plates from breaking. Although its homogeneity is discussed, it has been observed that ZnO is coated with Bi_2O_3 and the powder has a yellowish homogeneous color. The sintering process was carried out under the determined standard conditions. Humidification was done in the air as in all experiments. Figure 4.32 a, the density of the sample containing MicNo after sintering was determined as 1.41g/cm^3. The theoretical density is 5.72g/cm^3. Sintering of the platelet shaped powder has not been achieved sufficiently, it was broken easily as seen at Figure 4.32 b.

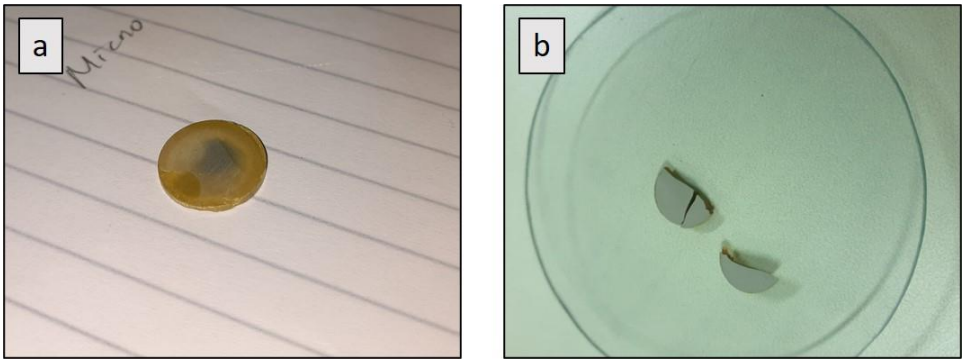

Figure 4.32. *Photo of samples produced with MicNo as ZnO source, a) Sintered micro sample containing 1% mol Bi_2O_3 b) broken sample after silvering*

Dispersing and solubility

Among these factors, the environment around the grain can be changed by pH. In addition, the liquid medium can also be used as an important tool. Pure water with

adjusted pH is the solvent at this study. Experiments at different pHs were made in previous studies. In all experiments, pH ranges were chosen as acidic. Because dissolution is an important factor for the CSP, it was aimed to obtain higher densities with increasing solubility. An untested study was conducted, and liquids with pH 9.5 – pH 10.5 – pH 11.5 were prepared using ammonia and CSP trials were carried out with these liquids. The aim here was to turn the partial solubility of ZnO powder into an advantage at these pH ranges and to enable the Bi_2O_3 solubility to compete with ZnO. However, in all three pH experiments, bulk samples could not be obtained as a result of CSP. All samples were broken out of the mold. Partial dissolution was not sufficient to maintain density during the process. For this reason, after all the trials in which the powder was mixed in the mill, it was decided to carry out CSP trials by coating ZnO with Bi_2O_3. The purpose was to ensure that the solubilizing liquid primarily interacts with Bi_2O_3, so that the dissolving Bi_2O_3 has a higher ratio at the grain boundaries and the varistor properties can be improved for the CSP method. We have seen that the effective mechanism in the CSP process is possible by the dissolution of the materials and their precipitation into regions with lower energy. All research in the literature give chase this attitude of mind, [25,137]. Understanding the dissolution mechanisms and acting accordingly is the method that should be applied to achieve the desired structure in the CSP process.

For this reason, its dissolution properties should be studied in more detail. Figure 4.33 and 4.34 show the equilibrium phase stability diagrams for ZnO and Bi_2O_3 that describes dissolution of such compounds as a function of pH, respectively. The pH 5.5 range we work with is marked in red on the ZnO chart. At pH 5.5, ZnO appears to have the ability to dissolve almost completely. In the previous zeta measurement experiments we conducted in our own laboratory, the pH could not be lowered below 6.5 because ZnO was completely dissolved. Bi_2O_3 is also a well soluble material, but it is not completely soluble, see at Figure 4.34. There is some solid phase Bi_2O_3 in the system. It is a material with limited solubility.

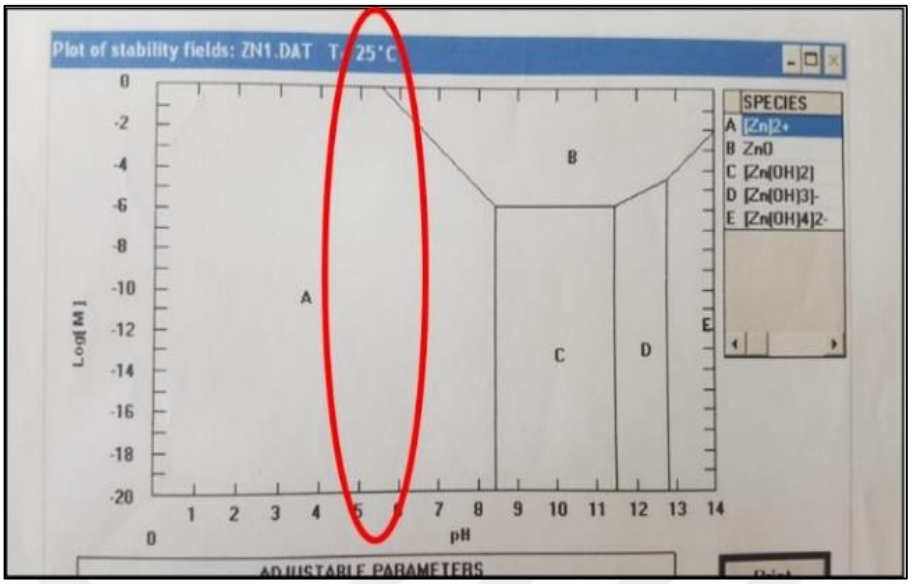

Figure 4.33. *pH dependent dissolution graphs of a) ZnO and b)Bi_2O_3*

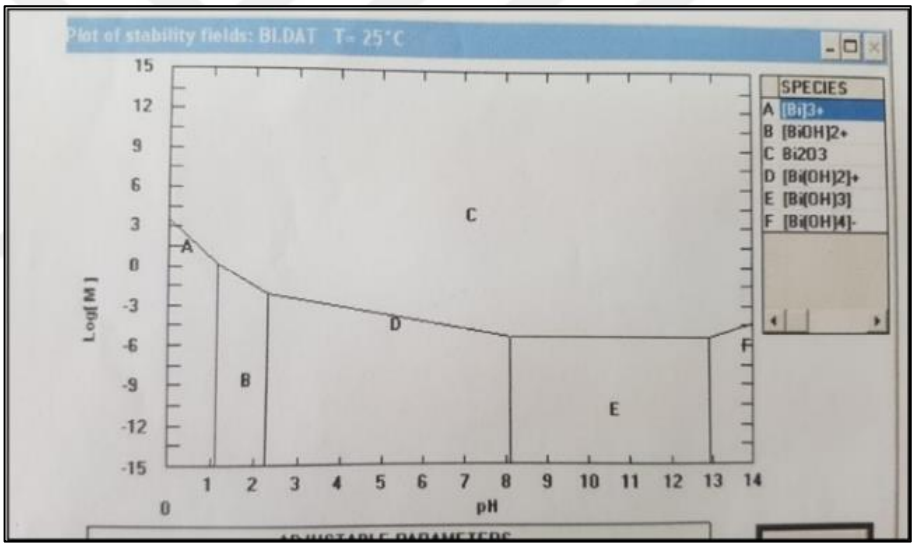

Figure 4.34. *pH dependent dissolution graphs of a) ZnO and b)Bi_2O_3*

For the pre-trials, ZnO and Bi_2O_3 were mixed in the mill for 2 hours. When the bulk samples produced with CSP were examined by SEM, it was determined that the samples were not homogeneous sufficiently. In Figure 4.34, there is a SEM image showing the general view of the sample. While it is back scattered image, white grains should be considered as bismuth oxide and dark areas should be considered as zinc oxide. Theoretical density of the sample is 94.45 % and although it's not very clear, there are fine textured cracks on the sample. It is estimated that this fine crack appearance occurs as a result of rapid evaporation during the removal of water from the system. This sample

was the first good sample without lamination, just before optimization of sintering parameters, mentioned in Thesis Part 1. However, when the SEM and EDX results in Figure 4.35 and Figure 4.36 were examined, it was seen that the Bi distribution was not homogeneous.

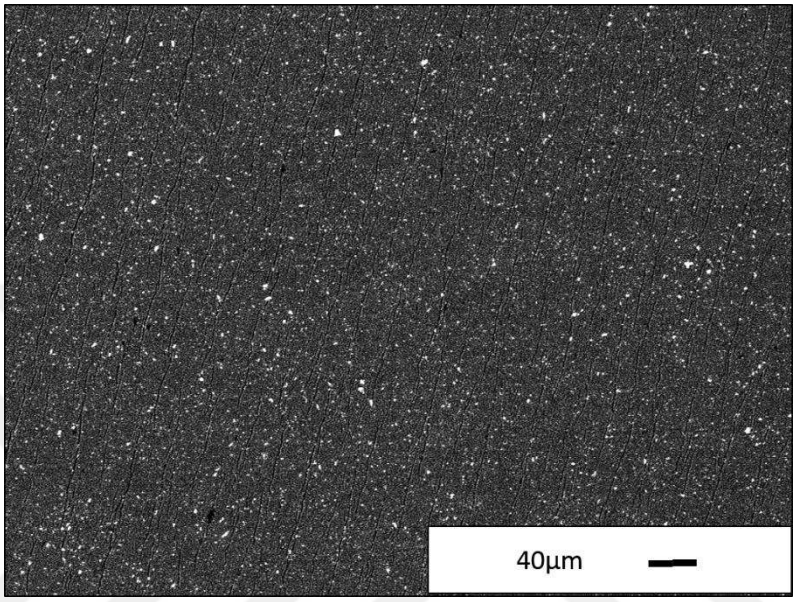

Figure 4.35. *BSE SEM image showing the overall microstructure*

In Figure 4.35, EDX analysis was taken from the white grain and overall dark grey area. Obtained atomic weight percent ratios are given in Table 4.3. When bismuth oxide added with 1% mol to the system, the Zn/Bi ratio to be seen is approximately 15. There is a difference of approximately 9.6 times as seen at the Table 4.3 Agglomerated bismuth grains in the analysis area may also have influence on the bismuth rate in the measurement result. However, in general, it is possible to say that there is enough dispersed bismuth in the system.

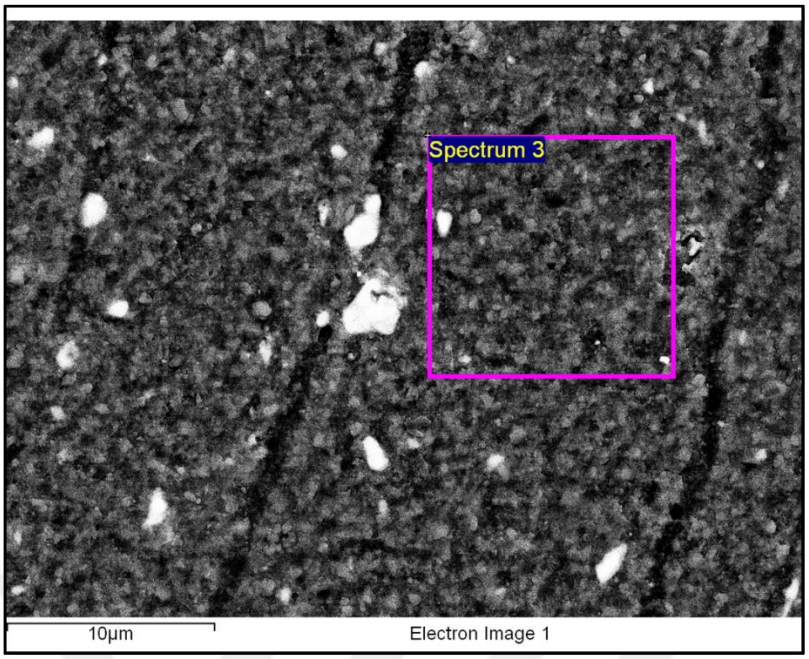

Figure 4.36. *SEM image showing the EDX analysis region*

Table 4.3. *EDX analysis result, general distribution*

Element	Wt %	Atomic %
O K	15.23	43.97
Zn K	76.81	54.28
Bi M	7.96	1.76
Total	100.00	

As a result of the white grain analysis in Figure 4.36, it is seen that there is intense bismuth. Bismuth-rich agglomerates are evenly distributed throughout the material. Table 4.4 shows the results of the analysis. The white grains appear to be rich in bismuth.

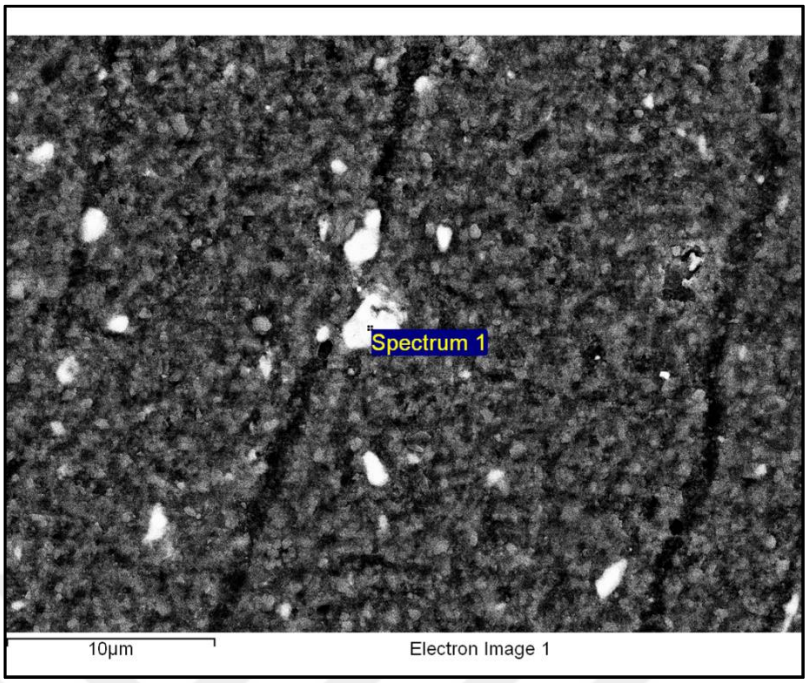

Figure 4.37. *SEM image showing the EDX analysis region*

Table 4.4. *EDX analysis result, white point analysis*

Element	Wt %	Atomic %
O K	13.79	62.20
Zn K	10.58	11.68
Bi M	75.63	26.11
Total	100.00	

When the grains and grain boundaries are examined at Figure 4.38 b, it is seen that the grains are of equal size and the average grain size is about 100 – 150 nm. The SEM image of the powder used is given in Figure 4.38 a. The grains formed by the raw material with a grain size of 100 – 150 nm as a result of sintering are almost the same. Accordingly, it is seen that there is not much growth in the average grain size. BET analysis of the ZnO powder was performed in Chapter 1 and surface area of 5.8796 m^2/g was obtained.

It is seen that the grains touch each other, but the grain boundaries are not clear. The sample was first examined as a broken surface without being polished, then the polishing and etching conditions were determined and the samples polished under these conditions and etched with HCl - water solution were examined. Etching solution taken from Ö. Özer thesis [138]. The water/acid ratio was used as 40/1.

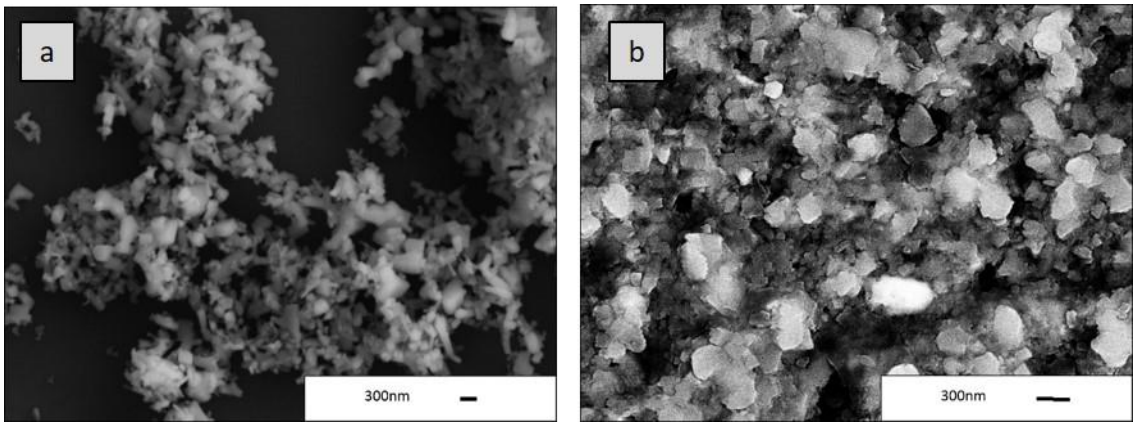

Figure 4.38. *a) ZnO raw material and b) Top surface view from the polished sample, BSE SEM*

In the EDX mapping analysis shown in Figure 4.39 and 4.40, it is seen that both atoms have a balanced distribution. It is not clear from the images whether the Bi_2O_3 atoms are at the grain boundaries or not. In order to understand this situation, it would be appropriate to perform a TEM analysis.

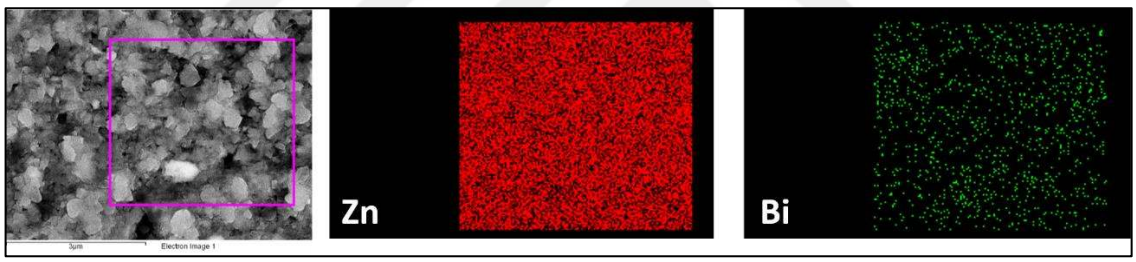

Figure 4.39. *SEM EDX mapping, Zn and Bi ion distributions, polished top surface view*

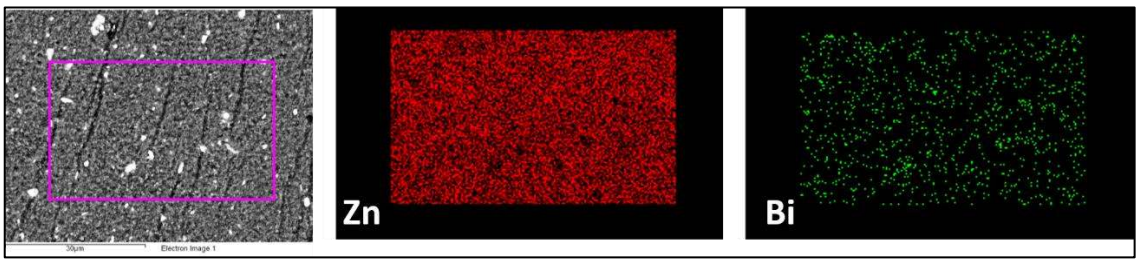

Figure 4.40. *SEM EDX mapping, Zn and Bi ion distributions, polished section view*

When we look at the structure of the samples up to this time, it is seen that there is no homogeneity for the Bi_2O_3 distribution. Varistors are ceramics that stand out with their internal structures. The homogeneity of the structure is as important as the grain size and the structure of the grain boundaries. For the CSP process, powder preparation is even more important, because at low temperature Bi_2O_3 will not have a chance to form a liquid

phase and disperse throughout the entire structure. The non-homogeneous structure will also create fluctuations in the electrical properties, causing the desired values not to be achieved. In this case, as a process improvement step, it was decided to make some trials for the appropriate dispersant system and then to study the mixing times of Bi_2O_3 and ZnO in the mill. It is necessary to use the appropriate dispersant during mixing in the mill and to optimize the mixing time in the mill.

For dispersant selection, sedimentation test was performed. Powder and ethanol were prepared by weighing in 3 different beakers and mixed for 1 minute with an ultrasonic probe, and the mixtures were placed in 100 ml measuring tapes. Crash conditions were checked at regular intervals. The test showed itself completely within 24 hours. The powder containing the PAA dispersant precipitated in the first 1 hour, Figure 4.41. The powder containing Darvan C settled in halfly in 1 day. Tego-containing powder, on the other hand, did not fully settle for 1 day. In this case, it was decided that Tego was the most suitable dispersant for ZnO. Tego will be used as dispersant for mixing procedure. Figure 4.42 shows settling behavior of powders over time as graph. It's seen that for the Tego, curve in orange colour, even after 1 day holding time, nearly no collapsing.

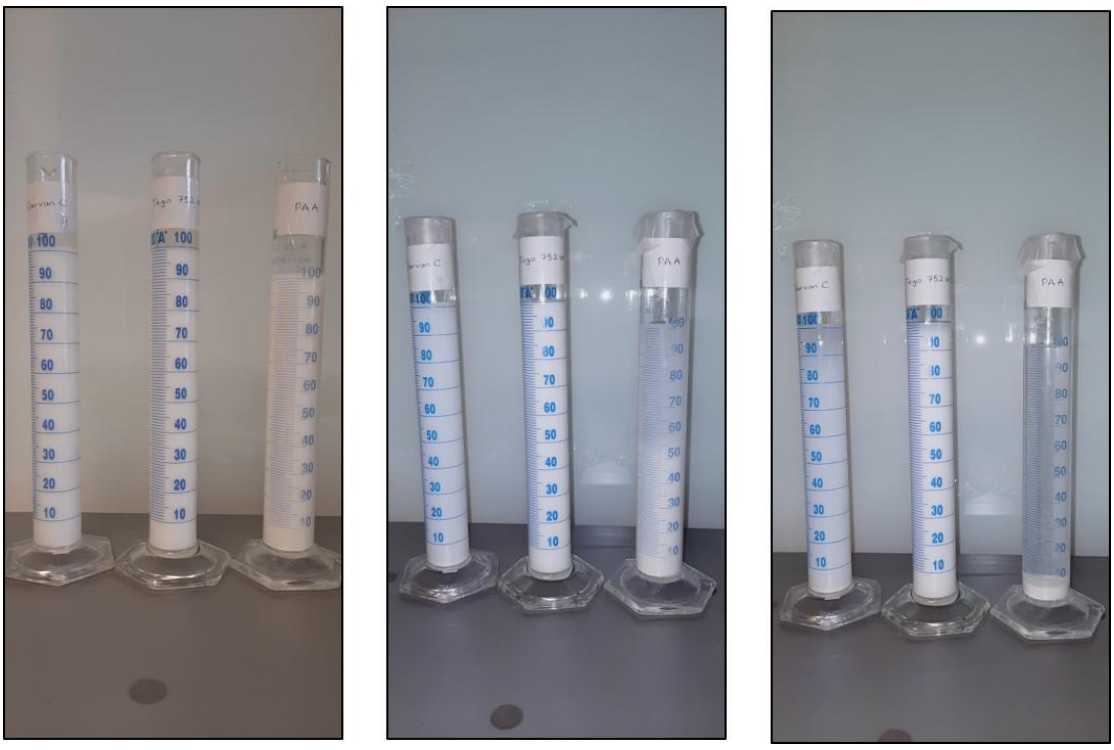

Figure 4.41. *Photographs of sedimentation test after a) 0 hour, b) 1 hour, c) 1 day*

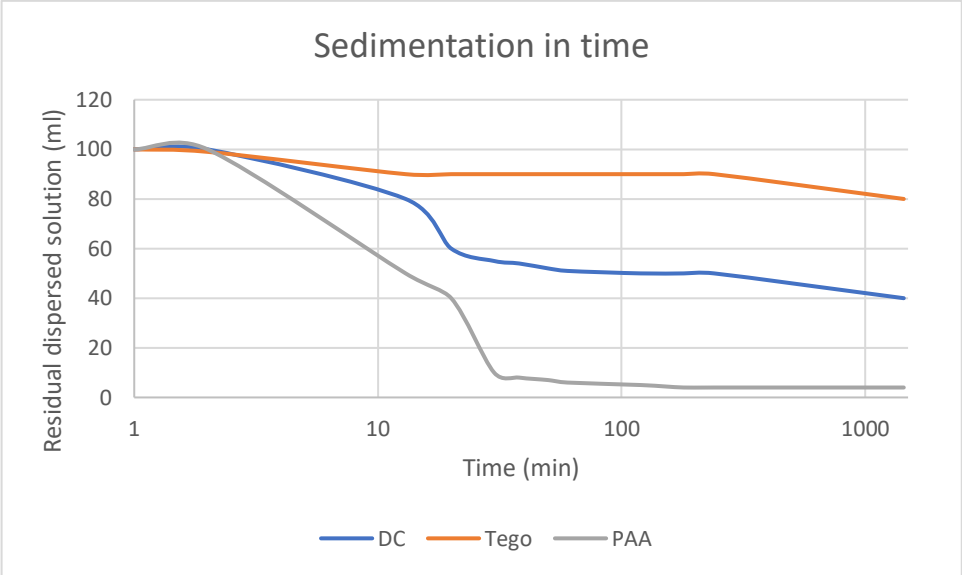

Figure 4.42. *Sedimentation test of ZnO with different dispersant in time*

Another homogenization study is the determination of milling times. After different mill mixing times, the samples were sintered and analyzed by SEM. The aim here is to determine the homogeneity on the bulk sample. First, general images were examined with SE technique, Figure 4.43. No significant differences were observed between the microstructures. Milling times are written on the images and show mixing time ZnO and Bi_2O_3 together.

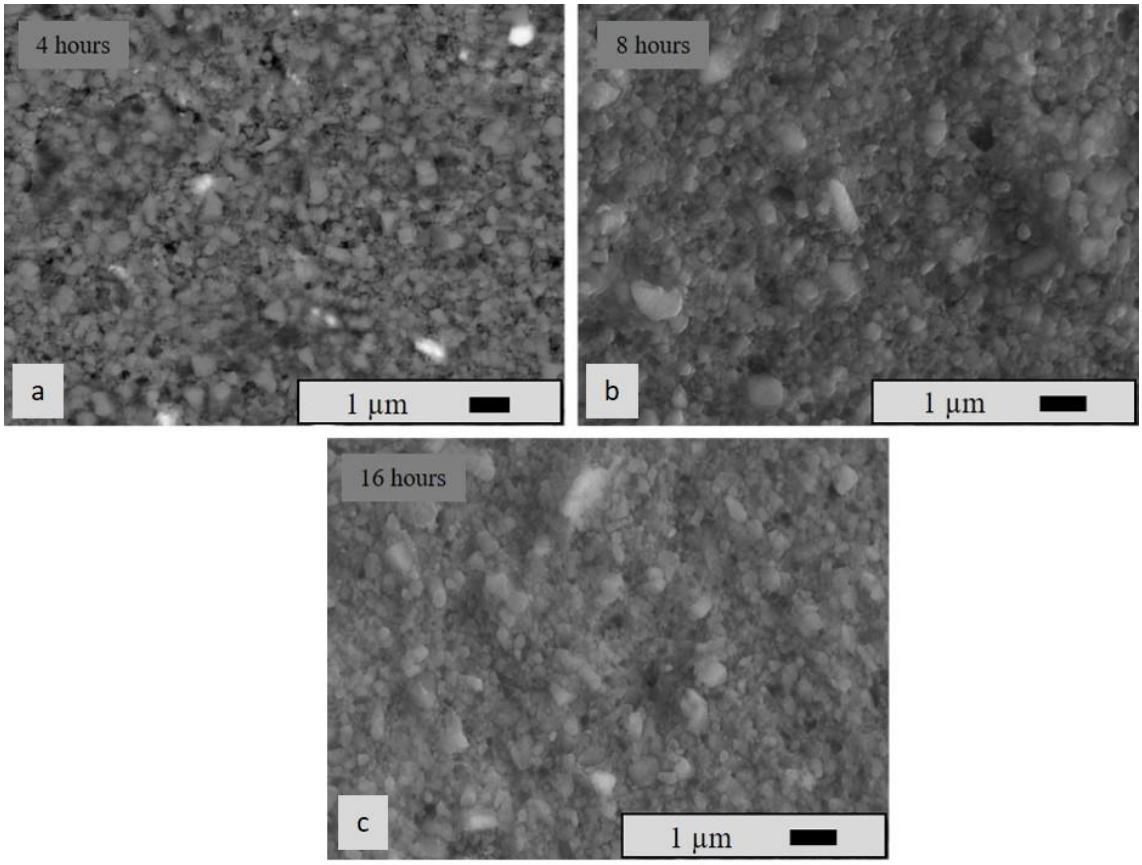

Figure 4.43. *SE SEM image of ZnO bulk materils, powders of the samples were mixed in the mill for different times, a)4 hours, b)8 hours, c)16hours*

When the BSE images were examined, it was determined that there was a difference between the microstructures, Figure 4.44. The white dots in the images show the Bi_2O_3 distribution. The color of the heavy element is reflected on the screen more clearly. In this case, it is possible to say that the sample is more homogeneous at the end of the mill mixing period of 16 hours. At other mixing times, there are still undispersed Bi_2O_3 agglomerates. In this case, it would be a more accurate approach to increase the time to prepare the powder mixture.

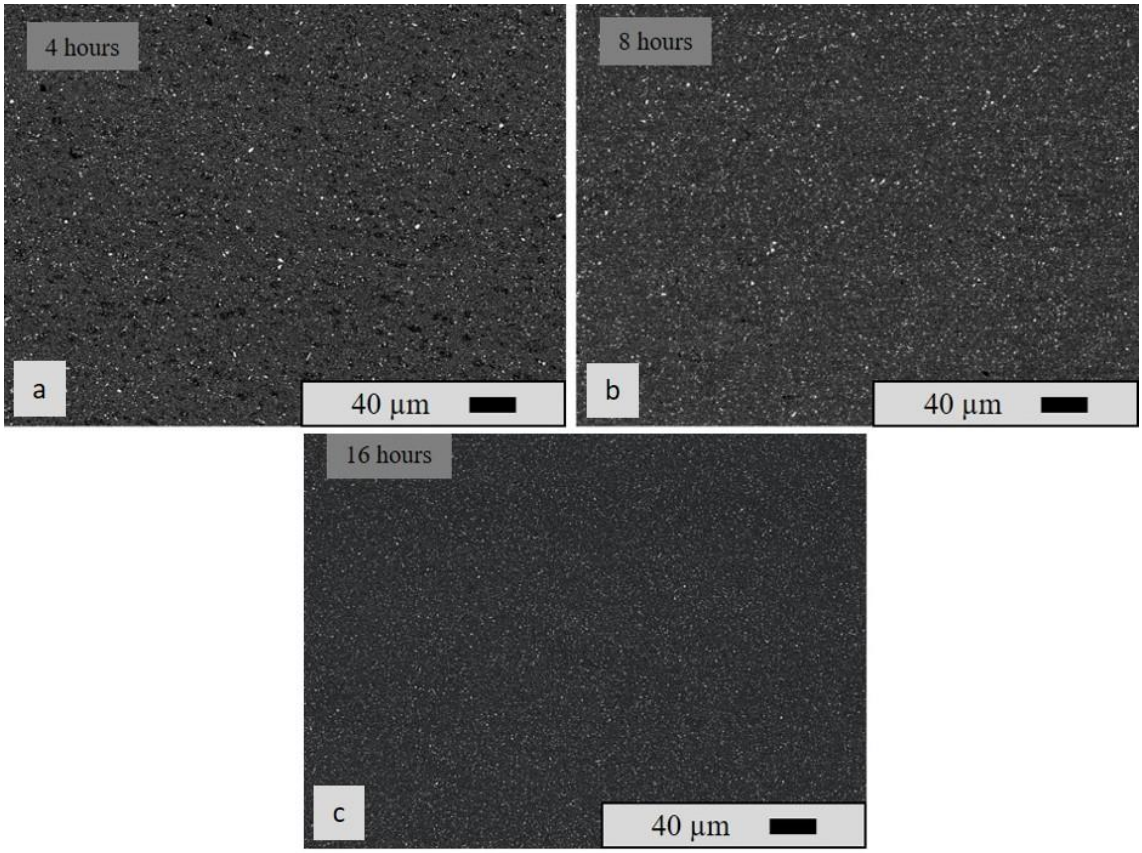

Figure 4.44. *BSE SEM image of ZnO bulk material, mixed in the mill for different times after sintering, a)4 hours, b)8 hours, c)16hours*

Bulk materials were examined to see homogenity by EDX method, Figure 4.45. In this case, field chemical analysis was made from different parts of the bulk samples and it was checked whether the amount of Bi_2O_3 was homogeneously distributed. Initial EDX analysis shows 8 hours of mill time. Accordingly, it is possible to say that the Bi_2O_3 distribution has closer values than the 16-hour milling period in the next figure, Figure 4.46. However, despite this analysis result, 16 hours mill mixing time will be used since it was determined in visual analysis that the dispersion of agglomerates and the homogeneity of the image were better in 16 hours mixing time.

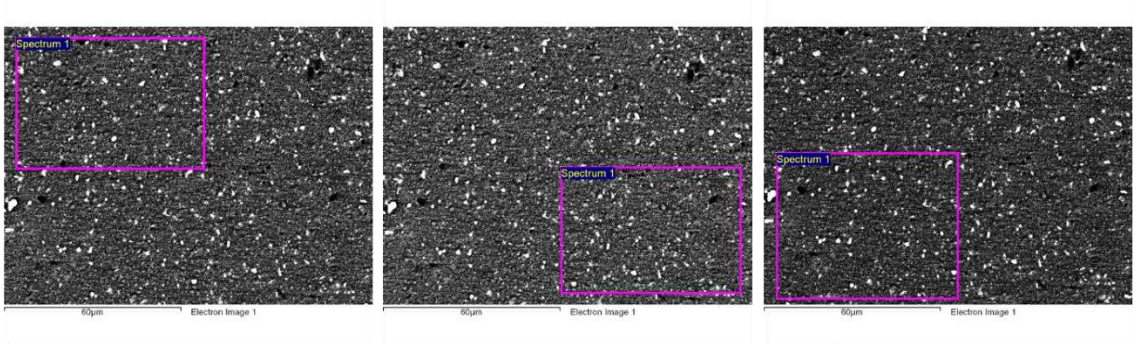

Element	Weight%	Atomic%
O K	18.18	49.27
Zn L	74.04	49.12
Bi M	7.79	1.62
Totals	100.00	

Element	Weight%	Atomic%
O K	17.31	47.61
Zn L	75.64	50.91
Bi M	7.05	1.48
Totals	100.00	

Element	Weight%	Atomic%
O K	17.82	48.44
Zn L	75.38	50.14
Bi M	6.79	1.41
Totals	100.00	

Figure 4.45. *Area EDX analysis of bulk ceramic after sintering of the powder prepared by mixing in the mill for 8 hours*

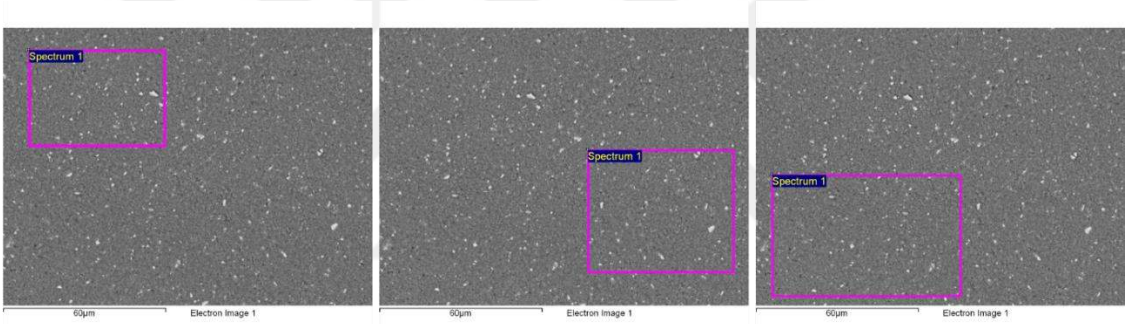

Element	Ağ.%	Atomik%
O K	15.72	45.20
Zn L	74.99	52.76
Bi M	9.28	2.04
Total	100.00	

Element	Ağ.%	Atomik%
O K	17.64	48.47
Zn L	74.00	49.77
Bi M	8.36	1.76
Total	100.00	

Element	Ağ.%	Atomik%
O K	16.46	46.01
Zn L	76.87	52.57
Bi M	6.67	1.43
Total	100.00	

Figure 4.46. *Area EDX analysis of bulk ceramic after sintering of the powder prepared by mixing in the mill for 16 hours*

CSP of ZnO-Bi_2O_3 system

Bi_2O_3 usage rate in varistor production was determined as 1% mol in previous studies in literature. Detailed information about the selection of this ratio is given in the study of Bernik et al. Bernik states in his study that the optimum Bi_2O_3 addition is 1.0 % mol [139]. Although this amount can be optimized for CSP in the future, the Bi_2O_3 ratio was kept constant in the current studies.

In the first trials, the optimum water ratio was adjusted for the material by using the CSP conditions, which had the best results previously. Other conditions were fixed as pH

5.5, final temperature 300°C, press pressure 155 MPa. The water ratios used in the first trials were 2.01 – 2.16 – 2.83 – 3.39 – 5.66 – 4.01 – 4.32 wt %. The liquid ratio with the highest density obtained as 5.66 %.

The temperatures were changed between 100 – 260°C for the temperature adjustment, Figure 4.47. The density values obtained accordingly are given in Table 4.5. The highest theoretical density observed at 140°C sintering temperature, and was 96.14 %. However, it has been seen in more trials with the liquid ratio that there is an increase in density at the extreme values of 5.0 % and 8.5 % water ratio, Figure 4.48 a. When the theoretical densities are examined by increasing the number of samples, it is seen that the densities fluctuate, Figure 4.48 b.

Figure 4.48 b the average theoretical density for all liquid ratios was determined as 93.97 %. The green curve in the graph shows the average density. The standard deviation is 1.91 % and indicated by red lines. The yellow lines are the values where the lowest and highest density is seen. It is not desirable for the highest and lowest density values to go beyond the standard deviation values. This indicates that there are uncontrolled points in the process. The most obvious variable in the process is the method of distribution of moisture. Moisture is dispersed in the powder at mortar and pestle for 1 minute. Some of this moisture evaporates during processing. In the studies in the first chapter, the amount of liquid supplied to the system and the amount of moisture measured in TG-DTA were different. In the last stage of sintering, the amount of liquid dispersed in the system will change the diffusion rate. Liquid film thickness will cause the diffusion paths to decrease or increase. The application of water in the system can be an important factor, since the change in the amount of this liquid will be effective even if it is very small. The applicability of such a sensitive process in an industrial environment should be discussed further in the future. Theoretical densities were measured by the Archimedes method and theoritical density was used as 5.72g/cm^3. General CSP conditions used were 1.5 g powder (ZnO +1 mol % micron-Bi_2O_3), liquid pH 5.5, sintering was at 140°C and 350MPa for 50 min. Unless otherwise stated, these conditions are determined as general conditions. The standard liquid ratio was used as 6.5 wt. %.

Table 4.5. *Theoretical density variation of pure ZnO and ZnO with the addition of 1% mol Bi_2O_3 with varying temperature*

Sample	Pressure (Mpa)	Time (min.)	Temp. (°C)	Liq. (wt %)	pH	T.D. (%TD)
ZnO-Bi	540	50	100	6,47	5,5	91,68
ZnO-Bi	540	50	140	6,47	5,5	96,14
ZnO-Bi	540	50	180	6,47	5,5	95,52
ZnO-Bi	540	50	220	6,47	5,5	93,13
ZnO-Bi	540	50	260	6,47	5,5	sticking
ZnO-Bi	540	50	260	6,47	5,5	sticking

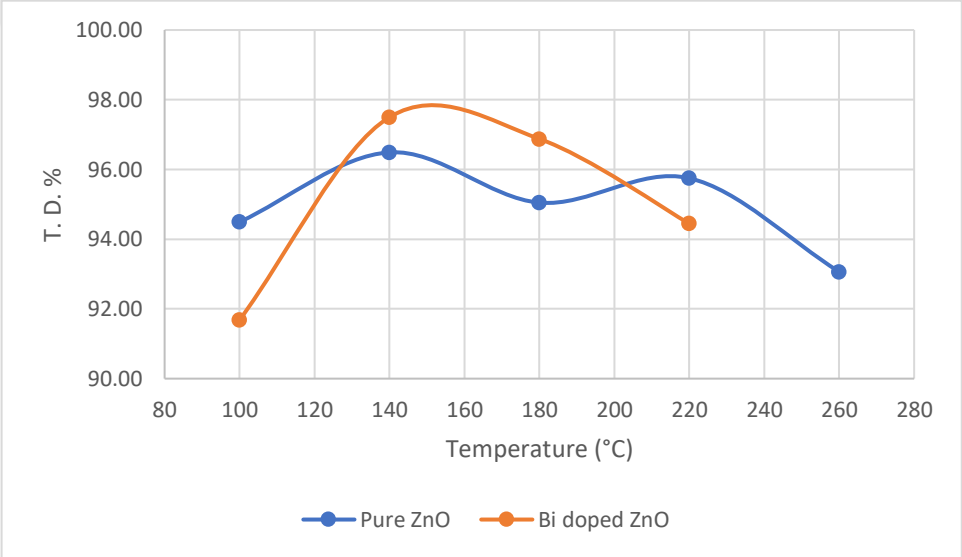

Figure 4.47. *Theoretical Density change as a function of the temperature of pure ZnO and ZnO with Bi_2O_3 addition*

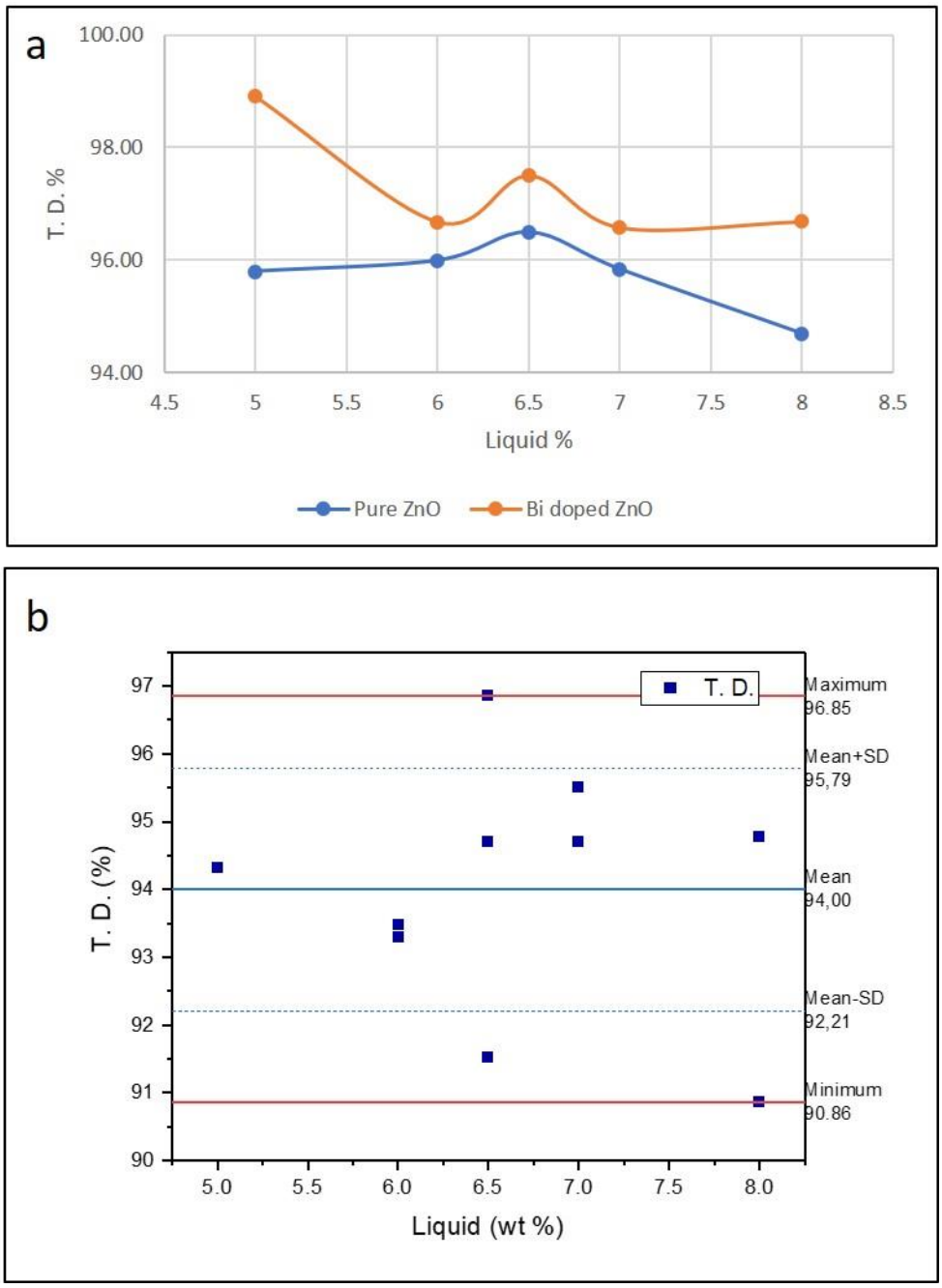

Figure 4.48. *a) T.D. % change according to pure ZnO and Bi_2O_3 added ZnO liquid ratio, b) Graph of theoretical densities and statistical limit values depending on the liquid wt. ratio*

While the density fluctuations at different liquid ratios persist, the SEM images below give us information about the microstructure, Figure 4.49. At the SEM images, it was observed that the pores were more prominently located at the grain boundaries in the sample containing 8.0 % water. This sample, in which the most liquid was used, was examined more closely. Figure 4.49 show SEM images of the sample containing 8.0 wt % water.

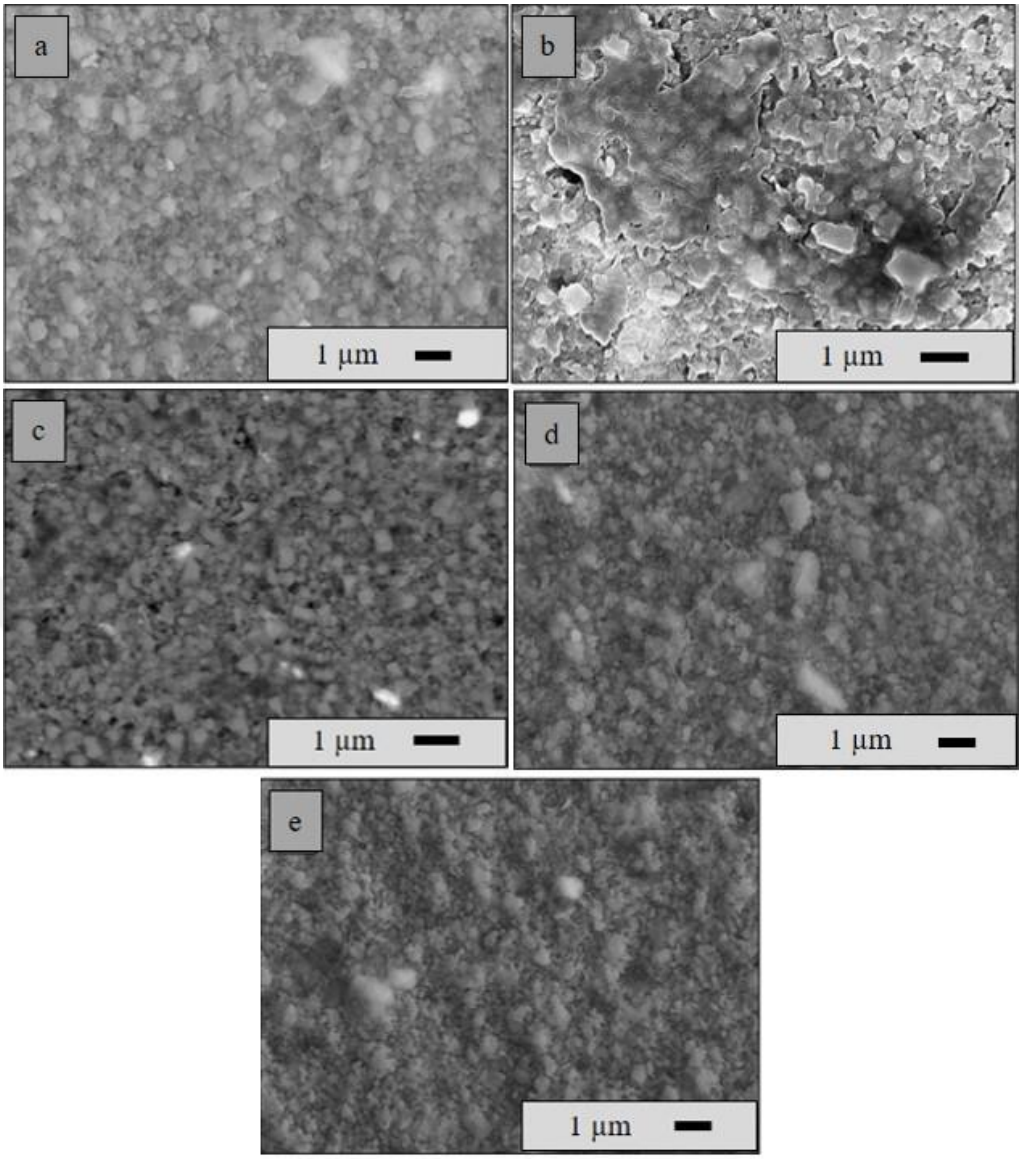

Figure 4.49. *ZnO SEM images containing 5.0%, 6.0%, 6.5%, 7.0%, 8.0% and 1% mol Bi_2O_3 by weight, respectively*

At Figure 4.50, grains and grain boundaries can be easily selected. It is possible to say that sintering is in the 2nd stage; In the second stage, the material's theoretical density is almost 90-95%, the pores become connected, as fort the general observations of the literature. Grain boundaries are not closed, pores are not completely destroyed. The sample theoretical density was measured as 97.7 % and close but not the same with the obsevations. Pore structure can be more easily selected at Figure 4.50 b, from the back scatter image.

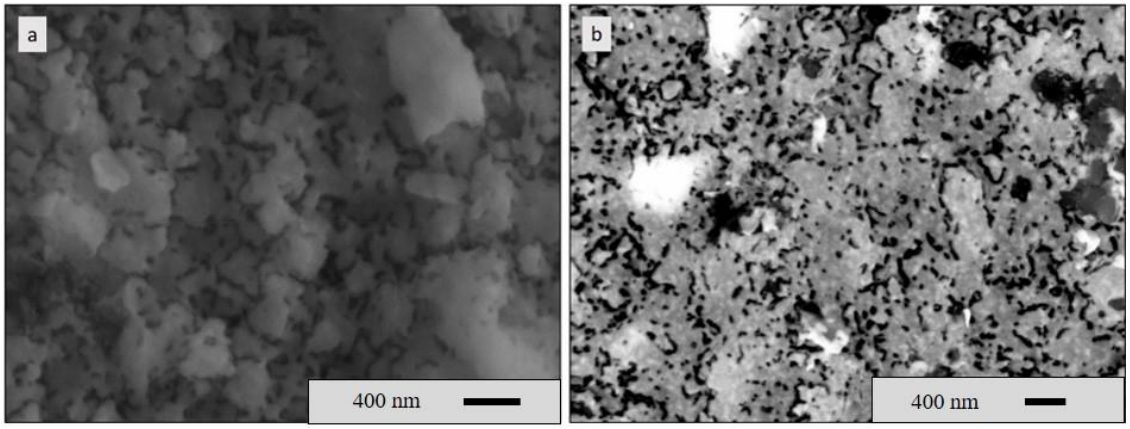

Figure 4.50. *a) SE and b) BSE, SEM images of ZnO sample containing 8.0 wt % liquid*

XRD analysis was performed on the ZnO bulk materials obtained from the experiments using different liquid ratios and different temperatures, Figure 4.51 and Figure 4.52 respectively. Although it is thought that the temperature or liquid ratio does not change over the phases, tests were performed to determine this situation and compared with the literature, see in Figure 4.53. Accordingly, the same phases are present in the system at all temperatures and liquid ratios. ZnO and β-Bi_2O_3 phases show similar peaks with XRD in the literature. Figure 4.53 shows the phases formed in the ZnO varistor system sintered at different temperatures, produced with traditional methods [106].

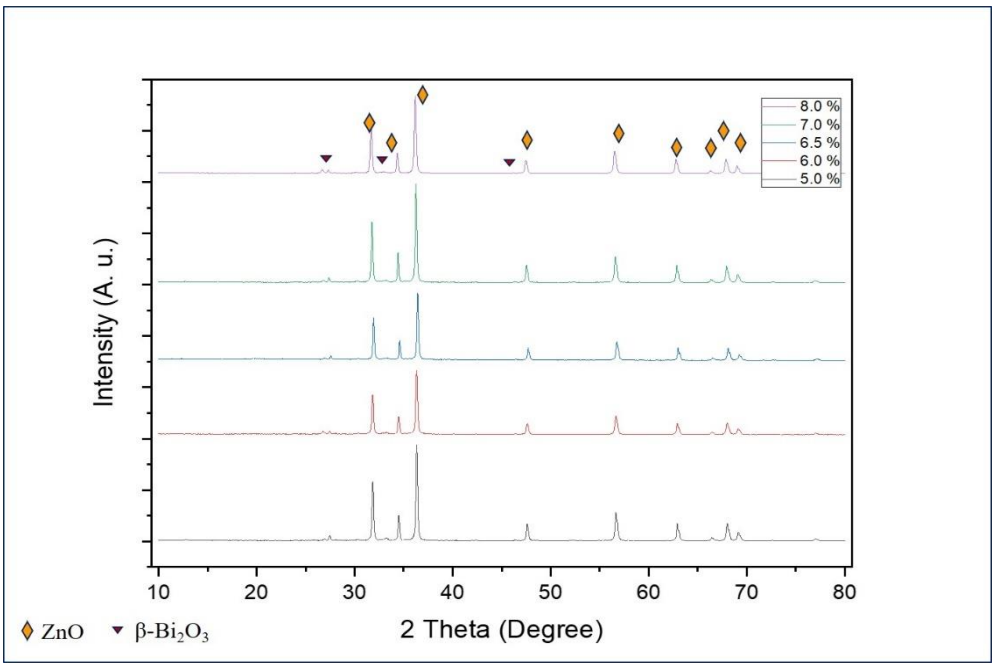

Figure 4.51. *XRD analysis of ZnO bulk sample containing 1 % mol Bi_2O_3 sintered under the same conditions and containing different ratios of liquid.*

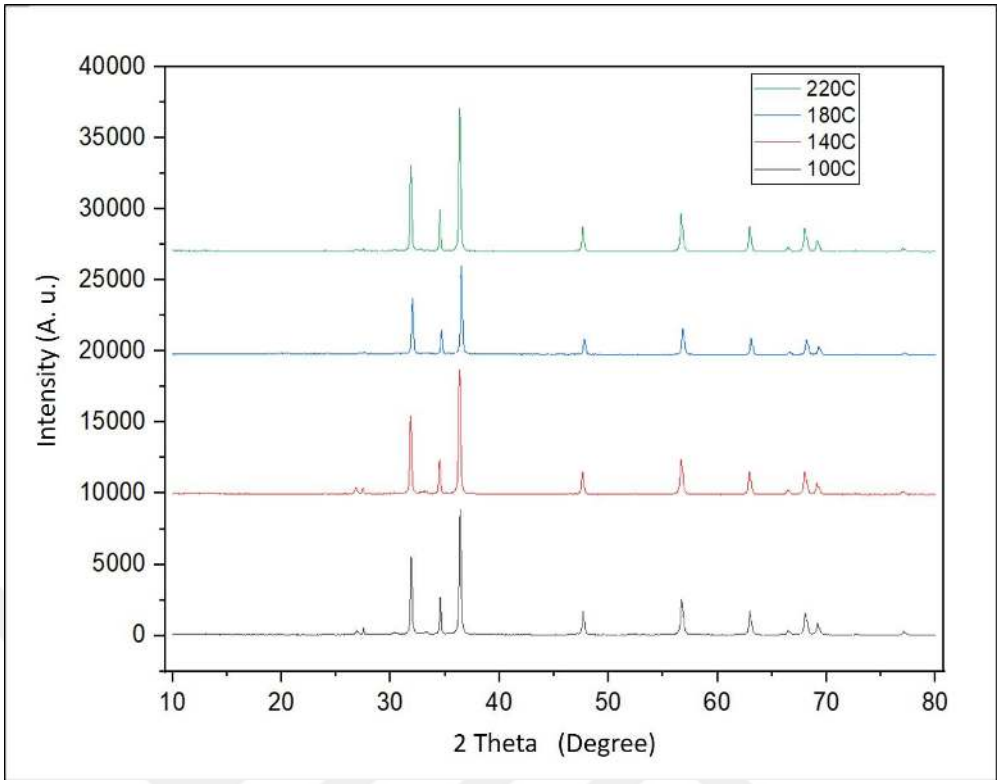

Figure 4.52. *XRD analysis of ZnO bulk sample containing 1 % mol Bi_2O_3 sintered at different temperatures.*

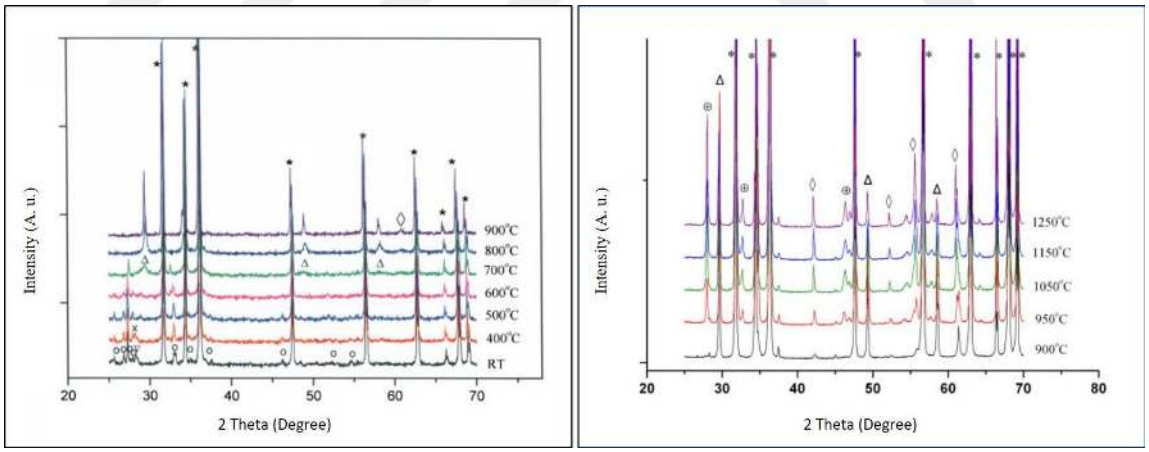

Figure 4.53. *a) XRD graphs of phases ranging from room temperature to 900°C in ZnO varistors * ZnO, Δ pyrochlor, o α-Bi_2O_3, ▽ Sb_2O_3, ◊ spinel phases. B) XRD graphs of phase change between 900°C-1250°C *ZnO, ⊕ β- Bi_2O_3, Δ pyrochlore, ◊ spinel phases [106].*

Looking at the SEM images in Figure 4.54 below, no large grain size or porosity ratio difference could be detected between the sample containing with different liquid ratios as 7.00 % liquid and the 6.46 % water. However, the grain size and structure of the material containing nano Bi_2O_3 given in c appears to be different. Samples in b and c were sintered using the same amount of liquid.

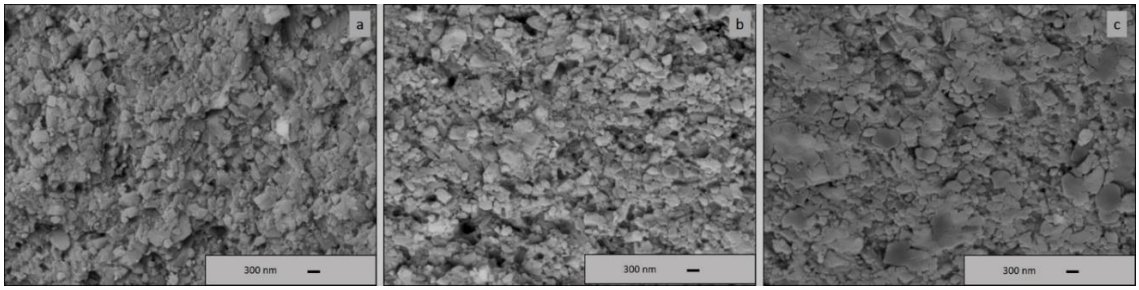

Figure 4.54. *Broken surface BSE-SEM images after Bi_2O_3-ZnO, 140°C, CSP a) 6.46% b) 7.00% liquid, 1mol % micron-Bi_2O_3 c) 7.00% liquid, 1% mol nano-Bi_2O_3*

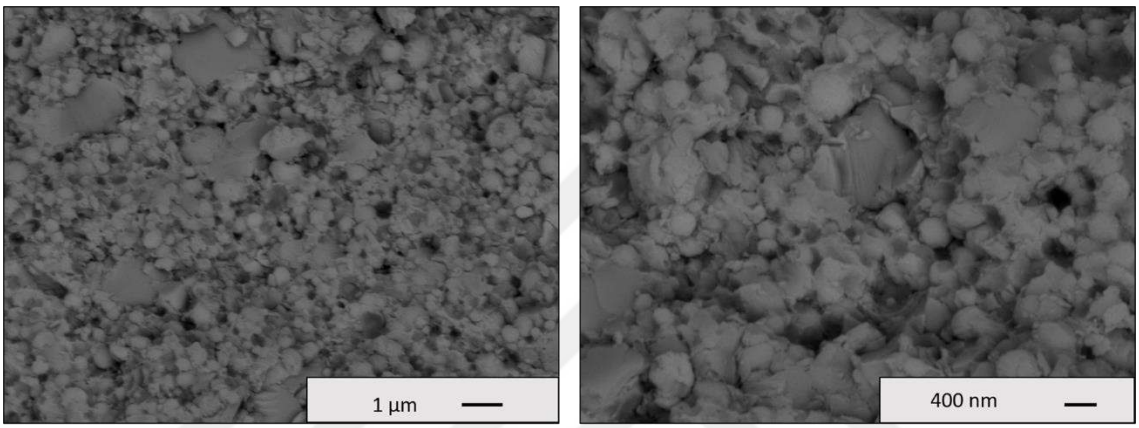

Figure 4.55. *Broken surface, BSE-SEM images after CSP, 6.46 % liquid, 1 mol % nano-Bi_2O_3*

Figure 4.55 shows the SEM images of the sample containing nano Bi_2O_3. Sample sintered with 6.46% liquid grain size is around 300-400 nm. It is seen that there are approximately 200 nm pores in the material.

Figure 4.56 shows the broken surface BSE-SEM image of ZnO containing micron-Bi_2O_3. In the sample containing 7.00 % liquid, the particle size is in the range of 200-400 nm. It is seen that finer grains are also present. It is thought that the particle size distribution is more homogeneous in the material produced with nano-Bi_2O_3. This result is similar to the results obtained with nano Bi_2O_3 in previous studies in terms of grain size.

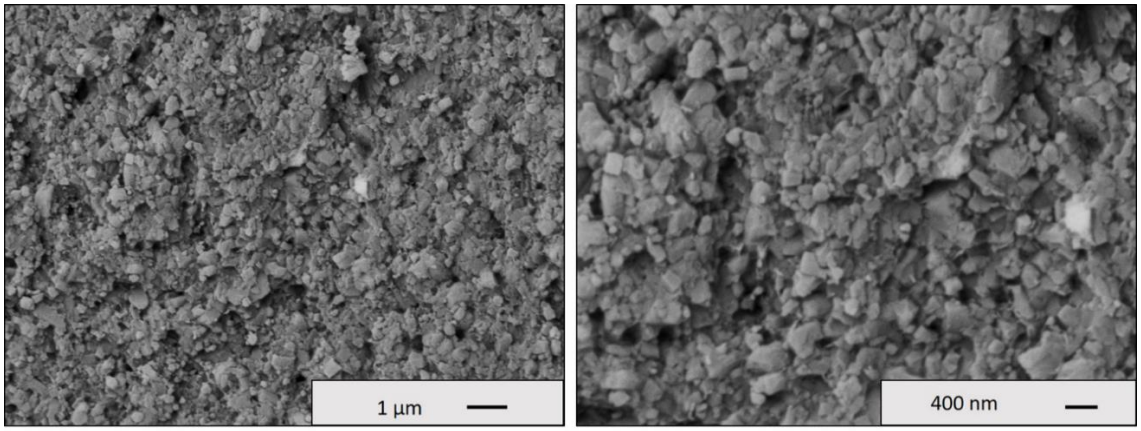

Figure 4.56. *Broken surface, BSE-SEM images after CSP, 7.00 % liquid, 1 mol % micron-Bi_2O_3*

Electrical Poperties of the CSPed Binary ZnO-Bi_2O_3 System

Mixing of the powder at mill was peformed for ZnO was mentioned at experimental procedure of this chapter. Figure 4.55 shows I-V curves of the samples containing nano-Bi_2O_3, sintered for 50 min. at 140°C and under 539 MPa pressure. The two samples had different liquid ratios as 7.0 and 8.0 wt % as shown in Table 4.6. The theoretical densities of both samples were over 90.00 %T.D. According to the I-V curves, varistor behavior is observed in both samples. There is no linear conductivity. However, in order to see the non-linearity behavior, Table 4.6, which includes the α values, should be examined. It was observed that the α values were 4.70 and 4.04, respectively. These values are higher than the pure ZnO mean α value of 2.24. In this case, it can be thought that varistor properties can be enhanced when the CSP is performed to the binary system, as well. It is seen that the threshold voltages are 190 V/mm and 268 V/mm, respectively.

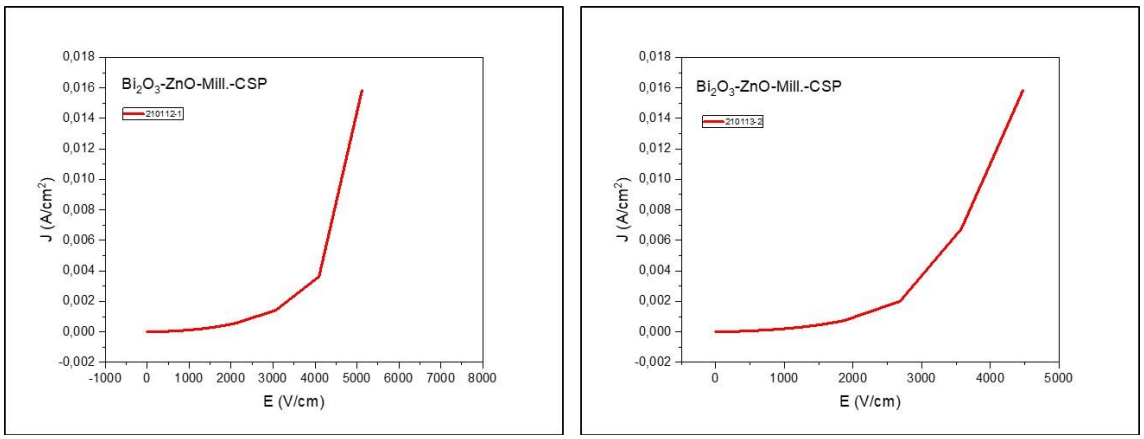

Figure 4.57. *Nano-Bi_2O_3-ZnO, I-V curves, a) 7.0 % wt liq., b) 8.0 % wt liq.*

Table 4.6. *Nano-Bi_2O_3-ZnO, electrical characterization results and sample properties*

Sample	Liq. (wt %)	T.D. (%TD)	α	V_{Th} (V/mm)
a	7.00	96.28	4.70	190
b	8.00	93.81	4.04	268

The I-V graphs for the samples with 6.46; 7.0 and 8.0 wt% liquid phase, sintered for 50 min. at 140°C and under 539 MPa pressure. CSP experiments using micron grain size Bi_2O_3 were also examined, as shown in Figure 4.58. When the curves are analyzed, similarly to the nano-Bi_2O_3 used samples, varistor behavior was observed. The sample with the lowest α value and the sample with the highest density was the sample sintered with the 6.46% liquid. It was determined that the α values were similar with nano-Bi_2O_3 containing samples. Threshold voltages were 179, 282 and 213 V/mm for the samples with the 6.46; 7.0 and 8.0 wt% liquid phase contents, respectively, see at Table 4.7.

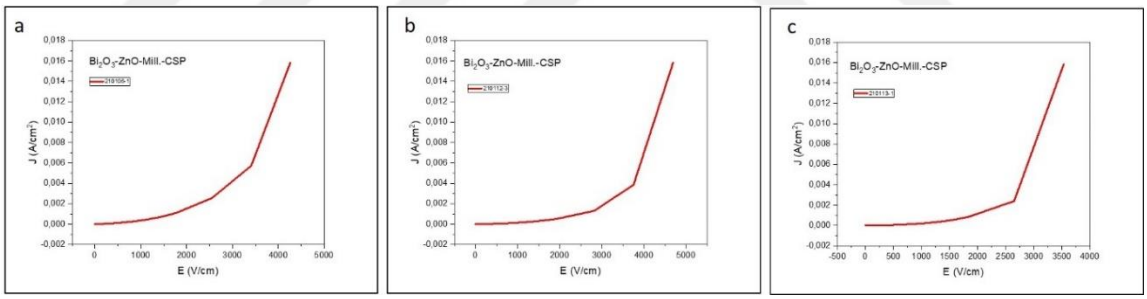

Figure 4.58. *Micron-Bi_2O_3-ZnO, I-V curves*

Table 4.7. *Micron-Bi_2O_3-ZnO α values and Threshold Voltages*

Sample	Liq. (wt %)	T.D. (%TD)	α	V_{Th} (V/mm)
a	6.46	96.28	2.99	179
b	7.00	93.81	4.89	282
c	8.00	94.24	4.49	213

In order to obtain high density in conventional sintering trials, different temperature and time trials were carried out. A box furnace was used for sintering of ZnO-Bi_2O_3 conventional sintering. The sintering regimes were 4 h at 771°C, 4h at 790°C, and 4 h at 810°C. The resulting theoretical density value for the sample sintered at 771C was 93.55 %TD. as seen at Table 4.8. The α value of 4.29 was the highest obtained for conventional sintering and is approximately close to the α value obtained by the CSP method samples. I-V graph of the conventionally sintered ZnO is at the Figure 4.59. On the other hand, the threshold voltage was determined as 265 V/mm with the conventional sintering. Higher theoretical density values would probably result in improved electrical properties.

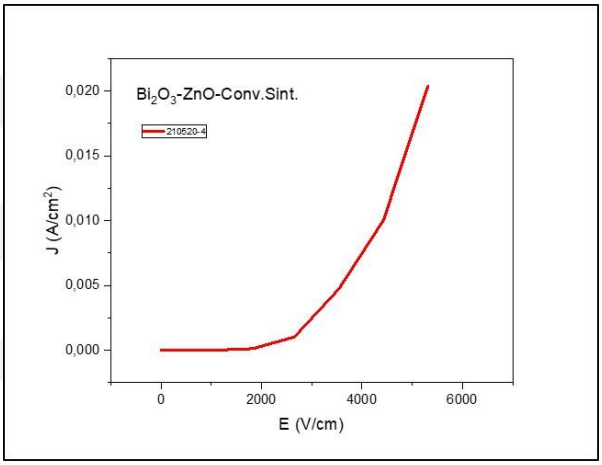

Figure 4.59. *Conventionally sintered micron-Bi_2O_3-ZnO, I-V curve*

Table 4.8. *Conventionally sintered micron-Bi_2O_3-ZnO, α values and Threshold Voltages*

Temp. (°C)	**T.D. (%)**	**α**	**V_{th} (V/mm)**
771	93.55	4.29	265

4.3.1.3. Coating ZnO by Bi_2O_3

Resolution is a very important factor for the CSP process. Resolution reviews are valuable to us for two reasons. First, the mechanism of dissolution and precipitation during the CSP process requires knowing which of the different powders used in the system will dissolve during sintering. As mentioned before, the solubility of ZnO is quite high at certain pH values. However, we do not expect the same degree of resolution for Bi_2O_3. We tried to test this situation in our own conditions and with our powder. When

the results of the experiments were examined, the following pH-dependent zeta graphs were obtained, 3.4.1.3.1 and 3.4.1.3.2.

The zeta potential values, which are examined in solubility studies, are also important when coating is considered. Zeta plots and isoelectric points were investigated to see whether Bi_2O_3 coated ZnO could be produced by heterocoagulation.

The graph in Figure 4.60 shows the pH-dependent zeta curve of micron-sized ZnO particles. Nitric acid and NaOH were used to adjust pH values. According to this curve, the isoelectric point of ZnO is around pH 9.0. It is similar to the values in the literature. It is stated in the literature that pH 9 - 10 is zero point of charge. Again at the same study, ZnO is positively charged between pH 6 and 8, and negatively charged between 10 and 12, [140,141].

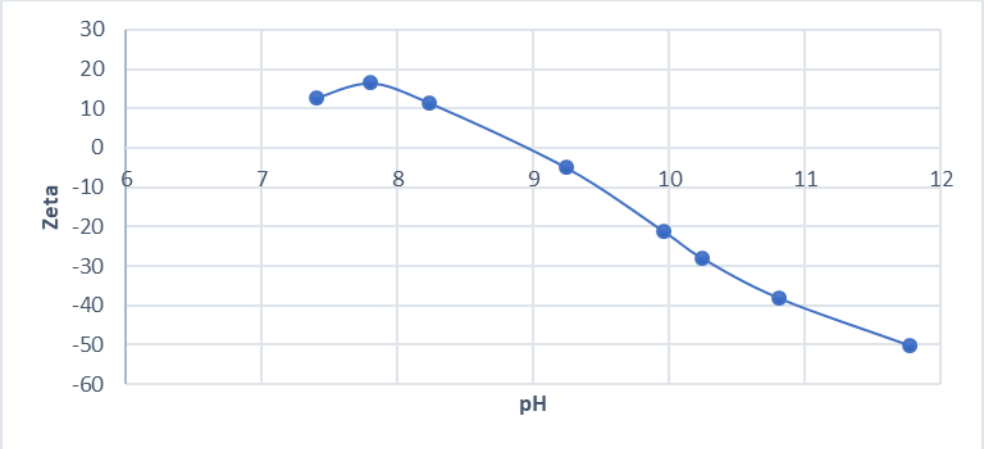

Figure 4.60. *Zeta potential plot of ZnO versus pH*

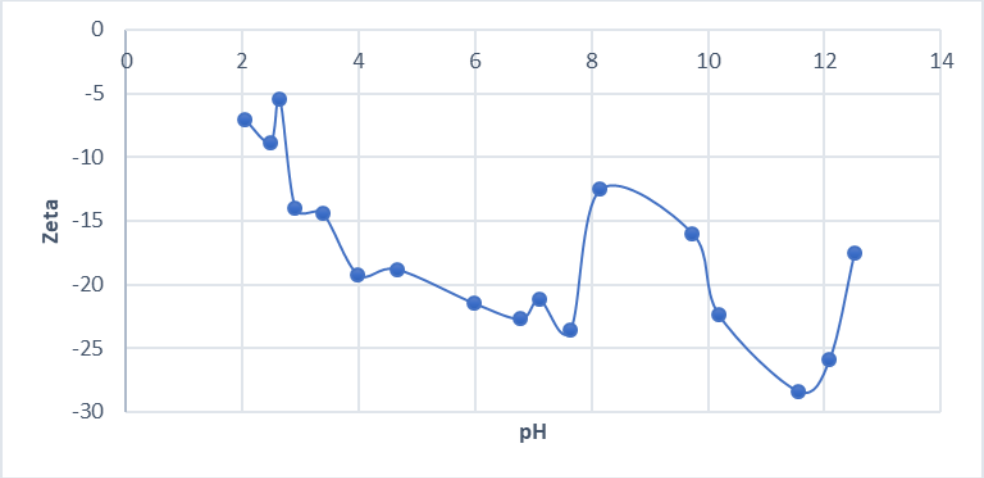

Figure 4.61. *pH-dependent Zeta Potential plot of Nano-Bi_2O_3*

Zeta potential graph of nano-Bi_2O_3 at Figure 4.61 shows the measurement results taken between pH 2.0 and pH 12.5. It was tried to reduce the pH by adding nitric acid, but despite the addition of acid at high rates, it was very difficult to lower the pH below 2.6. NaOH was used as the base. The isoelectric point was not observed. In the literature, it is stated that the isoelectric point is around pH 2.0 to 3.0 for Bi_2O_3 [142].

When pH<PCN the surface charge is positive, if pH>PCN the surface charge is negative [141]. In this case, the required pH value could not be obtained if we want to take advantage of the ion charge differences for synthesis or coating. Bi_2O_3 is negative above pH 2.0. ZnO is positive below pH 9.0. However, since ZnO starts to dissolve rapidly below pH 7.0, it is not possible to coat it with Bi_2O_3.

Coating of ZnO by Bi_2O_3 via pH controlled method

-Coating of ZnO

Various analyzes were carried out to understand whether the resulting powder was coated or not. The first of these is the measurement of Zeta potential values. First of all, suspensions of raw materials and a powder called S1, indicating the pH-controlled coating, in pure water with a pH of 7.33 were prepared in separate beakers and the zeta potential values were measured, see at Table 4.9. Since there was no significant difference between the zeta potential values, it was considered to try measuring again at high pH values as presented in Table 4.10. The milled powder obtained by mechanical mixing of ZnO and Bi_2O_3. Zeta value of mixed powder is similar with pure ZnO. S1 powder has Zeta value between Bi_2O_3 and ZnO values. This result indicates that the coated powder system is different from the powder mixed system.

Table 4.9. *Zeta potential values of raw material and Produced S1 powder in pure water*

Powder type	Zeta at pH 7.0
ZnO	-0.02370
Micron-Bi_2O_3	0.05820
Nano-Bi_2O_3	0.00557
S1 powder	0.00153
S2 powder	

Table 4.10. *Zeta potential values of raw material and produced S1 powder for pH 11.8 in pure water*

Powder type	Zeta at pH 11.8
ZnO	-54
Micron-Bi_2O_3	-30
Nano-Bi_2O_3	-33
Milling (ZnO-Bi_2O_3)	-51
S1 powder	-41
S2 powder	

TG-DTA analysis was performed to the obtained S1 powder, see at Figure 4.62. It is not known whether the powder from the uncalcined Bi-nitrate turns into an oxide or if the nitrates were completely removed by washing. An endothermic peak was observed only around 730°C, see at Figure 4.62. An endothermic peak is formed by melting and these temperatures are close to the Bi_2O_3 melting temperature. However, this is not exact information. On the other hand, it is stated in some studies that the endothermic peak formed at 730°C occurs with the conversion of α-Bi_2O_3 to ϱ-Bi_2O_3 in the literature [143].

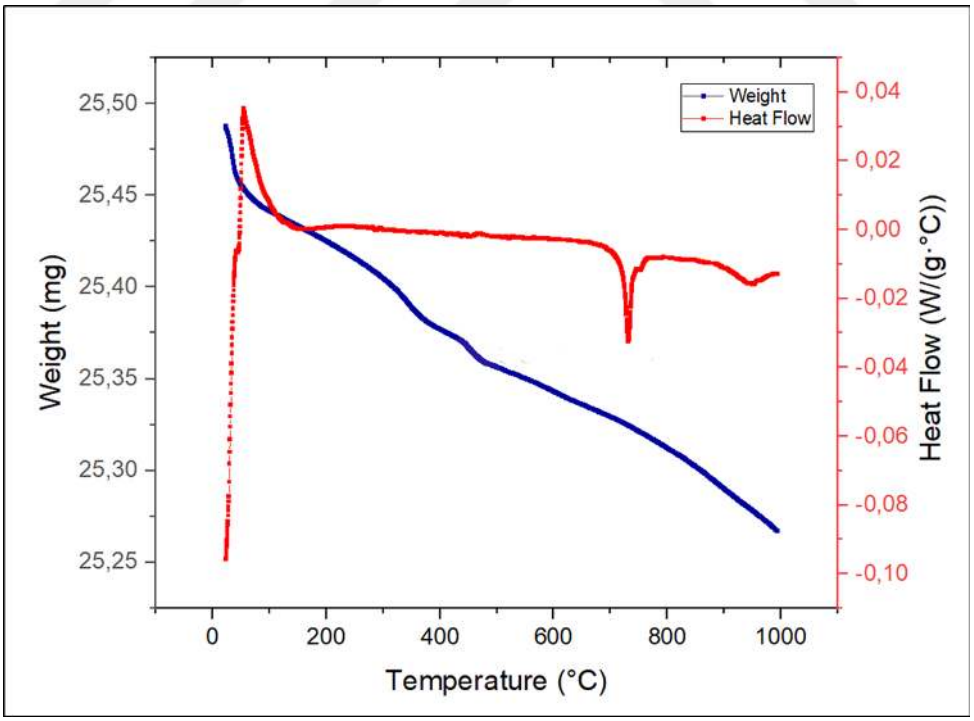

Figure 4.62. *TG-DTA graph of S1 powder*

Fourier Change Infrared Spectroscopy (FTIR) analysis was performed on the produced powders, Figure 4.63. By the FTIR analysis, the chemical bonds formed can be

analyzed to differ for each material. Differences for the bonds formed in the system, and the pure powders tried to be determined, and mill-mixed Bi_2O_3-ZnO powder was also used for comparison. It was seen that the peak at 1300 is different for ZnO and Bi_2O_3 and this peak for the S1 powder is much more similar with Bi_2O_3-ZnO mixed powder. When looking at another peak in the 2300 range, it is seen that the mill sample shows more similarity with ZnO, while the S1 sample has similar shapes with the Bi_2O_3 peak. In order to examine the FTIR analysis in a little more detail, the region where the peaks intensified was examined in detail. Figure 4.64 a shows the detailed analysis and at b, ZnO, Bi_2O_3 and ZnO-Bi_2O_3 FTIR analyzes obtained from the literature [144]. There are some differences between the data from the literature and our measurement. However, Bi_2O_3 characteristic peaks are shown in the literature and some of these peaks are included in our analysis. When our analysis was re-evaluated, it was thought that the peak at 850 cm^{-1} in S1 powder is similar to the peak of 850 cm^{-1} in Bi_2O_3 in the literature. At the same time, it is seen that the peak at 1350 cm^{-1} is similar to pure ZnO. S1 powder FTIR analysis shows similarity with both of the starting raw materials.

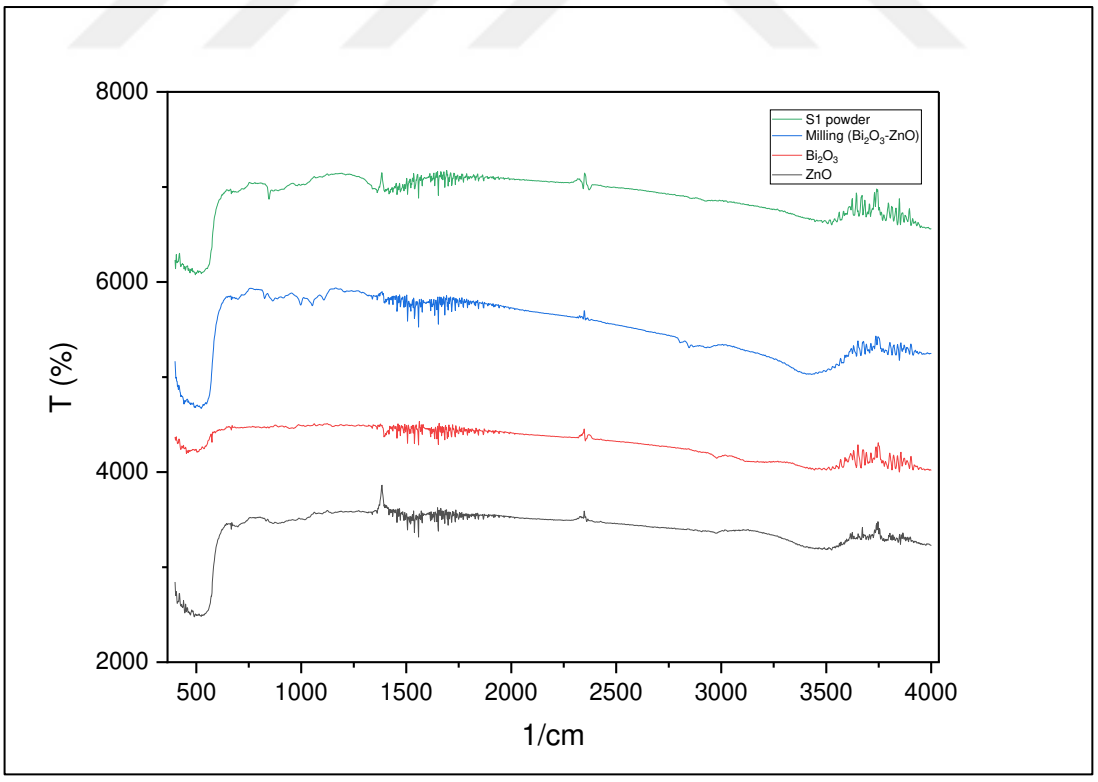

Figure 4.63. *FTIR Analyses of S1 powder*

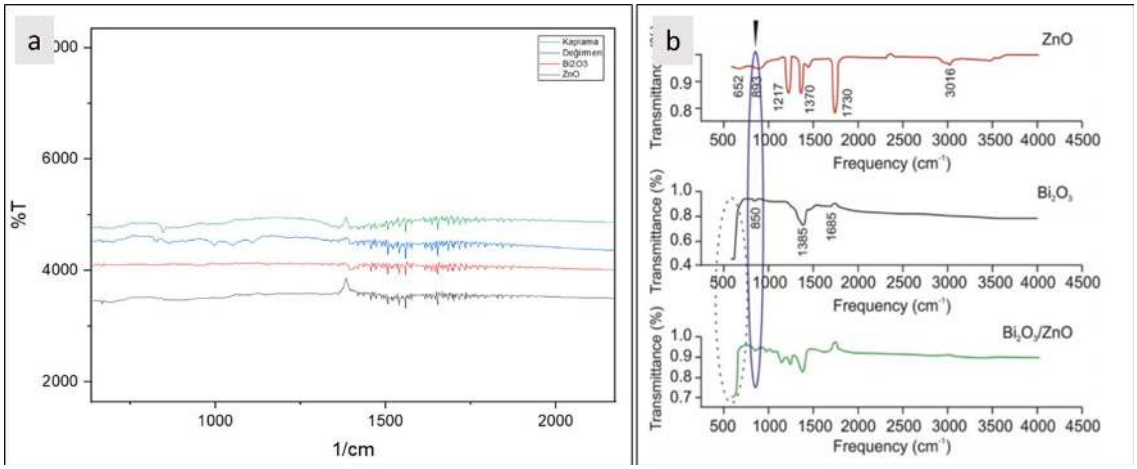

Figure 4.64. *a) S1 powder FTIR analyses, detailed peak analyses and b) ZnO-Bi_2O_3 FTIR analysis [144].*

All raw materials, ZnO-Bi_2O_3 mixed powder produced as standard in the mill, S1 and S2 powder, were examined by XRD analysis. Figure 4.65 shows the XRD patterns of the powders for comparison. It has been observed that the powder belonging to S1 shown in purple has a similar structure with ZnO-Bi_2O_3 mixture obtained from the mill. However, ZnO powders that are not completely coated may also have caused this. Along with the ZnO peaks, there are peaks thought to belong to β-Bi_2O_3 in the XRD examinations in the Bi_2O_3 section that was examined before.

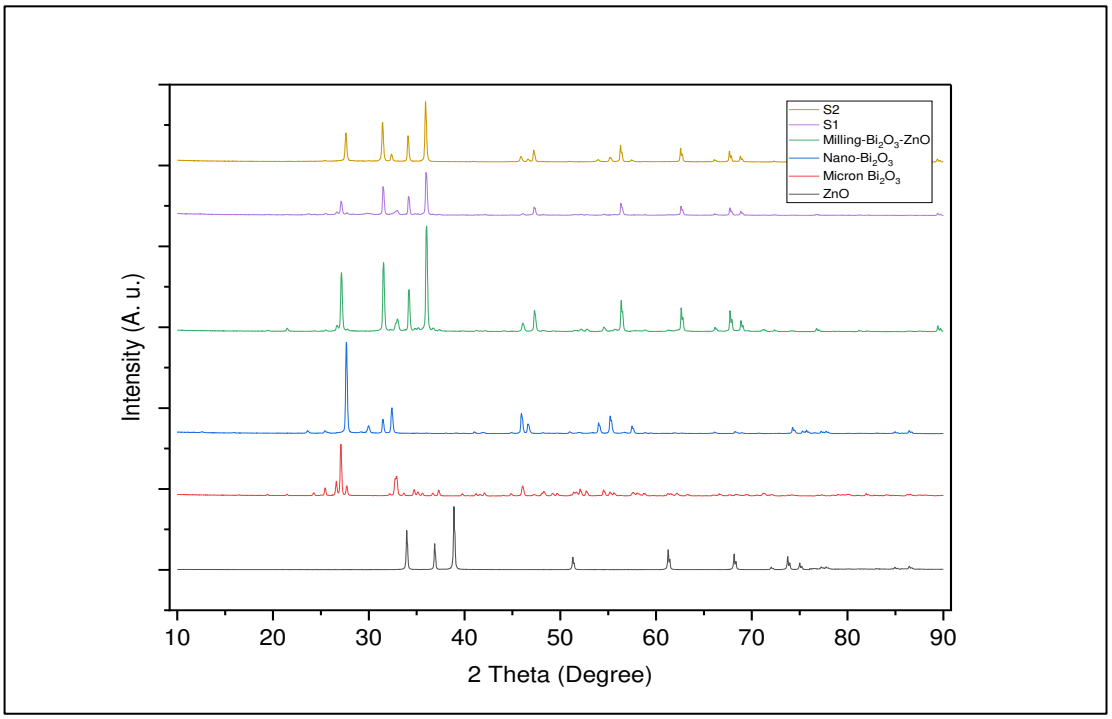

Figure 4.65. *XRD graphics of raw materials, milled Bi_2O_3-ZnO, S1 and S2 powders*

BSE-SEM images of S1 powder with raw materials were examined. ZnO in Figure 4.66 a was used for coating, other raw material images are for information purposes only. Bi-nitrate, on the other hand, was used completely dissolved in the system and its image is not available. We can say that Bi_2O_3 crystallizes with a very fine grain size distribution. In Figure 4.68, the dimensions and quantities of the rod-like particles can be seen more clearly. They vary in size from 2 to 10µm. However, it is also stated in the reference article that the powder produced by precipitation may have a rod-like morphology, [119].

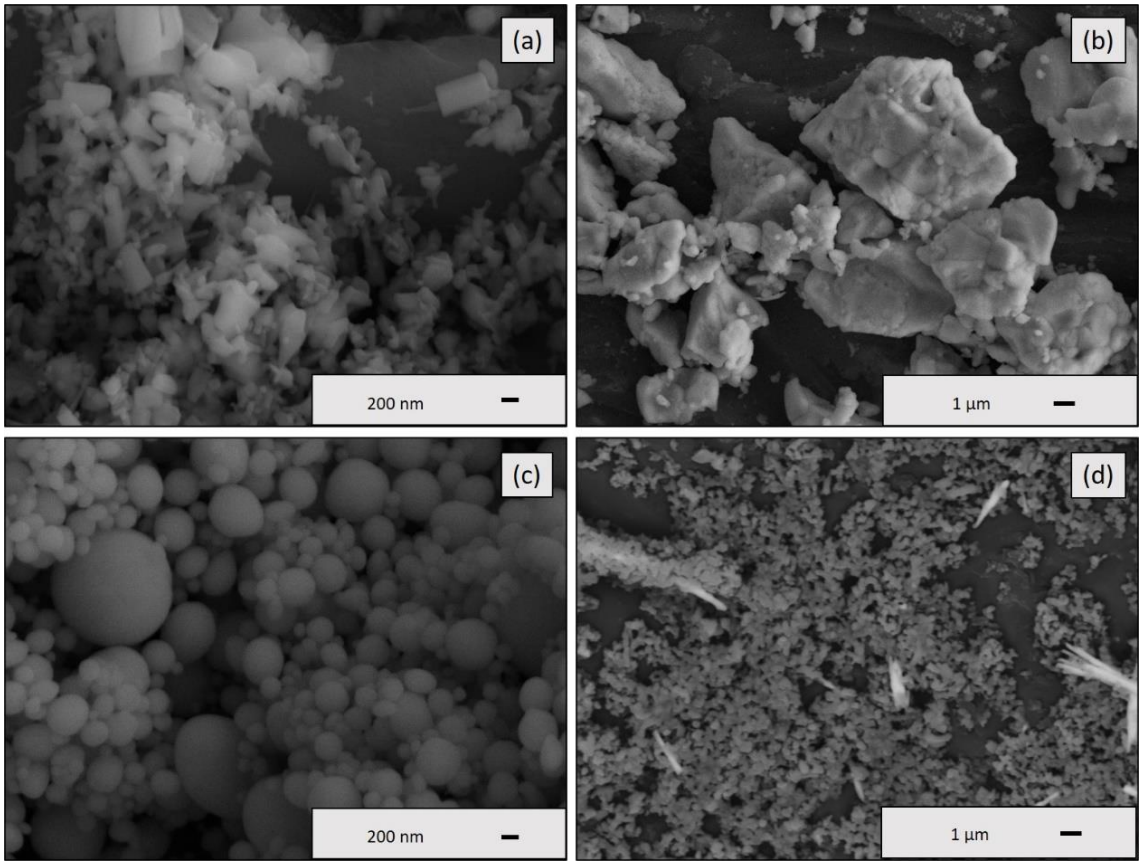

Figure 4.66. *BSE-SEM images of a) ZnO, b)micron-Bi_2O_3, c)nano-Bi_2O_3, d)S1 powder*

Figure 4.67 shows a closer (40000X) BSE-SEM image of S1 powder. It is seen that the grains are in the range of 80-300 nm, but there are rod-shaped Bi_2O_3 grains in between. The content of these grains was tried to be determined by EDX analysis.

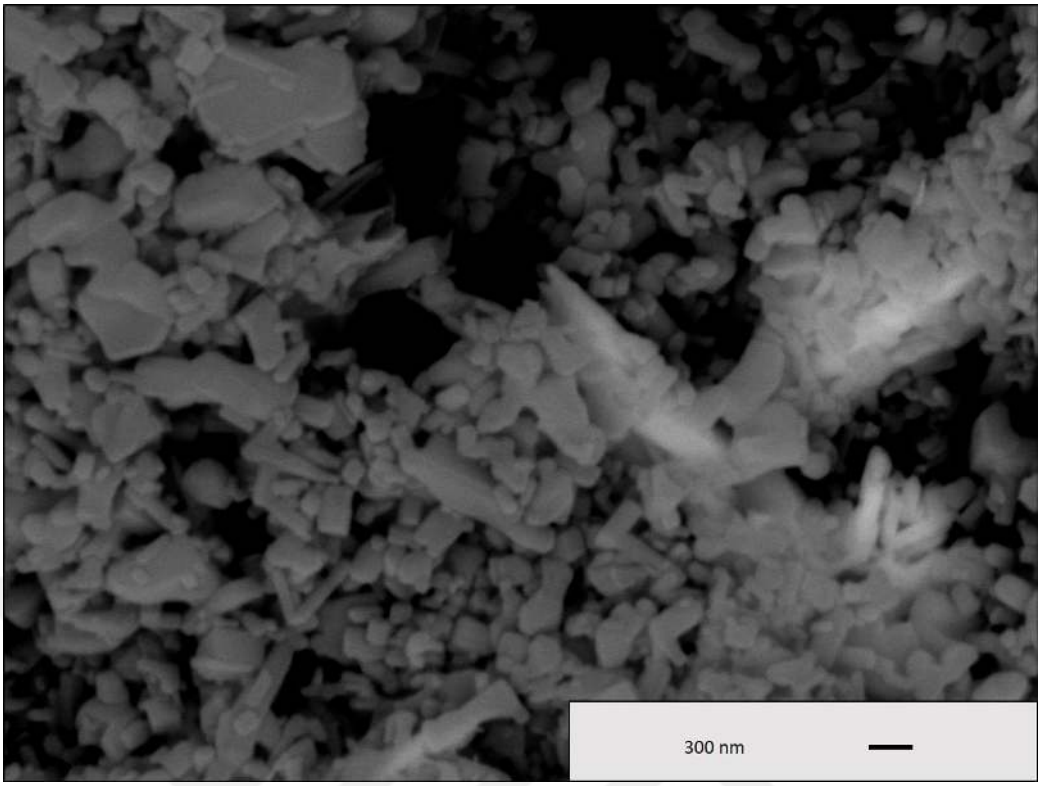

Figure 4.67. *BSE-SEM image of S1 powder*

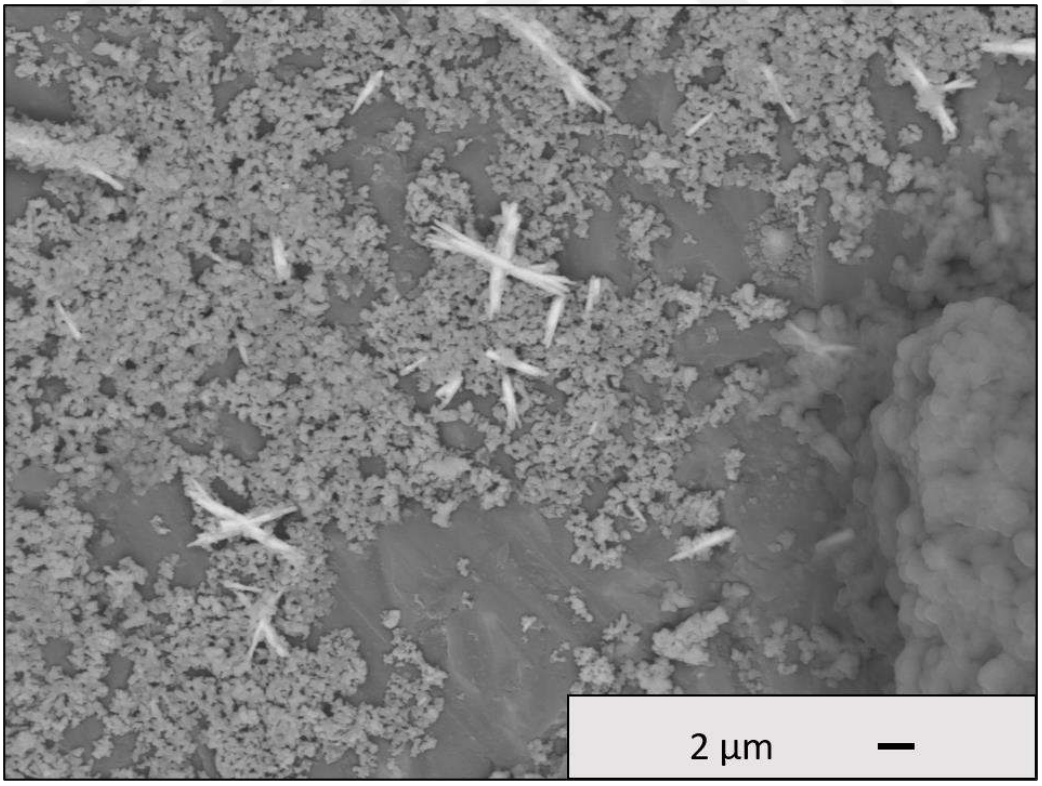

Figure 4.68. *BSE-SEM image showing the overall distribution of rod-like particles in S1 powder*

EDX analysis of the S1 powder was performed for elemental analysis. Figure 4.69 shows the EDX results of the rod-like grains. The EDX analysis was originally taken from a general area. It was observed that composition was 69 wt%, Zn and 13 wt% Bi atoms. Then, point analysis was taken from the region where the grains appear as white and have a rod-like morphology. Accordingly, the weight ratio of 25 % ZnO and 61 % Bi atoms was determined, se at Figure 4.70. Exact values may not be obtained, because in EDX analysis, although point analysis is performed, information comes also from its surrounding. However, it is understood that these rod like particles are richer in bismuth.

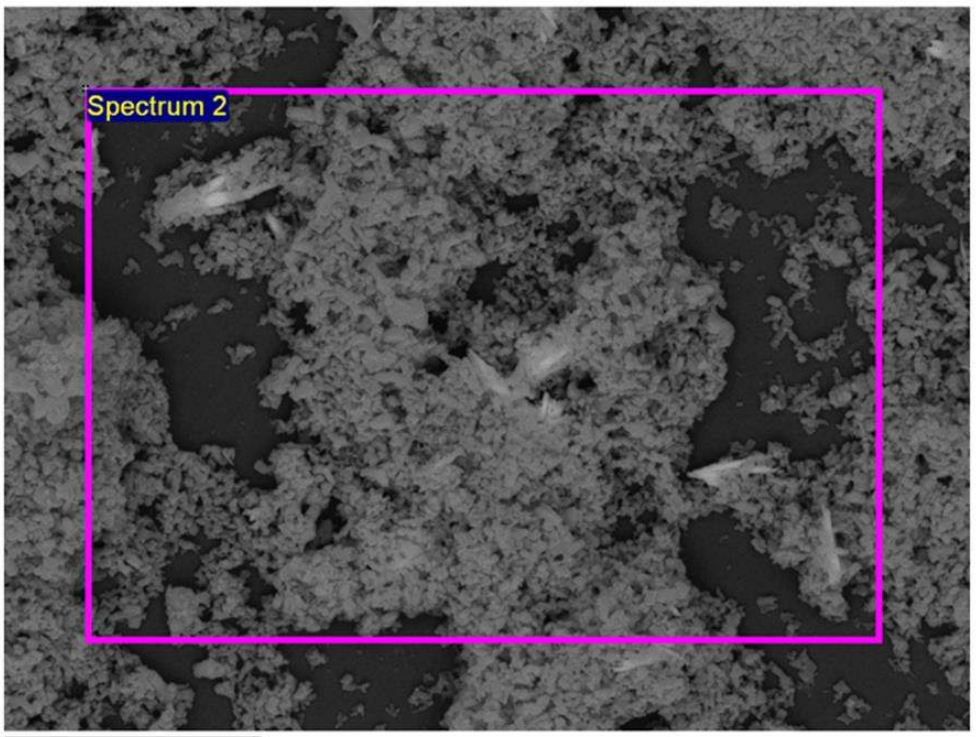

Element	Weight%	Atomic%	Compd%	Formula
Zn K	68.73	46.57	85.55	ZnO
Bi M	12.96	2.75	14.45	Bi2O3
O	18.31	50.69		
Totals	100.00			

Figure 4.69. *EDX analysis of S1 powder, overall*

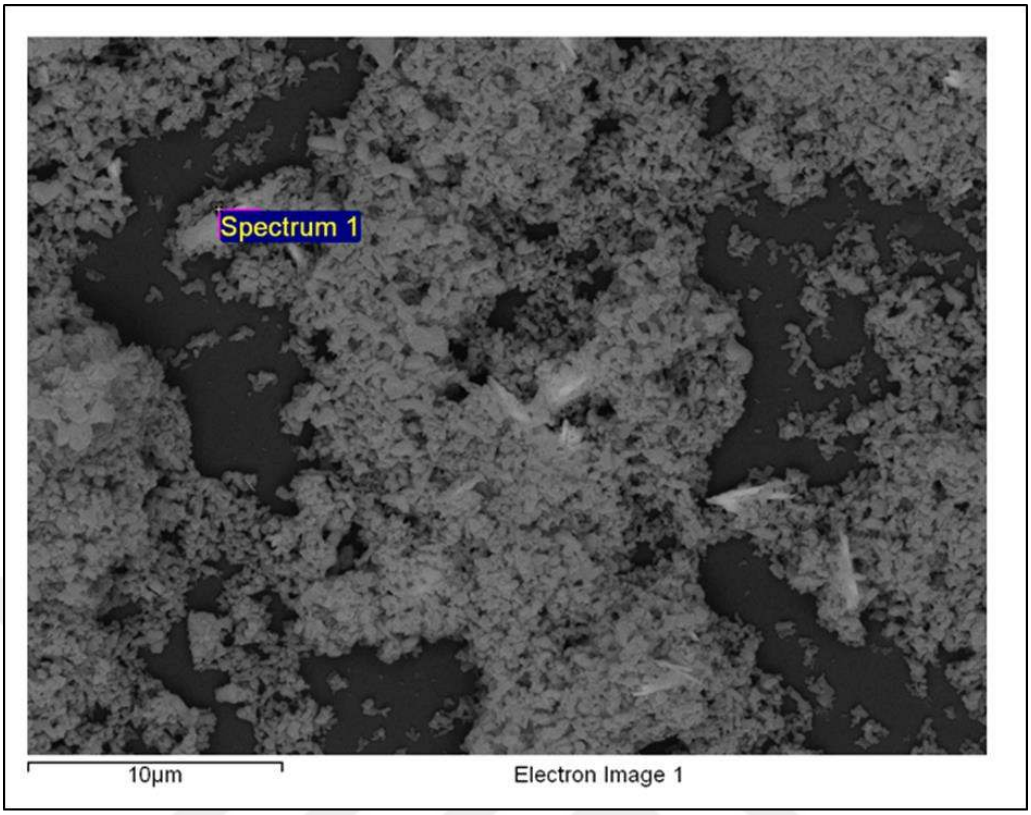

Element	Weight%	Atomic%	Compd%	Formula
Zn K	25.43	25.74	31.65	ZnO
Bi M	61.31	19.41	68.35	Bi2O3
O	13.26	54.85		
Totals	100.00			

Figure 4.70. *EDX analysis of S1 powder, rod-like grain*

CSP of Bi_2O_3 coated ZnO – S1

CSP trials were conducted with S1 powder, see at Table 4.11. All density values are above 90.00 % T.D.. No significant difference was observed at the sintering behavior when compared to the production made with the powders taken from the mill. However, when working with S1 powder, it was observed that the powder showed a hydrophilic property when adding the liquid to the powder in a mortar, Figure 4.71. This property was almost similar with pure Bi_2O_3 and this is not the case with ZnO powder. This is actually an important difference because it indicates that the ZnO surface energy has changed and is more similar to Bi_2O_3.

Figure 4.71. *Photograph showing the S1 powder encountering water in the mortar*

Table 4.11. *Sintering conditions and Theoretical Densities of the samples produced with S1 powder.*

Sample	Pressure (Mpa)	Time (min.)	Temp. (°C)	Liquid (wt %)	pH	T.D. (%)
S1-CSP	539	50	140	8.00	5.5	98.98
S1-CSP	539	50	140	7.81	5.5	93.28
S1-CSP	539	50	140	7.81	5.5	97.27
S1-CSP	539	50	140	7.81	5.5	96.34
S1-CSP	539	50	140	7.81	5.5	96.02
S1-CSP	539	50	140	7.81	5.5	98.25
S1-CSP	539	50	140	8.10	5.5	98.25
S1-CSP	539	50	135	7.81	5.5	96.25

CSP study was carried out using different liquid ratios. The resulting theoretical density values are shown in the curve in Figure 4.72. According to this, the highest density was reached at 8.00 wt % liquid.

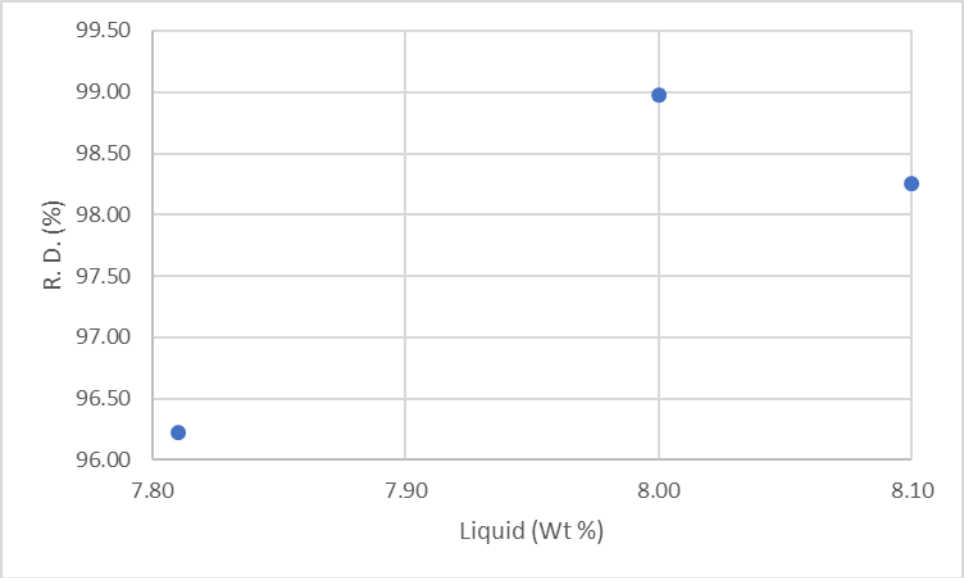

Figure 4.72. *Graph of T.D. %, CSP at 140°C using S1 powder and with different water ratios.*

SEM images of the samples sintered with 8.00 % liquid were examined, Figure 4.73 It is seen that the particle size distribution varies between 100-300 nm. No rod-like grains were not found after sintering. The reason for this may be the dissolution of the grains or their breakage during sintering.

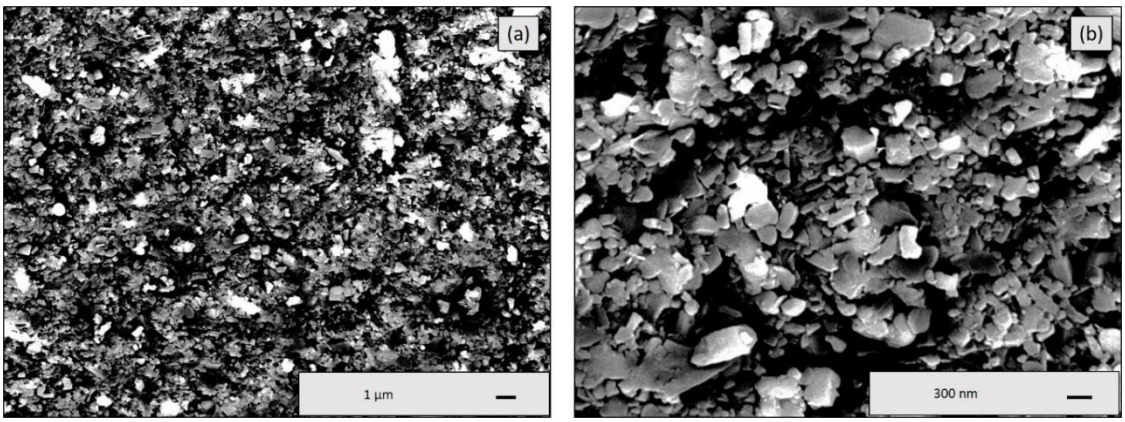

Figure 4.73. *BSE-SEM images of CSP sample at 140°C with 8.0 wt % liquid*

Electrical characterizations of CSPed Bi_2O_3 coated ZnO powder – S1

Electrical characterization was performed for S1 powder used samples, sintered with different liquid ratios. Varistor behavior was not achieved for 7.00 wt % liq. amount. This may be a feature of that sample, or it may be due to insufficient sintering as a result of insufficient liquid ratio. For the other two samples, higher densities were reached during sintering, see at Table 4.12. Varistor behavior was observed in I-V graphs, Figure

4.74. Two samples with 8.00 and 8.67 wt % liq. containing samples had α values of 6.32 and 25.24, respectively, at Table 4.12. In the experiments with the Bi_2O_3 powder mixed in the mill, α values were obtained around 4.89 – 4.49, for sintering at the same conditions. It is possible to say that alpha values were significantly improved by the coating process. Similarly, while the CSP results of the milled powders provided a maximum threshold voltage of 544 and 820 V/mm, it was seen that threshold voltage value was increased nearly three times when the samples produced with the coated powder. The highest threshold voltage obtained using the conventional sintering method was 265 V/mm. The maximum threshold voltage of 282 V/mm was reached by the CSP of the powder obtained from the mill. Threshold voltage value of 820 V/mm was the highest value with the coated S1 powder. These results clearly showed that uniform distribution of the bismuth oxide phase via coating enhances the CSP and hence varistor properties significantly.

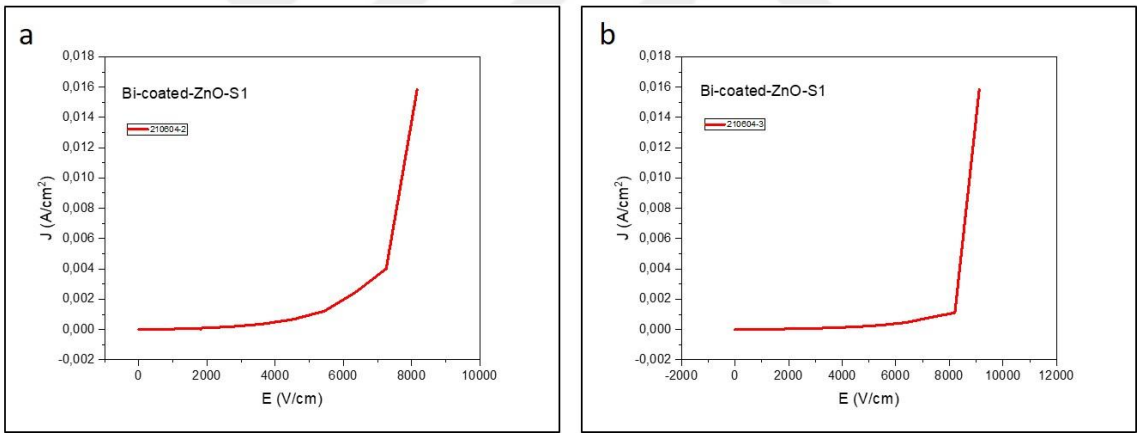

Figure 4.74. *S1 powder, CSP sintering, I-V curves, a 8.00 wt %, b 8.67 wt % liq.*

Table 4.12. *S1 powder CSP α values and Threshold Voltages*

Sample	**Liq. (wt %)**	**% TD**	**α**	**V_{Th} (V/mm)**
a	8.00	98.25	6.32	544
b	8.67	96.25	25.24	820

Coating of ZnO by Bi_2O_3 via slurry based method

Figure 4.75 shows the XRD pattern of the S2 powders produced by the solution method. When this pattern was compared with the XRD patterns, reported in the literature (Figure 4.76) it was observed that the peak at 27° diffraction angle in the XRD pattern belongs to β-Bi_2O_3. This result suggests that the Bi-nitrate converts to Bi_2O_3 during the calcination which was performed at 600°C for 2 hours.

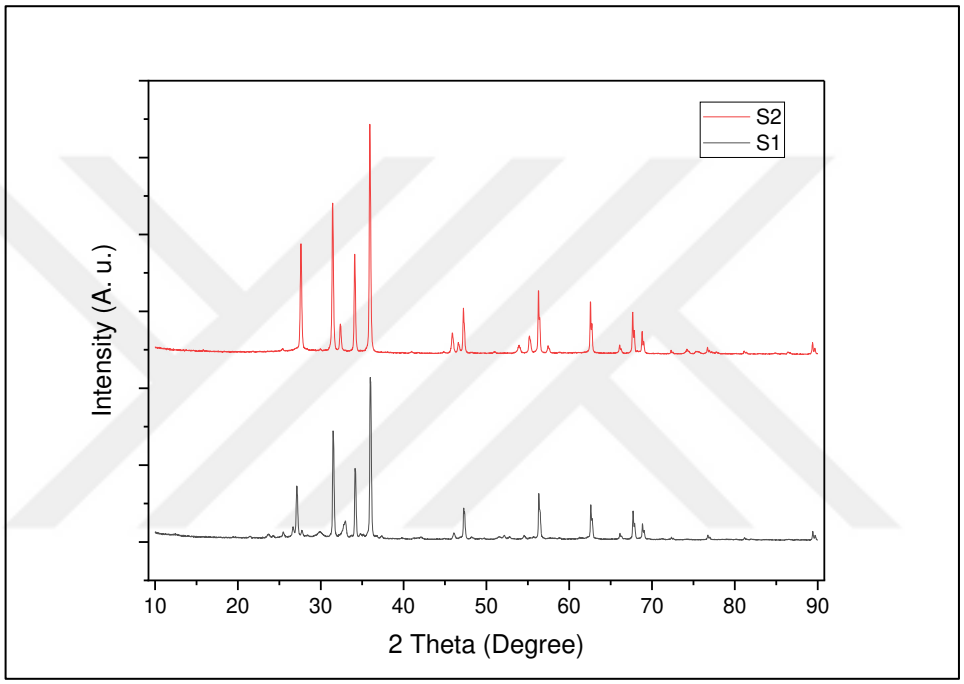

Figure 4.75. *XRD graphs of S1 and S2 powders*

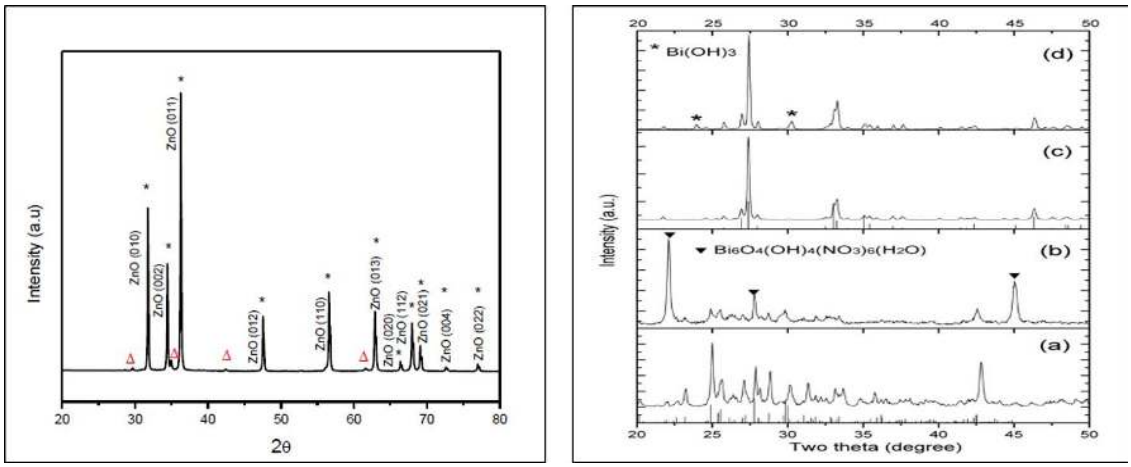

Figure 4.76. *XRD plots of ZnO and Bi-nitrate and Bi-hydrate [126].*

EDX analysis was performed from a general area of the powder as shown in Figure 4.77 EDX results revealed the compostion of the powder was 67 wt% Zn and 15 wt% Bi.

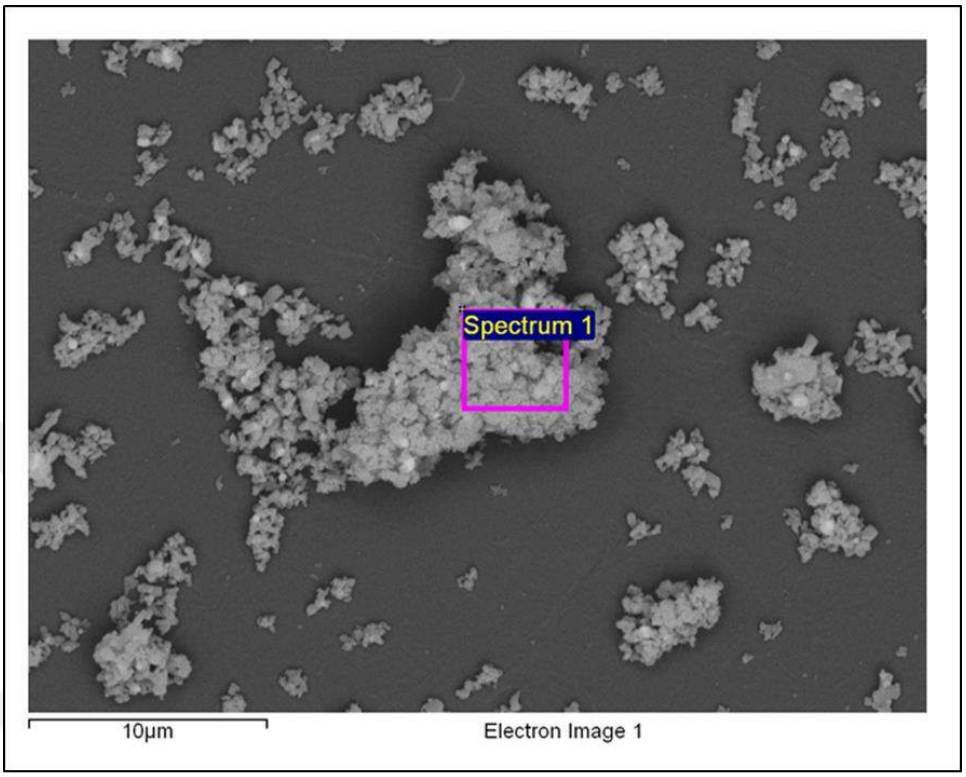

Element	Weight%	Atomic%	Compd%	Formula
Zn K	67.30	46.10	83.77	ZnO
Bi M	14.55	3.12	16.23	Bi2O3
O	18.14	50.78		
Totals	100.00			

Figure 4.77. *EDX analysis of S2 powder, overall*

There were white particles in the powder mixture, to evaluate their composition, EDX point analysis was performed on white particles as shown Figure 4.78. It was determined that there were 64 wt% Zn and 18 wt% Bi atoms. This composition was close to the general analysis result. However, the fact that the analysis result was not exactly at the desired point and the signal coming from its surrounding may have caused this.

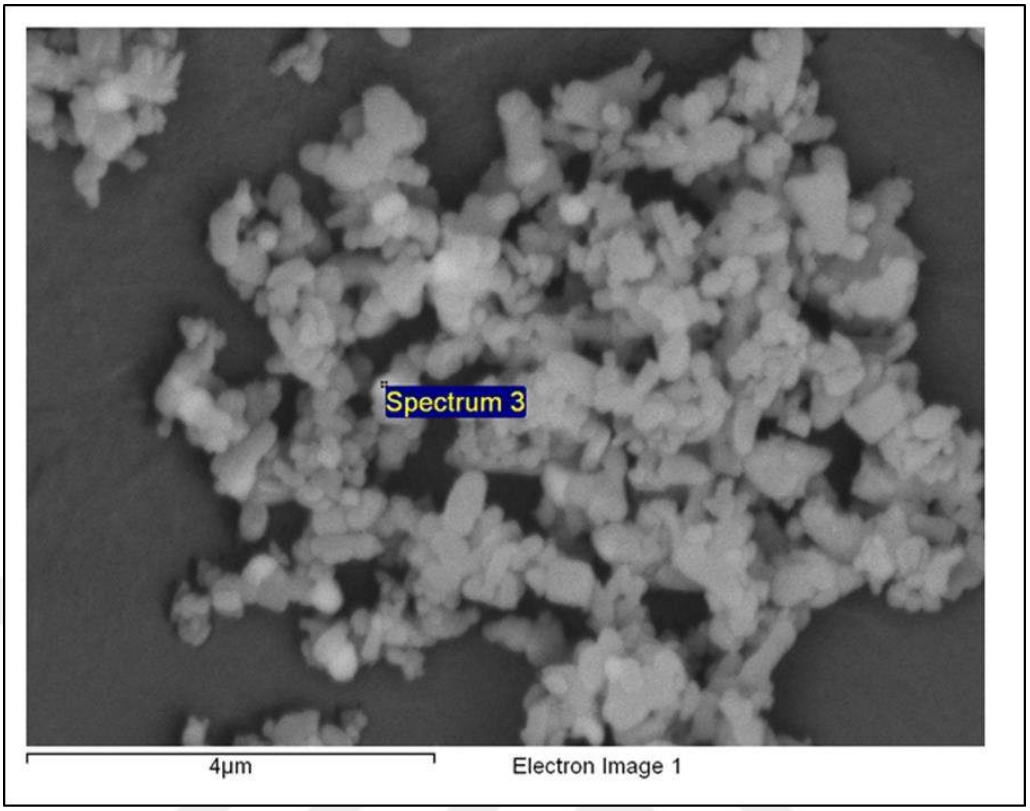

Element	Weight%	Atomic%	Compd%	Formula
Zn K	64.31	45.09	80.05	ZnO
Bi M	17.90	3.93	19.95	Bi2O3
O	17.79	50.98		
Totals	100.00			

Figure 4.78. *EDX analysis of S1 powder, white grain*

CSP of Bi_2O_3 coated ZnO – S1

CSP trials were carried out with the obtained S2 powder, see at Table 4.13. Accordingly, it was observed that the densities were approximately 4-6 % lower than the experiments with S1 powder, but still more than 90.00 % T.D.. Accordingly, the highest density was obtained when 8.00 wt % liquid ratio was used. The curve below shows the T.D. values due to liquid amount, see at Figure 4.79.

Table 4.13. *Sintering conditions Theoretical Density % of the samples made CSP with S2 powder.*

Sample	Pressure (Mpa)	Time (min.)	Temp. (°C)	Liquid (wt %)	pH	T. D. (%)
S2-CSP	539	50	140	9.00	5.5	87.96
S2-CSP	539	50	140	7.81	5.5	91.05
S2-CSP	539	50	140	7.81	5.5	92.54
S2-CSP	539	50	140	7.81	5.5	92.59
S2-CSP	539	50	140	7.81	5.5	94.00
S2-CSP	539	50	140	7.81	5.5	97.69
S2-CSP	539	50	140	8.10	5.5	93.25
S2-CSP	539	50	135	7.81	5.5	87.92

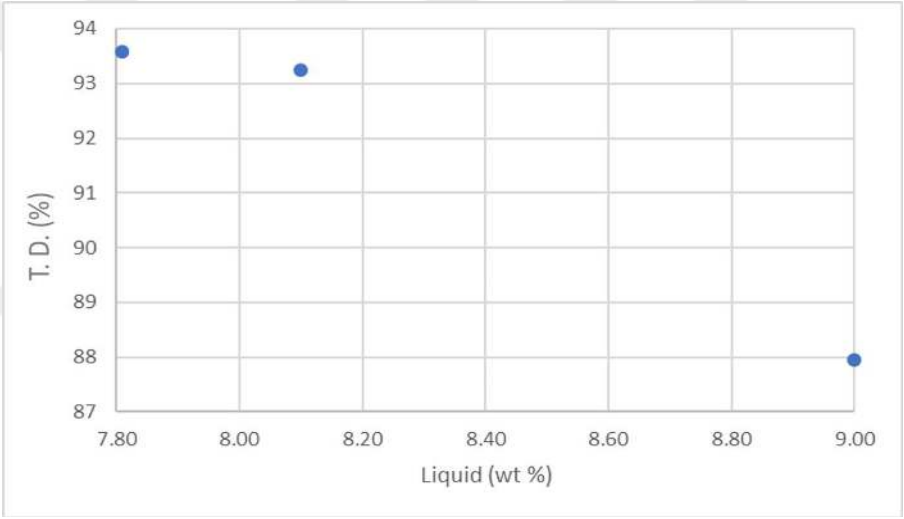

Figure 4.79. *Graph of T.D. %, CSP at 140°C using S2 powder and with different water ratios.*

Figure 4.80 shows the SEM image of the sample produced with S2 powder, sintered at 140°C and used 9.00 wt % liquid. It is seen that the grain size is 200 – 300 nm after sintering. The white grains known to be Bi_2O_3 are homogeneously dispersed.

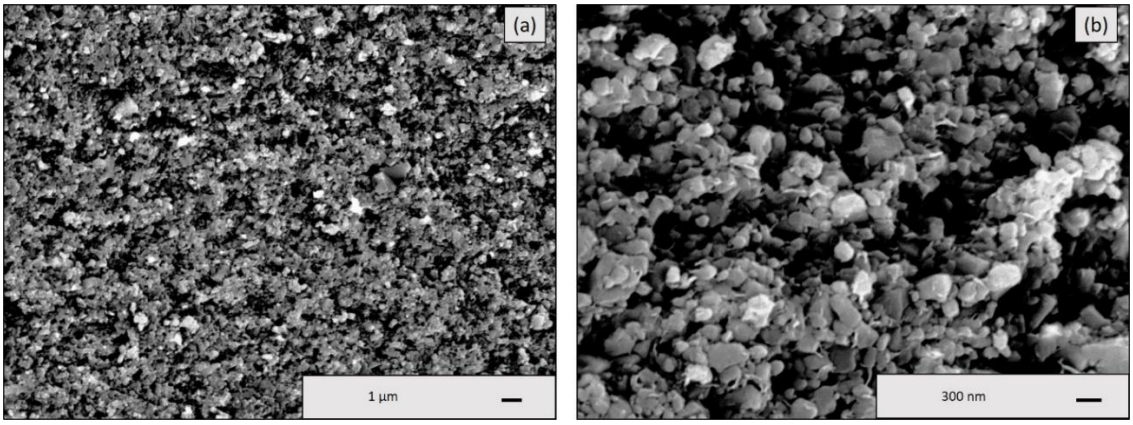

Figure 4.80. *BSE-SEM images of CSP sample at 140°C with 8,0 % liquid*

In Figure 4.81, the broken surface BSE-SEM images of the sintered sample of S1 powder produced with 8.00 wt % liq in a and the sample using S1 powder produced with 9.00 % liquid in b are placed. Although the liquid ratios are not equivalent, the overall appearance of both samples were compared. They both show similar microstructural properties. The grain sizes, shapes and pore size distributions were similar.

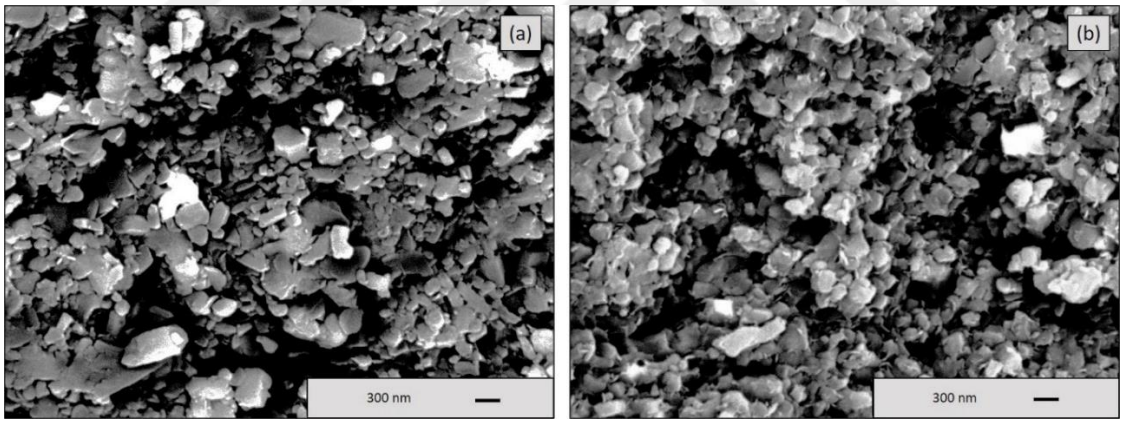

Figure 4.81. *BSE-SEM images of CSP sample at 140°C with a)S1, 8.0 wt % liquid b)S2, 9.0 wt % liquid*

Electrical characterizations of CSPed Bi_2O_3 coated ZnO powder – S2

When the I-V curves of the samples produced with the S2 powder were examined, it was observed that there were some incomprehensible differences in the electrical behavior of both samples. It is seen that they do not fully reach the varistor characteristics. Figure 4.82 shows the best I-V curve that was obtained with the S2 powder. Density values of the sample are shown in the Table 4.14. The straight gap in the middle is a very short region for varistor behavior. When the measurement was evaluated, we saw that the α value was 1.80 and the threshold voltage was 936 V/mm. It was decided to try to

develop the CSP samples produced by using S1 and S2 powders by annealing to see the electrical behaviour changes with an additional heat treatment.

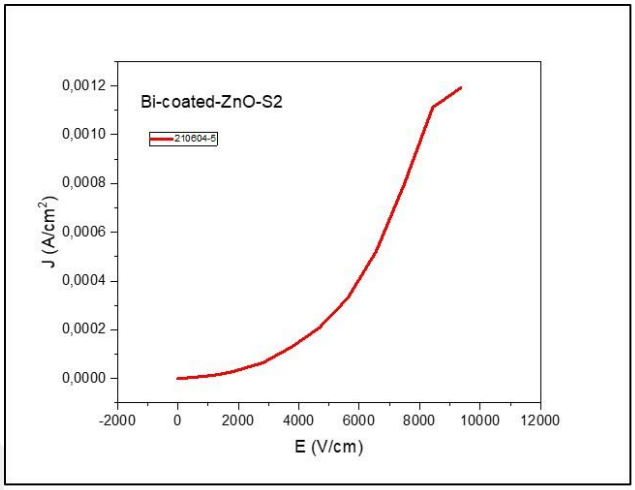

Figure 4.82. *S2 powder, CSP sintering, I-V curves*

Table 4.14. *S2 powder, electrical characterization samples properties*

Liq. (wt %)	**T.D. (%)**	**α**	**V_{Th} (V/mm)**
8.00	93.25	1.80	936

4.3.1.4. Annealing of the cold sintered ZnO-Bi_2O_3 varistors

The samples produced with the S1 powder were kept at 400°C, 600°C and 800°C temperatures for 1 hour and then XRD analyzes were evaluated, Figure 4.83. There was a similarity in XRD analyzes after 400°C and 600°C. However, when annealed at 800°C, the peak of the Bi_2O_3 phase at 27 degrees disappeared. In this case, it is thought whether Bi_2O_3 may have been removed from the system. Although the probability of this situation is low, the situation will become clear with electrical measurements.

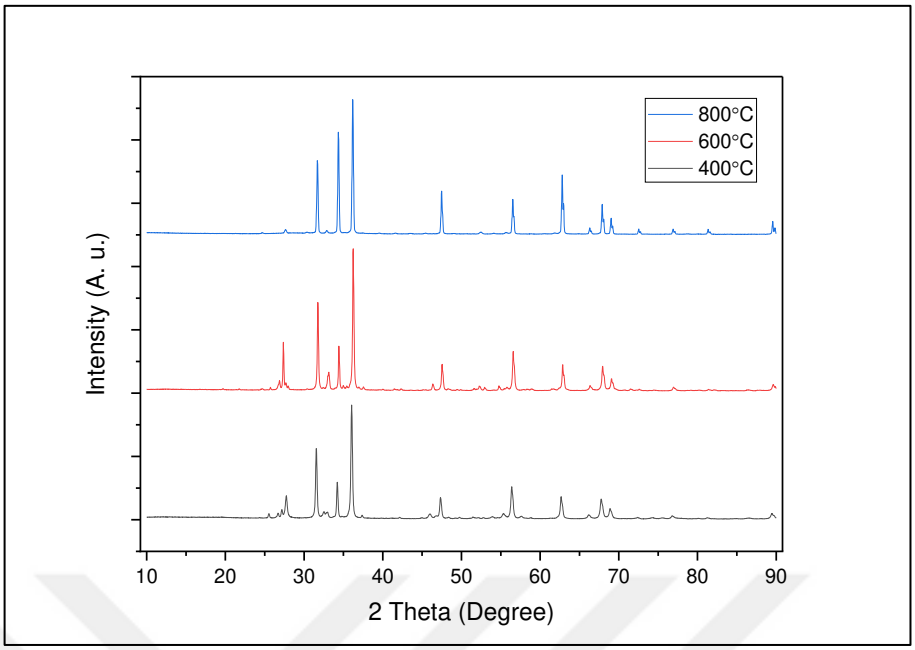

Figure 4.83. *CSP with S1 powder, XRD analysis after annealing*

The samples produced with the S2 powder were annealed at the same temperatures. XRD analyzes were performed on these samples. In this analysis, there was no phase change in the sample annealed at 800°C. In this case, the electrical properties of both samples will be compared.

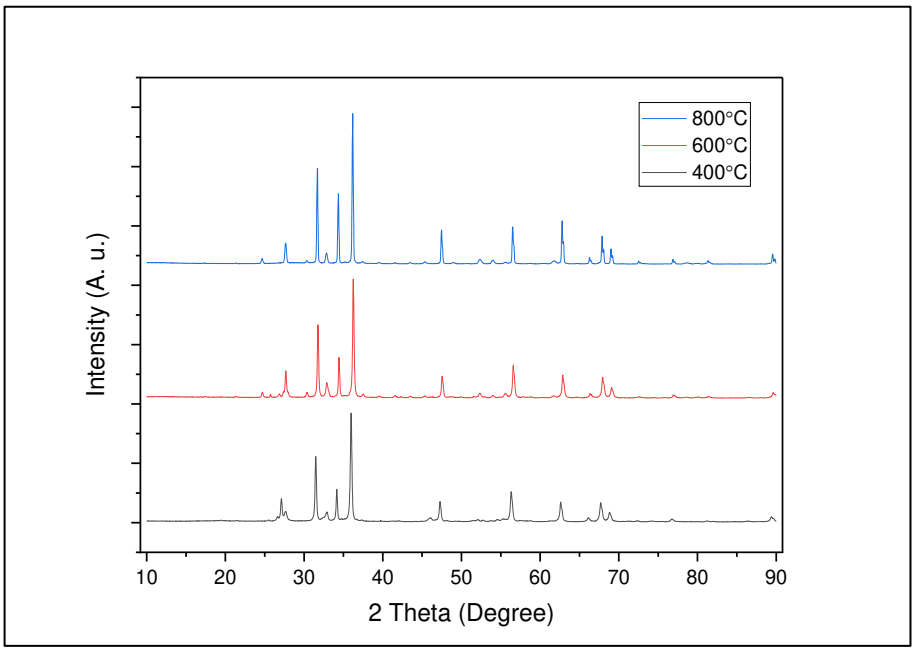

Figure 4.84. *CSP with S2 powder, XRD analysis after annealing*

As a result of annealing at 400°C, there was no improvement in the α value of the material, Figure 4.85 a. When the α value of the sample is examined as a result of annealing at 600°C, it is seen that there is no improvement, and even the α value decreases. After annealing at 800°C, the α value was 12.01, Figure 4.85 c. This value is the highest α value obtained throughout the annealing study. It was seen that the threshold voltage was 464 V/mm and lower than the non-annealed samples, see at Table 4.15. densities are downward trend due to annealing temperature increment. This may be due to hydrate decomposition at the body or due to phase changes of Bi_2O_3.

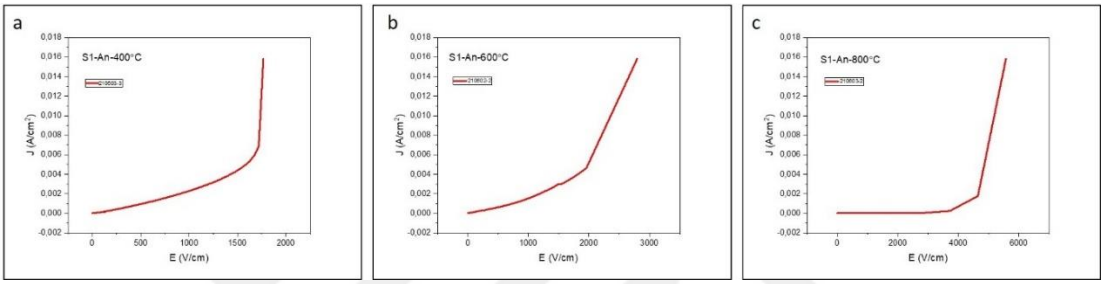

Figure 4.85. *S1 powder, I-V curves after sintering with CSP, annealing*

Table 4.15. *α values and Threshold Voltages, S1*

An. Temp. (°C)	T.D. (%TD)	α	V_{Th} (V/mm)
400	94.84	2.27	53
600	91.57	2.08	75
800	90.43	12.01	464

The I-V curves for the samples produced with the S2 powder were also examined, see at Figure 4.86. It was determined that the varistor curve behavior, which was not seen before annealing, could be seen after annealing when the curves were examined. However, examining the α values will give a more accurate perspective on this issue, see at Table 4.16. After annealing at 400°C, the α value decreased. In fact, varistor behavior had disappeared. After annealing at 600°C, the α value was 14.95. In S2 samples, a maximum value of 1.80 was obtained before annealing. In this case, it was possible to say that there was some increase of α value. As the result of annealing at 800°C, an α

value of 7.45 was obtained. Although this value is not as high as the 12.01 value obtained by annealing the S1 powder at 800°C before, it was seen that it is considerably higher when evaluated within itself. The threshold voltage for this sample was measured as 454 V/mm.

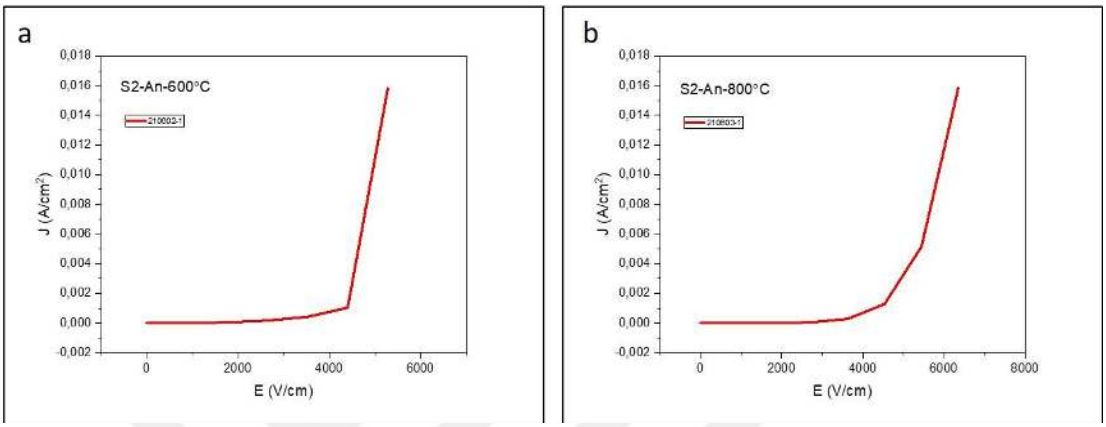

Figure 4.86. *S2 powder, I-V curves after sintering with CSP, annealing*

Table 4.16. *α values and Threshold Voltages, S2*

An. Temp. (°C)	T.D. (%)	α	V_{Th} (V/mm)
600	88.17	14.95	440
800	89.83	7.45	454

4.3.2. ZnO-Bi_2O_3-Co_2O_3 varistor production via CSP

4.3.2.1. Mixed powder method

In our study, α value was determined as 25.24 at most for ZnO-Bi_2O_3 coated system. Further experiments were made with the additions of Co_2O_3, Mn_2O_3, Sb_2O_3 to increase the α value. However, although Zhao and Randall used the mixing powder method in their study, we could not obtain similar results in our studies [24].

Table 4.17 showing the theoretical densities of the experiments with the powders produced, the errors that occurred and the process parameters used is given below. At the table, it is seen that the density can be increased as a result of many trials, by changing CSP conditions. However, it was determined that the strength of the samples were low.

At the same time, although high densities were obtained with pure ZnO at 140°C, high densities could not be reached at the same temperature with the varistor powders. For this reason, experiments were carried out at different temperatures. Electrical measurements could be done with a few samples that had 94-95 % T.D. values.

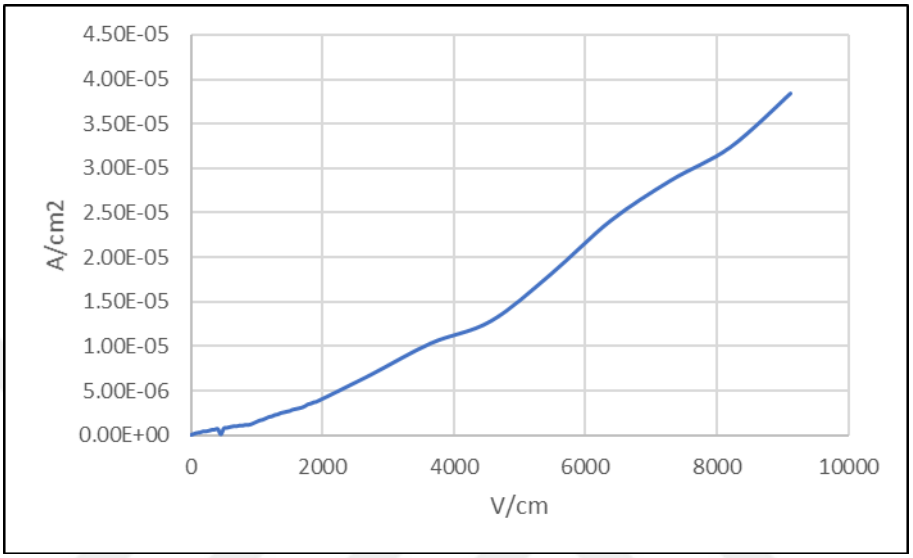

Figure 4.87. *I-V curve of CSPed powders, mixed at mill*

Electrical measurement made with the produced samples, the desired varistor behavior could not be determined. For this reason, α values and threshold voltages could not be reached. The sample whose I-V measurement is given in Figure 4.87 was sample 210922-1, it was produced with ZBCM – 210909-1 powder and its theoretical density was determined as 90.64 %. Since the results obtained from the experiments with these powders could not provide sufficient density and electrical properties, it was decided to try the previously tried powder coating method. The reason for not obtaining sufficient values may be that insoluble particles have a reducing effect on sintering in the system. The idea of making the coating on ZnO with insoluble particles and adding Bi_2O_3 to the system at the mill will be used.

Table 4.17. *The CSP experiments with powders produced in the mill*

Sample	Powder	Temp. (°C)	Pressure (Mpa)	Other parameters	R. D. (%)	Comments
210914-1	ZBCM-2109	140	540	8wt%,pH5.5	88.02	Elect. char./insulator
210914-2	ZBCM-2109	140	540	8wt%,pH5.5	77.70	
210914-3	ZBCMS-2109	140	540	8wt%,pH5.5	-	crack
210914-4	ZBCM-2109	135	540	8wt%,pH5.5	87.18	crack
210915-1	ZBCMS-2109	135	540	8wt%,pH5.5	76.71	
210915-2	ZBCMS-2109	135	540	8wt%,pH5.5	76.50	crack
210915-3	ZBCMS-2109	135	540	7,5wt%,pH5.5	-	crack
210916-1	ZBCM-2109	135	540	7,5wt%,pH5.5	83.86	Elect. char./insulator
210916-2	ZBCMS-2109	135	540	7,5wt%,pH5.5	-	
210920-1	ZBCM-2109	160	540	8wt%,pH5.5	86.21	
210920-2	ZBCM-2109	180	540	8wt%,pH5.5	88.64	crack
210920-3	ZBCM-2109	200	540	8wt%,pH5.5	94.00	
210921-1	ZBCM-2109	220	540	8wt%,pH5.5	93.57	
210921-2	ZBCM-2109	240	540	8wt%,pH5.5	-	
210921-3	ZBCMS-2109	200	540	8wt%,pH5.5	-	
210922-1	ZBCM-2109	200	540	8wt%,pH5.5	90.64	
210922-2	ZBCMS-2109	200	540	8wt%,pH5.5	-	crack
210922-3	ZBCMS-2109	180	540	8.1wt%,pH5.5	-	crack
210923-1	ZBCMS-2109	180	540	8.3wt%,pH5.5	-	crack
210923-2	ZBCMS-2109	200	540	8.3wt%,pH5.0	77.48	good outlook
210923-3	ZBCMS-2109	190	540	8.3wt%,pH5.0	-	crack
210924-1	ZBCMS-2109	180	540	8.3wt%,pH4.5	74.30	good outlook
210924-2	ZBCMS-2109	220	540	8wt%,Ph4.5	74.30	crack
211125-3	ZBCM-2109	100-140-220	540	8wt%,pH5,5	92.16	
211126-1	ZBCM-2109	100-220-260	540	8wt%,pH5.5	-	crack
211126-2	ZBCM-2109	100-180-220	540	8wt%,pH5.5	-	crack
211126-3	ZBCM-2109	100-220-140	540	8wt%,pH5.5	91.95	
211126-4	ZBCM-2109	110-300-140	540	8wt%,pH5.5	95.79	
211128-1	ZBCM-2109	110-330-140	540	8wt%,pH5.5	95.68	

4.3.2.2. Coating ZnO by cobalt oxide

Additions to be used in the coating process will first be started with Co_2O_3. The reason for choosing cobalt is that it is known to cause an increase in alpha value, means non-linearity, [145-147]. Other additives in the system may be the matter of further studies.

The process used was obtained by examining the pH ranges of the articles produced Co_2O_3 from Co-nitrate powder, [148-151]. J.M. Xu et al. studied cobalt nitrate and as a result, oxide cobalt powders were obtained in different shapes and forms according to pH ranges. G. Allaedini, on the other hand, mentioned about the importance of different pH ranges in powder synthesis and examines the effect of other parameters. In the coating of the powder, the process was started with the necessary cobalt-nitrate so that the oxide cobalt to be formed on ZnO is 0.5 % by mole. Since cobalt-nitrate powder can be easily dissolved in pure water, the process had been started without the need for acid dissolving. It was said that the dissolved powder precipitates after pH 8.0, but it was desired that the pH level be above 9.0 with the temperature in order to become an oxide. Just before the precipitation process, ZnO powder was added to the system and used as the core. It was observed that the powder precipitated in a yellowish color. However, some characterization processes were applied to determine the form of the precipitate and the presence of the coating. These are analysis by XRD, Raman analysis, UV-spectrometry, Zeta measurement, FTIR analysis and imaging analysis by SEM. Although the presence of cobalt has been detected in the system, it has not been determined exactly in which form it was. Detection was started with XRD analysis.

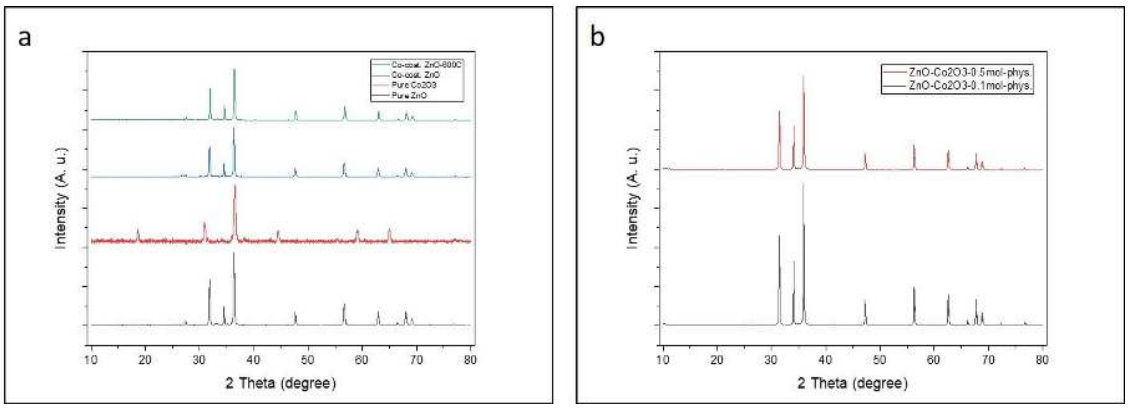

Figure 4.88. *The XRD Patterns of Pure ZnO, Co_2O_3, Co-coated ZnO, Co-coated ZnO-600°C calcinated, ZnO-Co_2O_3, 0.1 mol physical mix and ZnO-Co_2O_3, 0.5 mol physical mix*

XRD graph of the powder coated with cobalt was examined, Figure 4.87. XRD graphs were also utilized to pure ZnO powder used for comparison and Co_2O_3 powder (Alpha aeser) available as raw material. The curves seen in Figure 4.87 a belong to the coated powder and pure raw materials. In addition, XRD analyzes were performed again on the powder made by TG-DTA. The purpose here is to see the change that may occur if the cobalt precipitate as oxide. It is seen that the peaks are compatible with pure ZnO powder. In Figure 4.87 b, the raw material Co_2O_3 is physically mixed with ZnO at the ratios of 0.1 mol and 0.5 mol. It was thought that seeing the peaks of Co_2O_3, which is present in a small amount in the system, can shed light on whether we can see the small amount of addition. It was seen that the physical mixing peaks were similar with pure ZnO. For this reason, it was not possible to determine whether there was coating by XRD analysis.

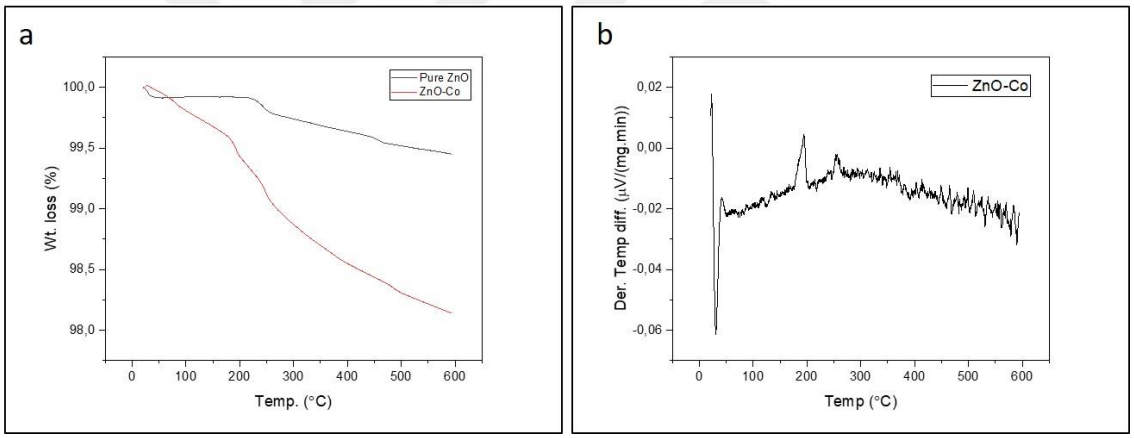

Figure 4.89. *a) Pure ZnO and Co-coated ZnO weight loss, b) Co-coated ZnO temperature difference derivative curve*

At Figure 4.88, when the TG-DTA graphs are examined, it is seen that the weight loss is 0.5 % for pure ZnO and approximately 2.0 % for Co-coated ZnO powder. It was determined that there was a difference in material color after coating. However, it was not certain that this coating on ZnO is oxide or not. It was also possible that cobalt precipitating in the form of hydrates. Exothermic peak was observed at 180°C and 220°C, Figure 4.88 b. These peaks are clearly present even though the curve is very noisy. The reason for these peaks was not fully understood, However, was considered reactions in the system continue with temperature.

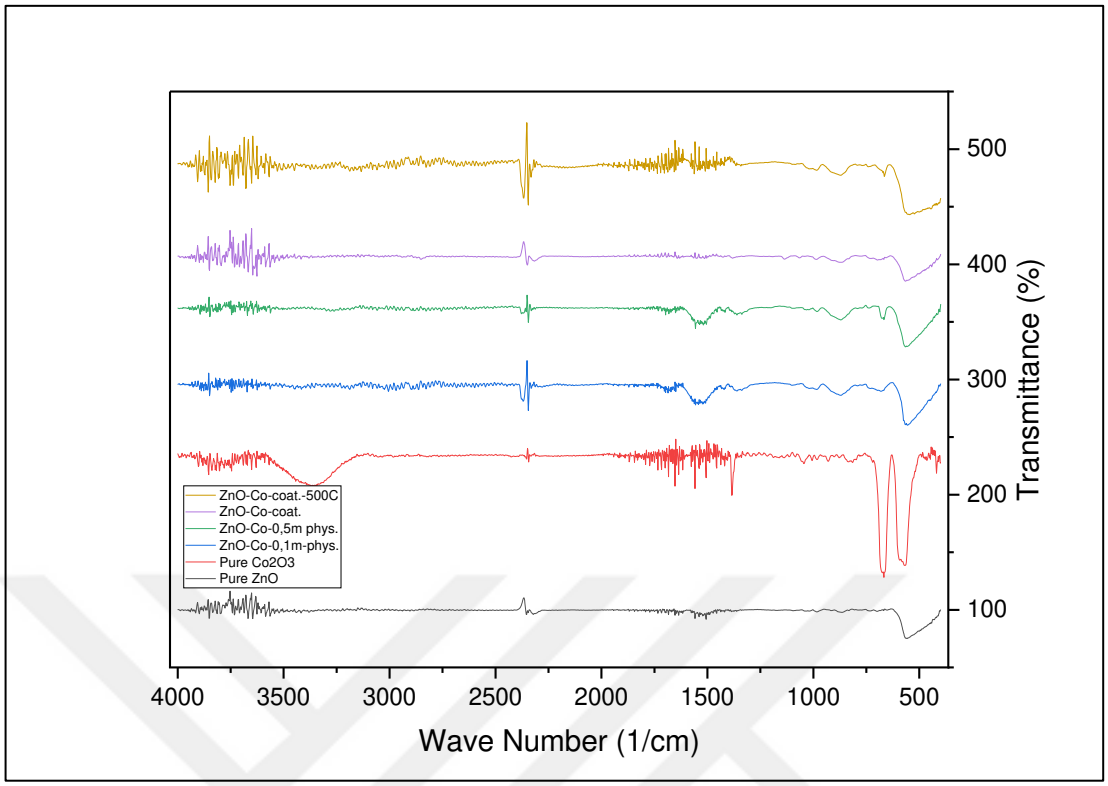

Figure 4.90. *FTIR analyses results of Pure ZnO, Co_2O_3, Co-coated ZnO, Co-coated ZnO-500°C calcination, ZnO-Co_2O_3, 0.1 mol physical mix and ZnO-Co_2O_3, 0.5 mol physical mix*

When we investigate FTIR curves of Co_2O_3 powder and two powders with physical Co_2O_3 mixing, the differences with the pure ZnO curve can be clearly seen, see at Figure 4.90. The difference of the peak at 1500 is evident at the physical mixtures. In this way, no clear difference could be seen in coated, calcined and uncalcined powders. However, when looking at the peak in the 2300s in the calcined powder curve, it was seen that the peak of the physical mixtures is similar to the same degree. However, since there is no clear distinguishing peak, no precise information could be obtained.

Raman analysis of pure ZnO powder and Raman analysis of pure Co_2O_3, Co-coated ZnO and calcined Co-coated ZnO powders were compared, see at Figure 4.91. Looking at these curves, it is seen that Co-coated ZnO powder is quite similar to pure ZnO. However, after calcining, a clear difference emerges. The reason for this is thought to be due to the differences in the vibration of the cobalt oxide bonds. It was seen that the main peak of the cobalt oxide at the 690 cm^{-1} is also included in the calcined Figure 4.91 d curve. However, the fact that the peaks of both materials do not change may indicate that there is no structural union [152]. The physical appearance of the powder changed after it was calcined. After coating, the cream color powder turned to gray. In this case, it is

possible to say that the ZnO powder has a cobalt coating on it. Zeta analyzes of the powders were also examined.

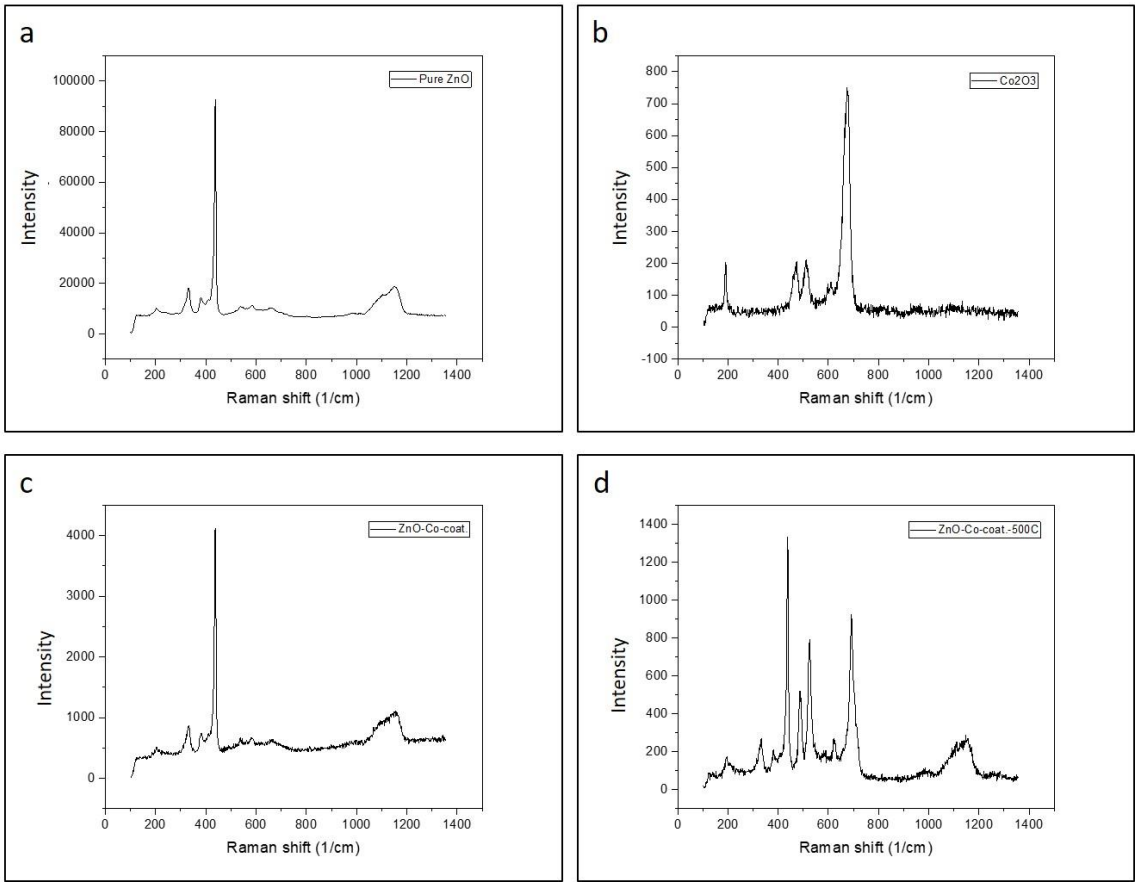

Figure 4.91. *a)Pure ZnO, b)Co_2O_3, c)Co-coated ZnO, d)Co- coated ZnO-500°C calcination Raman spectrums*

Zeta analyzes show that there is a difference in surface charges, see at Table 4.18. Measurements could not be taken with Co_2O_3 because it collapses very easily and does not disperse in water, but when the physical mixture results are examined, it can be specified that the addition of Co_2O_3 increases the zeta value. The zeta values of pure ZnO and Co-coated ZnO were obtained as 12.8 and 14.9, respectively. If cobalt was attached to the surface as hydrate, it was possible that the charges are similar. After calcining the Co-coated ZnO, the zeta value was measured again. It was seen that the zeta value of the calcined powder was 24.0. This indicates the presence of another oxide, namely Co_2O_3 coating, which was different from ZnO on the surface, as in the Raman analysis. In this case, mass sample production was started.

Table 4.18. *Pure ZnO, Co_2O_3, Co-coated ZnO, Co- coated ZnO-600°C calcination, ZnO-Co_2O_3, 0.1 mol physical mix and ZnO-Co_2O_3, 0.5 mol physical mix Zeta potential values*

Sample	**Zeta potential (mV)**
Pure ZnO	12.8
Pure ZnO-0.1 mole Co_2O_3-physical mix.	26.5
Pure ZnO-0.5 mole Co_2O_3-physical mix.	35.0
Co_2O_3-Bi_2O_3-ZnO (coating)	14.9
Co_2O_3-Bi_2O_3-ZnO (coating) – 600°C	24.0

4.3.2.3. ZnO – Bi_2O_3 – Co_2O_3 varistor production with the CSP

Experiments were made with the produced coated and calcined powders. In these experiments, different conditions were studied in order to increase the density. There were no successful result in the trials with powders used in the form of conventionally mixed powder method. The addition of the additives to the system with the coating method has been tried before with ZnO-Bi_2O_3 varistors and it has been determined that there is an increase in both alpha and breakdown voltage values [153]. It is stated that a more homogeneous structure is provided and there is a uniform potential barrier throughout the microstructure [154]. For this study, it was thought that the desired point in terms of homogeneity and solubility could be reached with the coating method. Thereafter CSP trials with the coated powder, SEM analyzes and electrical characterization were applied to some of the samples obtained.

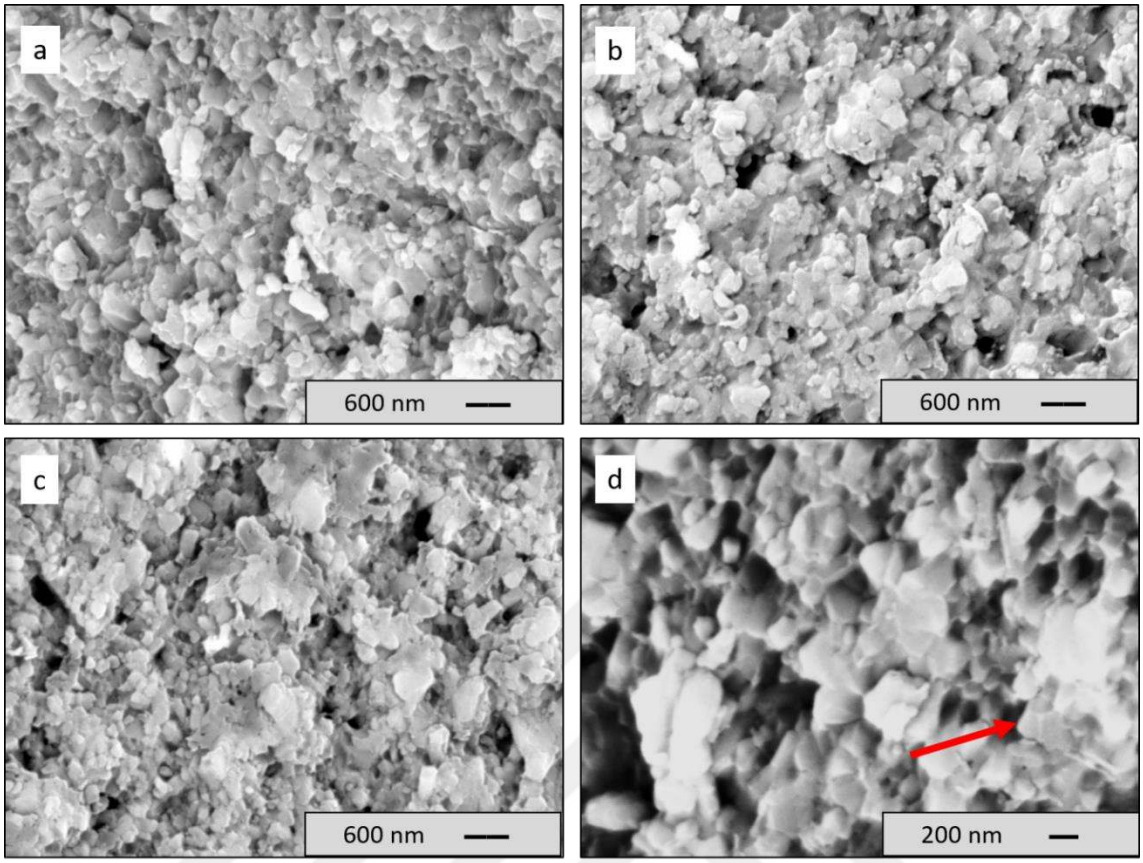

Figure 4.92. *SEM images of a) Powder of Co-ZnO coated, calcinated with Bi_2O_3, 9.7 wt % liq., pH 5.5, 250°C/5 min, 540MPa, 93.93 % T.D., b) powder of Co-ZnO coated, Bi_2O_3 addition after calcination, 9.7 wt % liq, pH 5.5, 140°C/45, min 540MPa, 94.6 % T.D., c)powder of Co-ZnO coated, Bi_2O_3 addition after calcination, 9.7 wt % liq., pH 5.5, 140°C/45 min, 540MPa, 93.9 % T.D., d) powder Co-ZnO coated, calcinated with Bi_2O_3, 9.7 wt % liq, pH 5.5, 250°C/5 min, 540MPa, 93.93 % T.D.*

At Figure 4.92, it can be seen that densification could be achieved. The density of the sample in Figure 4.92 a could not be measured dimensionally, as a result of the dimensional measurement, a density greater than the theoretical density of 5.72 g/cm^3 was calculated. In this case, it is possible that there was an error in the measurements. In order to correct this error, density measurement was made with Archimedes on the remaining sample and 93.93 % theoretical density was obtained. The high difference with the dimensional measurement indicates that it was necessary to increase the densities. Electrical measurements taken with low densities may not provide us with sufficient data or we may obtain lower values than they actually can have. This is something that needs to be developed. In the SEM image of the same sample, seen in Figure 4.92 d, it was seen that the ZnO grains merge with the sintering in the region indicated by the arrow and the grain boundaries, which are seen in white in between, are formed as a different phase. This is an important result. Because interphase could not be seen in any of the previous

studies. It can be understood from the color difference that the interface was different at grain boundary regions, which was white in colour, as like traditionally sintered varistors. By the images taken as BSE, the regions with Bi_2O_3 appear whiter, while ZnO appears grayer due to the phase difference. This opens a door for us to obtain varistors. On the other way, it was stated that the breakdown field of varistors depends on the grain size of the metal oxide grain size. If the grain size of the material is (< 10 μm) it is able to be used for high-voltage applications, whereas if the average grain size larger (> 30 μm) it is mostly used for low-voltage applications, [155,156]. Here, it is seen that avarage grain size is approximately 150 nm and able to be used for high voltage applications, theoritically.

4.3.2.4. Electrical characterizations

I-V graphs of Co-Bi-ZnO varistor system, produced by CSP were evaluated at Figure 4.93. In all graphs, it was seen that the threshold voltages exceed 1000 V/mm. The threshold voltage is the point at which the material becomes conductive. This situation can be seen more clearly in Figure 4.93 a. The density of the sample was higher than others, so it was proven the process conditions were also effective for the result property. At the previously examined SEM images, the formation of interphase was noticed in the sample, which was heated to 150°C and sintered with the same powder. This may also have a positive effect on varistor formation. The samples in Figure 4.93 b and c also belong to the samples sintered with the same powder. However, the behavior is not as clear as seen in a. It was seen that the density value in b is low. The density of the sample in Figure 4.93 c may be lower than the calculated value. The sample in Figure 4.93 d was prepared only by calcination of Co-coated ZnO powder. Afterwards, Bi_2O_3 was added freely and mixed in the mill. It is seen that the density and threshold voltage values of this sample was lower.

When the α values were calculated from the obtained I-V graphs, the α value was calculated as 27.90 for the sample in Figure 4.93 a, 6.01 for the sample in b, 6.45 for the sample in c, and 5.02 for the sample in d. The α values increased with the addition of cobalt to the system. The result is close to a sample produced with the S1, but still higher. The threshold voltages were 1754 V/mm, 2188 V/mm, 1864 V/mm and 1398 V/mm, respectively. The threshold voltage values are much more higher than previous studies.

In this case, it can be said that the addition of cobalt with coating method improves the varistor properties in production with the CSP method.

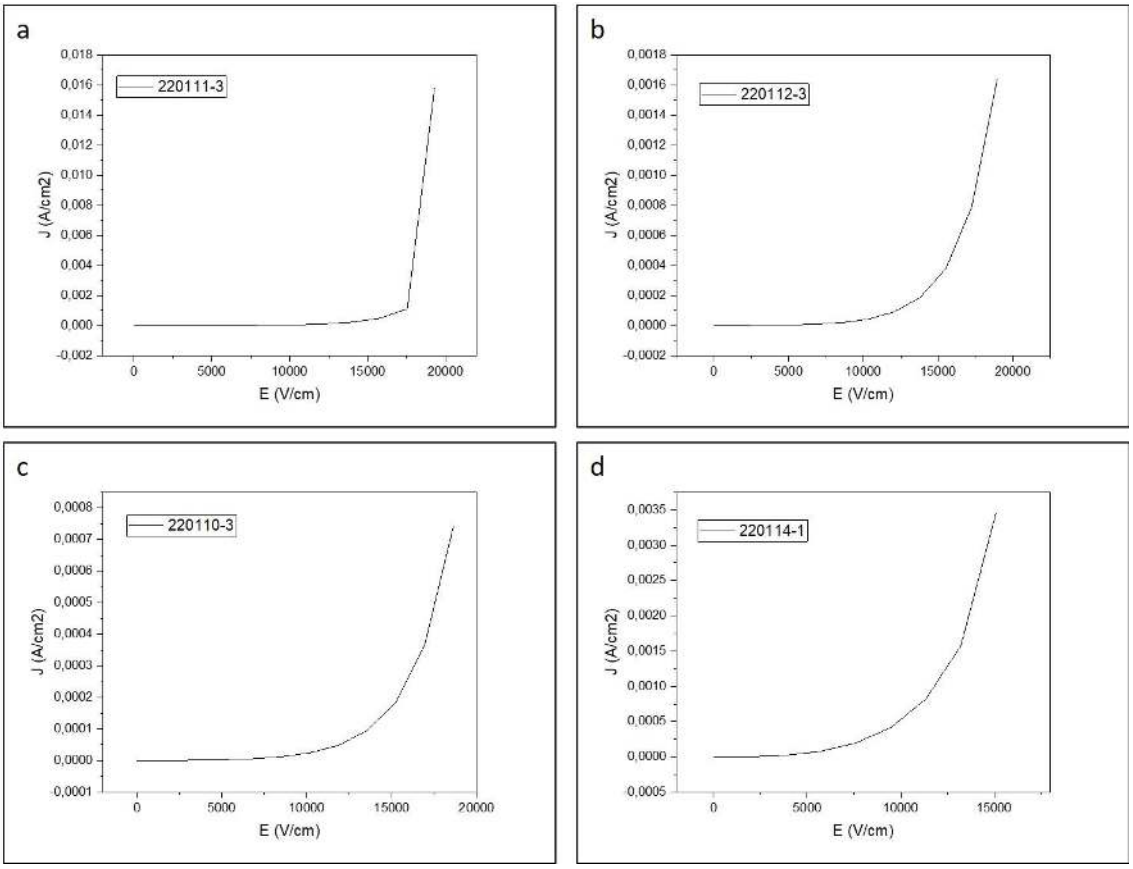

Figure 4.93. *J-E graphs of a) Powder of Co-ZnO coated, calcinated with Bi_2O_3, 9.7 wt % liq., pH 5.5, 250°C/1 min., 540MPa, 97.96 % T.D., b) powder of Co-ZnO coated, calcinated with Bi_2O_3, 9.7 wt % liq., pH 5.5, 250°C/5 min., 540MPa, 94.89 % T.D.,, c) powder of Co-ZnO coated, calcinated with Bi_2O_3, 9.7wt % liq., pH 5.5, 250°C/5 min., 540MPa, 98.5 % T.D.,, d) powder of Co-ZnO coated, Bi_2O_3 addition after calcination, 9.7 wt % liq., pH 5.5, 250°C/5 min-first 10 min of sintering reached 250°C, 540MPa, 96.33% T.D.*

The results were confirmed by repeated processing and the tests. The electrical measurement was applied to the samples produced with the same powders under similar conditions. Figure 4.94 are the I-V graphs of the repeated tests. All α values are over 20 as seen at Table 4.19. Results were compared with pre-results that were given above for Co-coated-ZnO-Bi_2O_3 system. Both alpha values and the threshold voltages are similar. Cobalt-containing ZnO varistors with fine grain size are considered to be electrically suitable and repeatable for high voltage applications.

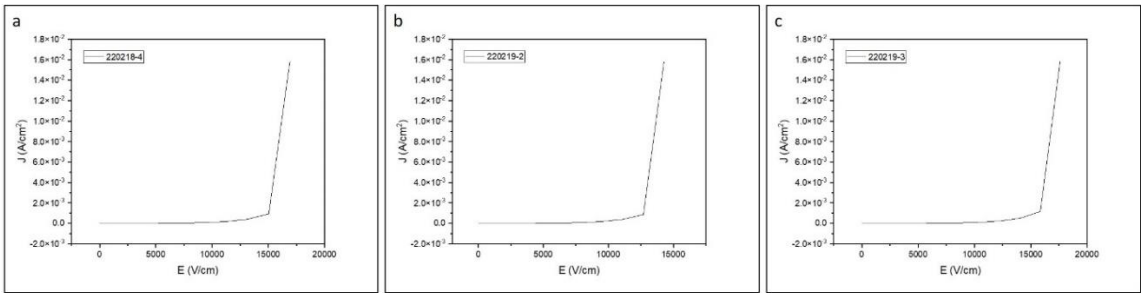

Figure 4.94. *J-E graphs of Powder of Co-ZnO coated, calcinated with Bi_2O_3, 9.5 wt % liq., pH 5.5, 250°C/1 min., 540MPa a) 99.00 % T.D., b) 98.40 % T.D., c)95.40 % T.D.*

Table 4.19. *Repeated experimemtal results for Co-coated ZnO-Bi_2O_3 varistor systems*

SEM sample name	T.D. (%)	α	V_{Th} (V/mm)
a	99.00	24.02	1504
b	98.40	24.66	1270
c	95.40	24.69	1588

4.3.3. Conclusions

For high voltage varistor applications, electrical properties of nonlinear coefficient value >30 and breakdown/threshold voltage > 1000 V/mm are expected.

These results show that varistor properties can be achieved with a binary system of ZnO and Bi_2O_3 via the cold sintering process at relatively low temperatures. The maximum nonlinear coefficient (α) value of 25.24 was obtained by the coated ZnO by Bi_2O_3 (S1) powder. With the traditional method, the alpha value was at most 4.89. In this case, it is possible to say that the coating has positive effects on CSP and microstructurel evolution. Annealing was utilized for some samples, but the improvement of α was insufficient. Evenmore, threshold voltages were disappeared by annealing. MnO/Mn_2O_3, Sb_2O_3, Co_2O_3 were used as additives to the ZnO-Bi_2O_3 varistor system. Mixed powder method was unsuccessful for CSP. Therefore, coating of ZnO by the cobalt oxide additive was approved.

It was determined by the experiments that the addition of cobalt improved the α value and increased the threshold voltage. The highest breakdown/threshold voltage was measured as 2188 V/mm, while the highest α value was measured as 27.90 and the values were repeatable as well. This result is compatible with the literature [105]. To achieve a

high voltage varistor, alpha value should be improved for our studies. Some more additives can be used for improvement. Sb_2O_3 is the best candidate for enhancing varistor properties. The breakdown voltage value is suitable for high voltage applications and still can be improved. Smaller grains and homogeneous microstructure will be effective for enhancing breakdown voltage.

As the result, ZnO-Bi_2O_3-Co_2O_3 system can be sintered with CSP and high voltage varistors can be produced with current method. Coating can be necessary for non-dissolving particles for CSP systems. It is a suitable method for high voltage applications since materials with fine grain size can be produced. Industrial production can be difficult due to the sensitive nature of production. Since the mechanical strengths are low, the application area is important. Density measurements are difficult because it is sensitive to water and has low mechanical strength. However, it is remarkable for the ease of production method for suitable areas and the reduction of sintering temperature from 800-1000˚C to 250˚C ranges. In microstructures, it can be seen that the interphase is different from the grains, as in the materials produced by conventional sintering. This microstructural property show that varistor characteristics earned via CSP, as well.

5. CONCLUSIONS

In this thesis, technical and scientific investigations of the CSP were discussed by using ZnO as model material. Within the scope of this thesis, ZnO bulk ceramics with a theoretical density (T.D.) >99.00 % were successfully obtained and the CSP method was used for the production of ZnO-based varistors.

ZnO bulk ceramics with >99.00 % T.D. were obtained under two different conditions:

1- Pre-pressing at 89 MPa pressure for 4 minutes at 100°C and afterwards 540 MPa pressure, at 140˚C temperature after 50 minutes dwell time and 7.00 wt % liquid with pH 5.5 via CSP.

2- Pre-pressing at 89 MPa pressure for 4 minutes at 100°C and afterwards 250 MPa pressure, at 300˚C temperature after 1 minute dwell time and 8.00 wt % liquid with pH 5.5 via CSP.

For pure ZnO, the Vickers hardness of the CSP sample applied at 135°C was 2.98 GPa and the hardness of the sample sintered at 300°C was 1.70 GPa.

Interrupted experiments were performed to analyze the CSP process from a thermodynamic and kinetic perspective. Experiments were carried out under 540 MPa pressure, 140˚C and 7.00 weight % liquid with pH 5.5 via CSP. When the variation of the film thickness with time was examined, it was observed that the film thickness did not decrease in the samples sintered at 140˚C. For CSP at 300°C, there was a reverse situation. It was determined that the decrease in film thickness in samples sintered at 300˚C was due to acetate evaporation. Another study is related to the growth of grains during sintering. The grain growth constant was determined as n~2. The n value of 2 indicates that the grain growth process is controlled by the interface reaction during the applied CSP conditions. In addition, the activation energy for grain growth was determined as 40.7 kJ.

For detailed interactions of the sintering variables, responce surface methodology (RSM) using Minitab software was used with Cental Composite Design (CCD) method. The variables of temperature, pressure, pH, amount of liquid and time were applied. The most effective parameter for the tested variables was determined as pH. While pH could affect the system linearly, the effect of other parameters was mostly seen as a binary effect. Optimum conditions in the determined research area were determined with pH 5.9, pressure of 560 MPa, dwell time at 150°C for 40 minutes and humidity of 6.33 wt %.

According to this research result, the best sintering conditions for pure ZnO can be achieved in this way with the investigated parameters and applied conditions. Theoretical intensities were obtained above 97.00 % in validity experiments. Although the results do not reach 99.00 % T.D., it is seen that the internal structure is more homogeneous as a result of sintering under the given conditions. The electrical conductivity of different samples was evaluated for different conditions. However, the electrical conductivity value was low in the sample produced under optimum conditions. Conductivities were determined as $1.94x10^{-5}$ S/cm for CSPed at 540 MPa-135˚C, $3.95x10^{-5}$ S/cm for CSPed at 560 MPa-150˚C, $1.27x10^{-6}$ S/cm for CSPed at 350 MPa-300˚C, $7.17x10^{-6}$ S/cm for CSPed at 250 MPa-300˚C. These conductivities for pure ZnO are all less than 9 S/cm that was mentioned by A. Baker et al., [19].

After scientific and technological investigations on the pure ZnO system, experiments were utilized on the production of varistors via CSP, using ZnO powder with additives. ZnO-Bi_2O_3 and ZnO-Bi_2O_3-Co_2O_3 varistor systems were produced by CSP method. For high voltage varistor applications, electrical properties of nonlinear coefficient value >30 and breakdown/threshold voltage > 1000 V/mm were expected.

The results show that the varistor properties can be achieved with a binary system of ZnO and Bi_2O_3 by sintering through CSP at relatively low temperatures such as 135-140˚C. With the uncoated ZnO-Bi_2O_3 powder system, the α value was at most 4.89. The nonlinear coefficient (α) value of 25.24 was obtained with ZnO coated with Bi_2O_3 powder, (S1). In this case, it is possible to say that the coating has positive effects on CSP and microstructural development. The effect of annealing on electrical properties was also investigated. Annealing was used for some samples, but it was determined that α did not increase. Moreover, the threshold voltages decreased with annealing.

Trials were made using MnO/Mn_2O_3, Sb_2O_3, Co_2O_3 as additives to the ZnO-Bi_2O_3 varistor system. The mixed powder method was unsuccessful for CSP. For this reason, it was decided to coat ZnO powder with cobalt oxide additive. In this way, it was aimed that the insoluble addition surrounds ZnO and Bi_2O_3 was used as the soluble intermediate phase.

It has been determined by experiments that the addition of cobalt improves the α value and increases the threshold voltage in production with CSP. The highest threshold voltage was measured as 2188 V/mm, while the highest α value was measured as 27.90 and the values are repeatable. A nonlinear coefficient of about 19 and a threshold voltage

of 76 V/mm were found by W. Onreabroy et al., [157], in a ZBC varistor conventionally sintered for 4 hours at 1000–1100°C. The homogeneous microstructure, due to the fine-grained structure formed by CSP and the coating of ZnO particles with insoluble additives, was effective in increasing the nonlinearity and breakdown voltage. These electrical properties can still be improved by using more additives. The addition of Sb_2O_3 is the best candidate to improve varistor properties. This may be the first area of future study of CSPed ZnO varistor studies.

As a result, the ZnO-Bi_2O_3-Co_2O_3 system can be sintered with CSP and suitable properties for high voltage varistor applications can be obtained. The creation of a ceramic microstructure with fine grain size as a result of sintering at low temperatures has been effective in obtaining the desired electrical properties. However, the ease of the production method and the reduction of the sintering temperature from 800-1000˚C to 250˚C are remarkable, [157]. This reduction in sintering temperature means that the energy consumption degrades from 2000 kJ/g for 800-1000˚C for liquid phase sintering [50] to 42 kJ for CSP sintering at 250˚C. The 48-times reduction in production energy is quite significant considering the importance of energy consumption studies of todays world. The relevant calculations used in the production of varistors with CSP are proportional to the data given for $BaTiO_3$, “The energy consumption in sintering of $BaTiO_3$ powder can decrease from 2800 kJ/g for conventional sintering, to 2000 kJ/g for liquid phase sintering, to 1050 kJ/g for FAST sintering, to 540 kJ/g for microwave sintering, to 130 kJ/g for fast-firing, to even 30 kJ/g for the CSP.” [1]

On the other hand, there will be some factors that should be considered in the use of the CSP method in the production of ZnO varistor systems. Coating of powders may be necessary to incorporate insoluble particles into the CSP system. Industrial production of varistors can be difficult due to the delicate nature of manufacture and the low mechanical properties of bulk materials.

In microstructures, as in materials produced by conventional sintering, it can be seen that the grain boundary phase is different from the grains. Finally, the theoretically designed microstructure can be created and it has been proven that varistor properties can also be obtained with CSP. These varistor characteristics are suitable for high voltage applications.

[1] D. S. B.Heidary et al., Contrasting energy efficiency in various ceramic sintering processes, 2018

REFERENCES

[1] Rahaman M.N. Ceramic Processing and Sintering. vol. 53. 2018. https://doi.org/10.1017/CBO9781107415324.004.

[2] Gokce Y. Sintering of (K0.5Na0.5)NbO3 system with the addition of ZnO. Anadolu University, 2018.

[3] Kang S-JL. Sintering-Densification, Grain Growth, and Microstructure. 2005.

[4] Kwon O. Liquid-Phase Sintering n.d.

[5] Zamora V, Ortiz AL, Guiberteau F, Nygren M. Crystal-size dependence of the spark-plasma-sintering kinetics of ZrB 2 ultra-high-temperature ceramics. J Eur Ceram Soc 2012;32:271–6. https://doi.org/10.1016/j.jeurceramsoc.2011.08.027.

[6] Thompson M, Fahrenholtz WG, Ãã GH. Effect of Starting Particle Size and Oxygen Content on Densification of ZrB 2 2011;435:429–35. https://doi.org/10.1111/j.1551-2916.2010.04114.x.

[7] German RM. Fundamentals of Sintering n.d.

[8] German RM, Suri P, Park SJ. Review: Liquid phase sintering. J Mater Sci 2009;44:1–39. https://doi.org/10.1007/s10853-008-3008-0.

[9] Guillon O, Gonzalez-Julian J, Dargatz B, Kessel T, Schierning G, Räthel J, et al. Field-assisted sintering technology/spark plasma sintering: Mechanisms, materials, and technology developments. Adv Eng Mater 2014;16:830–49. https://doi.org/10.1002/adem.201300409.

[10] Cologna M, Rashkova B, Raj R. Flash sintering of nanograin zirconia in <5 s at 850°C. J Am Ceram Soc 2010;93:3556–9. https://doi.org/10.1111/j.1551-2916.2010.04089.x.

[11] Guo H, Baker A, Guo J, Randall CA. Cold Sintering Process: A Novel Technique for Low-Temperature Ceramic Processing of Ferroelectrics. J Am Ceram Soc 2016;99:3489–507. https://doi.org/10.1111/jace.14554.

[12] Yamasaki N, Yanagisawa K, Nishioka M, Kanahara S. A hydrothermal hot-pressing method: Apparatus and application. J Mater Sci Lett 1986;5:355–6. https://doi.org/10.1007/BF01748104.

[13] Guo J, Guo H, Baker AL, Lanagan MT, Kupp ER, Messing GL, et al. Cold Sintering: A Paradigm Shift for Processing and Integration of Ceramics. Angew Chemie - Int Ed 2016;55:11457–61. https://doi.org/10.1002/anie.201605443.

[14] Guo J, Berbano SS, Guo H, Baker AL, Lanagan MT, Randall CA. Cold Sintering Process of Composites: Bridging the Processing Temperature Gap of Ceramic and Polymer Materials. Adv Funct Mater 2016;26:7115–21. https://doi.org/10.1002/adfm.201602489.

[15] Guo H, Baker A, Guo J, Randall CA. Protocol for Ultralow-Temperature Ceramic Sintering: An Integration of Nanotechnology and the Cold Sintering Process. ACS Nano 2016;10:10606–14. https://doi.org/10.1021/acsnano.6b03800.

[16] Ma JP, Chen XM, Ouyang WQ, Wang J, Li H, Fang JL. Microstructure, dielectric, and energy storage properties of BaTiO3ceramics prepared via cold sintering. Ceram Int 2018;44:4436–41. https://doi.org/10.1016/j.ceramint.2017.12.044.

[17] Grasso S, Biesuz M, Zoli L, Taveri G, Duff AI, Ke D, et al. A review of cold sintering processes. Adv Appl Ceram 2020;0:1–29. https://doi.org/10.1080/17436753.2019.1706825.

[18] Guo J, Baker AL, Guo H, Lanagan M, Randall CA. Cold sintering process: A new era for ceramic packaging and microwave device development. J Am Ceram Soc 2017;100:669–77. https://doi.org/10.1111/jace.14603.

[19] Baker A, Guo H, Guo J, Randall C, Green DJ. Utilizing the Cold Sintering Process for Flexible–Printable Electroceramic Device Fabrication. J Am Ceram Soc 2016;99:3202–4. https://doi.org/10.1111/jace.14467.

[20] Funahashi S, Guo J, Guo H, Wang K, Baker AL, Shiratsuyu K, et al. Demonstration of the cold sintering process study for the densification and grain growth of ZnO ceramics. J Am Ceram Soc 2017;100:546–53. https://doi.org/10.1111/jace.14617.

[21] Berbano SS, Guo J, Guo H, Lanagan MT, Randall CA. Cold sintering process of Li1.5Al0.5Ge1.5(PO4)3 solid electrolyte. J Am Ceram Soc 2017;100:2123–35. https://doi.org/10.1111/jace.14727.

[22] Gonzalez-Julian J, Neuhaus K, Bernemann M, Pereira da Silva J, Laptev A, Bram M, et al. Unveiling the mechanisms of cold sintering of ZnO at 250 °C by varying applied stress and characterizing grain boundaries by Kelvin Probe Force Microscopy. Acta Mater 2018;144:116–28. https://doi.org/10.1016/j.actamat.2017.10.055.

[23] Jiang X, Zhu G, Xu H, Dong L, Song J, Zhang X, et al. Preparation of high density ZnO ceramics by the Cold Sintering Process. Ceram Int 2019;45:17382–6. https://doi.org/10.1016/j.ceramint.2019.05.298.

[24] Zhao X, Liang J, Sun J, Guo J, Dursun S, Wang K, et al. Cold sintering ZnO based varistor ceramics with controlled grain growth to realize superior breakdown electric field. J Eur Ceram Soc 2021;41:430–5. https://doi.org/10.1016/j.jeurceramsoc.2020.09.023.

[25] Kang X, Floyd R, Lowum S, Cabral M, Dickey E, Maria JP. Mechanism studies of hydrothermal cold sintering of zinc oxide at near room temperature. J Am Ceram Soc 2019;102:4459–69. https://doi.org/10.1111/jace.16340.

[26] Lowum S, Floyd R, Bermejo R, Maria J-P. Mechanical strength of cold-sintered zinc oxide under biaxial bending. J Mater Sci 2018. https://doi.org/10.1007/s10853-018-3173-8.

[27] Lowum S, Floyd R, Bermejo R, Maria JP. Mechanical strength of cold-sintered zinc oxide under biaxial bending. J Mater Sci 2019;54:4518–22. https://doi.org/10.1007/s10853-018-3173-8.

[28] Guo J, Berbano SS, Guo H, Baker AL, Lanagan MT, Randall CA. Cold Sintering Process of Composites: Bridging the Processing Temperature Gap of Ceramic and Polymer Materials. Adv Funct Mater 2016;26:7115–21. https://doi.org/10.1002/adfm.201602489.

[29] Dargatz B, Gonzalez-Julian J, Bram M, Jakes P, Besmehn A, Schade L, et al. FAST/SPS sintering of nanocrystalline zinc oxide-Part I: Enhanced densification and formation of hydrogen-related defects in presence of adsorbed water. J Eur Ceram Soc 2016;36:1207–20. https://doi.org/10.1016/j.jeurceramsoc.2015.12.009.

[30] Dargatz B, Gonzalez-Julian J, Guillon O. Improved compaction of ZnO nano-powder triggered by the presence of acetate and its effect on sintering. Sci Technol Adv Mater 2015;16. https://doi.org/10.1088/1468-6996/16/2/025008.

[31] E.Y.Gutmanas AR. Cold Sintering Under High PRessure. Scr Metall 1979;13:11–5.

[32] Liao SC, Chen YJ, Kear BH, Mayo WE. High pressure/low temperature sintering of nanocrystalline alumina. Nanostructured Mater 1998;10:1063–79. https://doi.org/10.1016/S0965-9773(98)00125-1.

[33] Yalamaç E, Trapani A, Akkurt S. Sintering and microstructural investigation of gamma–alpha alumina powders. Eng Sci Technol an Int J 2014;17:2–7. https://doi.org/10.1016/j.jestch.2014.02.001.

[34] Yanagisawa K, Feng Q, Yamasaki N. Preparation of ceramics by hydrothermal hot-pressing. High Press Res 2001;20:343–9. https://doi.org/10.1080/08957950108206182.

[35] Yanagisawa K, Ioku K, Yamasaki N. Formation of anatase porous ceramics by hydrothermal hot-pressing of amorphous titania spheres. J Am Ceram Soc 1997;80:1303–6. https://doi.org/10.1111/j.1151-2916.1997.tb02982.x.

[36] Li J, Hashida T. Preparation of hydroxyapatite ceramics by hydrothermal hot-pressing method at 300 °c. J Mater Sci 2007;42:5013–9. https://doi.org/10.1007/s10853-006-0613-7.

[37] Guo H, Guo J, Baker A, Randall CA. Cold sintering process for ZrO2-based ceramics: significantly enhanced densification evolution in yttria-doped ZrO2. J Am Ceram Soc 2017;100:491–5. https://doi.org/10.1111/jace.14593.

[38] Sohrabi Baba Heidary D, Lanagan M, Randall CA. Contrasting energy efficiency in various ceramic sintering processes. J Eur Ceram Soc 2018;38:1018–29. https://doi.org/10.1016/j.jeurceramsoc.2017.10.015.

[39] Funahashi S, Guo J, Guo H, Wang K, Baker AL, Shiratsuyu K, et al. Demonstration of the cold sintering process study for the densification and grain growth of ZnO ceramics. J Am Ceram Soc 2017;100:546–53.

https://doi.org/10.1111/jace.14617.

[40] Schwarz S, Thron AM, Rufner J, Van Benthem K, Guillon O. Low temperature sintering of nanocrystalline zinc oxide: Effect of heating rate achieved by field assisted sintering/spark plasma sintering. J Am Ceram Soc 2012;95:2451–7. https://doi.org/10.1111/j.1551-2916.2012.05205.x.

[41] Dargatz B, Gonzalez-julian J, Bram M, Shinoda Y, Wakai F, Guillon O. Journal of the European Ceramic Society FAST / SPS sintering of nanocrystalline zinc oxide — Part II : Abnormal grain growth , texture and grain anisotropy. J Eur Ceram Soc 2016;36:1221–32. https://doi.org/10.1016/j.jeurceramsoc.2015.12.008.

[42] German RM. Liquid Phase Sintering. 1985.

[43] Ac OF, For P. Patent Application Publication Pub. No.: US 2017/0139001 A1 2017;1.

[44] Guo H, Guo J, Baker A, Randall CA. Cold sintering process for ZrO2-based ceramics: significantly enhanced densification evolution in yttria-doped ZrO2. J Am Ceram Soc 2017;100:491–5. https://doi.org/10.1111/jace.14593.

[45] Kimura T, Dong Q, Yin S, Hashimoto T, Sasaki A, Sato T. Synthesis and piezoelectric properties of Li-doped BaTiO3 by a solvothermal approach. J Eur Ceram Soc 2013;33:1009–15. https://doi.org/10.1016/j.jeurceramsoc.2012.11.007.

[46] Munir ZA, Anselmi-Tamburini U, Ohyanagi M. The effect of electric field and pressure on the synthesis and consolidation of materials: A review of the spark plasma sintering method. J Mater Sci 2006;41:763–77. https://doi.org/10.1007/s10853-006-6555-2.

[47] Anselmi-Tamburini U, Garay JE, Munir ZA. Fundamental investigations on the spark plasma sintering/synthesis process. Mater Sci Eng A 2005;407:24–30. https://doi.org/10.1016/j.msea.2005.06.066.

[48] Grasso S, Sakka Y, Maizza G. Electric current activated/assisted sintering (ECAS): A review of patents 1906-2008. Sci Technol Adv Mater 2009;10.

https://doi.org/10.1088/1468-6996/10/5/053001.

[49] Chaim R, Levin M, Shlayer A, Estournes C. Sintering and densification of nanocrystalline ceramic oxide powders: A review. Adv Appl Ceram 2008;107:159–69. https://doi.org/10.1179/174367508X297812.

[50] Sohrabi D, Heidary B, Lanagan M, Randall CA. Contrasting Energy Efficiency in Various Ceramic Sintering Processes Damoon Sohrabi Baba Heidary*, Michael Lanagan, and Clive A. Randall Center for Dielectrics and Piezoelectrics, Materials Research Institute, the Pennsylvania State University, University n.d.

[51] Anselmi-Tamburini U, Garay JE, Munir ZA. Fast low-temperature consolidation of bulk nanometric ceramic materials. Scr Mater 2006;54:823–8. https://doi.org/10.1016/j.scriptamat.2005.11.015.

[52] M.N.Rahaman. Ceramic Processing and Sintering. 2003. https://doi.org/10.1017/CBO9781107415324.004.

[53] Randall CA, Wang SF, Laubscher D, Dougherty JP, Huebner W. Structure property relationships in core-shell BaTiO3—LiF ceramics. J Mater Res 1993;8:871–9. https://doi.org/10.1557/JMR.1993.0871.

[54] Rahaman MN. Sintering of ceramics. Sinter Ceram 2007:1–389. https://doi.org/10.1201/b15869-2.

[55] West AR, Andres-Verges M. Impedance and Modulus Spectroscopy of ZnO Varistors. J Electroceramics 1997;1:125–32. https://doi.org/10.1023/A:1009906315725.

[56] Magnusson KO, Wiklund S. Interface formation of Bi on ceramic ZnO: A simple model varistor grain boundary. J Appl Phys 1994;76:7405–9. https://doi.org/10.1063/1.357966.

[57] Greuter F. Electrically active interfaces in ZnO varistors. Solid State Ionics 1995;75:67–78. https://doi.org/10.1016/0167-2738(94)00181-Q.

[58] Badev A, Marinel S, Heuguet R, Savary E, Agrawal D. Sintering behavior and non-linear properties of ZnO varistors processed in microwave electric and magnetic fields at 2.45 GHz. Acta Mater 2013;61:7849–58.

https://doi.org/10.1016/j.actamat.2013.09.023.

[59] Gupta TK, Carlson WG. A grain-boundary defect model for instability / stability of a ZnO varistor Di ? ordered Layer 1985;20:3487–500.

[60] Ndayishimiye A, Sengul MY, Bang SH, Tsuji K, Takashima K, Hérisson de Beauvoir T, et al. Comparing hydrothermal sintering and cold sintering process: Mechanisms, microstructure, kinetics and chemistry. J Eur Ceram Soc 2020;40:1312–24. https://doi.org/10.1016/j.jeurceramsoc.2019.11.049.

[61] Nielsen AE. A. E. Nielsen 1970;42:319–33.

[62] Guo H, Guo J, Baker A, Randall CA. Hydrothermal-Assisted Cold Sintering Process: A New Guidance for Low-Temperature Ceramic Sintering. ACS Appl Mater Interfaces 2016;8:20909–15. https://doi.org/10.1021/acsami.6b07481.

[63] Biesuz M, Taveri G, Duff AI, Olevsky E, Zhu D, Hu C, et al. A theoretical analysis of cold sintering. Adv Appl Ceram 2019;0:1–15. https://doi.org/10.1080/17436753.2019.1692173.

[64] Goglio G, Ndayishimiye A, Elissalde C, Randall CA. Cold Sintering and Hydrothermal Sintering. Ref Modul Mater Sci Mater Eng 2020:1–16. https://doi.org/10.1016/b978-0-12-803581-8.12113-7.

[65] Sengul MY, Guo J, Randall CA, van Duin ACT. Water-Mediated Surface Diffusion Mechanism Enables the Cold Sintering Process: A Combined Computational and Experimental Study. Angew Chemie 2019;131:12550–4. https://doi.org/10.1002/ange.201904738.

[66] Sengul MY, Guo J, Randall CA, van Duin ACT. Water-Mediated Surface Diffusion Mechanism Enables the Cold Sintering Process: A Combined Computational and Experimental Study. Angew Chemie - Int Ed 2019;58:12420–4. https://doi.org/10.1002/anie.201904738.

[67] Liu Y, Sun Q, Wang D, Adair K, Liang J, Sun X. Development of the cold sintering process and its application in solid-state lithium batteries. J Power Sources 2018;393:193–203. https://doi.org/10.1016/j.jpowsour.2018.05.015.

[68] Kolodziejczak-Radzimska A, Jesionowski T. Zinc oxide-from synthesis to

application: A review. Materials (Basel) 2014;7:2833–81. https://doi.org/10.3390/ma7042833.

[69] Djurišić AB, Chen X, Leung YH, Man Ching Ng A. ZnO nanostructures: Growth, properties and applications. J Mater Chem 2012;22:6526–35. https://doi.org/10.1039/c2jm15548f.

[70] Cun T, Dong C, Huang Q. Ionothermal precipitation of highly dispersive ZnO nanoparticles with improved photocatalytic performance. Appl Surf Sci 2016;384:73–82. https://doi.org/10.1016/j.apsusc.2016.05.008.

[71] Mudunkotuwa IA, Rupasinghe T, Wu CM, Grassian VH. Dissolution of ZnO nanoparticles at circumneutral pH: A study of size effects in the presence and absence of citric acid. Langmuir 2012;28:396–403. https://doi.org/10.1021/la203542x.

[72] Jing Y, Luo N, Wu S, Han K, Wang X, Miao L, et al. Remarkably improved electrical conductivity of ZnO ceramics by cold sintering and post-heat-treatment. Ceram Int 2018;44:20570–4. https://doi.org/10.1016/j.ceramint.2018.07.192.

[73] Farhat S, Rekaby M, Awad R. Vickers microhardness and indentation creep studies for erbium-doped ZnO nanoparticles. SN Appl Sci 2019;1:1–12. https://doi.org/10.1007/s42452-019-0559-4.

[74] Roy TK. Assessing hardness and fracture toughness in sintered zinc oxide ceramics through indentation technique. Mater Sci Eng A 2015;640:267–74. https://doi.org/10.1016/j.msea.2015.05.107.

[75] Nur K, Zubair M, Gibson JSKL, Sandlöbes-Haut S, Mayer J, Bram M, et al. Mechanical properties of cold sintered ZnO investigated by nanoindentation and micro-pillar testing. J Eur Ceram Soc 2022;42:512–24. https://doi.org/10.1016/j.jeurceramsoc.2021.10.011.

[76] Reed J. Principles of Ceramic Processing. Wiley-Inte. Jonh Wiley & Sons, Inc.; 1995.

[77] Zahabi M, Said A, Memari A. Cold Sintering of Calcium Carbonate for Construction Material Applications. ACS Omega 2021;6:2576–88.

https://doi.org/10.1021/acsomega.0c04617.

[78] Anandan M, Dinesh S, Krishnakumar N, Balamurugan K. Tuning the crystalline size of template free hexagonal ZnO nanoparticles via precipitation synthesis towards enhanced photocatalytic performance. J Mater Sci Mater Electron 2017;28:2574–85. https://doi.org/10.1007/s10854-016-5833-2.

[79] Hanif MA, Lee I, Akter J, Islam MA, Zahid AASM, Sapkota KP, et al. Enhanced photocatalytic and antibacterial performance of ZnO nanoparticles prepared by an efficient thermolysis method. Catalysts 2019;9. https://doi.org/10.3390/catal9070608.

[80] Bang SH, Ndayishimiye A, Randall CA. Anisothermal densification kinetics of the cold sintering process below 150 °C. J Mater Chem C 2020;8:5668–72. https://doi.org/10.1039/d0tc00395f.

[81] Rana N, Ghosh KS, Chand S, Gathania AK. Investigation of ZnO nanoparticles for their applications in wastewater treatment and antimicrobial activity. Indian J Pure Appl Phys 2018;56:19–25.

[82] Horzum N, Hilal ME, Isik T. Enhanced bactericidal and photocatalytic activities of ZnO nanostructures by changing the cooling route. New J Chem 2018;42:11831–8. https://doi.org/10.1039/c8nj01849a.

[83] Yu T, Cheng J, Li L, Sun B, Bao X, Zhang H. Current understanding and applications of the cold sintering process. Front Chem Sci Eng 2019:1–11. https://doi.org/10.1007/s11705-019-1832-1.

[84] Grasso S, Biesuz M, Zoli L, Taveri G, Duff AI, Ke D, et al. A review of cold sintering processes. Adv Appl Ceram 2020;119:115–43. https://doi.org/10.1080/17436753.2019.1706825.

[85] Yu T, Cheng J, Li L, Sun B, Bao X, Zhang H. Current understanding and applications of the cold sintering process. Front Chem Sci Eng 2019;13:654–64. https://doi.org/10.1007/s11705-019-1832-1.

[86] Maria JP, Kang X, Floyd RD, Dickey EC, Guo H, Guo J, et al. Cold sintering: Current status and prospects. J Mater Res 2017;32:3205–18.

https://doi.org/10.1557/jmr.2017.262.

[87] Kang X. Hydrothermal Cold Sintering. 2017.

[88] Andrews J, Button D, Reaney IM. Advances in Cold Sintering. Johnson Matthey Technol Rev 2020:219–32.

[89] Floyd RD, Lowum S, Maria JP. Cold sintering zinc oxide with a crystalline zinc acetate dihydrate mass transport phase. J Mater Sci 2020;55:15117–29. https://doi.org/10.1007/s10853-020-05100-9.

[90] Keramat E, Hashemi B. Modelling and optimizing the liquid phase sintering of alumina/CaO–SiO2–Al2O3 ceramics using response surface methodology. Ceram Int 2021;47:3159–72. https://doi.org/10.1016/j.ceramint.2020.09.153.

[91] M. LL, R. PH. Zinc oxide varistors — a review. Am Ceram Soc Bull 1986;65.

[92] Matsuoka M. Nonohmic properties of zinc oxide ceramics. Jpn J Appl Phys 1971;10:736. https://doi.org/10.1143/JJAP.10.736.

[93] Philipp HR, Levinson LM. ZnO varistors for protection against nuclear electromagnetic pulses. J Appl Phys 1981;52:1083–90. https://doi.org/10.1063/1.328807.

[94] Martzloff FD, Co GE, Golden FB. Metal-oxide varistor halts component 1977;1972.

[95] He J. Metal Oxide Varistors. vol. 17. 1987. https://doi.org/10.1146/annurev.ms.17.080187.001503.

[96] He J. Introduction of Varistor Ceramics. Met. Oxide Varistors From Microstruct. to Macro-Characteristics, 2019, p. 1–30. https://doi.org/10.1002/9783527684038.ch1.

[97] Tan DQ, Cao Y, Chu B. High voltage metal oxide varistors for surge protection. SAE Tech Pap 2008. https://doi.org/10.4271/2008-01-2850.

[98] Gromov OG, Savel'ev YA, Tikhomirova EL, Belyaevskii AT, Lokshin EP. Optimization of the composition and sintering conditions of high-voltage ZnO varistor ceramics. Inorg Mater 2017;53:536–9.

https://doi.org/10.1134/S0020168517050089.

[99] He J. Metal Oxide Varistors: from microstructure to macrocharacteristics 2019:482.

[100] Global Metal Oxide Varistor Market , By Type (Disc Metal Oxide Varistor , Strap Metal Oxide Varistor , Block Metal Oxide Varistor , Ring Metal Oxide Varistor , Others), By End User , By Construction , By Sales Channel , By Region , Competition Forecast. 2022.

[101] Xu D, Shi L, Wu Z, Zhong Q, Wu X. Microstructure and electrical properties of ZnO-Bi2O3-based varistor ceramics by different sintering processes. J Eur Ceram Soc 2009;29:1789–94. https://doi.org/10.1016/j.jeurceramsoc.2008.10.020.

[102] Olsson E, Dunlop G, Österlund R. Development of Functional Microstructure during Sintering of a ZnO Varistor Material. J Am Ceram Soc 1993;76:65–71. https://doi.org/10.1111/j.1151-2916.1993.tb03690.x.

[103] Mehring M. From molecules to bismuth oxide-based materials: Potential homo- and heterometallic precursors and model compounds. Coord Chem Rev 2007;251:974–1006. https://doi.org/10.1016/j.ccr.2006.06.005.

[104] Daneu N, Rec A. Grain Growth Control in Sb 2 O 3 -Doped Zinc Oxide 2003;84:1379–84.

[105] He JL, Hu J, Lin YH. ZnO varistors with high voltage gradient and low leakage current by doping rare-earth oxide. Sci China, Ser E Technol Sci 2008;51:693–701. https://doi.org/10.1007/s11431-008-0085-x.

[106] Fan J, Poosimma P, Freer R. Phase development in ZnO varistors. Adv Appl Ceram 2015;114:14–7. https://doi.org/10.1179/1743676114Y.0000000179.

[107] Gupta TK, Straub WD. Effect of annealing on the ac leakage components of the ZnO varistor. I. Resistive current. J Appl Phys 1990;68:845–50. https://doi.org/10.1063/1.346766.

[108] Wu A, Zhu Z, Wang X, Yan N, Zhou H, Huang R, et al. High-performance ZnO varistor ceramics prepared by arc-induced flash sintering with low energy consumption at room temperature. High Volt 2022;7:222–32.

https://doi.org/10.1049/hve2.12161.

[109] Beynet Y, Izoulet A, Guillemet-Fritsch S, Chevallier G, Bley V, Pérel T, et al. ZnO-based varistors prepared by spark plasma sintering. J Eur Ceram Soc 2015;35:1199–208. https://doi.org/10.1016/j.jeurceramsoc.2014.10.007.

[110] German RM. Sintering With a Liquid Phase. 2014. https://doi.org/10.1016/b978-0-12-401682-8.00009-4.

[111] De Jonghe LC, Rahaman MN. Sintering of Ceramics. Handb Adv Ceram Mater Appl Process Prop 2003;1–2:187–264. https://doi.org/10.1016/B978-012654640-8/50006-7.

[112] Buckton G, Beezer AE. The relationship between particle size and solubility. Int J Pharm 1992;82:7–10. https://doi.org/10.1016/0378-5173(92)90184-4.

[113] Bernik S, Cheng L, Podlogar M, Li G. Low-Temperature Sintering Of Zno – Bi_2O_3-Based Varistor Ceramics For Enhanced Microstructure Development And Current-Voltage Characteristics 2018;62:8–14. https://doi.org/10.13168/cs.2017.0040.

[114] Kang S-JL. Sintering Densification, Grain Growth and Microstructure. 2005.

[115] Rupasinghe RP. Dissolution and aggregation of zinc oxide nanoparticles at circumneutral pH ; a study of size effects in the presence and absence of citric acid 2011.

[116] Fatehah MO, Aziz HA, Stoll S. Stability of ZnO Nanoparticles in Solution. Influence of pH, Dissolution, Aggregation and Disaggregation Effects. J Colloid Sci Biotechnol 2014;3:75–84. https://doi.org/10.1166/jcsb.2014.1072.

[117] Sletson Lc, Potter Me, Alim Ma. Influence of Sintering Temperature on Intrinsic Trapping in Zinc Oxide-Based Varistors. J Am Ceram Soc 1988;71:909–13. https://doi.org/10.1111/j.1151-2916.1988.tb07557.x.

[118] Yuan F, Ryu H. Microstructure of varistors prepared with zinc oxide nanoparticles coated with Bi2O3. J Am Ceram Soc 2004;87:736–8. https://doi.org/10.1111/j.1551-2916.2004.00736.x.

[119] Wu YC, Chaing YC, Huang CY, Wang SF, Yang HY. Morphology-controllable

Bi2O3 crystals through an aqueous precipitation method and their photocatalytic performance. Dye Pigment 2013;98:25–30. https://doi.org/10.1016/j.dyepig.2013.02.006.

[120] Olsson E, Dunlop GL. The effect of Bi2O3 content on the microstructure and electrical properties of ZnO varistor materials. J Appl Phys 1989;66:4317–24. https://doi.org/10.1063/1.343978.

[121] Branković ZM, Branković GO, Poleti DD, Karanović L, Varela JA. Correlation between chemical composition of the γ-Bi2O3 phase and the properties of ZnO varistors. Chem Ind Chem Eng Q 2005;11:169–72. https://doi.org/10.2298/CICEQ0504169B.

[122] Morris WG. Electrical Properties of ZnO-Bi , O , Ceramics 1973;56:360–4.

[123] Varistors ZO. Application of Zinc Oxide Varistors 1990.

[124] nonohmic properties of zinc oxide ceramics - matsuoka1971.pdf n.d.

[125] Liang J, Zhao X, Sun J, Ren L, Liao R, Yang L, et al. Enhanced electrical properties of ZnO varistor ceramics by spark plasma sintering: Role of annealing. Ceram Int 2020:0–1. https://doi.org/10.1016/j.ceramint.2020.03.042.

[126] Shiva LU, Ayachit NH, Udachan LA. Electrical And Microstructural Properties Of ZnO-Bi_2O_3-TiO_2-Sb_2O_3-Al_2O_3-Based Varistor Ceramics Fabricated By Solution Coating Method. Int J Nanoelectron Mater 2019;12:221–36.

[127] Yanagida H. A discussion on the Mevhanism for the Non-linear Voltage-Current Charateristic of ZnO-Bi2O3 Composite Ceramic 1971:64–7.

[128] Levinson LM, Philipp HR. Zinc Oxide Varistors - a Review. Am Ceram Soc Bull 1986;65:639–46.

[129] Industrial, Matsushita Electric, Kazuo E. Zinc Oxide Varistors. IEEE Electr Insul Mag 1989;5.

[130] Elfwing M, Österlund R, Olsson E. Differences in Wetting Characteristics of Bi2O3 Polymorphs in ZnO Varistor Materials. J Am Ceram Soc 2004;83:2311–4. https://doi.org/10.1111/j.1151-2916.2000.tb01552.x.

[131] Byrn SR, Zografi G, Chen XS. Solubility and Dissolution. Solid State Prop Pharm Mater 2017:249–64. https://doi.org/10.1002/9781119264408.ch17.

[132] Entekno Materials. Entekno-MicNo-All-Brochures 2020.

[133] Ikono R, Maulana NN, Dewinggih T, Effendi M, Widayanto WB. Effect of Polyacrylic Acid Addition to Improve Nano Zinc Oxide Dispersion Stability. Int J Eng 2012:95–9.

[134] Jabeen Fatima MJ, Niveditha C V., Sindhu S. α-Bi2O3 photoanode in DSSC and study of the electrode-electrolyte interface. RSC Adv 2015;5:78299–305. https://doi.org/10.1039/c5ra12760b.

[135] Chitrada K, Raja KS. Stability of the Nanoporous Bismuth Oxide Photoanodes for Solar Water Splitting 2014:173–99. https://doi.org/10.1007/978-1-4939-1628-3_9.

[136] Shi Y, Luo L, Zhang Y, Chen Y, Wang S, Li L, et al. Synthesis and characterization of α/β-Bi2O3 with enhanced photocatalytic activity for 17α-ethynylestradiol. Ceram Int 2017;43:7627–35. https://doi.org/10.1016/j.ceramint.2017.03.057.

[137] Vakifahmetoglu C, Karacasulu L. Current Opinion in Solid State & Materials Science Cold sintering of ceramics and glasses : A review 2020;24. https://doi.org/10.1016/j.cossms.2020.100807.

[138] O. Ozer. ZnO Esaslı Varistörlerde Yönlenme Gelişimi, Evrik Sınırların Yönlenme Gelişimine Etkisi Ve Yönlenme İle Elektriksel Özelliklerin İlişkisi. 2006.

[139] Rečnik A, Bernik S, Daneu N. Microstructural engineering of ZnO-based varistor ceramics. J Mater Sci 2012;47:1655–68. https://doi.org/10.1007/s10853-011-5937-2.

[140] Brayner R, Dahoumane SA, Yéprémian C, Djediat C, Meyer M, Couté A, et al. ZnO nanoparticles: Synthesis, characterization, and ecotoxicological studies. Langmuir 2010;26:6522–8. https://doi.org/10.1021/la100293s.

[141] Jolivet J-P., Henry M., Livage J. and BE. Metal Oxide Chemistry and Synthesis. 2000.

[142] Weng CH, Weiw WCJ. Synthesis and properties of homogeneous Nb-doped

bismuth oxide. J Am Ceram Soc 2010;93:3124–9. https://doi.org/10.1111/j.1551-2916.2010.03836.x.

[143] Jabeen Fatima MJ, Navaneeth A, Sindhu S. Improved carrier mobility and bandgap tuning of zinc doped bismuth oxide. RSC Adv 2015;5:2504–10. https://doi.org/10.1039/c4ra12494d.

[144] Ansari S, Ansari MS, Satsangee SP, Jain R. Bi2O3/ZnO nanocomposite: Synthesis, characterizations and its application in electrochemical detection of balofloxacin as an anti-biotic drug. J Pharm Anal 2021;11:57–67. https://doi.org/10.1016/j.jpha.2020.03.013.

[145] Ma S, Xu Z, Chu R, Hao J, Cheng L, Li G. Low-temperature sintering and electrical properties of Co-doped ZnO varistors. J Mater Sci Mater Electron 2014;25:3878–84. https://doi.org/10.1007/s10854-014-2102-0.

[146] Wang YJ, Wang JF, Li CP, Chen HC, Su WB, Zhong WL, et al. Improved varistor nonlinearity via sintering and acceptor impurity doping. EPJ Appl Phys 2000;11:155–8. https://doi.org/10.1051/epjap:2000157.

[147] Clarke DR. Varistor Ceramics 1999;502:485–502.

[148] Prabaharan DDM, Sadaiyandi K, Mahendran M, Sagadevan S. Precipitation method and characterization of cobalt oxide nanoparticles. Appl Phys A Mater Sci Process 2017;123:1–6. https://doi.org/10.1007/s00339-017-0786-8.

[149] Sinkó K, Szabó G, Zrínyi M. Liquid-phase synthesis of cobalt oxide nanoparticles. J Nanosci Nanotechnol 2011;11:4127–35. https://doi.org/10.1166/jnn.2011.3875.

[150] Xu JM, Zhang J, Wang BB, Liu F. Shape-regulated synthesis of cobalt oxide and its gas-sensing property. J Alloys Compd 2015;619:361–7. https://doi.org/10.1016/j.jallcom.2014.09.020.

[151] Allaedini G, Muhammad A. Study of influential factors in synthesis and characterization of cobalt oxide nanoparticles. J Nanostructure Chem 2013;3:1. https://doi.org/10.1186/2193-8865-3-77.

[152] Kumbhar D, Kumbhar S, Dhodamani A, Delekar S, Harale N, Nalawade R, et al. Enhanced photoelectrochemical cell performance of Co doped ZnO nanoparticles

sensitized by affordable mixed dyes as sensitizer. Inorg Nano-Metal Chem 2021;51:1258–71. https://doi.org/10.1080/24701556.2020.1835963.

[153] Li Y, Li G, Yin Q. Preparation of ZnO varistors by solution nano-coating technique. Mater Sci Eng B Solid-State Mater Adv Technol 2006;130:264–8. https://doi.org/10.1016/j.mseb.2006.03.010.

[154] Banerjee A, Ramamohan TR, Patni MJ. Smart technique for fabrication of zinc oxide varistor. Mater Res Bull 2001;36:1259–67. https://doi.org/10.1016/S0025-5408(01)00611-0.

[155] Daneu N, Novak Gramc N, Rečnik A, Maček Kržmanc M, Bernik S. Shock-sintering of low-voltage ZnO-based varistor ceramics with Bi 4Ti 3O 12 additions. J Eur Ceram Soc 2013;33:335–44. https://doi.org/10.1016/j.jeurceramsoc.2012.08.023.

[156] Shahraki MM, Golmohammad M, Safaee I, Chermahini MD. The control of abnormal grain growth in low-voltage SnO2 varistors by microseed addition. Ceram Int 2018;44:3388–93. https://doi.org/10.1016/j.ceramint.2017.11.129.

[157] Onreabroy W, Sirikulrat N. Effects of cobalt doping on nonlinearity of zinc oxide. Mater Sci Eng B Solid-State Mater Adv Technol 2006;130:108–13. https://doi.org/10.1016/j.mseb.2006.02.058.

CURRICULUM VITAE

ORCID ID: 0000-0002-6425-2851

Name Surname : Gökçe ÖZARSLAN

Foreign Language : English

Education and Working Experinces:

- **2008, Anadolu University**, High Tecnologies Departmant, Nanotechnology, MSc degree, "Sintering of $(K_{0.5}Na_{0.5})NbO_3$ system with the addition of ZnO".
- **2005, Anadolu University**, Materials Science and Engineering, Undergraduate degree, "Improving electrical properties of zinc oxide by texturing its microstructure on <001> direction via TGG Method".

- 2019-2020 TUBITAK Project; “Lead Free Electrocaloric Ceramics”
- 2006-2009 BAP Project; “Lead Free Piezoelectric Ceramics” (Finished successfully)
- 2006-2009 TUBITAK Project; “Lead Free Piezoelectric Ceramics” (Finished successfully) / Master degree thesis
- ECERS, International Ceramic Conference, Krakow, Poland, June 2009, Poster presentation.
- 5S, Quality Course, June 2009
- Piezoelectric Conference, Manchester, September 2008, poster
- ASTMD International Conference of Textured Materials, Gebze, June 2008, Poster presentation
- KMM (European Virtual Institute on Knowledge-Based Multifunctional Materials), Summer School, invited student, Imperial Collage, London, England, June 2007
- Petrol Ofisi A.Ş. (POAŞ) Nanotechnology Summer Camp (July 2006)
- Nano-Tr International Conference, 2004, Antalya
- “Project Design, Project Planning, Project Management” certificate (Ankara Ostim Kosgeb-2004)
- “ISO 9001-2000 Primary Training” quality certificate (Ankara Ostim Kosgeb-2004)
- “ISO 9001-2000 documentation” quality certificate (Ankara Ostim Kosgeb-2004)
- “ISO 9001-2000 internal auditor” quality certificate (Ankara Ostim Kosgeb-2004)
- Anadolu University 2005 honor certificate
- 1992 Anatolian High School, first 1600 of Turkey.